



THE HONG KONG  
POLYTECHNIC UNIVERSITY

香港理工大學

Pao Yue-kong Library

包玉剛圖書館

---

## Copyright Undertaking

This thesis is protected by copyright, with all rights reserved.

**By reading and using the thesis, the reader understands and agrees to the following terms:**

1. The reader will abide by the rules and legal ordinances governing copyright regarding the use of the thesis.
2. The reader will use the thesis for the purpose of research or private study only and not for distribution or further reproduction or any other purpose.
3. The reader agrees to indemnify and hold the University harmless from and against any loss, damage, cost, liability or expenses arising from copyright infringement or unauthorized usage.

### IMPORTANT

If you have reasons to believe that any materials in this thesis are deemed not suitable to be distributed in this form, or a copyright owner having difficulty with the material being included in our database, please contact [lbsys@polyu.edu.hk](mailto:lbsys@polyu.edu.hk) providing details. The Library will look into your claim and consider taking remedial action upon receipt of the written requests.

**IDENTIFICATION OF POTENTIAL MOLECULAR PATHWAYS  
AND GENES THAT INDUCED HEPATOCELLULAR  
CARCINOMA BY VARIOUS GENOTYPES OF HBX GENE IN  
TRANSGENIC MOUSE MODEL**

**CHIU PAN HEUNG**

**PhD**

**THE HONG KONG POLYTECHNIC UNIVERSITY**

**2019**

**The Hong Kong Polytechnic University**

**Department of Applied Biology and Chemical Technology**

**Identification of potential molecular pathways and genes that  
induced hepatocellular carcinoma by various genotypes of HBx gene  
in transgenic mouse model**

**Chiu Pan Heung**

**A thesis submitted in partial fulfilment of the requirements for the degree of  
Doctor of Philosophy**

**August 2018**

## **CERTIFICATE OF ORIGINALITY**

I hereby declare that this thesis is my own work and that, to the best of my knowledge and belief, it reproduces no material previously published or written, nor material that has been accepted for the award of any other degree or diploma, except where due acknowledgement has been made in the text.

\_\_\_\_\_ (Signed)

Chiu Pan Heung (Name of student)

## Abstract

**Background & Aims:** Chronic hepatitis B viral (HBV) infection still raises a high threat for hepatocellular carcinoma (HCC) worldwide, especially in Asia. Different HBV genotypes are associated with varying levels of pathogenicity, while the genetic mechanisms behind this remain unclear. This study attempts to elucidate the mechanisms contributing to tumor progression of K130M/V131I mutant and wild-type variants of HBx genotypes A, B, C and D *in vivo*.

**Methods:** To compare the potential tumorigenic effects of various HBx genotypes on HCC, the *Sleeping Beauty* (SB) transposon system was used to deliver different HBx genotypes into the livers of fumarylacetoacetate hydrolyase (*Fah*)-deficient mice by hydrodynamic tail vein injection. Short hairpin RNA directed against transformation-related protein (*Trp53*) was co-injected to determine the combinational effect of *Trp53* dysfunction in HBV-associated HCC.

**Results:** The most tumorigenic genotype of HBx gene was genotype D for both wild-type and K130M/V131I mutant variants; while genotype A was the least tumorigenic. Mutant variant of genotype B exerted a stronger tumor burden than its wild-type counterpart; while both wild-type and mutant variants of genotype C induced similar tumorigenic evidence as mutant variant of genotype B. In general, both wild-type and mutant variants of all HBx genotypes played an important role in liver hepatitis by activating the arachidonic acid metabolic pathway. Significant up-regulation of major urinary protein 14 (*Mup14*) (>100-fold increase) and down-regulation of cytochrome P450, family 4, subfamily f, polypeptide 14 (*Cyp4f14*) or cytochrome P450, family 4, subfamily f, polypeptide 15 (*Cyp4f15*) (~3-fold decrease) caused accumulation of pro-inflammatory factors, prostaglandin D<sub>2</sub> (PGD<sub>2</sub>) and leukotriene B<sub>4</sub> (LTB<sub>4</sub>) in liver; at the same time, suppression of anti-inflammatory factors epoxyeicosatrienoic acids (EETs) production by down-regulating cytochrome P450 CYP2 (CYP2) encoding genes was observed in mutant and wild-type variants of all HBx genotypes studied. At the transcriptional level, we identified insulin growth factor 2 (*Igf2*) was commonly up-regulated in tumors induced by mutant variants of HBx genotypes B, C and D; while p21 (RAC1) activated kinase 6 (*Pak6*) and Rho GTPase activating protein 27

(*Arhgap27*) were commonly up-regulated in tumor induced by wild-type variants of HBx genotypes A, C and D. Up-regulation of *Igf2* was reported to be associated with phosphatidylinositol 3-kinase (PI3K)/AKT serine/threonine-protein kinase (AKT) and mitogen-activated protein kinase (MAPK) signalling pathways; while *Pak6* has been reported to regulate actin cytoskeleton via RAC/PAK signalling pathway. Additionally, at the translational level, HBx genotype B mutant variant induced phosphorylation of AKT and reduction of FOXO1; while genotype C wild-type variant suppressed PPARG and induced accumulation of CTNNB1.

**Conclusion:** HBx-D K130M/V131I mutant demonstrated the strongest tumorigenic effect. HBx-B mutant, HBx-C mutant and wild-type displayed similar tumorigenic effect; while HBx-B wild-type, HBx-A mutant and wild-type were the least tumorigenic. HBx induced inflammation by accumulation of pro-inflammatory factors in the liver via arachidonic acid metabolism. At the transcriptional level, we identified *Igf2* as a commonly up-regulated gene in tumor induced by mutant HBx and *Pak6* and *Arhgap27* as a commonly up-regulated gene in tumor induced by wild-type HBx. Last but not least, we discovered that different genotypes induced tumor development via different signalling pathways predominantly. HBx genotype B induced tumor progression mainly via AKT/FOXO1 signalling cascade; while genotype C induced tumor progression predominantly via PPARG/CTNNB1 signalling cascade.

## List of publications

### Publications:

1. **Chiu AP**, Tschida BR, Sham TT, Lo LH, Moriarity BS, Li XX, Lo CL, Hinton DE, Rowlands DK, Chan CO, Mok KW, Largaespada DA, Warner N, Keng VW. HBx-K130M/V131I Promotes Liver Cancer in Transgenic Mice via AKT/FOXO1 Signalling Pathway and Arachidonic Acid Metabolism. *Mol Cancer Res* May 3 2019 DOI: 10.1158/1541-7786.MCR-18-1127.
2. **Chiu AP**, Keng VW. Liver-Specific Delivery of Sleeping Beauty Transposon System by Hydrodynamic injection for Cancer Gene Validation. *Methods Mol Biol* 2019;1907:185-196.
3. **Chiu AP**, Tschida BR, Lo LH, Moriarity BS, Rowlands DK, Largaespada DA, Keng VW. Transposon mouse models to elucidate the genetic mechanisms of hepatitis B viral induced hepatocellular carcinoma. *World Journal of Gastroenterology*. 2015;21(42):12157-12170.
4. Li XX, Zhang SJ, **Chiu AP**, et al. Targeting of AKT/ERK/CTNNB1 by DAW22 as a potential therapeutic compound for malignant peripheral nerve sheath tumor. *Cancer Med*. 2018;7(9):4791-4800.
5. Li XX, Zhang SJ, **Chiu AP**, et al. Conditional Inactivation of *NF1* and *Pten* in Schwann Cells Results in Abnormal Neuromuscular Junction Maturation. *G3: GENES, GENOMES, GENETICS*. 2018.
6. Li XX, Lu XY, Zhang SJ, **Chiu AP**, et al. Sodium tanshinone IIA sulfonate ameliorates hepatic steatosis by inhibiting lipogenesis and inflammation. *Biomed Pharmacother*. 2018 Dec 18;111:68-75.

### **Posters:**

7. **Chiu AP**, et al. “HBx induces hepatocarcinogenesis via activation of cancerous signaling pathways and alteration of metabolism” was presented at the 77<sup>th</sup> Annual meeting of the Japanese Cancer Association, Osaka, Japan, 27-29 September, 2018. Poster-3006.
8. **Chiu AP**, et al. “Explicating the molecular pathways of HBx-induced HCC using the Sleeping Beauty Transposon System in vivo” was presented at the 76<sup>th</sup> Annual meeting of the Japanese Cancer Association, Yokohama, Japan, 28-30 September, 2017. Poster-1044.
9. **Chiu AP**, Tschida BR, Lo LH, et al. Validating the effects and genetic mechanisms of hepatitis B viral (HBV) gene components in liver tumorigenesis in vivo using a transposon-based reverse genetic system. Conference on Transposition and Genome Engineering 2015.
10. **Chiu AP**, Tschida BR, Lo LH, et al. Elucidating the effects and genetic mechanisms of various hepatitis B viral gene components in vivo. Sunney I. and Irene Y. Chan Lecture in Chemical Biology 2015.
11. **Chiu AP**, Tschida BR, Lo LH, et al. Elucidating the effects and genetic mechanisms of various hepatitis B viral gene components in vivo. International Symposium on “Frontiers in cancer biology & drug development” 2015.

### **Awards:**

1. **2017:** Travel Grant, the 76<sup>th</sup> Annual meeting of the Japanese Cancer Association, Yokohama, Japan
2. **2015:** Best Poster Award in Life Sciences – First Prize, Sunney I. and Irene Y. Chan Lecture in Chemical Biology

## **Acknowledgements**

I would like to thank my supervisor, Dr. Vincent Keng, for providing me with great support and ideas for my project. He provided a good environment and equipment for me to conduct the experiments. I am especially grateful for his patience and opportunities throughout my PhD study.

I am grateful to have collaborations with Prof. David A. Largaspada, Dr. Barbara R. Tschida, and Dr. Branden S. Moriarity, from the University of Minnesota, US; Dr. Nadia Warner, from the Victorian Infectious Diseases Reference Laboratory at The Peter Doherty Institute for Infection and Immunity, Australia. I would like to thank Prof. David A. Largaspada for his experimental advice; Dr. Barbara R. Tschida for designing and conducting part of the experiment; Dr. Branden S. Moriarity for the backbone plasmid constructs; and Dr. Nadia Warner for providing the human sequence of mutant and wild-type HBx genes of various genotypes and her ideas on the project.

I would also like to thank the team members, especially Irene Sham and On Chan in Dr. Daniel Mok's lab who helped out with the metabolomics analyses; Dr. Regina Lo from Department of Pathology of the University of Hong Kong, Dr. David E Hinton from Civil and Environmental Engineering of Duke University, Dr. Michael A Linden, Dr. Khalid Amin from Laboratory Medicine and Pathology of University of Minnesota for their help on the project with the histopathological analyses.

I would also like to thank the professors, scientific officers, technicians and staffs in ABCT, CAF and LASEC of the Chinese University of Hong Kong for their kind assistance and support on my research work.

Last but not least, I would like to thank all team members and ex-team members in Dr. Vincent Keng's lab, especially Cindy Li, Lilian Lo, Jeffrey To, Carlton Wong, Shijie Zhang, Karen Chan, Sheila Cui and Eleven Yin for their advice and support.

Most importantly, I would like to express my sincere gratitude to my family and friends for their love, care and support, without which this journey would not have been possible.

## **Table of Contents**

<b><u>CERTIFICATE OF ORIGINALITY</u></b>	<b><u>3</u></b>
<b><u>ABSTRACT</u></b>	<b><u>4</u></b>
<b><u>LIST OF PUBLICATIONS</u></b>	<b><u>6</u></b>
<b><u>ACKNOWLEDGEMENTS</u></b>	<b><u>8</u></b>
<b><u>LIST OF TABLES</u></b>	<b><u>16</u></b>
<b><u>ABBREVIATIONS</u></b>	<b><u>17</u></b>
<b><u>CHAPTER 1 – INTRODUCTION</u></b>	<b><u>22</u></b>
<b>1.1 LIVER CANCER EPIDEMIOLOGY</b>	<b>22</b>
1.1.1 HBV-INDUCED LIVER CANCER	22
1.1.2 HBV TRANSMISSION	23
1.1.3 HBV DIAGNOSIS	23
1.2 HBV INFECTION THERAPY	26
1.2.1 PREVENTION	26
1.2.2 ANTIVIRAL THERAPY	26
1.2.3 NEW TREATMENT STRATEGIES	27
<b>1.3 HBV EPIDEMIOLOGY</b>	<b>27</b>
1.3.1 HBV LIFE CYCLES	28
1.3.2 HBV GENOTYPES	29
1.3.3 HBV GENOME	31
1.3.4 FREQUENTLY MUTATED GENES IN HBV-INDUCED HCC	38
<b>1.4 SLEEPING BEAUTY TRANSPOSON SYSTEM</b>	<b>39</b>
<b>1.5 HYDRODYNAMIC TAIL VEIN INJECTION</b>	<b>40</b>
<b>1.6 PROJECT AIMS</b>	<b>41</b>
<b><u>CHAPTER 2 – METHODOLOGY</u></b>	<b><u>43</u></b>
<b>2.1 FAH-DEFICIENT/ROSA26-SB TRANSPOSASE TRANSGENIC MOUSE MODEL</b>	<b>43</b>
<b>2.2 PLASMID CONSTRUCTION</b>	<b>44</b>
<b>2.3 HYDRODYNAMIC TAIL VEIN INJECTION</b>	<b>46</b>

<b>2.4 LIVER TUMOR ANALYSES</b>	<b>47</b>
<b>2.5 HISTOLOGICAL ANALYSES</b>	<b>47</b>
<b>2.6 IMMUNOHISTOCHEMICAL (IHC) ANALYSES</b>	<b>47</b>
<b>2.6 SEMI-QUANTITATIVE REVERSE-TRANSCRIPTION POLYMERASE CHAIN REACTION (RT-PCR)</b>	<b>48</b>
<b>2.7 QUANTITATIVE PCR</b>	<b>49</b>
<b>2.8 WESTERN BLOTTING</b>	<b>50</b>
<b>2.9 SERUM METABOLITE ANALYSES</b>	<b>50</b>
<b>2.10 STATISTICAL ANALYSIS AND FIGURES ICONS</b>	<b>52</b>
<b><u>CHAPTER 3 - RESULTS</u></b>	<b><u>53</u></b>
<b>3.1 DIVERGENT EFFECT ON TUMOR BURDEN BY K130M/V131I MUTANT AND WILD-TYPE OF VARIOUS HBX GENOTYPES</b>	<b>53</b>
<b>3.2 HISTOPATHOLOGICAL PHENOTYPES IN HBX INJECTED ANIMALS</b>	<b>56</b>
<b>3.3 EXPRESSION OF TRANSGENES IN HBX INJECTED LIVER</b>	<b>58</b>
<b>3.4 INCREASED AKT AND CTNNB1 PROTEIN LEVELS IN HBX INJECTED MICE</b>	<b>61</b>
<b>3.5 RNA-SEQ REVEALED CRUCIAL ROLES OF METABOLISM REPROGRAMMING IN HBX INJECTED MICE</b>	<b>67</b>
3.5.1 RNA SEQUENCING RESULT OF HBX GENOTYPE A	69
3.5.2 RNA SEQUENCING RESULT OF HBX GENOTYPE B	75
3.5.3 KEGG PATHWAYS OF HBX GENOTYPE C	86
3.5.4 KEGG PATHWAYS OF HBX GENOTYPE D	99
3.5.5 LOW GENETIC DIFFERENCE BETWEEN NORMAL TISSUES OF K130M/V131I MUTANT AND WILD-TYPE VARIANTS OF VARIOUS HBX GENOTYPES	115
3.5.6 <i>ARHGAP27</i> AND <i>PAK6</i> WERE COMMONLY UP-REGULATED IN THE TUMORS OF GENOTYPES A, C AND D OF HBX WILD-TYPE GENE	117
3.5.7 <i>IGF2</i> WAS COMMONLY UP-REGULATED IN THE TUMORS OF GENOTYPES B, C AND D OF HBX MUTANT GENE	121
3.5.8 BIOLOGICAL ROLES OF THE COMMON GENES	124
3.5.9 ARACHIDONIC ACID METABOLISM AND HBX-INDUCED HCC	125
<b><u>CHAPTER 4 - DISCUSSION</u></b>	<b><u>127</u></b>
<b>4.1 HBX GENOTYPE A</b>	<b>127</b>
<b>4.2 HBX GENOTYPE B</b>	<b>129</b>

<b>4.3 HBx GENOTYPE C</b>	<b>134</b>
<b>4.4 HBx GENOTYPE D</b>	<b>136</b>
<b>4.5 ARHGAP27 AND PAK6 WERE COMMONLY UP-REGULATED IN THE TUMORS OF GENOTYPES A, C AND D OF HBx WILD-TYPE GENE</b>	<b>139</b>
<b>4.6 IGF2 WAS COMMONLY UP-REGULATED IN THE TUMORS OF GENOTYPES B, C AND D OF HBx MUTANT GENE</b>	<b>140</b>
<b>4.7 CONTRIBUTIONS OF THE STUDY AND FUTURE DIRECTIONS</b>	<b>142</b>
<b><u>CHAPTER 5 – CONCLUSION</u></b>	<b><u>145</u></b>
<b><u>REFERENCES</u></b>	<b><u>148</u></b>

## List of Figures

<b>Figure 1  Types of liver cancer.</b> .....	23
<b>Figure 2  Diagnosis for HBV infection.</b> .....	25
<b>Figure 3  HBV life cycle.</b> .....	29
<b>Figure 4  Geographical distribution of various HBV genotypes.</b> .....	30
<b>Figure 5  Schematic HBV genome.</b> .....	32
<b>Figure 6  Substitution mutation hot spots in MHR-S region of HBsAg.</b> .....	33
<b>Figure 7  Deletion mutations in HBsAg.</b> .....	34
<b>Figure 8  K130M/V131I dual substitution mutation in HBx.</b> .....	37
<b>Figure 9  Sleeping Beauty Transposon System.</b> .....	40
<b>Figure 10  Fumarylacetoacetate hydrolase (Fah)-deficient/SB knock-in transgenic mouse model.</b> .....	43
<b>Figure 11  Plasmid construction.</b> .....	45
<b>Figure 12  Hydrodynamic injection time line.</b> .....	46
<b>Figure 13  Isolated livers, number of tumor nodules and liver-to-whole body weight ratio of each experimental groups.</b> .....	55
<b>Figure 14  Histopathology of livers from HBx injected experimental animals.</b> ..	57
<b>Figure 15  Expression of transgenes in HBx injected animals.</b> .....	60
<b>Figure 16  Representative IHC stained images of experimental animals using anti-pAKT (S473) and anti-beta-Catenin (CTNNB1) primary antibodies.</b> 63	
<b>Figure 17  Representative Western blot and qPCR of experimental animals.</b> ..	67
<b>Figure 18  Differentially expressed genes (DEGs) identified in HBx-A injected animal groups.</b> .....	69
<b>Figure 19  RNA-seq result of HBx-A mutant and wild-type injected animals.</b> .	73
<b>Figure 20  Differentially expressed genes (DEGs) identified in HBx-B injected animal groups.</b> .....	75
<b>Figure 21  RNA-seq result of normal tissues of HBx-B mutant and wild-type injected animals.</b> .....	79
<b>Figure 22  RNA-seq result of normal and tumor tissues of HBx-B mutant injected animals.</b> .....	82
<b>Figure 23  Serum metabolites of HBx-B/shp53 injected animals.</b> .....	84

<b>Figure 24  Differentially expressed genes (DEGs) identified in HBx-C injected animal groups.....</b>	<b>86</b>
<b>Figure 25  RNA-seq result of normal tissues of HBx-C mutant and wild-type injected animals.....</b>	<b>89</b>
<b>Figure 26  RNA-seq result of normal and tumor tissues of HBx-C wild-type (WT) injected animals.....</b>	<b>92</b>
<b>Figure 27  RNA-seq result of normal and tumor tissues of HBx-C mutant (Mut) injected animals.....</b>	<b>95</b>
<b>Figure 28  RNA-seq result of tumor tissues of HBx-C mutant (Mut) and wild-type (WT) injected animals.....</b>	<b>98</b>
<b>Figure 29  Differentially expressed genes (DEGs) identified in HBx-D injected animal groups.....</b>	<b>99</b>
<b>Figure 30  RNA-seq result of normal tissues of HBx-D mutant (Mut) and wild-type (WT) injected animals.....</b>	<b>104</b>
<b>Figure 31  RNA-seq result of normal and tumor tissues of HBx-D wild-type (WT) injected animals.....</b>	<b>108</b>
<b>Figure 32  RNA-seq result of normal and tumor tissues of HBx-D mutant (Mut) injected animals.....</b>	<b>111</b>
<b>Figure 33  RNA-seq result of tumor tissues of HBx-D mutant (Mut) and wild-type (WT) injected animals.....</b>	<b>113</b>
<b>Figure 34  Combinatorial analyses on DEGs identified from comparing the RNA expression profile of normal tissues between mutant (Mut) and wild-type (WT) of HBx genotype A, B, C and D. ....</b>	<b>116</b>
<b>Figure 35  Combinatorial analyses on DEGs identified from comparing the RNA expression profile of tumor induced by wild-type (WT) HBx gene to its corresponding normal tissues in the same genotype. ....</b>	<b>118</b>
<b>Figure 36  The mRNA expression level of Pak6 in animals injected with genotype A, B, C and D of HBx-WT variant by qPCR.....</b>	<b>119</b>
<b>Figure 37  The mRNA expression level of Arhgap27 in animals injected with genotype A, B, C and D of HBx-WT variant by qPCR.....</b>	<b>120</b>
<b>Figure 38  Combinatorial analyses on DEGs identified from comparing the RNA expression profile of tumor induced by mutant (Mut) HBx gene to its corresponding normal tissues in the same genotype. ....</b>	<b>122</b>

<b>Figure 39  The mRNA expression level of Igf2 in animals injected with genotype A, B, C and D of HBx-WT variant by qPCR. ....</b>	<b>123</b>
<b>Figure 40  Expression level of IGF2 in HBV-positive and HBV-negative human biopsy samples.....</b>	<b>124</b>
<b>Figure 41  Combinatorial analyses on common DEGs found in wild-type (WT) and mutant (Mut) tumor identified in Figure 35 and 36. ....</b>	<b>125</b>
<b>Figure 42  Abundance of metabolites in arachidonic acid metabolism pathway. ....</b>	<b>126</b>
<b>Figure 43  Proposed schematic pathways involved in disease progression by HBx-A gene. ....</b>	<b>129</b>
<b>Figure 44  Proposed schematic pathways involved in disease progression by HBx-B gene.....</b>	<b>133</b>
<b>Figure 45  Proposed schematic pathways involved in disease progression by HBx-C gene. ....</b>	<b>136</b>
<b>Figure 46  Proposed schematic pathways involved in disease progression by HBx-D gene. ....</b>	<b>138</b>
<b>Figure 47  Proposed schematic genetic pathways involved in disease progression by HBx gene. ....</b>	<b>141</b>
<b>Figure 48  Survival rate of HBx expressing cell lines under different concentrations of AKT protein kinase inhibitor (AZD5363).....</b>	<b>144</b>
<b>Figure 49  Summarized proposed schematic pathways involved in disease progression by HBx gene. ....</b>	<b>146</b>

## **List of Tables**

**Table 1| Prevention and treatments for HBV infection.**

**Table 2| Primers for PCR genotyping.**

**Table 3| Antibodies for immunohistochemistry (IHC) staining.**

**Table 4| Primers for RT-PCR.**

**Table 5| Primers for qPCR.**

**Table 6| List of RNA samples for RNA sequencing.**

**Table 7| Expression level of genes in schematic genetic pathways induced by HBx expression.**

## Abbreviations

HBV	Hepatitis B virus
HCC	Hepatocellular carcinoma
<i>SB</i>	Sleeping Beauty
<i>Fah</i>	Fumarylacetoacetate hydrolase
<i>Trp53</i>	Transformation related protein
AKT	RAC-alpha serine/threonine-protein kinase
PI3K	Phosphatidylinositol 3-kinase
FOXO1	Forkhead box protein O1
FHCC	Fibrolamellar HCC
HCV	Hepatitis C virus
AFP	Alpha-fetoprotein
ALT	Alanine aminotransferase
AST	Aspartate aminotransferase
ALP	Alkaline phosphatase
CHB	Chronic hepatitis B
RT-PCR	Real-time polymerase chain reaction
PEG	Pegylated
IFN	Interferon
NAs	Nucleos(t)ide analogues
TAF	Tenofovir alafenamide fumarate
cccDNA	Covalently closed circular DNA
L	Large
M	Middle
S	Small
NTCP	Sodium taurocholate cotransporting polypeptide
mkNTCP	Macaca fascicularis NTCP
rcDNA	Relaxed circular DNA
pgRNA	Pregenomic RNA
sgRNA	Subgenomic RNA
ORFs	Open reading frame
HBcAg	Hepatitis core protein
HBeAg	Hepatitis B e Antigen

HBx	Hepatitis X protein
MHR	Major hydrophilic region
ROSs	Reactive oxygen species
NF- $\kappa$ B	Nuclear factor-kappa B
mTOR	Mammalian target of rapamycin
PTGS2	Prostaglandin-endoperoxide synthase 2
VEGF	Vascular endothelial growth factor
DNMT	DNA (cytosine-5-)-methyltransferase
CpG	Cytosine-guanine dinucleotide
<i>CDKN2A</i>	Cyclin dependent kinase inhibitor 2A
<i>CDH1</i>	Cadherin 1, type 1, E-cadherin (epithelial)
<i>RB1</i>	Retinoblastoma 1
<i>TP53</i>	Tumor protein 53
<i>AXIN1</i>	Axin 1
HIF1A	Hypoxia inducible factor 1, alpha subunit (basic helix-loop-helix transcription factor)
<i>CTNNB1</i>	Catenin (cadherin-associated protein), beta 1
WNT	Wingless-type MMTV integration site family
BCP	Basal Core Promotor
<i>TERT</i>	Telomerase reverse transcriptase
<i>ARIN1A</i>	AT rich interactive domain 1A (SWI-like)
GOI	gene-of-interest
IR	Inverted repeat
DR	Direct repeat
NTBC	2-(2-nitro-4-trifluoromethylbenzoyl)-1,3-cyclohexanedione
Mut	Mutant
WT	Wild-type
PHI	Post-hydrodynamic injection
PBS	Phosphate buffered saline
H&E	Hematoxylin-eosin
IHC	Immunohistochemical
Actb/ ACTB	Actin, beta

qPCR	Quantitative PCR
Myc	Myelocytomatosis oncogene
Ccnd1	Cyclin D1
UPLC-Orbitrap-MS	Ultra-Performance Liquid Chromatography-Orbitrap-Mass spectroscopy
QC	Quality control
H-ESI	Heated electrospray ionization
PLS-DA	Partial least squares-discriminant analysis
SD	Standard deviation
Gfp	Green fluorescent protein
DEG	Differentially expressed gene
KEGG	Kyoto Encyclopedia of Genes and Genomes
<i>Mup12</i>	Major urinary protein 12
<i>Susd4</i>	Sushi domain containing 4
Eda	Ectodysplasin-A
<i>Gm5779</i>	Ribosomal protein, large, P0 pseudogene
9,10-DiHOME	9,10-dihydroxy-12Z-octadecenoic acid
12,13-DiHOME	12,13-dihydroxy-9Z-octadecenoic acid
Cyp2C	Cytochrome P450 family 2 subfamily C
TCA	taurocholate
TCDCA	taurochenodeoxycholate
THDCA	taurohyodeoxycholate
TUDCA	tauroursodeoxycholate
BAs	Bile acids
TRP	transient receptor potential
ECM	Extracellular matrix
<i>Styk1</i>	Serine/threonine/tyrosine kinase 1
<i>Lrtm1</i>	Leucine-rich repeats and transmembrane domains 1
<i>Nat8f3</i>	N-acetyltransferase 8 (GCN5-related) family member 3
<i>Csrp3</i>	Cysteine and glycine-rich protein 3
<i>Slc7a1</i>	Solute carrier family 7 (cationic amino acid transporter), member 1
<i>Stmn1</i>	stathmin

<i>Cdc25a</i>	M-phase inducer phosphatase 1
<i>Cidea</i>	Cell death-inducing DNA fragment factor, alpha subunit-like effector A
<i>Tuba8</i>	Tubulin, alpha 8
<i>Gab1</i>	Growth factor receptor bound protein 2-associated protein 1
<i>Igf2</i>	Insulin-like growth factor 2
<i>Srp54b</i>	Signal recognition particle 54B
<i>Ugt1a6a</i>	UDP glucuronosyltransferase 1 family, polypeptide A6A
<i>Eif5b</i>	Eukaryotic translation initiation factor 5B
<i>Ccnb1ip1</i>	Cyclin B1 interacting protein 1
<i>Gm6710</i>	Predicted gene 6710
<i>Zfp820</i>	Zinc finger protein 820
<i>Xlr3a</i>	X-linked lymphocyte-regulated 3A
<i>Fam47e</i>	Family with sequence similarity 47, member E
<i>Mup14</i>	Major urinary protein 14
<i>Arhgap27</i>	Rho GTPase activating protein 27
<i>Pak6</i>	p21 (RAC1) activated kinase 6
<i>Bex1</i>	Brain expressed X-linked 1
<i>Fgd3</i>	FYVE, RhoGEF and PH domain containing 3
<i>Psca</i>	Prostate stem cell antigen
<i>Moap1</i>	Modulator of apoptosis 1
<i>Serpinb6b</i>	Serine (or cysteine) peptidase inhibitor, clade B, member 6b
<i>Spink1</i>	Serine peptidase inhibitor, Kazal type 1
GO	Gene Ontology
<i>Src</i>	Rous sarcoma oncogene
<i>Shc2</i>	(Src homology 2 domain containing) transforming protein 2
<i>Ptgds</i>	Prostaglandin D2 synthase
AA	Arachidonic acid
PGD <sub>2</sub>	Prostaglandin D2
LTB <sub>4</sub>	Leukotriene B <sub>4</sub>

Alox12	Arachidonate 12-lipoxygenase
Cyp4f15	Cytochrome P450, family 4, subfamily f, polypeptide 15
PLA2G	Secretory phospholipase A2
IGF1R	Insulin-like growth factor 1 receptor
EGF	Epidermal growth factor
Rho	Ras homologous
RhoGAP	Rho GTPase-activating protein
IR-A	Insulin receptor isoform A
<i>Diaph1</i>	Diaphanous 1
<i>Tmem117</i>	Transmembrane protein 117
ER	Endoplasmic reticulum
IGFBP	IGF binding protein
IGF2BP/IMP	IGF2 mRNA binding protein

## **Chapter 1 – Introduction**

### ***1.1 Liver cancer epidemiology***

#### **1.1.1 HBV-induced liver cancer**

Liver cancer is the second most common cause of cancer death around the world in 2015 (1). There are 5 types of liver cancer classified by the cell types that become cancerous, include hepatocellular carcinoma (HCC), fibrolamellar HCC (FHCC), cholangiocarcinoma, angiosarcoma and secondary liver cancer (**Figure 1**). HCC is derived from hepatocytes and accounts for more than 75% of liver cancer cases, with hepatitis B virus (HBV) infection being the leading cause of HCC (2). FHCC is a rare type of HCC which accounts for less than 1% of liver cancer cases and 95% of FHCC cases is not related to hepatitis or cirrhosis (3, 4). Cholangiocarcinoma is a type of intrahepatic bile duct cancer and accounts for 10-20% of liver cancer cases (5, 6). Angiosarcoma begins in the blood vessels of liver and accounts for about 1% of liver cancer cases (7). Secondary liver cancer, also known as liver metastasis, is the cancer that spreads from other parts of body to liver. Most liver metastasis originates from colon or colorectal cancer and more than 50% of patients who diagnosed with colorectal cancer had developed secondary liver cancer (8). Major risk factors for liver cancer include HBV and hepatitis C virus (HCV) infections, alcoholic consumption and non-alcoholic liver disease, aflatoxin exposure, tryosinemia and hemochromatosis. Apart from exposing to difference risk factors, liver cancer prevalence is also varied by age, gender and geographic regions. HCC is a gender bias disease; males are about three times more susceptible than the females to the disease in terms of incidence (12.1 hundred thousand males to 4.2 hundred thousand females in United States) and mortality (9.4 hundred thousand males to 3.8 hundred thousand females in United States) (9). Overall five-year survival rate for liver and intrahepatic bile duct cancer is 18% (9).

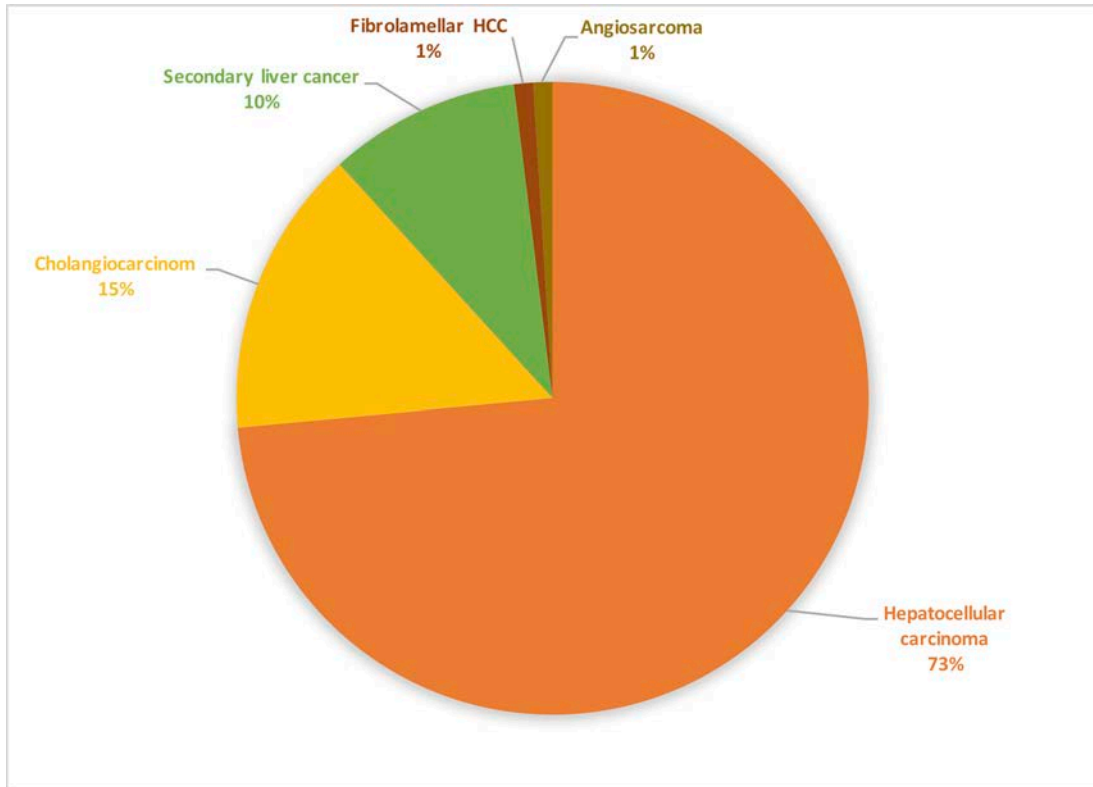


**Figure 1| Types of liver cancer.** Different types of liver cancer are classified by the types of cell that become cancerous. Hepatocellular carcinoma (HCC) is derived from hepatocellular cells. Cholangiocarcinoma is a type of intrahepatic bile duct cancer. Fibrolamellar HCC (FHCC) is the eosinophilic HCC with lamellar fibrosis. Angiosarcoma begins in the blood vessels of liver. Secondary liver cancer, also known as liver metastasis. The most common primary liver cancer is hepatocellular carcinoma (HCC).

### 1.1.2 HBV transmission

HBV is transmitted through the direct interaction with blood and body fluids of infected person. Adulthood HBV infection rarely leads to chronic hepatitis and only accounts for 5% of liver cancer cases (10). Perinatal transmission is the major path of HBV infection in many parts of the world, especially in China and South-East Asia, where HBV can be transmitted to infants at the time of, or shortly after birth (10).

### 1.1.3 HBV diagnosis

HBV infection can be diagnosed by testing viral components levels such as HBsAg, HBeAg, concentration of HBV DNA in serum; liver specific enzymes levels such as alpha-fetoprotein (AFP), alanine aminotransferase (ALT), aspartate aminotransferase

(AST), alkaline phosphatase (ALP), serum bilirubin, albumin, and prothrombin; and liver biopsy (**Figure 2**).

#### Serological markers

HBsAg persists for more than 6 months is diagnosed as chronic hepatitis B (CHB). Inactive HBsAg carriers are differentiated from active HBsAg carriers by quantitative HBsAg level (11). Positive HBeAg in CHB patients indicates HBV replication is active, while with the presence of anti-HBe, HBeAg level will decrease and ALT level will become normal, then no treatment is needed. However, HBeAg level might not thoroughly represent the disease condition as active HBV replication can occur in some HBeAg negative patients due to mutation of pre-core gene or different variants of HBV (10).

#### Virological detection - Serum HBV DNA concentration

HBV DNA concentration in serum of infected patients can be detected by real-time polymerase chain reaction (RT-PCR). The HBV DNA concentration is correlated with disease progression and are used to differentiate active HBeAg-negative disease from inactive chronic infection (12, 13). Measurement of serum HBV DNA concentration can be used to monitor the treatment efficacy and to discover treatment resistant variants.

#### Liver enzymes:

Measuring serum level of ALT, AST, albumin, bilirubin, platelet count and prothrombin time can be used to determine cirrhosis development. Since the serum level of aminotransferases can vary with time, AST/ALT ratio is usually used to monitor liver disease progression. Under normal condition, the concentration of ALT is higher than that of AST, resulting in low AST/ALT ratio. However, under cirrhosis progression, the AST/ALT ratio will be reversed. Additionally, a progressive decline in serum albumin concentrations, rise in bilirubin and prolongation of the prothrombin time are characteristic indicators for cirrhosis development.

#### Liver biopsy:

Liver biopsy is used to assess the degree of necro-inflammation and fibrosis. However, biopsy has its limitations, such as the risks of bleeding and pneumothorax, subjectivity in reporting, high costs, sampling error, discomfort to the patient, and the need for training and infrastructure in low- and middle-income countries.

### Non-invasive tests

Non-invasive tests are performed by testing the serum markers for fibrosis, for example, APRI and FIB-4. Commercial markers such as FibroTest and transient elastography (FibroScan) are established to assess advanced fibrosis (14-16).

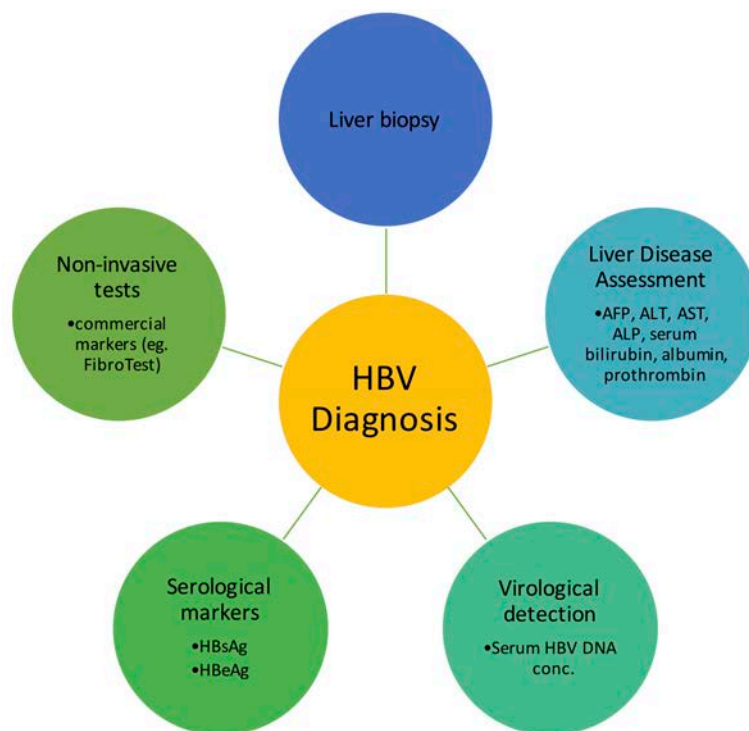


**Figure 2| Diagnosis for HBV infection.** HBV infection can be diagnosed with different tests, including testing viral component levels such as HBsAg, HBeAg, HBV DNA concentration in serum; liver specific enzymes levels such as AFP, ALT, AST, ALP, serum bilirubin, albumin, and prothrombin; and liver biopsy.

## **1.2 HBV infection therapy**

### **1.2.1 Prevention**

HBV infection can be prevented by vaccination, with HBV vaccines derived from recombinant DNA being established for more than two decades (10). A full HBV vaccination contains three doses. New-born who receives HBV vaccine within 24 hours after birth acquires 90-95% effective prevention of infection and reduces HBV transmission after injection of the other two doses (**Table 1**). The implementation of the HBV vaccination scheme has resulted in a drastic decrease in CHB prevalence. However, poor response to HBV vaccine has been diagnosed in a small proportion of vaccinated children (5-10%) and these children are susceptible to HBV infection later in adulthood (10).

### **1.2.2 Antiviral therapy**

Even though vaccination can prevent HBV infection, treating CHB patients at high risk of progression is still the ultimate goal to increase the survival rate associated with CHB. As time goes by, treatment outcomes for CHB patients have improved, from conventional to pegylated (PEG) interferon (IFN), then to nucleos(t)ide analogue (NAs). Seven antiviral agents: adefovir, entecavir, lamivudine, emtricitabine, telbivudine, tenofovir, and PEG-IFN, have been shown to delay cirrhosis progression, reduced risk of HCC and improved long-term survival. In general, all NAs target the HBV polymerase to prevent its replication. Adefovir inhibits the activity of reverse transcriptase; lamivudine, emtricitabine and tenofovir inhibit the synthesis of the viral (-) strand DNA; and entecavir inhibits HBV replication (10). These NAs have different action mechanisms, inhibitory capacity, pharmacokinetics, and resistance patterns (17). Although NAs can prevent the replication of HBV, they cannot cure the disease or clear HBsAg (**Table 1**).

Comparing NA therapy to IFN, NA has fewer side-effects and it can be administered orally in a “one-pill-a-day” manner, while IFN has its advantages of low resistance rate and effective clearance of HBeAg and HBsAg. However, less than 50% of CHB patients shown response to IFN treatment. Injection administration, common side-effects, as well as high-costs of IFN make it less favorable for HBV treatment (10) (**Table 1**).

### 1.2.3 New treatment strategies

Recently, a new prodrug of tenofovir - tenofovir alafenamide fumarate (TAF) has been established. It is an orally administered drug with less toxic effect, reduced dosage and improved delivery of active diphosphate metabolite and nucleotide into lymphoid cells and hepatocytes (18, 19). Moreover, this agent can eliminate all replicative forms of HBV, including covalently closed circular DNA (cccDNA) more effectively. Immunotherapeutic strategies that stimulate HBV-specific adaptive immune responses or innate intrahepatic immunity are also new targets for curative antiviral therapy (**Table 1**).

Approaches	Methods	Efficacy	Drawbacks
Prevention	<ul style="list-style-type: none"> <li>HBV vaccine within 24 hours after birth</li> </ul>	<ul style="list-style-type: none"> <li>90-95% effective prevention</li> </ul>	<ul style="list-style-type: none"> <li>5-10% vaccinated children had poor response to HBV vaccine</li> </ul>
PEG-IFN	<ul style="list-style-type: none"> <li>Delay the progression of cirrhosis</li> <li>Inhibit HBV replication</li> </ul>	<ul style="list-style-type: none"> <li>&lt;50% of CHB patients respond to IFN treatment</li> </ul>	<ul style="list-style-type: none"> <li>Cannot cure the disease or clear HBsAg</li> <li>Administrated by injection</li> <li>Side-effect</li> <li>Expensive</li> </ul>
Nucleos(t)ide analogues (NAs)			<ul style="list-style-type: none"> <li>Cannot cure the disease or clear HBsAg</li> </ul>
Tenofovir alafenamide fumarate (TAF)	<ul style="list-style-type: none"> <li>Prodrug of tenofovir</li> <li>Improved delivery of nucleotide and active diphosphate metabolite</li> <li>Eliminate all HBV replicative forms</li> </ul>		
Immunotherapy	<ul style="list-style-type: none"> <li>Stimulate HBV-specific adaptive immune response</li> <li>Active innate intrahepatic immunity</li> </ul>		

**Table 1| Prevention and treatments for HBV infection.** HBV infection can be prevented by vaccination. PEG-linked IFN and various types of NAs are commonly used to treat HBV infection. However, these antiviral agents were not effective enough to cure the disease. New treatments, such as derivative from NAs and immunotherapy have been established to increase the efficiency of the treatment.

### 1.3 HBV epidemiology

HBV infection is a major health issue globally, accounting for around 45% of HCC cases and 30% of cirrhosis, with around 880 000 people dying from complication associated of CHB (10). Symptoms of acute HBV infection is age-dependent: asymptomatic in most infected children, while, in adult, subclinical hepatitis with

increased transaminases in about 70% of cases and 30% of cases had transient jaundice and flu-like prodromal stage (20). Acute HBV infection are usually transient and self-limiting, yet it can also result in fulminant hepatitis with liver failure (less than 1% of cases) (20).

### 1.3.1 HBV life cycles

HBV is enveloped by three different surface proteins, namely large (L), middle (M), and small (S) surface proteins. Sodium taurocholate cotransporting polypeptide (NTCP), the receptor for HBV and HDV, was discovered in 2012 (21). NTCP is encoded by solute carrier family 10 member 1 (*Slc10a1*). It is a hepatic sodium ion-bile acid symporter and is responsible for the vast majority of sodium-dependent uptake of bile salts from enterohepatic circulation (22). It is mainly expressed in hepatocytes and localized to the sinusoidal plasma membrane (21, 22), and specifically interacts with the L proteins of HBV (21, 23-25), serving as a receptor for HBV. Human HBV affects only human, chimpanzees, and tree shrew (*Tupaia belangeri*), this host restriction phenomenon is highly related to the entrance of HBV into hepatocytes via the receptor (21, 22). NTCP is functionally conserved in mammals but the protein sequences vary amongst species (22). In 2012, Yan *et al.* confirmed the NTCP interacted with the amino acids (aa) 2-48 of the pre-S1 domain of the L protein (21). Yan *et al.* also reported that substitution of five residues from aa 157 to 165 of crab-eating monkey (*Macaca fascicularis*) NTCP (mkNTCP) with the corresponding human NTCP residues (from GRIILSLVP to KGIVISLVL, distinct residues are underlined), the non-functional mkNTCP could be converted to a functional receptor for pre-S1 binding and viral infection (21, 22).

HBV enters hepatocytes in many steps: During the initial phase, HBV enters hepatocytes via the interaction between L surface proteins of HBV and the NTCP receptors on the hepatocytes. Then, the virus is uncoated and the nucleocapsid is released into the cytoplasm and transported to the nucleus by microtubules. Nuclear pore complex that mediated by importins  $\alpha$  and  $\beta$  disintegrates the nucleocapsid and liberates HBV genome into the nucleus (26). In the nucleus, the relaxed circular DNA (rcDNA) is converted to a covalently closed circular DNA (cccDNA) by both viral and cellular enzymes (27). Specifically, the incomplete plus-strand of the rcDNA is

completed by the viral polymerase. Then the viral polymerase and the RNA-primers used for plus-strand DNA synthesis are eliminated by cellular enzymes, and eventually, both DNA strands are ligated by covalent ligation to give cccDNA (27). This cccDNA acts as template for transcription of all viral RNAs, such as the pregenomic RNA (pgRNA) and subgenomic RNAs (sgRNAs) (26) (**Figure 3**).

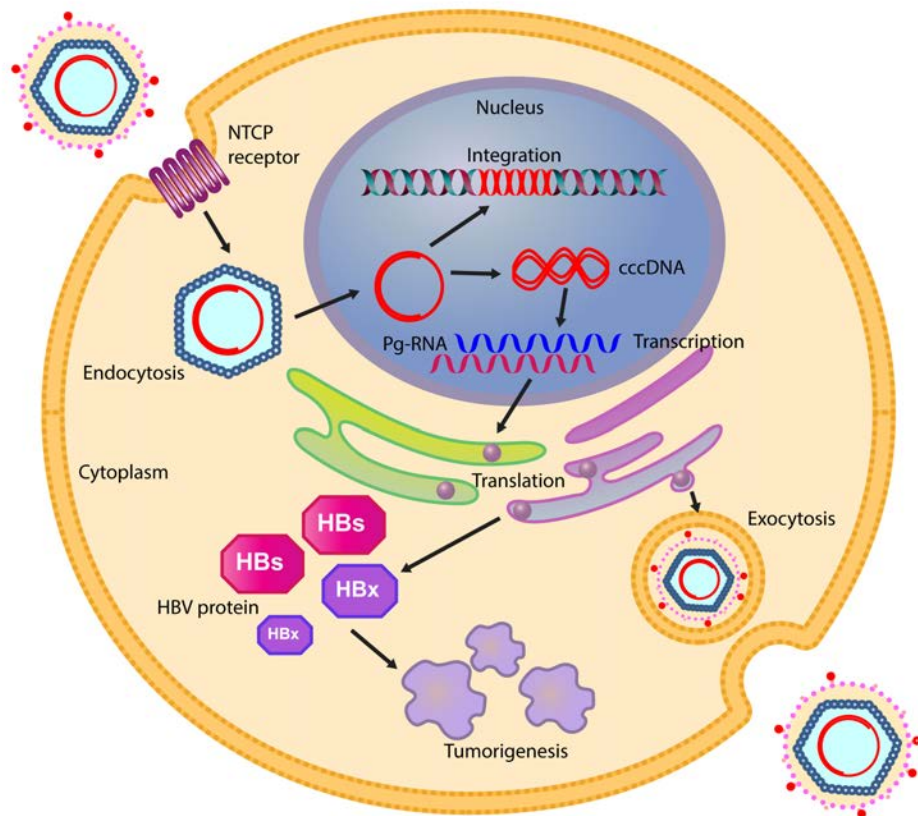


**Figure 3| HBV life cycle.** HBV enters the hepatocyte via the NTCP receptor. After entering the cell, HBV releases the viral genome into the nucleus of the hepatocyte. The HBV DNA can be integrated into the host genome and disrupt expression of the host genes; or converted to cccDNA. Transcription and translation of the cccDNA produces viral proteins for endocapsidation of infectious HBV. Prolong exposure to the viral proteins increases the risk of HCC development.

### 1.3.2 HBV genotypes

The prevalence of HBV infections varies in different geographical regions, with the highest rates in sub-Saharan Africa and East Asia, where 5-10% of the adult

population is chronically infected; while approximately 2-5% of the population in the Middle East and the Indian subcontinent is chronically infected, and less than 1% of the population in the Western European and North America is chronically infected (20). Up to date, there are ten genotypes, from A to J, have been identified and classified by geographical distribution (**Figure 4**). These genotypes have at least 8% nucleotide divergence in the genome (28, 29). Subgenotypes of some HBV genome were classified with more than 4% nucleotide difference (29).

Genotype A is commonly distributed in sub-Saharan Africa, Western Africa, and Northern Europe, including Brazil, Gambia, Nigeria, Haiti, Congo, Rwanda; Genotype B and C are widely spread in Asian countries, such as China, Hong Kong, Taiwan, South Korea, and Philippines, Vietnam and Indonesia; Genotype D is primarily observed in South Africa, Europe, Mediterranean countries and India, includes Iran, Mongolia, Italy, Egypt and Pakistan; Genotype E is distributed in Central African and Saudi Arabia; Genotype F is found in Tunisia, Brazil, Argentina, and Spain; Genotype G is reported in France, Germany, and the United States; Genotype H is observed in Central and South America (30). Genotype I is identified in Vietnam and Laos populations and genotype J is reported in Ryukyu Islands in Japan (30) (**Figure 4**).

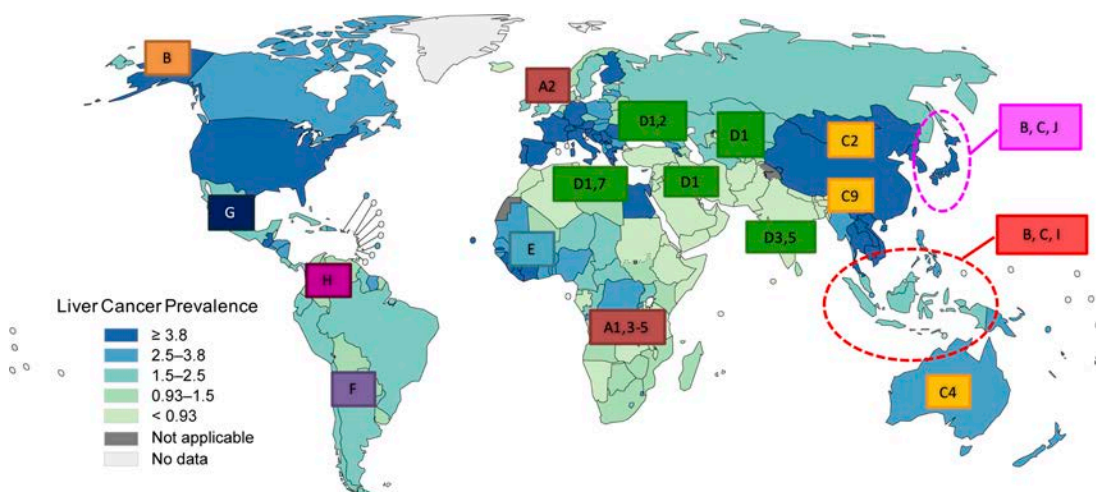


**Figure 4| Geographical distribution of various HBV genotypes.** Eleven HBV genotypes (from A to J) and subtypes (numbers) have been discovered and they are classified according to the geographical distribution. Genotype A is commonly distributed in European countries, sub-Saharan Africa, and Western Africa. Genotype B and C are widely spread in Asian

countries, such as China and Hong Kong. Genotype D is distributed in Mediterranean countries and India.

### 1.3.3 HBV genome

HBV is an enveloped virus with incomplete double-stranded DNA genome of 3.2 kb and is a member of the *hepadnaviridae* family (**Figure 5**). The double-stranded HBV genome contains four open reading frames (ORFs): surface proteins of HBV, namely large (L), middle (M), and small (S) are encoded by PreS1/PreS2/S ORF; hepatitis core protein (HBcAg) and HBeAg, a small molecular weight soluble protein derived from alternative start codon and post-translational modification of the core protein, are encoded by PreC/C ORF (31); POL ORF encodes the viral polymerases with four functional domains, including RNase H, viral DNA polymerase/reverse transcriptase, spacer, and terminal protein; X ORF encodes a multi-functional, non-structural hepatitis X protein (HBx). HBx is a transcriptional trans-activator and can promote HBV replication (32-34) (**Figure 5**). The effects of HBs and HBx protein on tumorigenesis have been widely studied but their molecular mechanisms remain unclear.

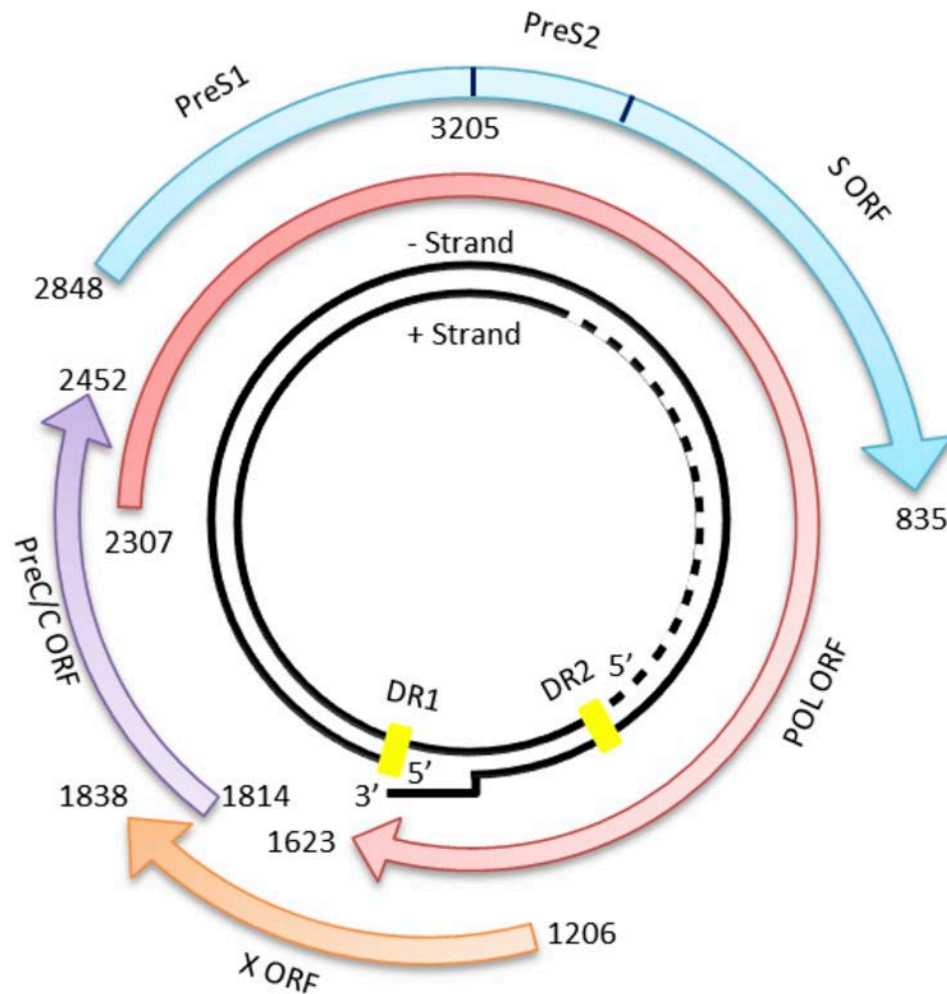


**Figure 5| Schematic HBV genome.** HBV genome is an incomplete double-stranded DNA with four open reading frames (ORFs). PreS1/PreS2/S ORF encodes the three surface proteins of HBV, namely large (L), middle (M), and small (S); PreC/C ORF encodes the hepatitis core protein (HBcAg) and HBeAg; POL ORF encodes the viral polymerases with four functional domains, including RNase H, viral DNA polymerase/reverse transcriptase, spacer, and terminal protein; X ORF encodes a multi-functional HBx protein.

### HBV PreS1/S2/S ORF

The synthesis of L, M and S surface proteins is determined by three individual promoters and start sites. Transcription initiated from the PreS1 promoter produces L surface protein; transcription initiated by the PreS2/S promoter produces M surface protein; while transcription of S ORF produces S surface protein (**Figure 7**). All these surface proteins are known as HBsAg. They have the same carboxyl (C)-terminus but

different amino (N)-terminal extensions: the S protein forms the HBsAg with only 226 amino acid (aa), the M protein has an additional 55 aa extension at its N-terminus, while the L protein has a further 108, 118 or 119 aa extension at its N-terminus, depending on the HBV genotype (35-39). Viral neutralization by either natural or vaccine-induced anti-HBs antibodies is targeting HBsAg (35, 36). Residues 103-173 of the HBsAg is known as the central major hydrophilic region (MHR) and is responsible for immune recognition (35). MHR is structured into five regions, including 3 central loops that held together by disulphide bonds. Loops 2 and 3 for the immunodominant “a” determinant (residues 124-147), which is the major target of HBsAg detection tests and against which most neutralizing antibodies are directed (35, 40) (**Figure 6**). HBsAg is important for activation of immune responses. Small insertions in loop 1 of HBsAg was identified from patients of HBsAg negative in serological test using monoclonal antibody, this suggests that the structure of “a” determinant is affected by any mutations even outside the “a” determinant region (40). Insertional mutation is rare and the most common HBsAg immune escape mutants, also known as “vaccine escape” mutants, are missense mutants that often involve only one residue substitutions (40). Many substitution mutations in “a” determinant had been reported, including I/T126A/N, A128V, Q129H/R, G130N, M133L/T, K141E, D144A/H, and G145R, in which G145R is the most common mutation reported so far (40). In addition, P120S/T is the most common substitution mutation found outside the “a” determinant (40). These immune escape mutants have reduced affinity for monoclonal antibodies against the “a” determinant or are less reactive in commercial HBsAg detection assays (40).

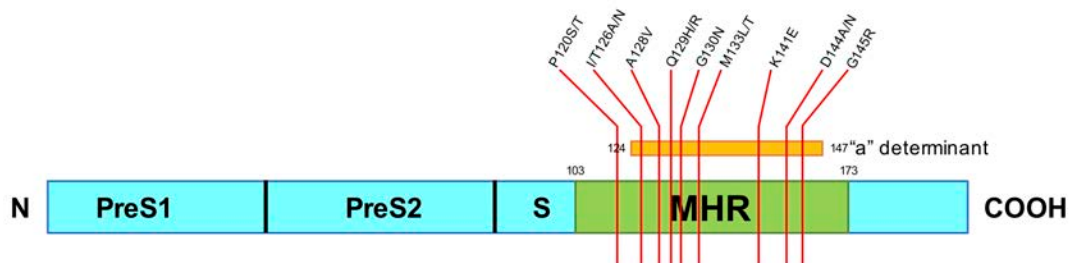


**Figure 6| Substitution mutation hot spots in MHR-S region of HBsAg.** I/T126A/N, A128V, Q129H/R, G130N, M133L/T, K141E, and D144A/H, and G145R substitution mutations

reported in “a” determinant. G145R is the most common mutation reported so far, while P120S/T is the most common substitution mutation found outside the “a” determinant.

The PreS1 and PreS2 regions of HBsAg contain multiple B cell and T cell recognition epitopes, so as to initiate host immune responses. Mutations in these two regions can lead to immune escape, resulting in chronic HBV infection (32, 41). Deletion, insertion and substitution mutations in the PreS1/PreS2/S ORF was reported and found to be closely correlated to HCC tumorigenesis (32, 41). Additionally, deletions in the 3’-end of PreS1 and 5’-end of PreS2 regions are frequently reported in chronic HBV infected patients (38, 41-43) (**Figure 7**). The common deletion mutations can be classified into four categories: start codon deletion at PreS1 or PreS2 regions and internal deletion on PreS1 or PreS2 regions (38, 43). Besides, substitution mutations cause premature termination of gene transcription, resulting in production of truncated HBsAg. Accumulation of truncated HBsAg in the hepatic endoplasmic reticulum increases oxidative stress of hepatocytes and eventually accelerate liver cell damage (38, 43).

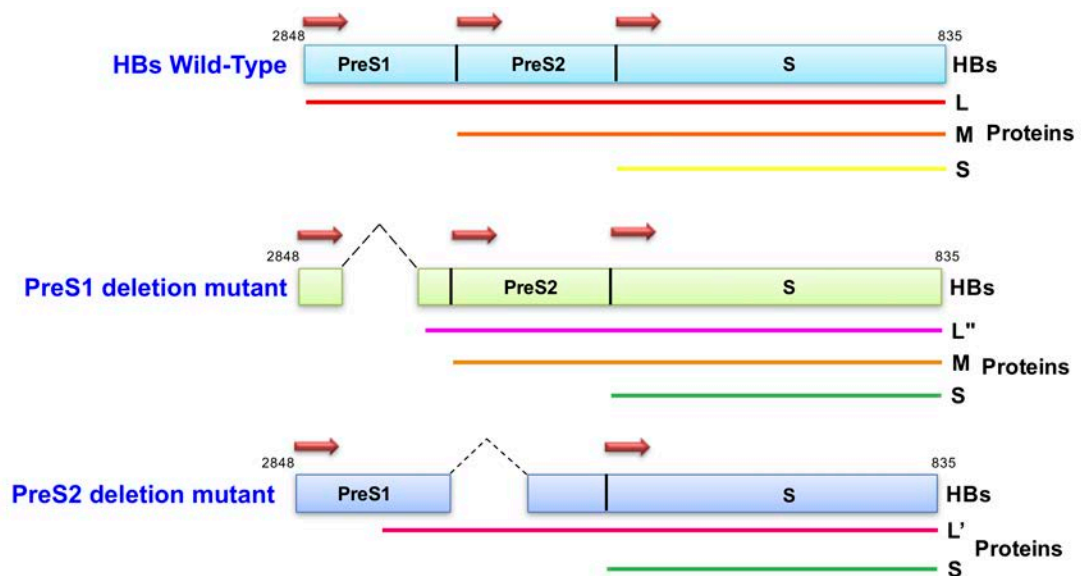


**Figure 7 | Deletion mutations in HBsAg.** Deletions in the PreS1 3’-end and PreS2 5’-end are frequently found in chronic HBV infected patients. Deletion in the 3’-end of PreS1 region produces truncated large protein (L’); and deletion in the 5’-end of PreS2 region produces truncated large protein (L’) and lack the middle protein (M).

PreS1 or PreS2 deletion mutants induce liver tumor formation in three approaches: (1) altering the PreS1-to-PreS2/S mRNA ratio; (2) inducing endoplasmic oxidative stress; and (3) allowing immune escape from host immune system. Deletion in 3'-end of the PreS2 domain and deletion of CCAAT element in the S promoter domain cause transcription reduction of the 2.1 kb PreS2/S mRNA (38). Generally, the CCAAT element is responsible for enhancing transcription of PreS2/S ORF and reducing transcription of PreS1 ORF, therefore, deletion of CCAAT element would reverse the PreS1-to-PreS2/S mRNA ratio. Moreover, reduced transcription of PreS2/S ORF resulting in reduced production of S protein and eliminated production of M protein. Without mutations, L protein is secreted in forms of sub-viral particles or mature virions by complexing with the M and S protein. Therefore, insufficient production of M and S proteins due to deletion mutation at 3'-end of PreS2/S ORF causes accumulation of L protein in hepatic ER creating high oxidative stress environment by generating increased amount of reactive oxygen species (ROSs). These ROSs cause oxidative DNA damage, induce genetic mutations, and ultimately promote HCC progression (38, 44).

In addition, PreS deletion mutants also prevent apoptosis of hepatocytes by activation of the nuclear factor kappa B subunit 1 (NFkB1) and AKT serine/threonine kinase (AKT)/mechanistic target of rapamycin kinase (mTOR) signalling pathways by increasing the prostaglandin-endoperoxide synthase 2 (PTGS2) and vascular endothelial growth factor A (VEGFA) protein production, respectively (38, 44). In addition, evasion of host immunity was reported in PreS2 deletion mutant transfected hepatocytes, due to the mutations in B-cell and T-cell recognition epitopes (b10, t5, t6) and/or reduction in binding affinity of the viral proteins to major histocompatibility complex I molecule (38, 44, 45).

### HBV X ORF

The multi-functional HBx protein consisting 154 aa is encoded by HBx ORF (33, 46). The genetic mechanism(s) by which HBx induces and/or contributes to HCC development is still not well discovered. However, it is suggested that HBx protein participated in hepatocyte transformation in three manners: (1) epigenetic status alteration; (2) genomic instability induction; and (3) signalling pathways modulation

(26, 47).

Changes of epigenetic status in hepatocytes by HBx lead to inactivation of host tumor suppressor genes and/or activation of host oncogenes through induction of DNA methyltransferases (47, 48). Histone hyperacetylation is initiated by binding of HBx to histone acetyltransferase complex and CREB binding protein, resulting in transactivation reactions (26, 46-48). In addition, HBx promotes H3-K4-specific methyltransferase production by up-regulating SET and MYND domain containing gene expression, hence, increasing H3 lysine K4 methylation (48). HBx inhibits expression of tumor suppressor genes via methylation by recruiting the binding of DNA (cytosine-5-)-methyltransferase 1 and 3A (DNMT1 and DNMT3A) onto tumor suppressor genes. In reverse, HBx promotes expression of tumor-promoting genes via demethylation by inhibiting the binding of DNMT3A to promoters of tumor-promoting genes (48). Association of *DNMT3A* on hepatocarcinogenesis has been reported, higher expression level of *DNMT3A* was detected in HCC patients (47). The transcriptional transactivation activity of HBx, includes the up-regulation of *DNMT1* and *DNMT3A*, induces cytosine-guanine dinucleotide (CpG) island methylation at the carbon-5 position of cytosine. Up-regulations of *DNMT1* and *DNMT3A* prevent binding of transcription factors and RNA polymerase II complexes to tumor suppressor genes, such as cyclin-dependent kinase inhibitor 2A (*CDKN2A*) and cadherin 1, type 1, E-cadherin (epithelial) (*CDH1*), resulting in their dysfunction (47, 48). Furthermore, HBx suppresses transcription of tumor suppressor genes by promoting binding of histone deacetylases on them (48).

Apart from epigenetic changes, HBx is also believed to intensify genomic instability. A lot of studies had reported that HBx can inactivate tumor suppressor genes, for example, retinoblastoma 1 (*RBI*), tumor protein p53 (*TP53*), and axin 1 (*AXINI*). HBx inhibits DNA repair by interacting with tumor suppressor proteins, leading to accumulation of mutations and deletions of genome, resulting in genome instability (49-52). HBx also promotes angiogenesis by up-regulating *VEGF* transcription and stabilizing hypoxia inducible factor 1, alpha subunit (basic helix-loop-helix transcription factor) (*HIF1A*) (46). Several *in vivo* research studies have discovered that over-expression of HBx caused up-regulation of catenin (cadherin-associated

protein), beta 1, 88 kDA (*CTNNB1*) in the important canonical wntless-type MMTV integration site family (WNT)/CTNNB1 signalling pathway implicated in hepatocarcinogenesis (46, 53, 54).

Substitution mutation at nucleotide T1753C (I127T aa), A1762T (K130M aa), G1764A (V131I aa) and T1768A (F132Y aa) are the four common mutation sites that have been reported in the HBx ORF (55). The combinatory effects of these mutations have been studied *in vitro* using the human liver cell line (CCL13) where dual-mutation at K130M and V131I had the potential to induce cell proliferation (55, 56) (**Figure 8**). K130M/V131I dual-mutation of HBx gene is overlapped with Basal Core Promoter (BCP), and has been consistently shown to have the highest potential to promote HCC progression (57-60). HBV patients with chronic hepatitis, fulminant hepatitis or HCC are often detected with mutations at K130M/V131I sites and diagnosed as HBeAg negative (60-62). These X protein changes are encoded by nucleotide changes in the BCP region A1762T/G1764A (BCP\_A1762T/G1764A), and have been shown to be associated with reduced synthesis of PreC/C RNA and expression of HBeAg (62), however the effect of the encoded protein changes on the tumorigenic potential of HBx is not well understood. Although several studies have reported the involvement of HBx in HCC development, the differential tumorigenicity of HBx mutations and the genetic mechanism(s) by which HBx induces and/or contributes to HCC development remains ambiguous, and most studies have been performed using transformed liver cell lines such as Huh7.

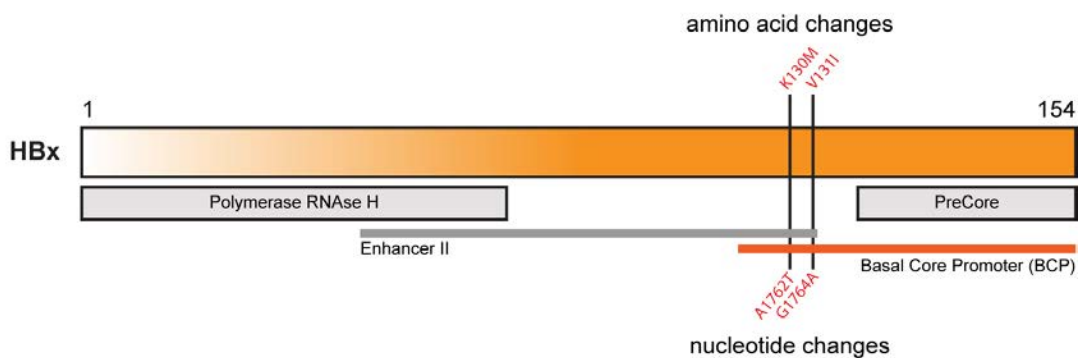


**Figure 8| K130M/V131I dual substitution mutation in HBx.** K130M/V131I dual-point mutations are the most common mutation sites in HBx gene. Its corresponding nucleotide

mutations at A1762T and G1764A sites overlapped with basal core promoter (BCP) resulting in reduced synthesis of PreC/C RNA and hence reduced expression of HBeAg.

C-terminal truncation in HBx was also reported in HBV infected patients. The role of The C-terminus of HBx gene contains the transactivation or co-activation domain in that can transactivate viral and cellular promoters (33). The 52-65 aa and 88-154 aa in the C-terminus of HBx had been shown to be strongly associated with its transactivation activity, cell cycle regulation, and HBx stability in transfected HepG2 and Huh7 cell lines (33, 63, 64). The 3'-end of HBx is often deleted during HBV integration into the host genome, resulting in production of C-terminal truncated HBx protein (65, 66). C-terminal truncated HBx has been consistently detected in tumors of HBV-related HCC patients (65, 67, 68). Moreover, comparing with full-length HBx, C-terminal truncated HBx has higher potential in promoting tumor cell proliferation and metastasis (65, 67, 69). However, the genetic mechanism(s) of how this C-terminal truncated HBx affects the tumorigenicity of HBV still remains unclear.

#### **1.3.4 Frequently mutated genes in HBV-induced HCC**

Recent study had shown that 37% of HBV-positive patients had mutation in promoter of telomerase reverse transcriptase (*TERT*), where the mutation site was consistently located at 124 bp upstream of the *TERT* start codon (70). Moreover, 22% focal amplification of *TERT* is reported in HBV-positive samples (70). Both promoter mutation and focal amplification of *TERT* lead to over-expression of *TERT* in HCC (70). An exome sequencing of HCC tumors had identified at least 30 significant putative HCC driver genes (70, 71). Amongst these putative driver genes, 10% of HCC samples had significant alteration in copy number and somatic mutations of *CTNNB1*, *TP53*, AT rich interactive domain 1A (SWI-like) (*ARID1A*) and *AXIN1* (70, 71). *TP53*, which is frequently mutated in most cancer types, was identified to be associated with HBV-related HCC in numerous studies (54, 70-72), and mutation of *TP53* at R249S site was reported in 16% of the HBV (genotype B)-related HCC cases (72-74).

#### ***1.4 Sleeping Beauty Transposon System***

Transposon systems can be used as genetic tools for both insertional mutagenesis in multiple tissue-types of most mammalian species as forward genetic screens (75-93) and/or validating the tumorigenic role of a specific gene(s) as reverse genetic screens (94, 95). The *Sleeping Beauty (SB)* transposon system is a member of the *Tc1/mariner* transposon superfamily and was genetically reconstructed from the genome of fossil elements in salmonid fish (96). The transposon is mobilized in a “cut-and-paste” manner in the *SB* system. The *SB* system consists of two key components: gene-of-interest (GOI) containing transposon cassette; and transposase. Transposon from the carrier plasmid is excised by the transposase and reintegrated into the host chromosome for long-term expression of the GOI (96) (**Figure 9**). The two ends of the transposon is flanked by the inverted repeat/direct repeat (IR/DR) sequences, which is 225-bp and 30-bp long, respectively (97). Transposition and integration occur upon the expression of both transposon and transposase in the same cell (96). During transposition, two *SB* transposase molecules bind to each end of the IR/DR sequences that bring the two ends together and cleave the transposon, then paste it into host chromosomes at TA-dinucleotide target sites. As part of the host DNA repair mechanism, the TA-dinucleotide site is duplicated after the transposon integration process (94, 96) (**Figure 9**). The mobilization of *SB* transposon is relatively random although there is a propensity for “local hopping” to occur (98-100).

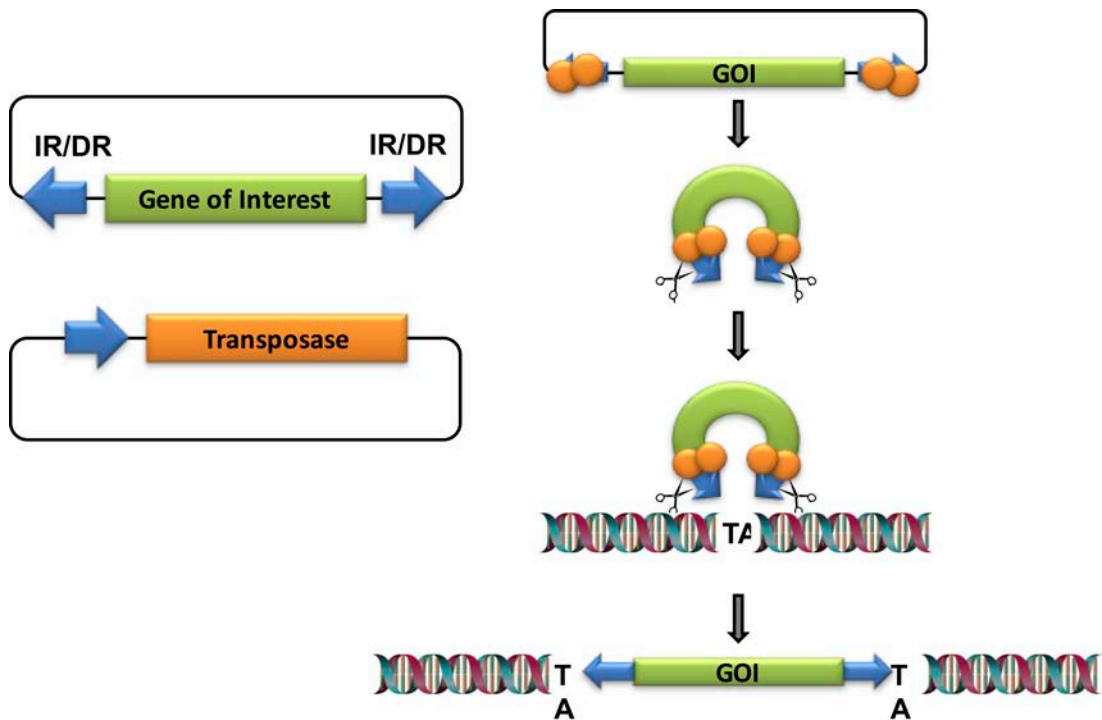


**Figure 9| Sleeping Beauty Transposon System.** The two main components of *Sleeping Beauty* (SB) transposon system are the transposon and the transposase. The transposon is flanked by inverted repeat/direct repeat (IR/DR) sequences, and two transposase molecules bind to each IR/DR sequences, then cut the transposon out and re-integrate it into the host genome at TA-dinucleotides sites.

### 1.5 Hydrodynamic tail vein injection

Delivery of naked plasmid DNA into the liver of the experimental animals can be achieved by hydrodynamic tail vein injection. It is an effective method for gene delivery *in vivo*, about 40% of the hepatocytes can take up the transgene(s) and more than 95% expression of transgene(s) are detected after injection (94). The DNA uptake rationale of hydrodynamic tail vein injection is still not well understood, but it is suggested that injection of high-volume DNA solution rapidly into animal causes over-stretch of myocardial fibres that induces cardiac congestion, resulting in delivery of DNA solution into liver (101). The animal model used in this study is fumarylacetoacetate hydrolase (*Fah*)-deficient mice with *SB* transposase 11 (SB11) gene knocked into the gene trap ROSA 26, Philippe Soriano (*Gt(ROSA)26Sor*) locus (102-104) (**Figure 10**). Lacking FAH in this mouse model causes accumulation of fumarylacetoacetate and succinyl acetone, which are toxic metabolites from tyrosine

catabolism. Therefore, to prevent the mouse from tyrosinemia, 2-(2-nitro-4-trifluoromethylbenzoyl)-1,3-cyclohexanedione (NTBC, Swedish Orphan International AB, Stockholm, Sweden) at final concentration of 6 µg/mL was added to the drinking water. NTBC inhibits the activity of *p*-hydroxylphenylpyruvate-dioxygenase, preventing the production of fumarylacetoacetate and succinyl acetone (102). NTBC water is replaced with normal drinking water after hydrodynamic tail vein injection. At this stage, the *SB* transposases that ubiquitously expressed in this mouse model mobilize the transposon into the mouse hepatocyte genome. Due to the presence of *Fah* cDNA in the transposon, only hepatocytes with stably integrated transposon can survive and repopulate under normal drinking water condition, while the hepatocytes lacking transposon integration will die due to the accumulation of toxic substances. This selective repopulation of transgenic hepatocytes mimics liver disease progression and is widely used to validate candidate genes involved in hepatocellular carcinoma (39, 54, 78, 79, 83, 103, 105, 106). However, wild-type or other transgenic mice can also be used with hydrodynamic delivery of *SB* transposon system for reverse genetic screening in the liver without selective repopulation (105). In addition, hydrodynamic injection has been used for delivery of DNA plasmids to the livers of large mammals, such as dog and swine (107, 108).

### **1.6 Project aims**

Due to the fact that there is no comparison on tumorigenicity amongst different genotypes, lacking effective and curable treatment to HBV infection, therefore, the genetic mechanism(s) of HBV-induced HCC should be clarified, and specific tumor markers for HBV-related HCC are needed. Additionally, as discussed in the previous session, HBV infected host with specific NTCP receptor sequence, so there is a shortage of laboratory animal model for the study of HBV-induced HCC. In this study, we attempted to elucidate the genetic mechanism(s) participated in HBx-induced HCC by expressing HBx gene of four genotypes (A, B, C and D) and each with K130M/V131I mutant and wild-type variants in *Fah*-deficient; *SB11* knock-in mouse model. First aim of this study was to deduce the differences in tumorigenicity between genotypes, then to compare the tumor burden between K130M/V131I mutant and wild-type of HBx gene in the same genotype. Next, we aimed to find out gene(s) and pathway(s) that are involved in tumor progression under expression of HBx. The final

aim of this study is to find out the association of these genes in disease progression in the context of HBx expression.

## Chapter 2 – Methodology

### 2.1 *Fah*-deficient/*Rosa26*-*SB* transposase transgenic mouse model

All animal work was conducted under approved animal welfare protocols of The Chinese University of Hong Kong and The Hong Kong Polytechnic University, HKSAR. Experimental animals with double mutant of fumarylacetoacetate hydrolase (*Fah*)-deficient and *Sleeping Beauty* transposase 11 (SB11) knock-in (*Fah*<sup>-/-</sup>; SB<sup>Tg/+</sup> or *Fah*/SB11) was obtained by breeding *Fah*-deficient mice (*Fah*<sup>-/-</sup>) with SB11 knock-in mice (*Fah*<sup>-/-</sup>; *Rosa26*-SB<sup>Tg/Tg</sup>) (**Figure 10**). All experimental mice were maintained at final concentration of 6 µg/mL 2-(2-nitro-4-trifluoromethylbenzoyl)-1,3-cyclohexanedione (NTBC, Swedish Orphan International AB, Stockholm, Sweden) in the drinking water before injection (102).

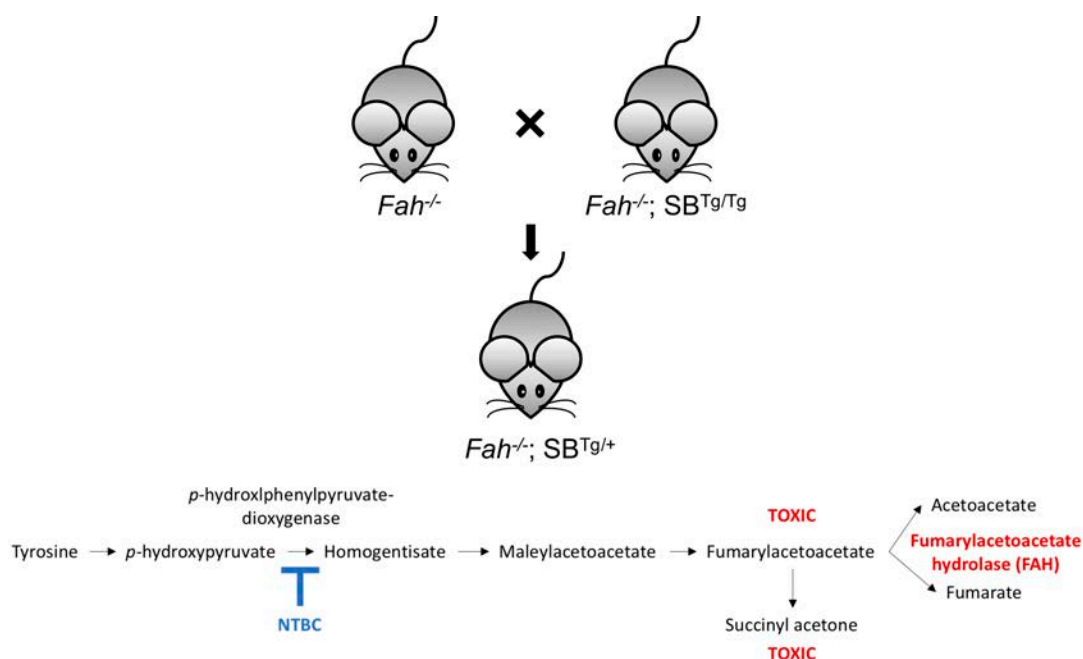


**Figure 10| Fumarylacetoacetate hydrolase (*Fah*)-deficient/SB knock-in transgenic mouse model.** The experimental mouse model (*Fah*<sup>-/-</sup>;SB<sup>Tg/+</sup>) was generated by breeding *Fah*-deficient mouse (*Fah*<sup>-/-</sup>) with *Fah*-deficient/SB knock-in mouse (*Fah*<sup>-/-</sup>;SB<sup>Tg/Tg</sup>). Since the mouse was lacking in FAH production and to prevent accumulation of toxic metabolites from breaking down of tyrosine, NTBC was added to the drinking water at final concentration of 6 µg/mL. NTBC inhibits the activity of *p*-hydroxylphenylpyruvate-dioxygenase, hence stop the tyrosine catabolic pathway.

The genotypes of *Fah*/SB11 transgenic mice were confirmed by extracting genomic DNA from clipped-tail samples. The clipped-tail samples were first dissolved in 500

$\mu$ L tail lysis buffer [10 mM Tris-HCl, 0.5 MEDTA, 1XSSC and 1% SDS] with 5  $\mu$ l Proteinase K at 55°C overnight, then extracted and precipitated with phenol-chloroform and isopropanol. Finally, the genomic DNA pellet was dissolved in sterile TE buffer [10 mM Tris-HCl (pH7.5), 1 mM EDTA (pH8)] and quantified using a Nanodrop spectrophotometer (Thermo Fisher Scientific, Massachusetts, USA). PCR genotyping was performed using 50 ng of genomic DNA as template in a 25  $\mu$ l PCR reaction volume following the GoTaq Green Master Mix protocol (Promega, Wisconsin, USA). PCR primers to confirm the genotype of the transgenic mouse are listed in **Table 2**. PCR conditions were set as follow: initial denaturing of 95°C for 15 min; 35-cycles of denaturing at 95°C for 25 sec, annealing at 55°C for 35 sec and extension at 72°C for 65 sec; followed by a final extension at 72°C for 5 min. PCR products were separated on a 2% agarose gel and genotype determined by the absence or presence of expected amplicons.

Primers	Sequence (5' --> 3')	Amplicon (bp)
<i>Fah</i>	Wild-type forward: CTAGGTCAATGGCTGTTTGG	<i>Fah</i> wild-type: 180 bp; <i>Fah</i> mutant: 240 bp
	Wild-type reverse: GGACATACCAATTTGGCAAC	
	Mutant forward: TAAAATGAGGAAATGCATCG	
<i>SB11</i>	Wild-type forward: CTGTTTTGGAGGCAGGAA	<i>Rosa26</i> wild-type: 420 bp; <i>Rosa26</i> - <i>SB11</i> : 317 bp
	Wild-type reverse: CCCAGATGACTACCTATCCTCCC	
	SB reverse: CTAAAAGGCCTATCACAAAC	

**Table 2| Primers for PCR genotyping of *Fah*/*SB11* transgenic mouse model.** Forward and reverse primers for *Fah* and *SB11* were listed in the above table.

## 2.2 Plasmid construction

The PCR products of K130M/V131I mutant (Mut) and wild-type (WT) variants of HBx genotype A, B, C and D were provided by Dr. Nadia Warner. These HBx genes were introduced into the Gateway entry clone pENTR11 Dual Selection Vector (pENTR11) (Life Technologies Thermo Fisher Scientific) by sticky end joining after enzymatically digesting both the HBx gene and pENTR11 vector with EcoR1 and XbaI to produce pENTR-HBx (**Figure 11A**). The HBx in the entry clone was then introduced into the destination vector (pT2/GD-DEST-EGFP) by LR clonase reaction using Gateway LR clonase II Enzyme mix (Life Technologies Thermo Fisher Scientific) to give the pT2/GD-HBx-EGFP plasmid for injection (**Figure 11A**). A

short-hairpin RNA directed against the *Trp53* gene was also incorporated into a transposon vector (pT2/GD-*shp53*) for stable integration into the mouse hepatocyte genome (54, 78, 79, 103) (**Figure 11A**). All vectors used for hydrodynamic tail vein injections were prepared using EndoFree Plasmid Maxi Kit (Qiagen, Hilden, Germany) following the instruction provided by the manufacturer.

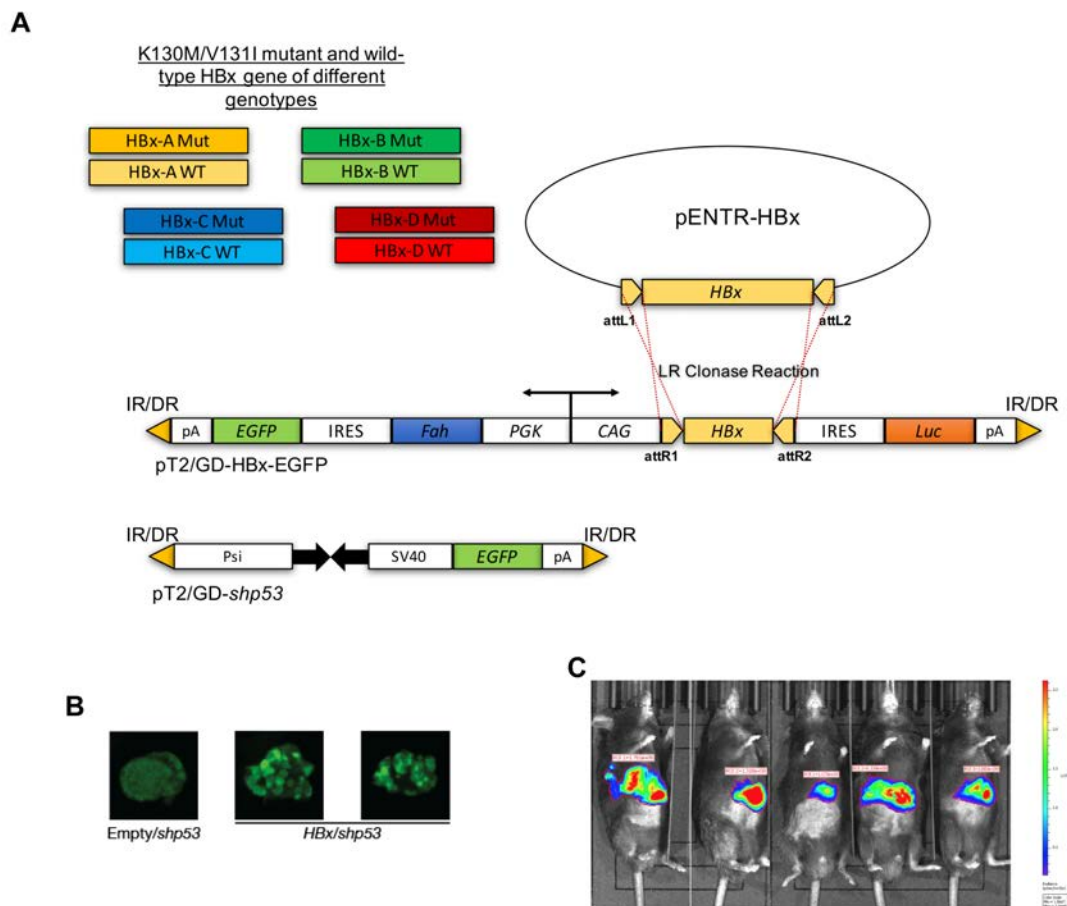


**Figure 11| Plasmid construction.** (A) The expression vector (pT2/GD-HBx-EGFP) was constructed by LR Clonase reaction. An intermediate vector (pENTR-HBx) was first constructed by inserting mutant and wild-type HBx of various genotypes into the pENTR11 dual selection vector individually. Then by LR Clonase reaction, pT2/GD-HBx-EGFP with individual HBx gene at correct position and orientation was generated. (B) EGFP genes in both pT2/GD-HBx-EGFP and pT2/GD-*shp53* vectors allowed bio-illumination of liver after necropsy. (C) Luciferase gene included in the pT2/GD-HBx-EGFP vector allowed for the monitoring of liver repopulation under the supply of luciferin in IVIS imaging system.

### 2.3 Hydrodynamic tail vein injection

Twenty micrograms of each pT2/GD-HBx-EGFP and pT2/GD-*shp53* plasmids were hydrodynamically injected into 45-day old *Fah*/SB11 mice (**Figure 12**). After injection, NTBC water was replaced with normal drinking water. The *Fah* cDNA in the expression vector was co-expressed and allowed selective repopulation of hepatocytes that integrated with the transposon. These mice were allowed to age and sacrificed at around 160-day post-hydrodynamic injection (PHI) (**Figure 12**). Historical controls for pT2/GD-empty-EGFP with pT2/GD-*shp53* were used in this study. Animal live imaging were performed at the Centralised Animal Facilities, The Hong Kong Polytechnic University. Experimental animals were observed for weight changes and *Luciferase* activity using the Xenogen IVIS Imaging System.

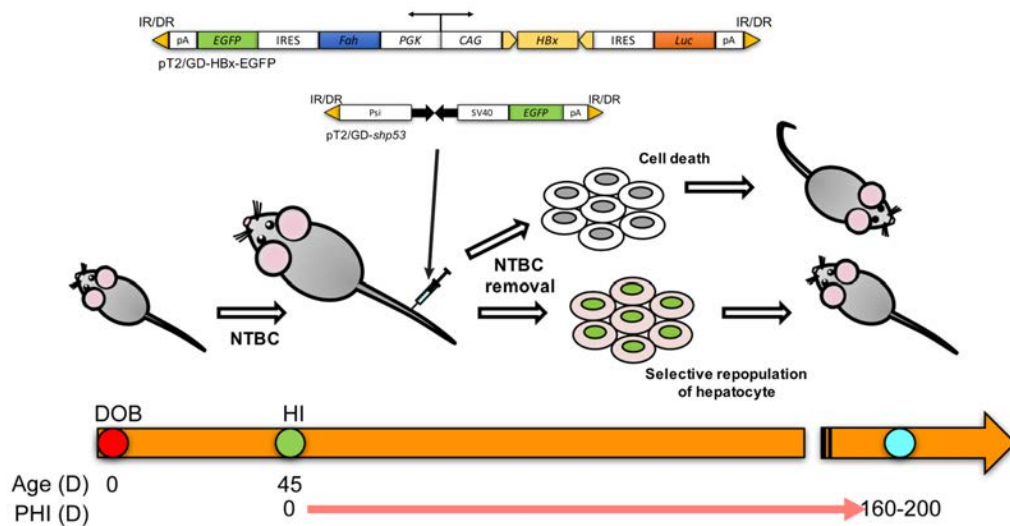


**Figure 12| Hydrodynamic injection time line.** The *Fah*<sup>-/-</sup>;SB<sup>Tg/+</sup> mouse model was treated under NTBC water before injection. At around 45-day old, the mouse was injected with both pT2/GD-HBx-EGFP and pT2/GD-*shp53* vectors by hydrodynamic tail vein injection. After injection, NTBC water was replaced with normal drinking water for the injected mouse and allowed to age. Only hepatocytes transgenic for the pT2/GD-HBx-EGFP vector could successfully repopulate the liver, due to the presence of *Fah* cDNA in the transposon. At about 160-day post-hydrodynamic injection (PHI), the injected mouse was sacrificed, liver and serum were isolated for experimental analyses.

#### ***2.4 Liver tumor analyses***

The whole liver was removed from the euthanized animal, weighed, rinsed, and placed in cold phosphate buffered saline (PBS). The number of liver tumor nodules on rostral and caudal surfaces of all liver lobes was counted and carefully isolated. These isolated tumor nodules were then cut into sections for DNA, RNA and protein extraction using a sterile razor blade. Histology sections were taken for larger tumor nodules. Tissue samples for RNA extraction were kept in 200  $\mu$ L of RNAlater Stabilization Solution (Life Technologies Thermo Fisher Scientific) and stored at -80°C before extraction. DNA extraction was performed as described in the PCR genotyping section. RNA was extracted using Trizol reagent (Life Technologies Thermo Fisher Scientific) following the protocol provided by the manufacturer. Protein was extracted using Qproteome Mammalian Protein Prep Kit (Qiagen) following the protocol provided by the manufacturer.

#### ***2.5 Histological analyses***

Formalin-fixed and paraffin-embedded liver tissues were sectioned at 5 microns using standard microtome (Leica Biosystems, Wetzlar, Germany). These sections were then mounted and heat-fixed onto glass slides at 55°C overnight. These tissue slides were used for hematoxylin-eosin (H&E) staining following standard protocols, and immunohistochemical (IHC) staining as described in the following section. Pathological analyses were performed by board-certified pathologists.

#### ***2.6 Immunohistochemical (IHC) analyses***

Dewaxing and rehydrating of the glass tissue section slides were performed by decreasing ethanol concentration gradually. Antigen epitopes on the tissue sections were unmasked using the citrate-based antigen unmasking solution (Vector Laboratories, California, USA). Endogenous peroxidases were removed by incubating the tissue sections with 3% hydrogen peroxide. Blocking was performed at room temperature using a M.O.M. mouse immunoglobulin-blocking reagent (Vector Laboratories) in a humidified chamber for 1 hour. Tissue sections were then incubated with primary antibodies with specific dilutions in M.O.M. diluent at 4°C overnight in a humidified chamber. Specific dilution for each antibody used in this study was listed in **Table 3** below. Tissue sections were washed thoroughly in PBS

after primary incubation, followed by incubation of horseradish peroxidase-secondary antibody raised against the source of primary antibody used. Freshly prepared DAB substrate (Vector Laboratories) was used to visualize tissue sections. Pigmentation for 5 seconds to 10 minutes before abolishing the reaction in water. Eventually, sections were lightly counter-stained with hematoxylin, dehydrated with increasing ethanol concentration, cleared in Clearene and mounted with CV mounting media (Leica Biosystems).

Primary Antibodies	Dilution	Source	Company
pAKT (Ser473)	1:250	Rabbit monoclonal	Cell Signaling Technology
Beta-Catenin (D10A8) XP	1:500	Rabbit monoclonal	Cell Signaling Technology
Ki67	1:200	Rabbit polyclonal	Abcam
FAH	1:250	Rabbit polyclonal	Abcam

**Table 3| Antibodies for immunohistochemistry (IHC) staining.** Specific dilution of primary antibodies used in IHC staining as listed in the table above.

### ***2.6 Semi-quantitative reverse-transcription polymerase chain reaction (RT-PCR)***

RNA from liver tissues was extracted using Trizol reagent (Life Technologies Thermo Fisher Scientific) following the protocol provided by the manufacturer. The first strand cDNA was synthesized from 250 ng mRNA using the SuperScript First-Strand Synthesis System for RT-PCR (Life Technologies Thermo Fisher Scientific). Reactions with (RT+) and without (RT-) the reverse transcriptase were performed for all samples. This cDNA was used as template for subsequent PCR with specific primers (**Table 4**). PCR conditions were similar to PCR genotyping with reduced cycles to avoid saturation of amplicon. Semi-quantitative analyses of unsaturated amplicons were measured using ImageJ software. Intensity of bands was calculated as an arbitrary value relative to actin, beta (*Actb*) expression level, and statistical analysis was generated using unpaired Student's *t*-test in Prism (version 6) (GraphPad Software, California, USA).

Primers	Sequence (5' --> 3')	Amplicon (bp)
<i>Afp</i>	Forward: CCTGTGAACTCTGGTATCAG	410
	Reverse: GCTCACACCAAAGCGTCAAC	
<i>Fah</i>	Forward: ATGAGCTTTATTCCAGTGGCC	503
	Reverse: ACCACAATGGAGGAAGCTCG	
<i>Gfp</i>	Forward: ACTTGTACAGCTCGTCCATGC	537
	Reverse: TCGTGACCACCCTGACCTAC	
<i>HBx</i>	Forward: ACCATGGCTGCTAGGCTGTGCTGCCAACTG	468
	Reverse: TTAGGCAGAGGTGAAAAAGTTGCATGGTGC	
<i>Actb</i>	Forward: GTGACGAGGCCAGAGCAAGAG	938
	Reverse: AGGGGCCGGACTCATCGTACTC	

**Table 4| Primers for RT-PCR.** Forward and reverse primers for each target gene as listed in the above table.

## 2.7 Quantitative PCR

Quantitative PCR (qPCR) was performed to determine the expression level of insulin growth factor 2 (*Igf2*), p21 (RAC1) activated kinase 6 (*Pak6*) and Rho GTPase activating protein 27 (*Arhgap27*) from extracted mRNA as mentioned previously. qPCR was performed using the QuantStudio 7 Flex Real-Time PCR System (University Research Facility in Life Sciences, The Hong Kong Polytechnic University). PCR reaction mixture consisted of a 1:50 dilution of cDNA in 20  $\mu$ L SYBR Green I containing GoTaq qPCR Master Mix (Promega) with specific primers (0.2  $\mu$ M final of each primer). Primers for target genes were listed in **Table 5**.

Primers	Sequence (5' --> 3')	Amplicon (bp)
<i>Igf2</i>	Forward: CCGTGTCCAGGAAAACGACT	233
	Reverse: CATTGGTACCACAAGGCCGA	
<i>Pak6</i>	Forward: CCTCGGCTGGCAGAATACAA	237
	Reverse: GCTTGGTGCTACCTGCACA	
<i>Arhgap27</i>	Forward: CCAGTACTGGGATGAGGAGA	203
	Reverse: GGTAAGTGGCCAGTAATTCGG	
<i>Actb</i>	Forward: AGAGCTACGAGCTGCCTGAC	184
	Reverse: AGCACTGTGTTGGCGTACAG	

**Table 5| Primers for qPCR.** Forward and reverse primers for each target gene as listed in the above table.

## 2.8 Western blotting

Protein was extracted from liver sections of injected mice using Qproteome Mammalian Protein Prep Kit (Qiagen) following the protocol provided by the manufacturer. Protein concentration was determined with standard protein assay (Bio-Rad). Protein (50 µg) was loaded into the SDS-PAGE and transferred onto PVDF membrane. Primary antibodies (pAKT, total AKT, non-phospho. (active) CTNNB1, total CTNNB1, FOXO1, peroxisome proliferator activated receptor gamma (PPARG) and ACTB) were diluted in 5% BSA at 1:2000 concentration. Secondary antibodies (anti-mouse or anti-rabbit) were diluted in 5% BSA at 1:2000 concentration. Membrane was blocked with 5% non-fat milk, then incubated with primary antibody at 4°C overnight followed by secondary antibody incubation at room temperature for an hour. The membrane was then washed with 1X TBST for 3 times in 10 minutes' interval. Afterwards, membrane was visualized using Immobilon Western Chemiluminescent HRP Substrate (MilliporeSigma, Massachusetts, USA) following the protocol provided by the manufacturer. Membrane was stripped with mild stripping buffer for binding with a new antibody when necessary.

## 2.9 Serum metabolite analyses

### *Serum preparation for injection:*

Serum was isolated by centrifuging blood at 4000 rpm for 5 to 10 minutes. To prepare serum for Ultra Performance Liquid Chromatography-Orbitrap-Mass spectroscopy

(UPLC-Orbitrap-MS), 60  $\mu$ L serum sample was mixed with 250  $\mu$ L methanol and vortexed for 30 seconds. The mixture was left at  $-20^{\circ}\text{C}$  overnight for the completion of deproteination. Then, 125  $\mu$ L aliquot of supernatant was collected after centrifugation at 18900g at  $4^{\circ}\text{C}$  for 20 minutes and dried under nitrogen gas. The dried supernatant was stored at  $-80^{\circ}\text{C}$  prior to UPLC-Orbitrap-MS analysis.

#### *Quality control*

An equal volume of each serum sample was pooled, vortexed and aliquoted to provide pooled quality control (QC) samples and went through the same extraction protocols of LC-MS as described above like all other samples. They were injected to UPLC-MS intermittently between samples for checking the stability of the instruments throughout the runs.

#### *UPLC-Orbitrap-MS analysis*

The dried supernatant was reconstituted in 60  $\mu$ L of 5% acetonitrile in water (5:90, v/v) and was centrifuged at 18900g for 15 minutes. A 3  $\mu$ L aliquot was injected into a Waters ACQUITY UPLC system (Waters, Milford, MA, USA). The UPLC separation was performed on a Waters ACQUITY UPLC HSS T3 column (2.1 mm x 100 mm, 1.8  $\mu\text{m}$ ) with HSS T3 guard column (2.1mm x 5 mm, 1.8  $\mu\text{m}$ ). The mobile phase consisted of solvent A (0.1% formic acid in water, v/v) and solvent B (0.1% formic acid in acetonitrile, v/v) at a flow rate of 0.3 mL/min with elution gradient as follows: 0 minutes, 5% B; 5 minutes, 50% B; 10 minutes, 60% B; 15 minutes, 65% B; 18 to 21 minutes, 95% B. A 3-minute post-run time was set to fully equilibrate the column. Column and sample chamber temperature were at  $40^{\circ}\text{C}$  and  $4^{\circ}\text{C}$ , respectively.

Mass spectrometry analysis was achieved by a Thermo Scientific Orbitrap Fusion Lumos Tribrid mass spectrometer equipped with a heated electrospray ionization (H-ESI) interface (Thermo Fisher Scientific). The mass-spectrometric conditions were optimized as follows: spray voltage, 2300V in negative H-ESI mode and 3500V in positive H-ESI mode; ion transfer tube and vaporizer temperature,  $300^{\circ}\text{C}$ . Nitrogen gas was used as the sheath gas and the aux gas with flow rate of 20 and 10 L/min, respectively. The instrument was operated in data-dependent acquisition mode, with

full MS scans over  $m/z$  90–1000 with Orbitrap (120k resolution) as detection. Mass fragmentation was carried out for peak identification at normalized collision energy of  $30 \pm 10\%$  higher energy collisional dissociation with detection in the Orbitrap (30k resolution) MS<sup>2</sup> detection. All the data analysis was carried out using the Thermo Xcalibur Qual Browser software (Thermo Fisher Scientific). Data processing was analysed by Progenesis QI software 2.0 (Nonlinear Dynamics, Newcastle upon Tyne, United Kingdom) and peak area was normalized by all compound with reference of quality control. Quality screening was done by filtering out those unstable metabolites (coefficient of variation > 30% in all pooled quality control samples). The remaining normalized data matrix was exported to the Extended Statistical tool (EZinfo v2.0 software, Umetrics AB) for partial least squares-discriminant analysis (PLS-DA) so as to evaluate their classification performance. The parameter  $Q^2$  is used to assess the goodness of prediction for performance of PLS-DA in a general acceptable threshold value of 0.5. The metabolites that had significant difference between HBx-B Mut and WT experimental samples were identified by comparing their  $m/z$ , mass fragmentation patterns and chromatographic retention times with commercially available reference standards and/or online metabolite databases such as Human Metabolome Database (<http://metlin.scripps.edu>), Metlin (<http://metlin.scripps.edu>) and literatures.

### ***2.10 Statistical analysis and figures icons***

Values are given as mean  $\pm$  standard deviation (SD). Statistical significance was assessed by Prism two-tailed Student's  $t$ -test with  $p$ -values (GraphPad Software).  $q$ -value was used to justify significantly differentially expressed genes (DEGs) in RNA sequencing result. Figure icons of cell components were adopted from an online bioinformatics tool – Reactome (109).

## Chapter 3 - Results

### *3.1 Divergent effect on tumor burden by K130M/V131I mutant and wild-type of various HBx genotypes*

The first goal of this study was to find out which genotype is the most tumorigenic. In order to achieve this, expression vectors expressing either K130M/V131I mutant and wild-type HBx gene of genotypes A, B, C and D were generated as described in the method section. Twenty micrograms of either mutant or wild-type clones were co-injected with a short hairpin RNA that targeted *Trp53* (*shp53*) containing vector into tail vein of *Fah*/SB11 mice by hydrodynamic tail vein injection. After injection, NTBC water was replaced by normal drinking water and the mice were allowed to age until 160-days post hydrodynamic injection (PHI). The body weight and condition of the injected mice were recorded in the first 6 weeks PHI. Since, the liver was undergoing regeneration in the first 6 weeks PHI, the weight of the mice was reduced in the first 3-4 weeks PHI and gradually increased afterwards (102).

During aging, due to the expression of luciferase in the expression vector, regeneration progress of liver in the experimental animals were monitored by animal live imaging via application of luciferin. Necropsy of experimental animals were performed at around 160-day PHI. Whole body weight and liver weight of the experimental animals were measured and recorded. GFP signal of the liver was observed under BLS<sup>®</sup> florescent goggle with specific emission filter, livers from all experimental animals, including empty control shown more than 95% GFP-positive hepatocytes; while no GFP signal could be observed in *Fah*/SB11 non-injected control and wild-type control animals. This indicated the successful expression of the transposon in hepatocytes after injection. The number of GFP-positive tumors were counted and isolated for further analyses (**Fig. 13A**). First of all, significant difference ( $p < 0.0001$ ) in liver-to-whole body weight ratio was observed in all HBx injected animals with either mutant or wild-type variants of each genotypes, which had an average liver-to-whole body weight ratio of about 7%, compared to the empty control groups, which had an average liver-to-whole body weight ratio of 5% ( $n = 9$ ) (**Fig. 13C**). However, there was no significant difference in liver-to-whole body weight ratio between mutant and wild-type of the same genotype, with the exception for genotype B. HBx-B mutant injected animals displayed significantly larger liver-to-

whole body weight ratio than HBx-B WT injected animals ( $p = 0.0473$ ). These results suggest that both mutant and wild-type of HBx genes in genotype A, B, C and D might induce hepatomegaly, while genotype B mutant variant displayed more severe phenotype than its wild-type counterpart (**Fig. 13C**).

Next, we compared the tumor burden efficacy between mutant and wild-type of each genotypes based on the number of GFP-positive tumor nodules formed in the experimental animals. From the result, both mutant and wild-type variants of genotype D induced the severest tumor burden ( $7.6 \pm 1.614$  tumor nodules per mouse,  $n = 10$  and  $3.1 \pm 0.9196$  tumor nodules per mouse,  $n = 9$ , respectively), in which its mutant variant induced significantly stronger tumor burden than its wild-type counterpart ( $p = 0.0315$ ) (**Figure 13B**). The second most tumorigenic genotype was genotype C, although there was no significant difference in tumor burden between mutant and wild-type variants of HBx genotype C ( $p = 0.5226$ ), both variants induced strong tumor burden: HBx-C Mut induced  $2.3 \pm 1.033$  ( $n = 10$ ) tumor nodules per mouse and HBx-C WT induced  $1.444 \pm 0.7658$  ( $n = 9$ ) tumor nodules per mouse (**Figure 13B**). For HBx genotype B, Mut and WT variants induced an average tumor burden of  $1.2 \pm 0.611$  ( $n = 10$ ) per mouse and  $0.2 \pm 0.1333$  ( $n = 10$ ) per mouse, respectively (**Figure 13B**). Although there was no significant difference in tumor burden efficacy between HBx-B Mut and WT experimental groups, HBx-B Mut injected mice displayed a trend toward higher tumor burden than HBx-B WT counterpart ( $p = 0.1272$ ) (**Figure 13B**). The genotype that displayed the least tumor burden effect was HBx genotype A, with no significant difference in number of tumor nodules induced by Mut and WT experimental animals. Both Mut and WT variants of HBx-A induced low tumor nodule formation with  $0.4 \pm 0.4$  ( $n = 10$ ) tumor nodule per mouse and  $0.5 \pm 0.3273$  ( $n = 8$ ) tumor nodules per mouse, respectively (**Figure 13B**).

Although genotype D of HBx gene was the most aggressive in tumor burden induction, its tumorigenic effect was studied in our previous study (54), thus more focus was placed on the Asian-related genotypes B and C in this study.

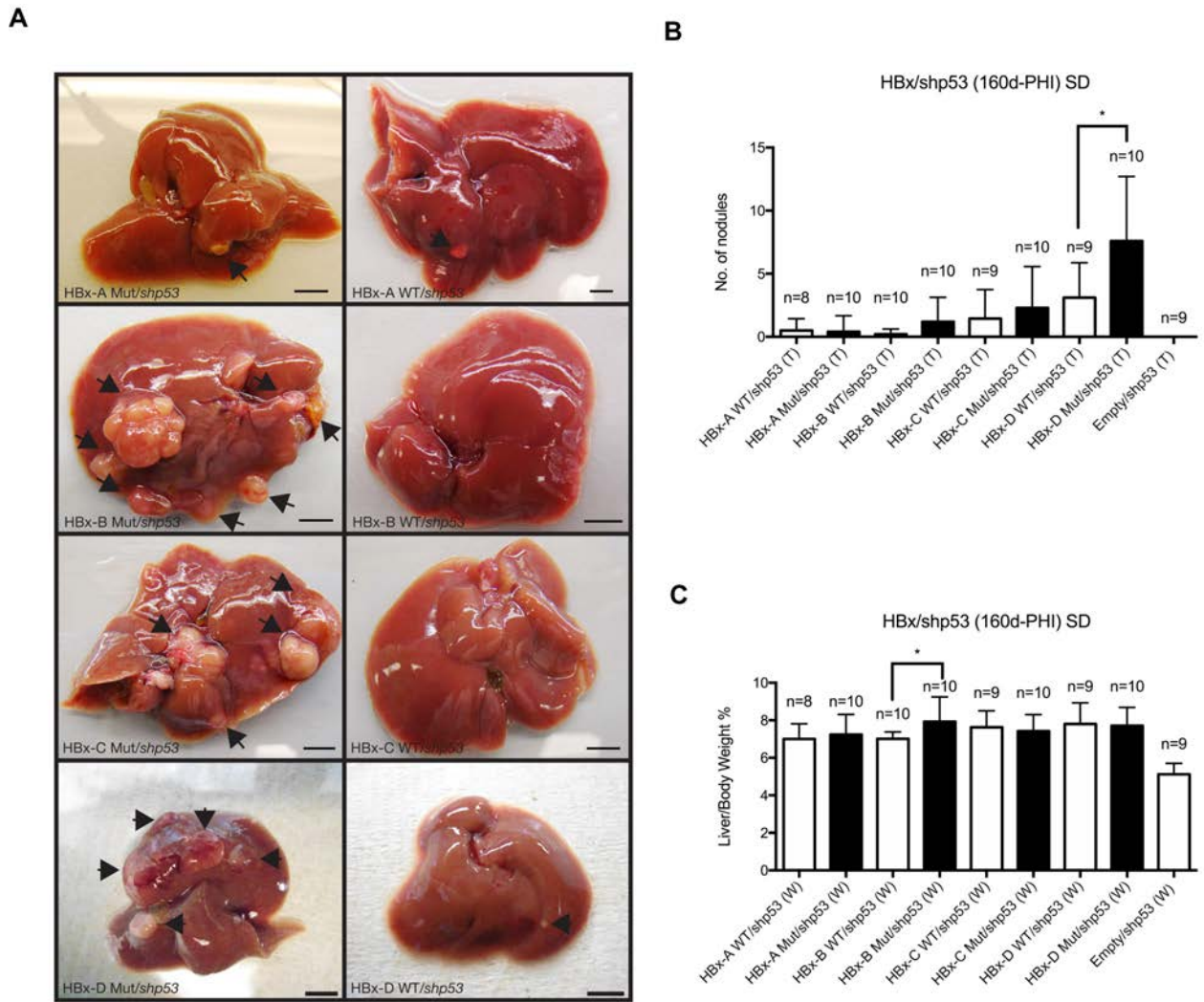


**Figure 13| Isolated livers, number of tumor nodules and liver-to-whole body weight ratio of each experimental groups. (A)** Representative isolated livers of necropsied animals from each experimental group. Generally, more nodules were found in animals injected with K130M/V131I mutant HBx gene of each genotypes. Arrows indicate tumor nodules; the orientation of the livers were optimized to show the most tumor nodules; scale bars, 0.5 cm. **(B)** Number of GFP+ tumor nodules found in each experimental group. HBx-D mutant (Mut) and wild-type (WT) variants induced the most tumor nodules formation ( $7.6 \pm 1.614$  nodules per mouse,  $n = 10$  and  $3.1 \pm 0.9196$  nodules per mouse,  $n = 9$ , respectively), in which its mutant variant induced significantly stronger tumor burden than its wild-type counterparts ( $p = 0.0315^*$ ). There was no significant difference in tumor burden between HBx genotype C Mut and WT variants ( $p = 0.5226$ ), HBx-C Mut induced  $2.3 \pm 1.033$  ( $n = 10$ ) tumor nodules per mouse and HBx-C WT induced  $1.444 \pm 0.7658$  ( $n = 9$ ) tumor nodules per mouse. HBx-B Mut injected mice displayed a trend toward higher tumor burden than HBx-B WT counterpart ( $p = 0.1272$ ). HBx-B Mut ( $n = 10$ ) and HBx-B WT ( $n = 10$ ) induced an average tumor burden of  $1.2 \pm 0.611$  nodules per mouse and  $0.2 \pm 0.1333$  tumor nodules per mouse, respectively. There was no significant difference in number of tumor nodules induced by HBx-A Mut and HBx-A WT experimental animals. HBx-A Mut induced  $0.4 \pm 0.4$  ( $n = 10$ ) tumor nodule per

mouse and HBx-A WT induced  $0.5 \pm 0.3273$  ( $n = 8$ ) tumor nodules per mouse. (C) There was significant difference in liver-to-body weight ratio between each HBx experimental groups compared with empty control groups. Liver-to-whole body weight ratio in HBx experimental groups was around 7%; while that in empty control group was around 5%. This indicated HBx might induce hepatomegaly. Additionally, a significant difference in liver-to-whole body weight ratio between HBx-B Mut and WT experimental groups was illustrated ( $p = 0.0473^*$ ).

### ***3.2 Histopathological phenotypes in HBx injected animals***

In order to find out the hepatic morphological changes of the experimental animals, liver tissues were stained with H&E solution and histopathological changes, including inflammation, necrosis, and fibrosis, were assessed by board certified pathologist. The severity of the histopathological changes was scored ranging grade 0 to grade 3, with grade 0 for no pathological changes, grade 1 for mild, grade 2 for moderate, and grade 3 for the most severe changes (**Figure 14A (i, ii, iii)**). Summarizing the histopathological changes, enlargement of hepatocyte nuclei with apparent pyknotic changes were observed and this indicated the development of hepatocellular necrosis (**Figure 14B (iii)**). Moreover, multi-nuclei and mitotic figures were found in the HBx injected animal sections (**Figure 14B (iii) and (iv)**). Additionally, individual cell necrosis was indicated from the slides injected with either mutant or wild-type HBx gene variants of genotype B (**Figure 14B (vii)**). Fibrosis and degenerative changes were also observed in liver sections of the HBx-B mutant and wild-type injected animals (**Figure 14B (viii)**). Furthermore, different degrees of inflammation were observed based on the amount of lymphocyte aggregation in the injected liver sections (**Figure 14B (ix)**). We found that higher degree of inflammation was observed in Asian-related genotypes B and C. Experimental animals injected with both mutant and wild-type HBx genes of genotype C induced severe inflammation, and HBx-B experimental groups induced moderate degree of inflammation; while both HBx-A and HBx-D experimental groups only induced mild inflammation. With the question if genotypes B and C played a more important role in promoting tumor progression, more effort was put on elucidating the molecular pathways induced by genotypes B and C of HBx gene.

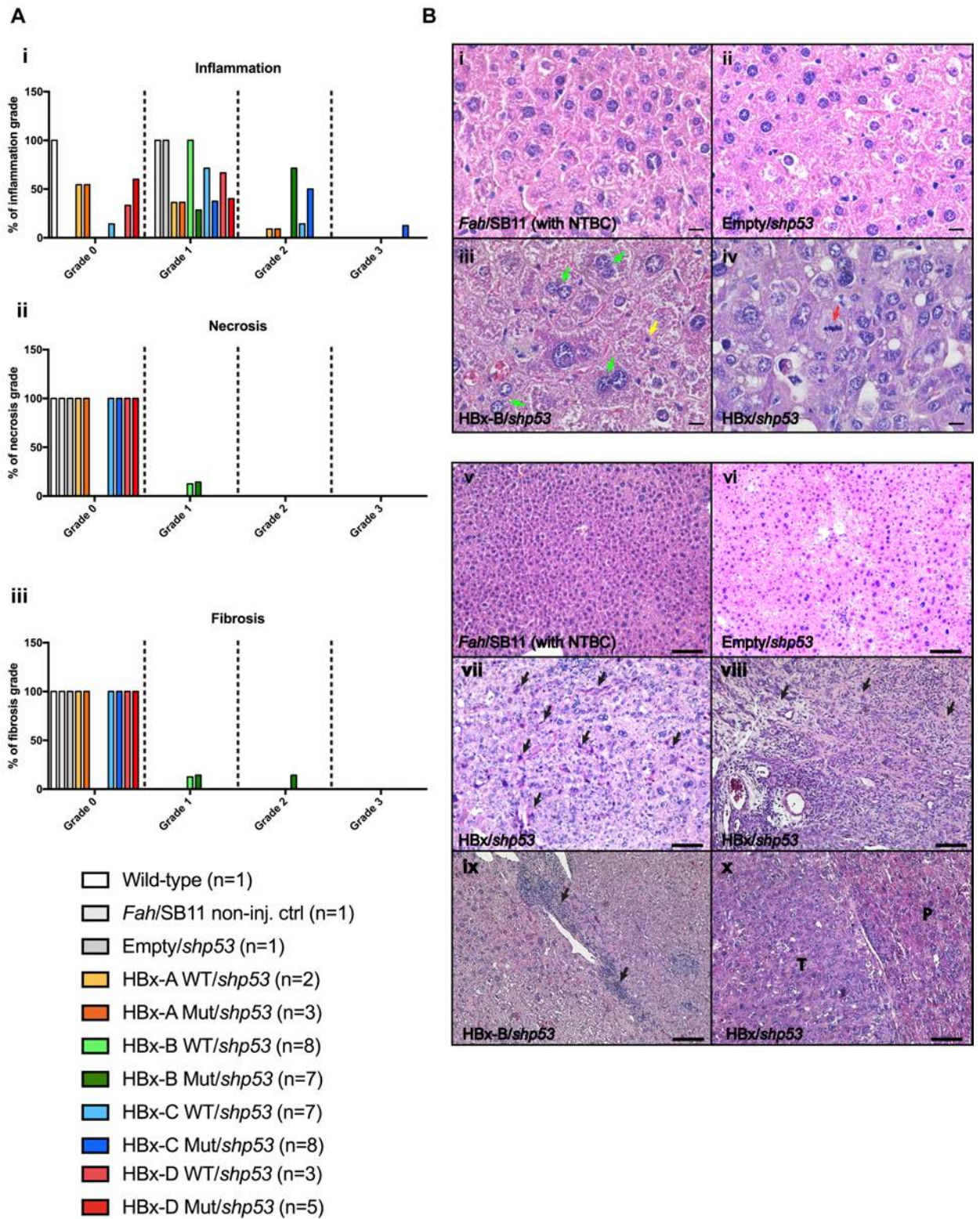


**Figure 14| Histopathology of livers from HBx injected experimental animals.** (A) inflammation (i), necrosis (ii), and fibrosis (iii) events were assessed by board-certified pathologist. Severity of each pathological events were graded from 0 to 3, 0 means the least severe, 1 means mild, 2 means moderate, and 3 means the most severe. (B) Representative H&E staining images illustrated dysplastic hepatic morphologies of the experimental animals.

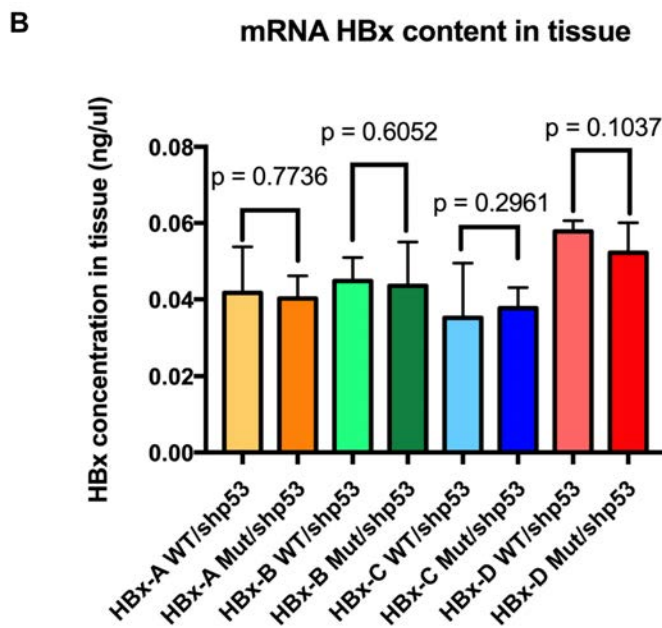
(i, v) Non-injected *Fah*/SB11 liver under continuous treatment of NTBC shown normal hepatocyte morphology. (ii, vi) *Fah*/SB11 liver injected with empty vector control in the context of *shp53*. (iii) Multinucleated cells (indicated with green arrow) and pyknotic nuclei (indicated with yellow arrow) of hepatocytes were found in HBx/*shp53* injected liver. (iv) More mitotic figures (indicated with red arrow) were noted in liver sections injected with HBx/*shp53*. Scale bars, 11  $\mu$ m. (vii) Necrosis (arrows) observed in the HBx injected animals with co-injection of *shp53*. (viii) Fibrosis observed in *Fah*/SB11 animals with HBx-B genotype co-injected with *shp53*. (ix) Areas of lymphocytic inflammation (arrows) seen in *Fah*/SB11 mice with HBx gene with co-injection of *shp53*. (x) Tumor nodule (T) observed in *Fah*/SB11 animals HBx gene co-injected with *shp53* with dysplastic hepatic morphology seen in peripheral hepatocytes (P). Scale bars, 100  $\mu$ m.

### 3.3 Expression of transgenes in HBx injected liver

To confirm the inflammation and tumor formed were driven by expression of the HBx gene, semi-quantitative RT-PCR was performed to examine the expression of green fluorescent protein (*Gfp*), *HBx* and *Fah* transgenes flanked in the transposon elements of the delivery vectors. Both normal tissues and tumors isolated from HBx injected mouse liver expressed the *Gfp*, *HBx* and *Fah* transgenes (**Figure 15A**), this indicated the successful integration and expression of transposons in the liver of the experimental animals. Next, the transcriptional level of alpha-fetoprotein (*Afp*), a well-known marker for HCC diagnosis, was analysed by semi-quantitative RT-PCR. The results showed that *Afp* was detected in all HBx injected animals, especially high mRNA expression of *Afp* was detected in tumor when compared with its corresponding adjacent microscopically normal liver samples ( $p = 0.0599$ ) (**Figure 15A**). As expected, the wild-type adult mouse liver control used for RT-PCR analyses did not express detectable levels of *Afp*, *Gfp* or *HBx* transgenes, but expressed high levels of endogenous *Fah* (**Figure 15A**). Additionally, to examine if the expression level of HBx would contribute to the tumorigenicity differences in mutant and wild-type variants in the same genotype of HBx gene, expression level of *HBx* in all experimental cohorts was quantified by qPCR (**Figure 15B**). From the qPCR result, there was no significant difference in *HBx* expression level between animals injected with mutant and wild-type variants of the same genotype (**Figure 15B**).

Furthermore, rescued activity of *Fah* in injected mice was also confirmed by IHC (**Figure 15C**), while control wild-type mouse livers were strongly *Fah*-positive, and

non-injected *Fah*/SB11 control animals (under NTBC treatment) were *Fah*-negative by IHC staining, indicating the successful integration, transcription and translation of genes flanked in transposon of injected animals. We also detected the level of Ki67, which is a marker for cell proliferation, in the experimental animal by IHC staining. As expected, normal non-proliferating livers were Ki67-negative, while liver tumor nodules isolated from experimental animals injected with HBx gene were strongly positive for Ki67 (**Figure 15C**).



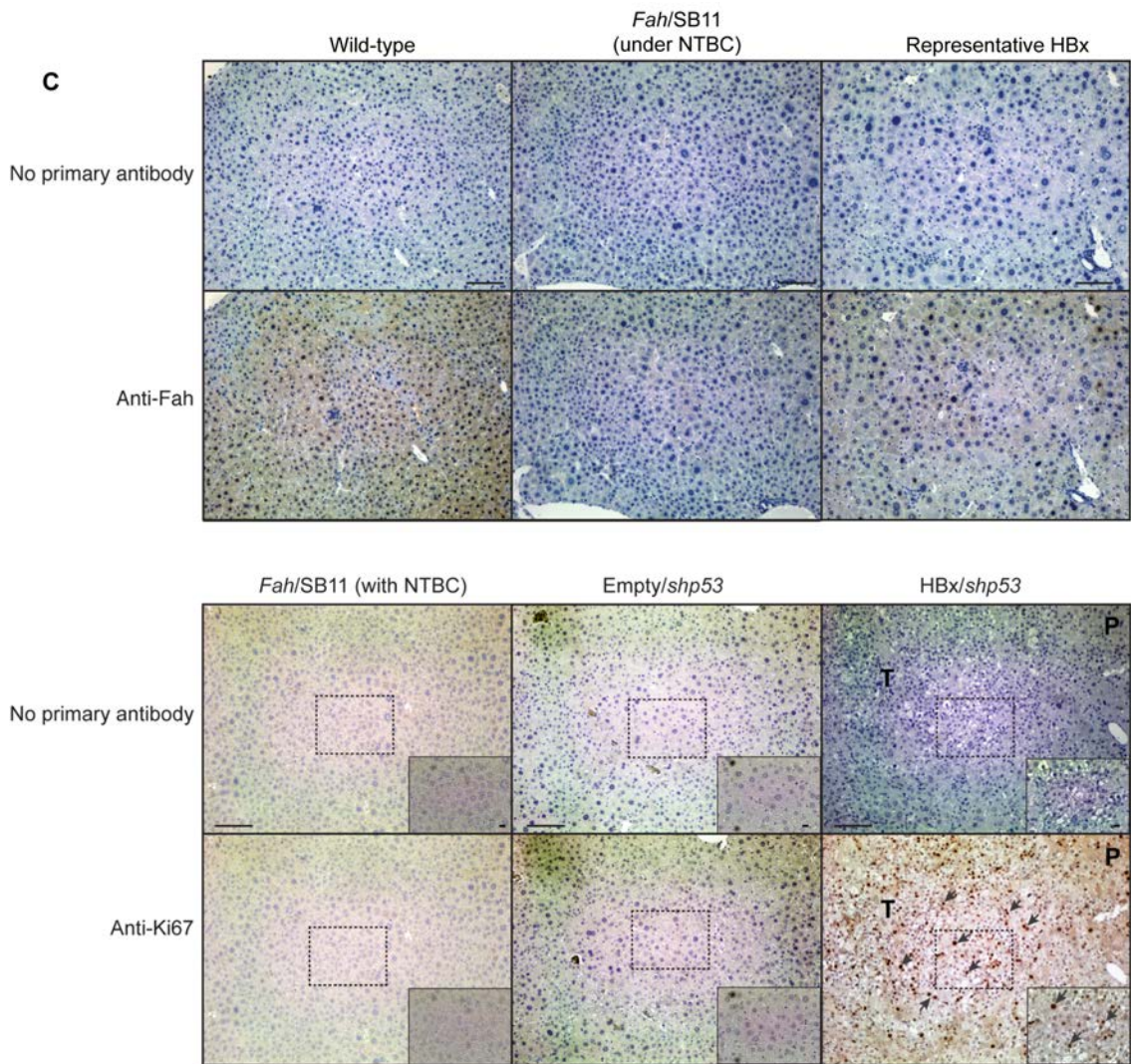


**Figure 15| Expression of transgenes in HBx injected animals.** (A) Representative RT-PCR on *Afp*, *Gfp*, *HBx*, *Fah* and *Actb* genes of HBx injected animals. The presence of *Gfp*, *HBx* and *Fah* bands in the RT-PCR products indicated successful integration and expression of transposon. Moreover, *Afp* mRNA expression level in HBx injected animals was higher than the wild-type mouse, additionally, its expression level in tumor was higher than that of normal tissues as well. (B) The mRNA expression level of *HBx* in different experimental groups. There was no significant different in *HBx* expression level between the mutant and wild-type variants of the HBx injected animals. (C) Representative IHC stained images for anti-Fah in controls and *Fah*/SB11 animals injected with various HBx and *shp53* transgenes. **Top panels**, no primary antibody was used. **Bottom panels**, anti-Fah primary antibody used. **Left column**, wild-type mouse liver showing strong anti-Fah activity. **Middle column**, no anti-Fah activity detectable in non-injected *Fah*/SB11 liver under NTBC supply. **Right column**, anti-Fah activity detected in *Fah*/SB11 livers with wild-type (WT) HBx-B genotype co-injected with *shp53*, with removal of NTBC after injection. Scale bars, 100  $\mu$ m. (C) Representative IHC stained images for anti-Ki67 in controls and liver tumors of *Fah*/SB11 animals injected with HBx and *shp53* transgenes. **Top panels**, no primary antibody was used. **Bottom panels**, anti-Ki67 primary antibody used. **Left column**, wild-type mouse liver showing no anti-Ki67

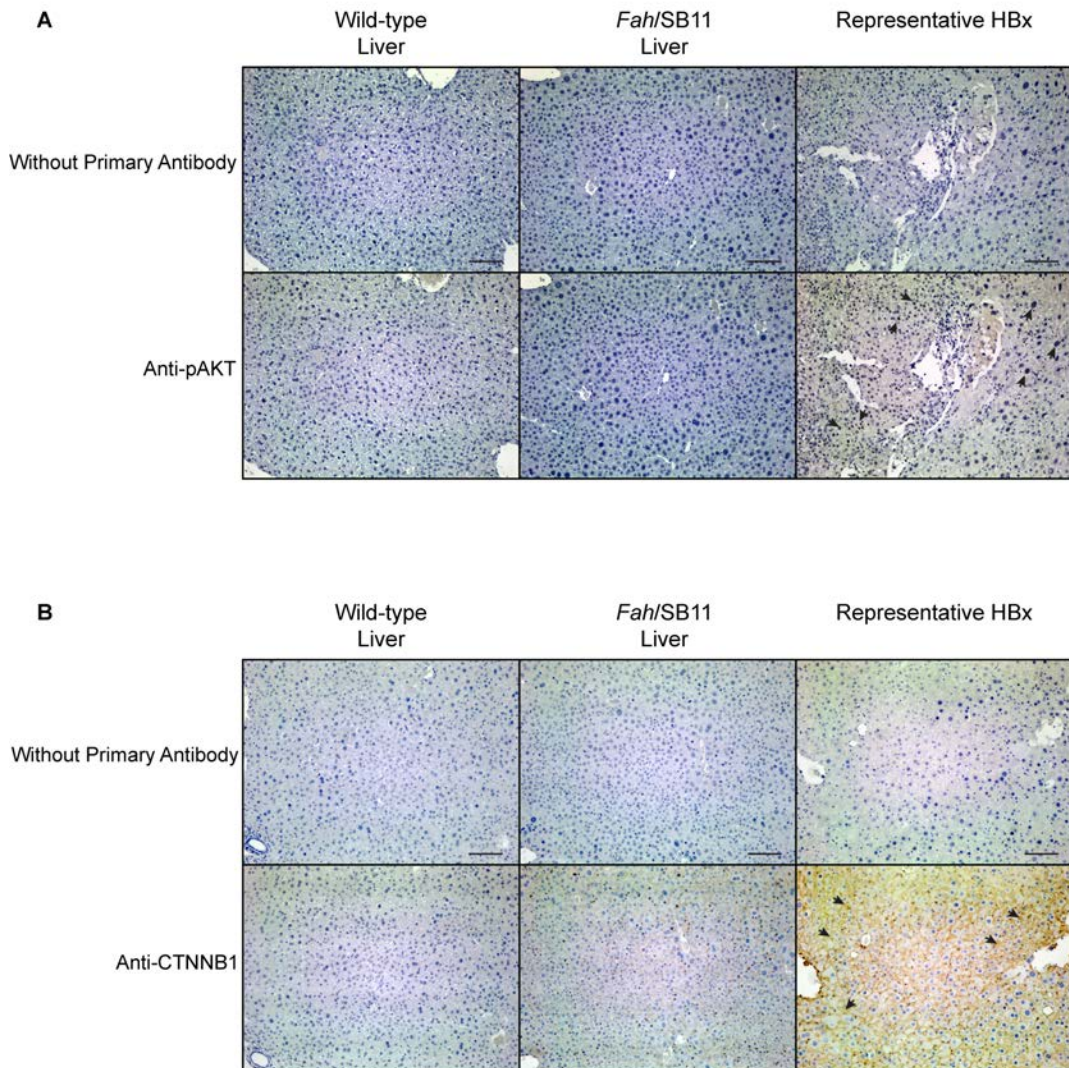
activity. **Middle column**, no anti-Ki67 activity detectable in empty liver. **Right column**, strong anti-Ki67 activity detected in tumors (T) of *Fah/SB11* livers with expression of HBx K130M/V131I mutant gene, while the peripheral hepatocytes (P) displayed low anti-Ki67 activity. Scale bars, 100  $\mu\text{m}$ . Magnified image was shown in right corner (solid-lined box) of each slide. Scale bars, 11  $\mu\text{m}$ .

### **3.4 Increased AKT and CTNNB1 protein levels in HBx injected mice**

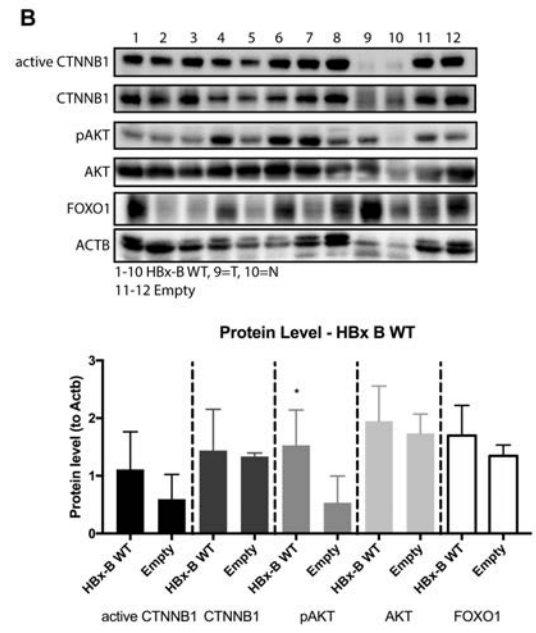
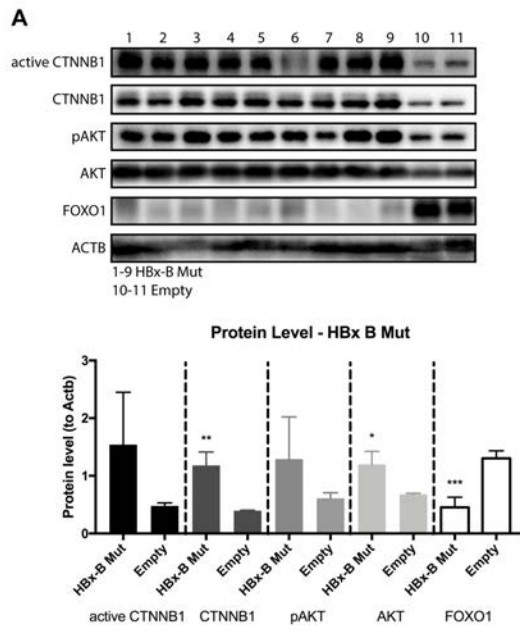
To elucidate the molecular pathways induced by various genotypes of HBx gene, we first focused on both PI3K/AKT and WNT/CTNNB1 signalling pathways, as they are commonly known to play vital roles in regulating cellular differentiation, proliferation and survival in HCC (110). IHC on liver sections of experimental animals were performed and liver tumor nodules isolated from mice injected with HBx in context of *shp53* predisposal background were strongly positive for nuclear pAKT and CTNNB1 (**Figure 16A and B**). Western blot analyses on protein extracted from HBx experimental mice was incubated with non-phospho (active) CTNNB1 (active CTNNB1), CTNNB1, phospho-AKT (ser473) (pAKT), and AKT primary antibodies (**Figure 17A and B**). After quantifying with the beta-actin (ACTB) level of empty control, the protein level of total CTNNB1 and total AKT were significantly higher in HBx-B Mut/*shp53* when compared with empty control, while FOXO1 protein level was significantly lower in HBx-B Mut/*shp53* than that of empty and there were a trend showing that protein level of active CTNNB1 and pAKT were higher in HBx-B Mut/*shp53* when compared with empty controls (**Figure 17A**). On the other hand, only pAKT protein level was significantly increased in HBx-B WT/*shp53* when compared with and there were no significant differences in AKT, active and total CTNNB1 and FOXO1 levels between HBx-B WT/*shp53* and empty controls (**Figure 17B**).

Furthermore, protein levels of active CTNNB1, total CTNNB1, pAKT, total AKT, FOXO1 and PPARG was examined for HBx-C Mut/*shp53* and WT/*shp53* injected animals. After quantification with the ACTB protein level, there was no significant alteration on expression of these proteins in normal tissues of HBx-C Mut/*shp53* and WT/*shp53* injected animals compared with that of empty control animals (**Figure 17C**). However, comparing the protein level from both tumor and normal tissues of

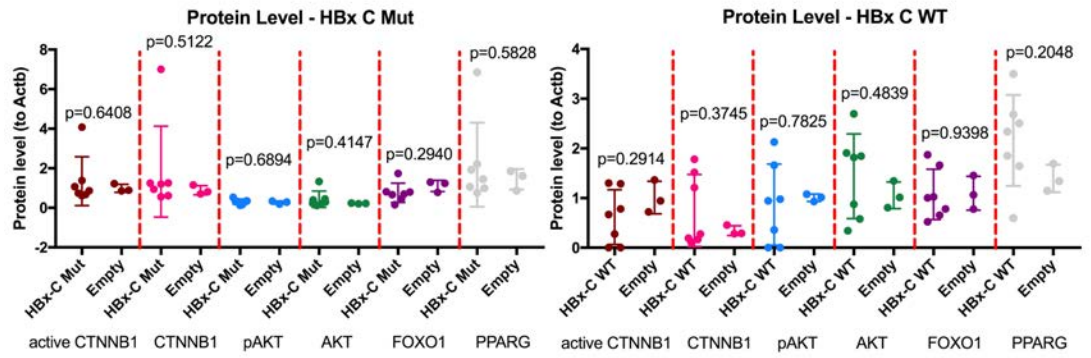
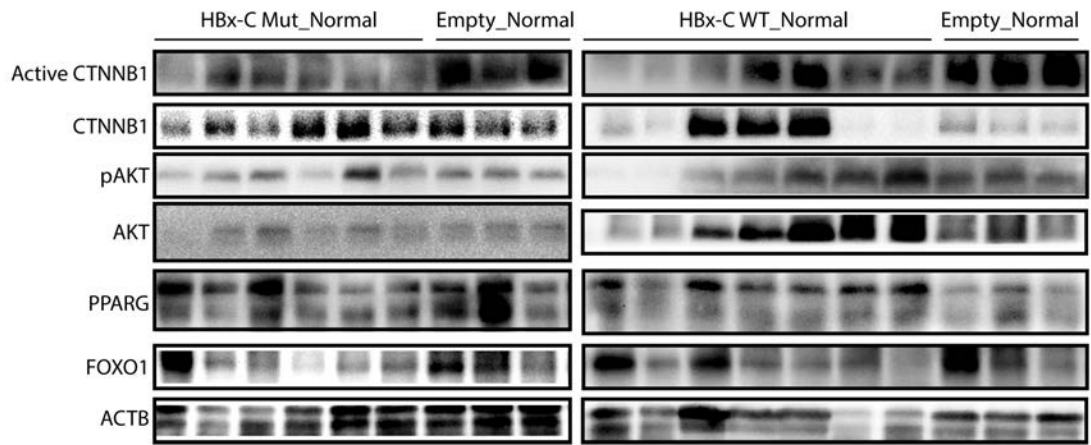
HBx-C WT/*shp53* injected animals with that from normal tissues of empty control, significantly higher expression of active CTNNB1 and pAKT level were detected in both normal and tumor tissues of HBx-C WT/*shp53* injected animals (**Figure 17D**). Surprisingly, there was no significant difference in FOXO1 expression level, yet PPARG expression level was significantly reduced in tumor of HBx-C WT/*shp53* injected animals compared with the empty control (**Figure 17D**). Therefore, we proposed that different genotypes of HBx gene would activate different signalling pathways predominantly, in which AKT/FOXO1 signalling pathway played a more significant role in triggering tumor development under over-expression of HBx-B K130M/V131I variant; while activation of PPARG/CTNNB1 signalling pathway was predominant under over-expression of HBx-C wild-type variant (**Figure 17E**).

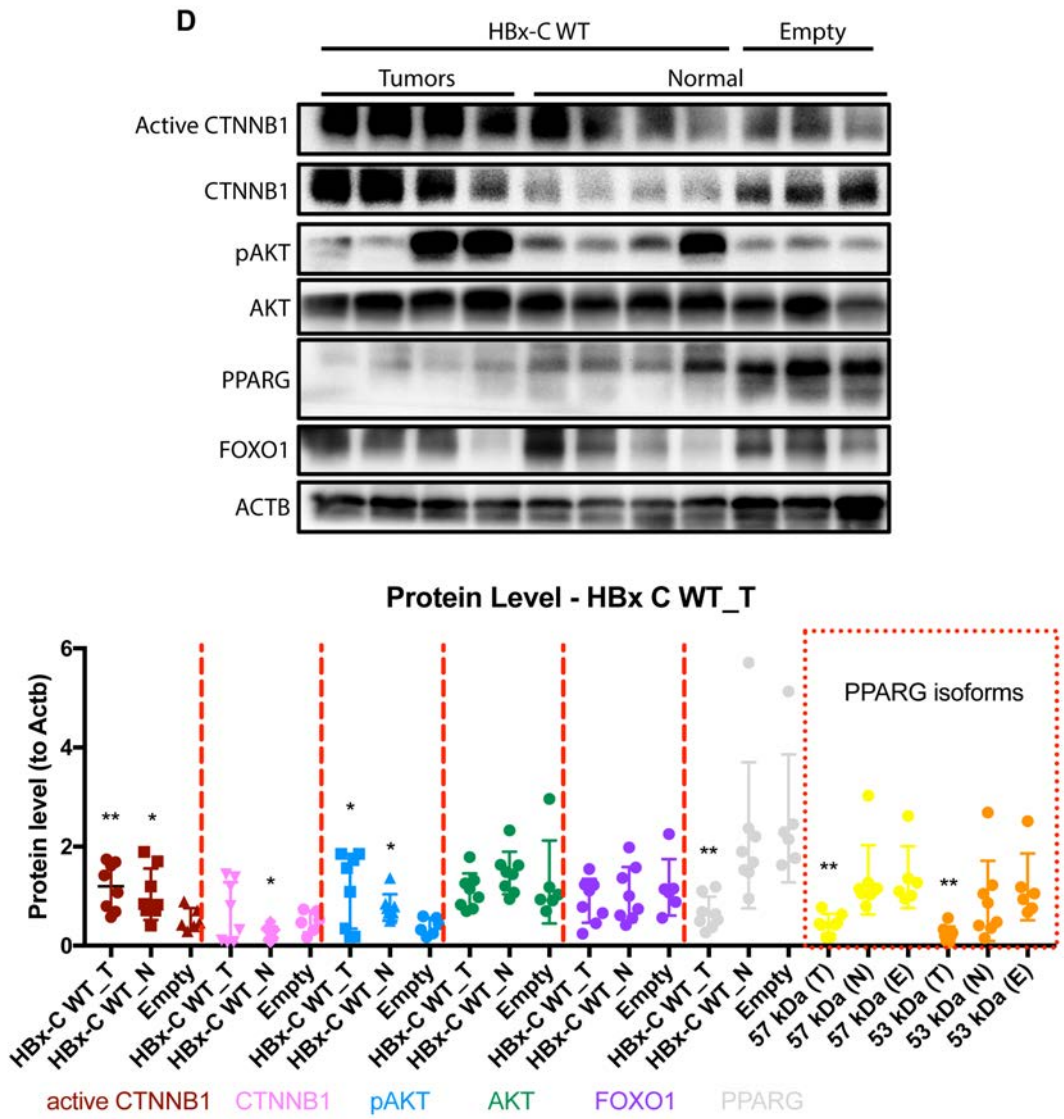


**Figure 16| Representative IHC stained images of experimental animals using anti-pAKT (S473) and anti-beta-Catenin (CTNNB1) primary antibodies. (A)** Representative liver sections stained with anti-pAKT (S473) primary antibody. **(Upper panel)** No primary antibody was added. **(Bottom panel)** pAKT (S473) primary antibody was added. **(Left panel)** Wild-type liver, **(middle panel)** Non-injected *Fah*/SB11 liver under continuous treatment of NTBC, and **(Right panel)** HBx/*shp53* co-injected liver. Nuclear staining by pAKT (S473) as indicated by the arrows. **(B)** Representative liver sections stained with anti- $\beta$ -Catenin primary antibody. **(Upper panel)** No primary antibody was added. **(Bottom panel)**  $\beta$ -Catenin primary antibody was added. **(Left panel)** Wild-type liver, **(middle panel)** Non-injected *Fah*/SB11 liver under continuous treatment of NTBC, and **(Right panel)** HBx/*shp53* co-injected liver. Cytoplasmic staining by  $\beta$ -Catenin as indicated by the arrows. Scale bars, 100  $\mu$ m.



**C**





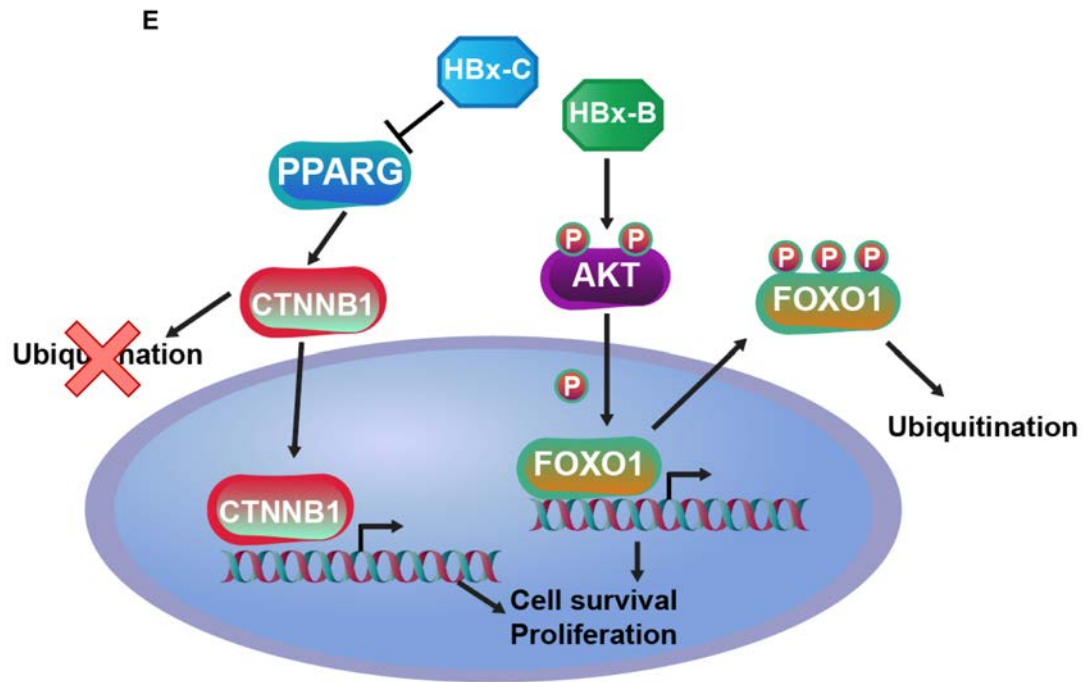


**Figure 17| Representative Western blot and qPCR of experimental animals.** (A) Representative Western blot of HBx-B Mut/*shp53* injected animals (**Upper panel**). (B) Representative Western blot of HBx-B WT/*shp53* injected animals (**Upper panel**). Active and total CTNNB1, phosphorylated and total AKT, total FOXO1 and ACTB levels of HBx-B mutant injected groups. Relative protein levels were quantified relative to the endogenous ACTB level of corresponding animals (**Bottom panel**). (C) Representative Western blot of protein extracted from normal tissues of HBx-C Mut/*shp53* and WT/*shp53* injected animals (**Upper panel**). Active and total CTNNB1, phosphorylated and total AKT, total FOXO1, PPARG and ACTB levels of HBx-C injected groups. Relative protein levels were quantified relative to the endogenous ACTB level of corresponding animals (**Bottom panel**). (D) Representative Western blot of protein extracted from both tumor and normal tissues of HBx-C WT/*shp53* injected animals (**Upper panel**). Active and total CTNNB1, phosphorylated and total AKT, total FOXO1, PPARG and ACTB levels of HBx-C injected groups. Relative protein levels were quantified relative to the endogenous ACTB level of corresponding animals (**Bottom panel**). (E) Proposed signalling pathways induced by over-expression of genotypes B and C of *HBx* gene. Mean  $\pm$  S.D.; *p*, unpaired student *t*-test, \**p*  $\leq$  0.05, \*\* *p*  $\leq$  0.01, \*\*\* *p*  $\leq$  0.001.

### 3.5 RNA-Seq revealed crucial roles of metabolism reprogramming in HBx injected mice

To determine gene expression alterations induced by over-expression of the HBx, RNA-Seq was performed to quantify the RNA expression profile of HBx injected animals. RNA expression of tumor and normal tissues of HBx/*shp53* experimental animals and empty/*shp53* control animals (samples were listed in **Table 6**) were

quantified by Illumina sequencing and expression level of each gene was calculated by fragments per kilobase of exon per million reads mapped (FPKM). Based on the gene expression level, differentially expressed genes (DEGs) were identified between groups. Fold of expression differences of gene expression between 2 samples were calculated by log<sub>2</sub> FPKM ratio of 2 samples. Significant gene expression difference was filtered with log<sub>2</sub> ratio greater or equal to 1 (for up-regulation) and smaller or equal to -1 (for down-regulation) and *p*-value less than 0.05. DEGs reported in the following sections were significantly altered with *p* < 0.05 and log<sub>2</sub> ratio greater than 1 for up-regulation and less than -1 for down-regulation cases.

Genotypes	Mutant (Mut) / Wild-type (WT)	Tumor (T) / Adjacent normal (N)	No. of samples
HBx-A	Mut	T	/
	Mut	N	3
	WT	T	1
	WT	N	4
HBx-B	Mut	T	3
	Mut	N	4
	WT	T	/
	WT	N	3
HBx-C	Mut	T	2
	Mut	N	2
	WT	T	3
	WT	N	3
HBx-D	Mut	T	3
	Mut	N	3
	WT	T	3
	WT	N	3
Empty	/	N	3

**Table 6| List of samples used for RNA sequencing.** Number and types of liver tissue in each experimental group used for RNA sequencing as listed in the above table.

### 3.5.1 RNA sequencing result of HBx Genotype A

In order to find out the genetic changes induced by K130M/V131I mutant and wild-type HBx of genotype A, we first compared the RNA expression profiles in normal and tumor tissue of HBx-A Mut and HBx-A WT experimental groups with empty control group, with the co-injection of *shp53*. There were relatively low genetic differences in RNA expression profiles of normal tissues between HBx-A Mut ( $n = 3$ ), HBx-A WT ( $n = 4$ ) and empty control ( $n = 3$ ) groups. Only 51 genes were up-regulated, and 98 genes were down-regulated in normal tissues of HBx-A Mut compared with empty control; and 34 genes were up-regulated, 51 genes were down-regulated in normal tissues of HBx-A WT compared with empty control (**Figure 18A**). There were large genetic differences between RNA expression profiles of HBx-A WT tumor ( $n = 1$ ) and that of empty normal control, in which 1204 genes were up-regulated, 791 genes were down-regulated (**Figure 18A**). There were 39 common DEGs identified in normal tissues of HBx-A WT and HBx-A Mut groups in referencing to the empty normal control, in which 12 DEGs were up-regulated, including major urinary protein 12 (*Mup12*), which participated in inflammatory pathway, and 27 DEGs were down-regulated, including *Fah* and sushi domain containing 4 (*Susd4*), which is a complement inhibitor (**Figure 18B**).

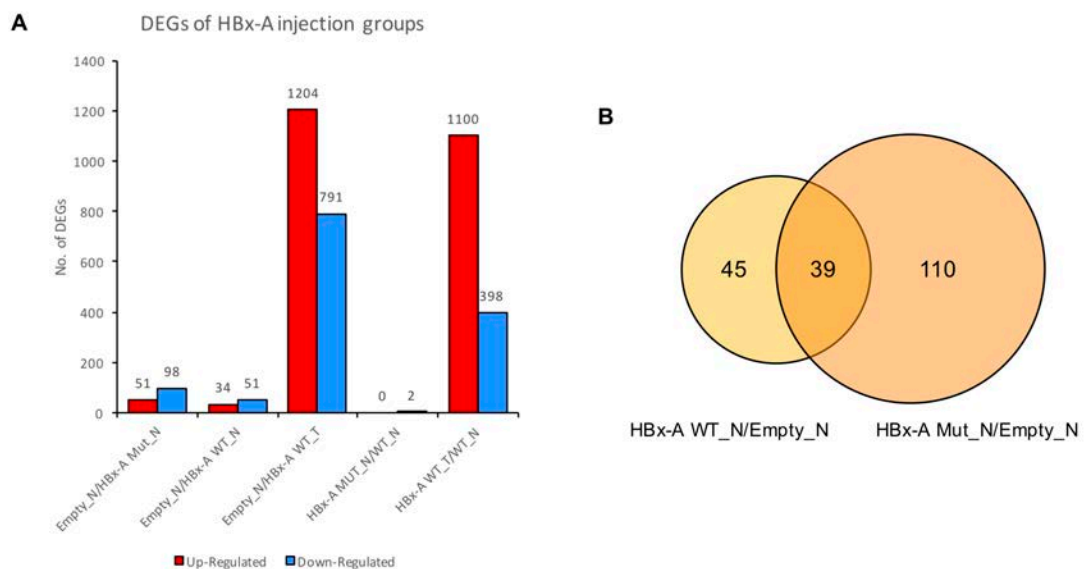


**Figure 18| Differentially expressed genes (DEGs) identified in HBx genotype A (HBx-A) injected. (A)** Number of DEGs in HBx-A Mut (149 DEGs,  $n = 3$ ) normal liver tissue was similar to that of HBx-A WT (85 DEGs,  $n = 4$ ) normal liver tissue compared with empty control ( $n =$

3); while gene expression in tumor induced by HBx-A WT ( $n = 1$ ) had a diverse difference comparing to empty normal control. Only two genes were differentially expressed in normal tissue of HBx-A Mut group compared with HBx-A WT normal group. High gene diversity was observed between tumor and normal tissue of HBx-A WT groups. Red bars represent up-regulated genes. Blue bars represent down-regulated genes. **(B)** Venn diagram showing overlapping DEGs identified in normal tissues of HBx-A WT and Mut injected animals in referencing to empty normal control. N represents normal tissue; T represents tumor tissue.

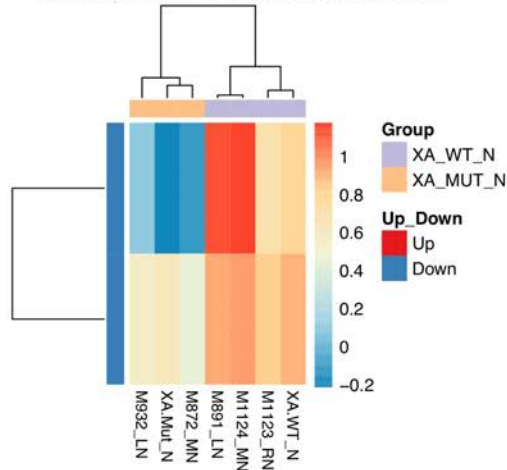
Next, we compared the normal tissues of HBx-A Mut to HBx-A WT, only X-linked lymphocyte-regulated 3A (*Xlr3a*) and family with sequence similarity 47, member E (*Fam47e*) were found to be differentially expressed (down-regulation) and they were not involved in any of the canonical KEGG pathways (**Figure 18A** and **Figure 19A**). A total of 1498 DEGs were identified when comparing the tumor tissue ( $n = 1$ ) to the normal tissues ( $n = 4$ ) injected with wild-type HBx genotype A, in which 1100 genes were found to be up-regulated and 398 genes were found to be down-regulated (**Figure 18A** and **Figure 19B**).

With the DEGs identified in tumor of HBx-A WT injected animal, KEGG analyses was performed. These genes were annotated in six functional classification branches of KEGG pathways including cellular process, environmental information processing, genetic information processing, human disease, metabolism and organismal systems. The top involvement functional pathways of each classification were cell growth and death in cellular process, signal transduction in environmental information processing, folding, sorting and degradation in genetic information processing, cancers: overview in human diseases, global and overview maps, metabolism and immune system in organismal systems (**Figure 19C**). We then matched DEGs with the KEGG pathways and found that the top 20 most significant pathway involved in tumor progression induced by HBx-A WT gene were chemokine signalling pathway ( $q = 1.126 \times 10^{-9}$ ), metabolic pathways ( $q = 8.116 \times 10^{-9}$ ), focal adhesion ( $q = 1.621 \times 10^{-8}$ ), Fc gamma R-mediated phagocytosis ( $q = 1.141 \times 10^{-7}$ ), regulation of actin cytoskeleton ( $q = 1.188 \times 10^{-7}$ ), osteoclast differentiation ( $q = 6.854 \times 10^{-7}$ ), tryptophan metabolism ( $q = 1.272 \times 10^{-6}$ ), AGE-RAGE signalling pathway in diabetic complications ( $q = 3.808 \times 10^{-6}$ ), amoebiasis ( $q = 3.808 \times 10^{-6}$ ), B cell receptor signalling pathway ( $q = 3.871 \times 10^{-6}$ ), arginine and proline metabolism ( $q = 7.238 \times 10^{-6}$ ), *staphylococcus aureus*

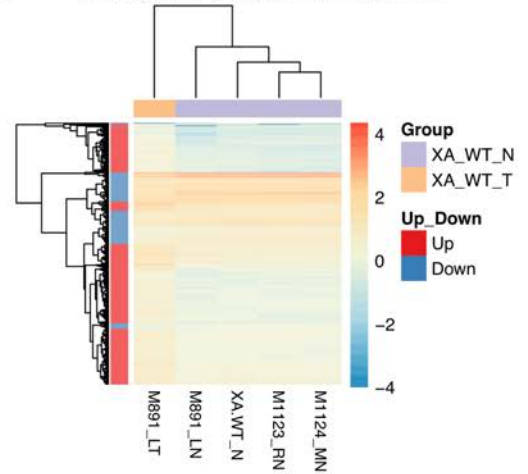
infection ( $q = 1.434 \times 10^{-5}$ ), Fc epsilon RI signalling pathway ( $q = 1.792 \times 10^{-5}$ ), arginine biosynthesis ( $q = 2.434 \times 10^{-5}$ ), leishmaniasis ( $q = 2.582 \times 10^{-5}$ ), Histidine metabolism ( $q = 3.203 \times 10^{-5}$ ), MAPK signalling pathway ( $q = 3.685 \times 10^{-5}$ ), alanine, aspartate and glutamate metabolism ( $q = 4.260 \times 10^{-5}$ ), T cell receptor signalling pathway ( $q = 5.614 \times 10^{-5}$ ), and natural killer cell mediated cytotoxicity ( $q = 5.853 \times 10^{-5}$ ) (**Figure 19D** and **19E**). While the top 5 pathways with the most number of DEGs involved were (i) metabolic pathway, in which 63 genes were up-regulated and 143 genes were down-regulated; (ii) focal adhesion with 59 DEGs, in which 54 genes were up-regulated and 5 genes were down regulated; (iii) regulation of actin cytoskeleton with 56 DEGs in total, in which 54 genes were up-regulated and 2 genes were down-regulated; (iv) MAPK signalling pathway with 54 DEGs, in which 49 genes were up-regulated and 5 genes were down-regulated; and (v) chemokine signalling pathway, in which 47 genes were up-regulated and 5 genes were down-regulated (**Figure 19D**).

To summarize the findings in HBx genotype A study, expression of *Mup12* was significantly up-regulated (760-fold increase) in normal tissues of both HBx-A WT and Mut injected animals referencing to empty normal control. There was low genetic difference between experimental animals injected with either mutant or wild-type HBx gene of genotype A for there was no significant difference in tumor burden rate and only 2 DEGs were identified between these groups. On the other hand, when comparing the tumor with the normal tissue of the HBx-A WT group, 1498 DEGs were identified, and most of the DEGs were found to be associated with signalling pathways, such as focal adhesion, regulation of actin cytoskeleton, MAPK signalling pathway, chemokine signalling pathway, and Rap1 signalling pathway.

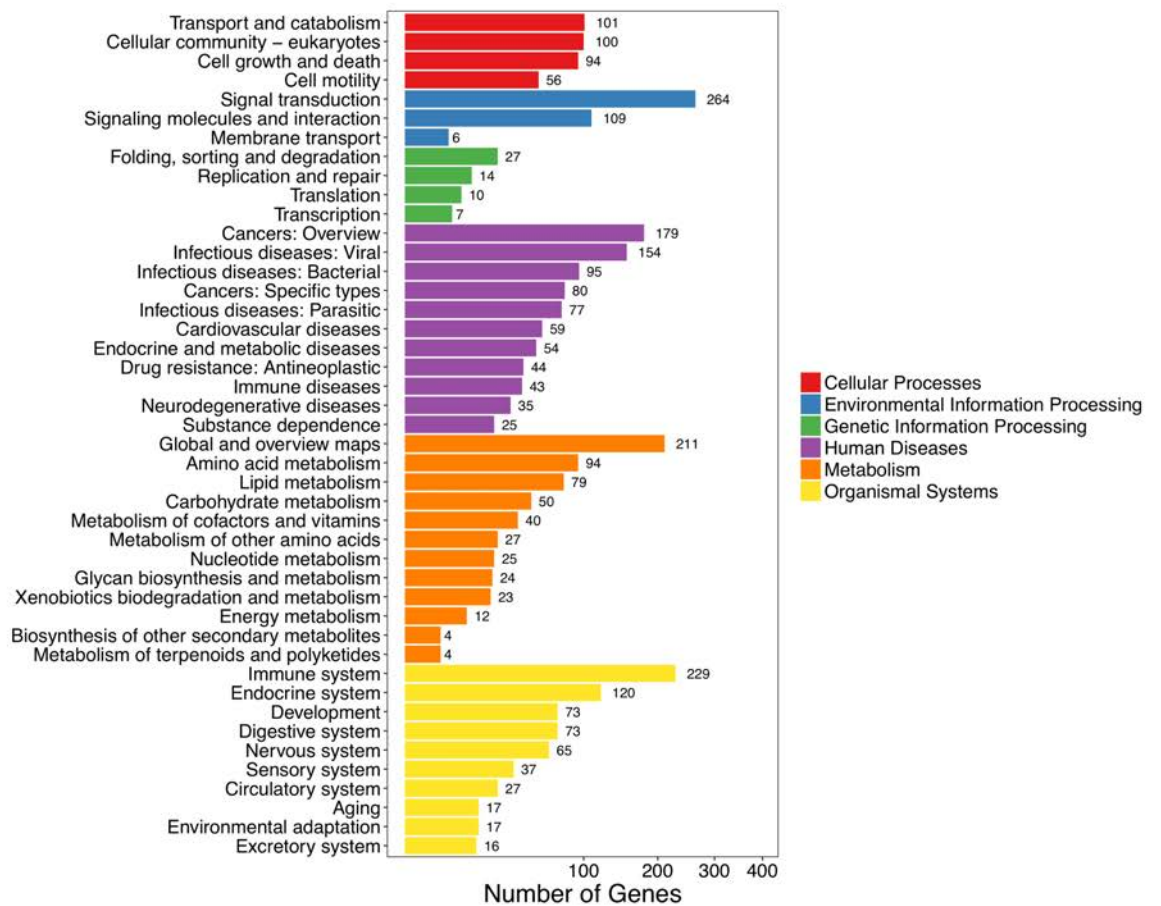
**A Heatmap of DEGs found between normal tissue of HBx-A Mut and WT**



**B Heatmap of DEGs found between normal and tumor tissues of HBx-A WT**



**C KEGG functional classifications of DEGs found between normal and tumor tissues of HBx-A WT**



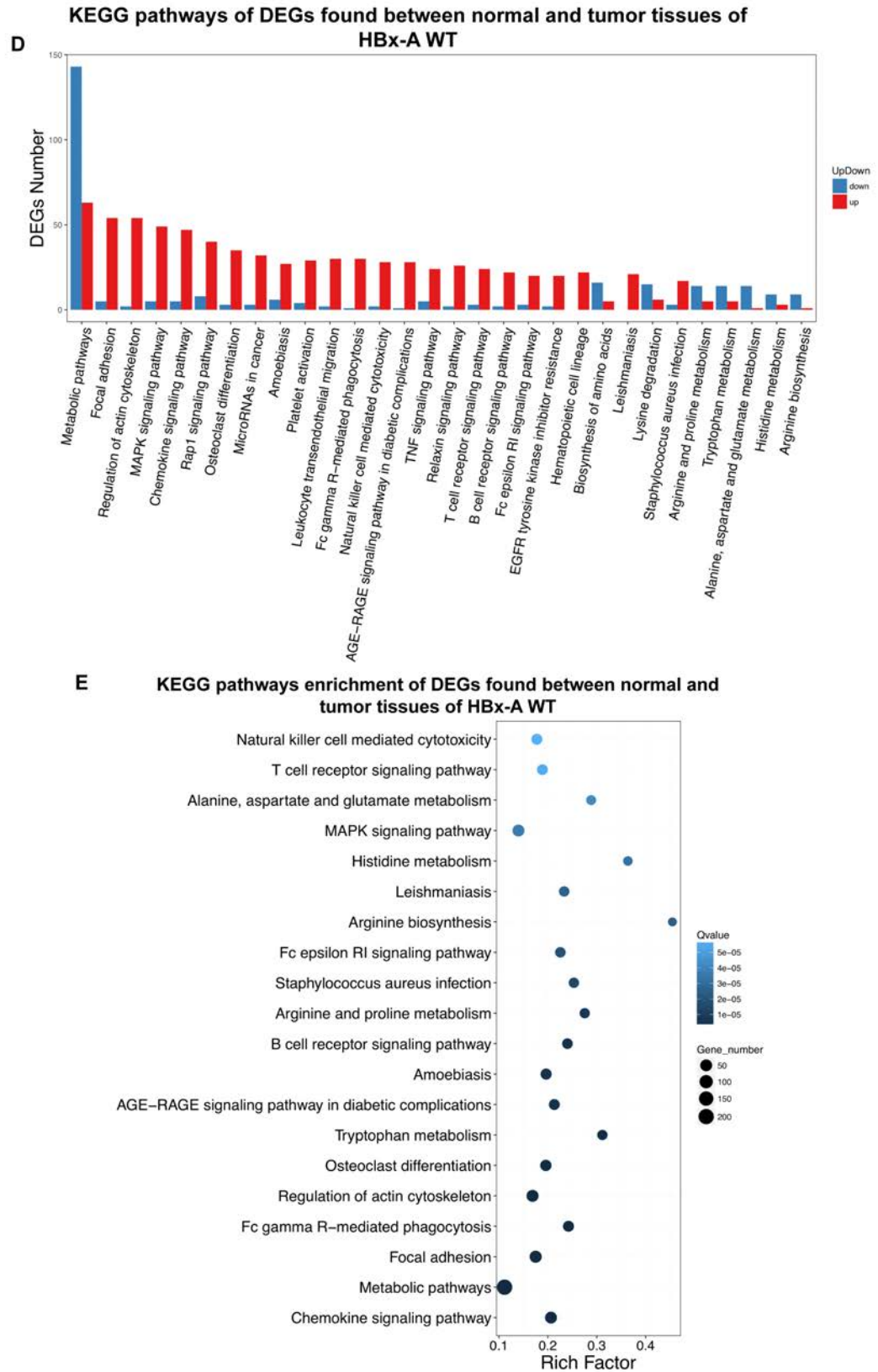


**Figure 19| RNA-seq result of HBx-A mutant and wild-type injected animals. (A)** Heatmap of DEGs found between normal tissues of HBx-A Mut and WT experimental animals. **(B)** Heatmap of DEGs found between normal and tumor tissues of HBx-A WT experimental

animals. **(C)** KEGG functional classifications of DEGs found between normal and tumor tissues of HBx-A WT experimental animals. **(D)** KEGG pathways of DEGs found between normal and tumor tissues of HBx-A WT experimental animals. **(E)** KEGG pathways enrichment of DEGs found between normal and tumor tissues of HBx-A WT experimental animals. N represents normal tissue; T represents tumor tissue. Red bars represent up-regulated genes. Blue bars represent down-regulated genes.

### 3.5.2 RNA sequencing result of HBx genotype B

Similar to genotype A, we first compared the RNA expression profiles in normal and tumor tissue of HBx-B Mut and HBx-B WT experimental groups with empty control group with the predisposal background of *shp53*. Since no solid tumor was isolated from HBx-B WT group, so RNA expression profile for tumor induced by HBx-B WT group was not included in the comparison of this study. There were relatively low genetic differences in RNA expression profile of normal tissues between HBx-B Mut ( $n = 4$ ), HBx-B WT ( $n = 3$ ) and empty control ( $n = 3$ ) groups. Only 13 genes were up-regulated and 26 genes were down-regulated in normal tissues of HBx-B Mut compared with empty control; and 7 genes were up-regulated and 20 genes were down-regulated in normal tissues of HBx-B WT compared with empty control (**Figure 20A**). Large genetic differences between RNA expression profiles of HBx-B Mut tumors ( $n = 3$ ) and that of empty normal control, in which 339 genes were up-regulated and 439 genes were down-regulated (**Figure 20A**). There were 10 common DEGs identified in normal tissues of HBx-B WT and HBx-B Mut groups in referencing to the empty normal control, in which only 1 DEGs were up-regulated and 9 DEGs were down-regulated, including *Fah* and *Susd4*, which were also commonly found in HBx-A Mut and WT injected animals (**Figure 20B**).

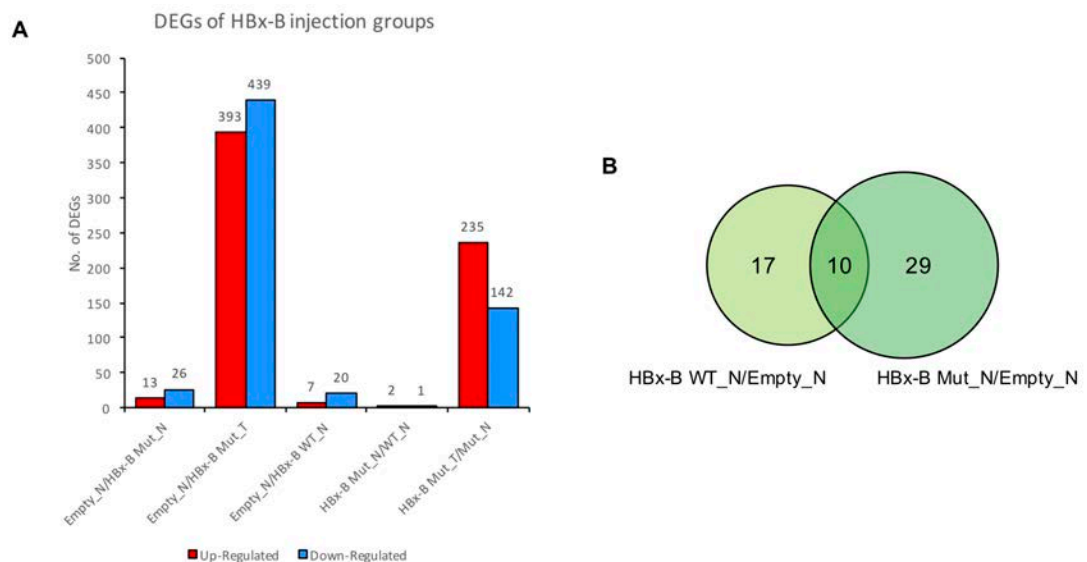


**Figure 20| Differentially expressed genes (DEGs) identified in HBx-B injected animal groups.** (A) Number of DEGs in HBx-B Mut (39 DEGs,  $n = 4$ ) normal liver tissue was similar to that of HBx-B WT (27 DEGs,  $n = 3$ ) normal liver tissue compared with empty control ( $n = 3$ ); while gene expression in tumor induced by HBx-B Mut (832 DEGs,  $n = 3$ ) had a diverse difference comparing to empty normal control. Only 3 genes were differentially expressed in

normal tissue of HBx-B Mut group compared with HBx-B WT normal group. High gene diversity (377 DEGs) was observed between tumor and normal tissue of HBx-B Mut groups. Red bars represent up-regulated genes. Blue bars represent down-regulated genes. **(B)** Venn diagram showing overlapping DEGs identified in normal tissues of HBx-B WT and Mut injected animals in referencing to empty normal control. N represents normal tissue; T represents tumor tissue.

Comparing the RNA expression profiles in normal tissues of HBx-B Mut to HBx-B WT group, three genes were found to be differentially expressed, in which *Mup14* and ectodysplasin-A (*Eda*) were up-regulated, while predicted gene 5779 (*Gm5779*) was down-regulated (**Figure 20A and 21A**). These DEGs played a role in arachidonic acid metabolism, ribosome, cytokine-cytokine receptor interaction and metabolic pathways of KEGG pathways (**Figure 21B, 21C and 21D**).

Next, we compared RNA expression profiles of the tumor ( $n = 3$ ) and normal tissues ( $n = 4$ ) of HBx-B Mut injected mice, 377 DEGs were totally identified, in which 235 genes were found to be up-regulated and 142 genes were found to be down-regulated in the tumor tissues compared to its normal tissues (**Figure 20A and 22A**). These DEGs were annotated in cellular processes, environmental information processing, genetic information processing, human diseases, metabolism and organismal systems. The highest amount of DEGs in each branch was cellular community – eukaryotes (26 DEGs) in cellular processes; signalling transduction (57 DEGs) in environmental information processing; folding, sorting and degradation (7 DEGs) in genetic information processing; cancers: overview (49 DEGs) in human diseases; global and overview maps (60 DEGs) in metabolism; and immune system (28 DEGs) in organismal systems (**Figure 22B**).

The top 20 KEGG pathways that were most significantly involved by these DEGs included chemical carcinogenesis ( $q = 1.441 \times 10^{-5}$ ), bile secretion ( $q = 4.085 \times 10^{-5}$ ), arginine biosynthesis ( $q = 1.645 \times 10^{-4}$ ), alanine, aspartate and glutamate metabolism ( $q = 2.527 \times 10^{-4}$ ), arachidonic acid metabolism ( $q = 3.657 \times 10^{-4}$ ), metabolic pathways ( $q = 5.120 \times 10^{-4}$ ), linoleic acid metabolism ( $q = 7.862 \times 10^{-4}$ ), biosynthesis of amino acids ( $q = 9.144 \times 10^{-4}$ ), steroid hormone biosynthesis ( $q = 1.609 \times 10^{-3}$ ), inflammatory mediator regulation of transient receptor potential (TRP) channels ( $q = 1.887 \times 10^{-3}$ ),

ECM-receptor interaction ( $q = 1.887 \times 10^{-3}$ ), cysteine and methionine metabolism ( $q = 6.172 \times 10^{-3}$ ), retinol metabolism ( $q = 1.697 \times 10^{-2}$ ), proximal tubule bicarbonate reclamation ( $q = 2.726 \times 10^{-2}$ ), glycine, serine and threonine metabolism ( $q = 2.842 \times 10^{-2}$ ), serotonergic synapse ( $q = 3.910 \times 10^{-2}$ ), focal adhesion ( $q = 5.072 \times 10^{-2}$ ), mineral absorption ( $q = 5.072 \times 10^{-2}$ ), seleno compound metabolism ( $q = 5.125 \times 10^{-2}$ ), and fluid shear stress and atherosclerosis ( $q = 6.008 \times 10^{-2}$ ) (**Figure 22C**). While the top 5 pathways with the most number of DEGs involved were (i) metabolic pathway with 59 DEGs, in which 13 genes were up-regulated and 46 genes were down-regulated; (ii) chemical carcinogenesis with 14 DEGs, in which 6 genes were up-regulated and 8 genes were down-regulated; (iii) focal adhesion with 14 DEGs up-regulated; (iv) arachidonic acid metabolism with 13 DEGs, in which 4 genes were up-regulated and 9 genes were down-regulated; and (v) Ras signalling pathway with 13 DEGs, in which 10 genes were up-regulated and 3 genes were down-regulated (**Figure 22D**).

#### ***Serum metabolites analysis using UPLC-Orbitrap-MS***

The RNA-seq results revealed the importance of metabolic disorder in tumor development of HBx injected mice. Therefore, metabolomics analysis on serum samples of HBx genotype B experimental mice performed using UPLC-Orbitrap-MS. This was used to determine changes in metabolites as a result of HBx expression. Fold-changes of metabolites were compared between mutant and wild-type groups. There was a significantly higher abundance of xanthine (67.23-fold increase) in HBx-B mutant compared to its wild-type variants, higher abundance of its downstream metabolites urate (2.15-fold increase) and 5-hydroxyisourate (3.55-fold increase) were detected (**Figure 23B**). These metabolites are produced during the break down of tumor cells (111), providing further evidence of the involvement of HBx-B mutant gene in liver tumorigenesis. Furthermore, metabolites 9,10-dihydroxy-12Z-octadecenoic acid (9,10-DiHOME) and 12,13-dihydroxy-9Z-octadecenoic acid (12,13-DiHOME) involved in linoleic acid metabolism were significantly reduced ( $p < 0.05$ ) in mutant serum than that in wild-type serum (**Figure 23C**). Both of the serum levels of these metabolites and RNA expression level of cytochrome P450 family 2 subfamily C (Cyp2C) proteins family encoding genes were down-regulated (**Figure 23C**). Additionally, the ion abundances of metabolites, such as taurocholate (TCA), taurochenodeoxycholate (TCDCa) and taurohyodeoxycholate

(THDCA)/tauroursodeoxycholate (TUDCA), in the synthesis of bile acids (BAs) from cholesterol were significantly reduced in the mutant serum compared to its wild-type serum (**Figure 23D**). This finding was matched with our RNA-seq result that the expression level of *Cyp7a1*, which encodes the key enzyme that converts cholesterol to BAs, was significantly down-regulated.

To summarize the RNA expression profiles of the wild-type and mutant HBx genotype B injected animals, there was relatively low genetic background differences in normal tissues of HBx-B Mut and WT groups compared to empty control group. And low genetic background differences in RNA expression profiles in normal tissues of HBx-B Mut and WT, only 3 DEGs were identified and no significant pathways were annotated. This indicated that the genetic background between the wild-type and mutant HBx genotype B injected animals were similar and DEGs found in tumor tissues were highly associated with disease progression. Next, in order to find out the genetic difference between the tumor and normal tissues, RNA expression profiles of which in HBx-B Mut injected animals identified 377 DEGs. These DEGs were highly associated with metabolic pathways, such as arachidonic acid metabolism, bile secretion, biosynthesis of amino acid and steroid hormone biosynthesis, and canonical signalling pathways including chemical carcinogenesis, focal adhesion, Ras signalling pathway, inflammatory mediator regulation of TRP channels, and ECM-receptor intermediation. Moreover, the participation of metabolic disorder was also confirmed by metabolomics analysis using the serum extracted from the HBx-B injected animals.

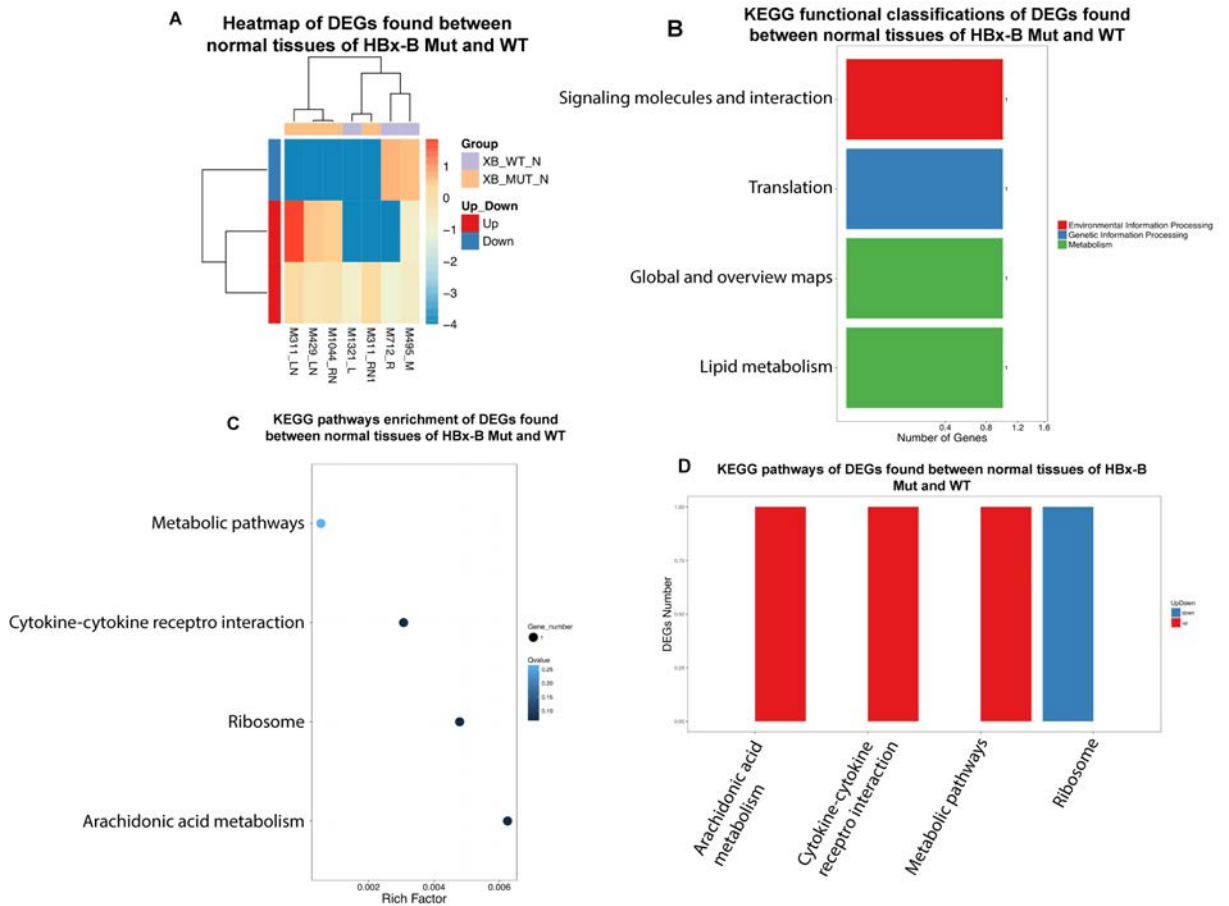
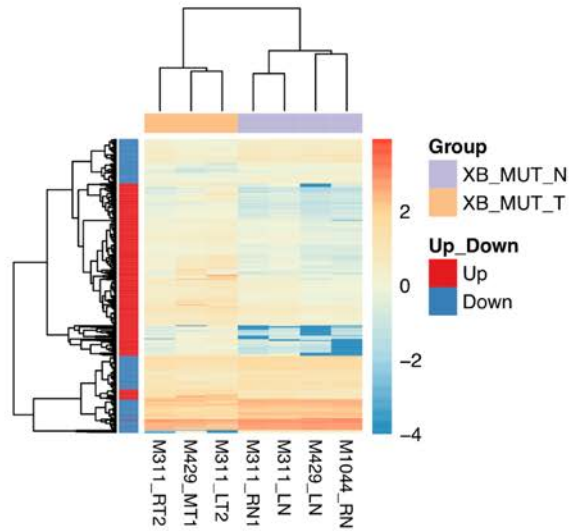
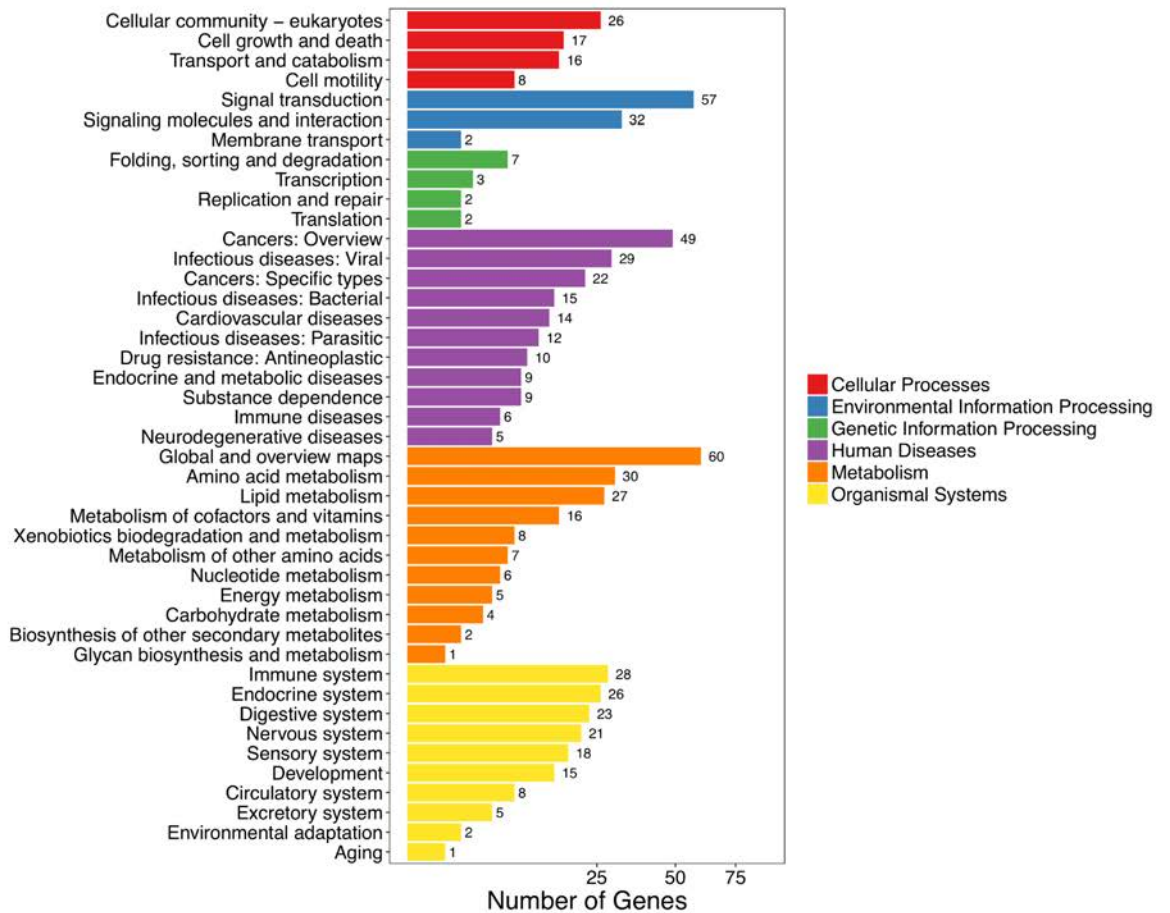


**Figure 21| RNA-seq result of normal tissues of HBx-B mutant and wild-type injected animals.** (A) Heatmap of DEGs found between normal tissues of HBx-B Mut and WT experimental animals. (B) KEGG functional classifications of DEGs found between normal tissues of HBx-B Mut and WT experimental animals. (C) KEGG pathways enrichment of DEGs found between normal tissues of HBx-B Mut and WT experimental animals. (D) KEGG pathways of DEGs found between normal tissues of HBx-B Mut and WT experimental animals. N represents normal tissue; T represents tumor tissue. Red bars represent up-regulated genes. Blue bars represent down-regulated genes.

**A Heatmap of DEGs found between normal and tumor tissues of HBx-B Mut**

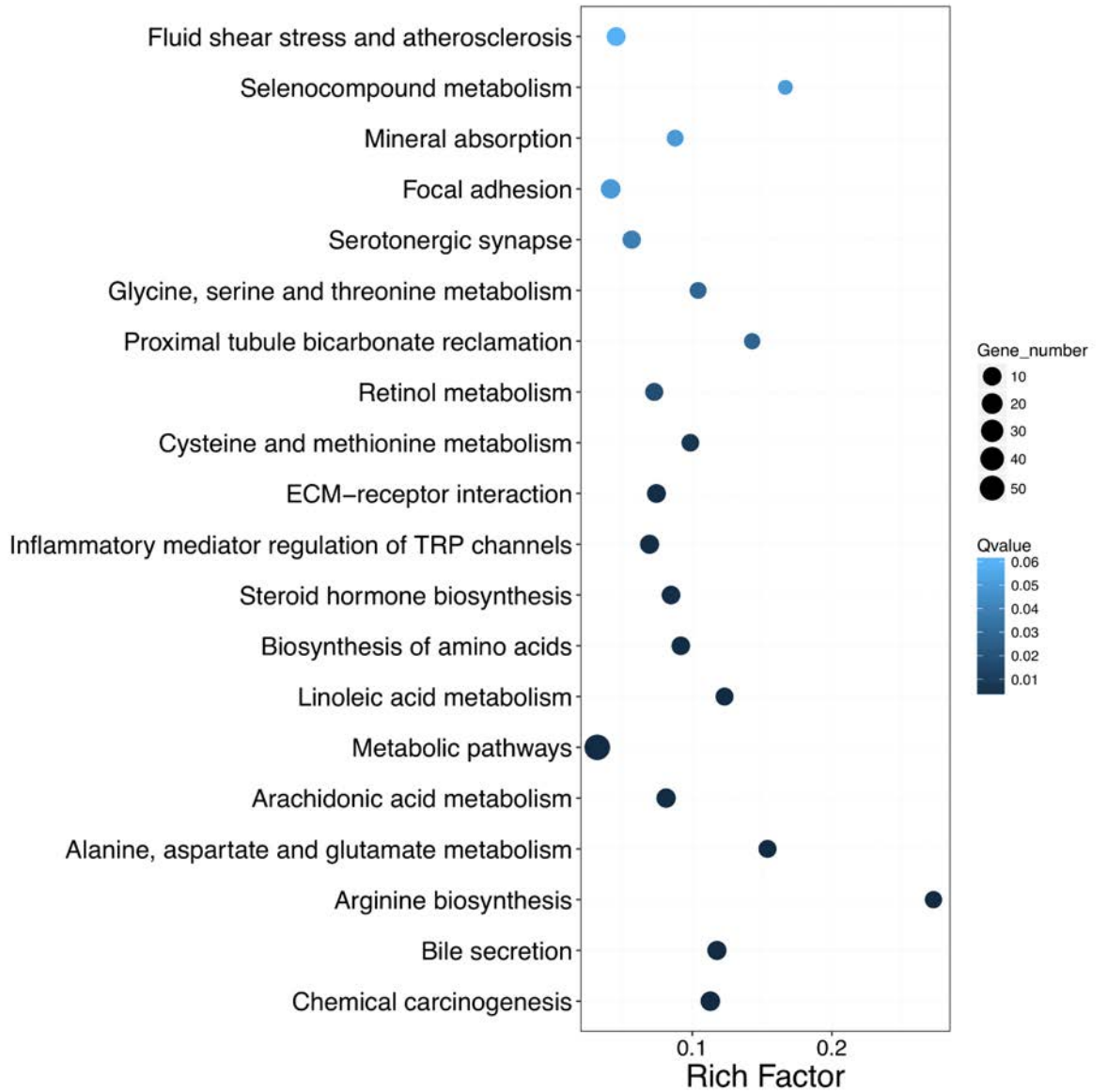


**B KEGG functional classifications of DEGs found between normal and tumor tissues of HBx-B Mut**

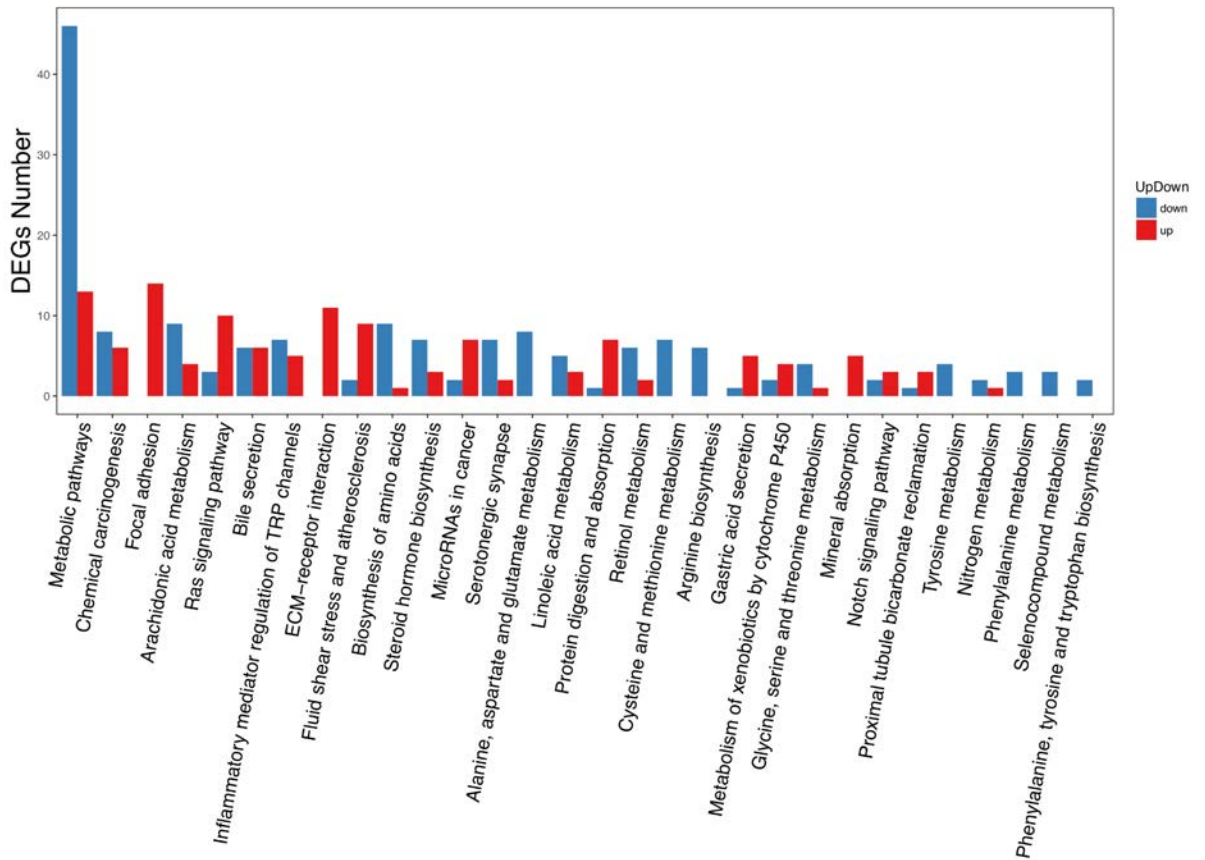


C

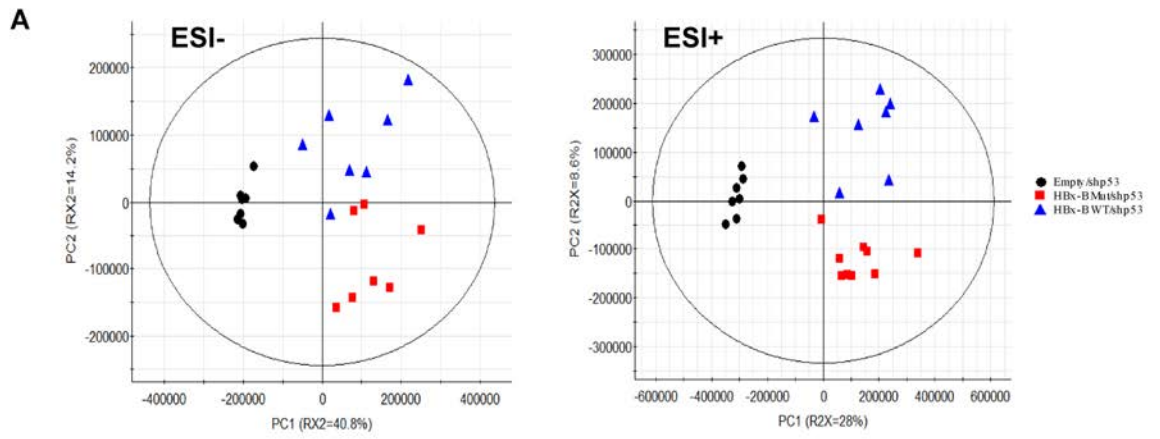
**KEGG pathways enrichment of DEGs found between normal and tumor tissues of HBx-B Mut**



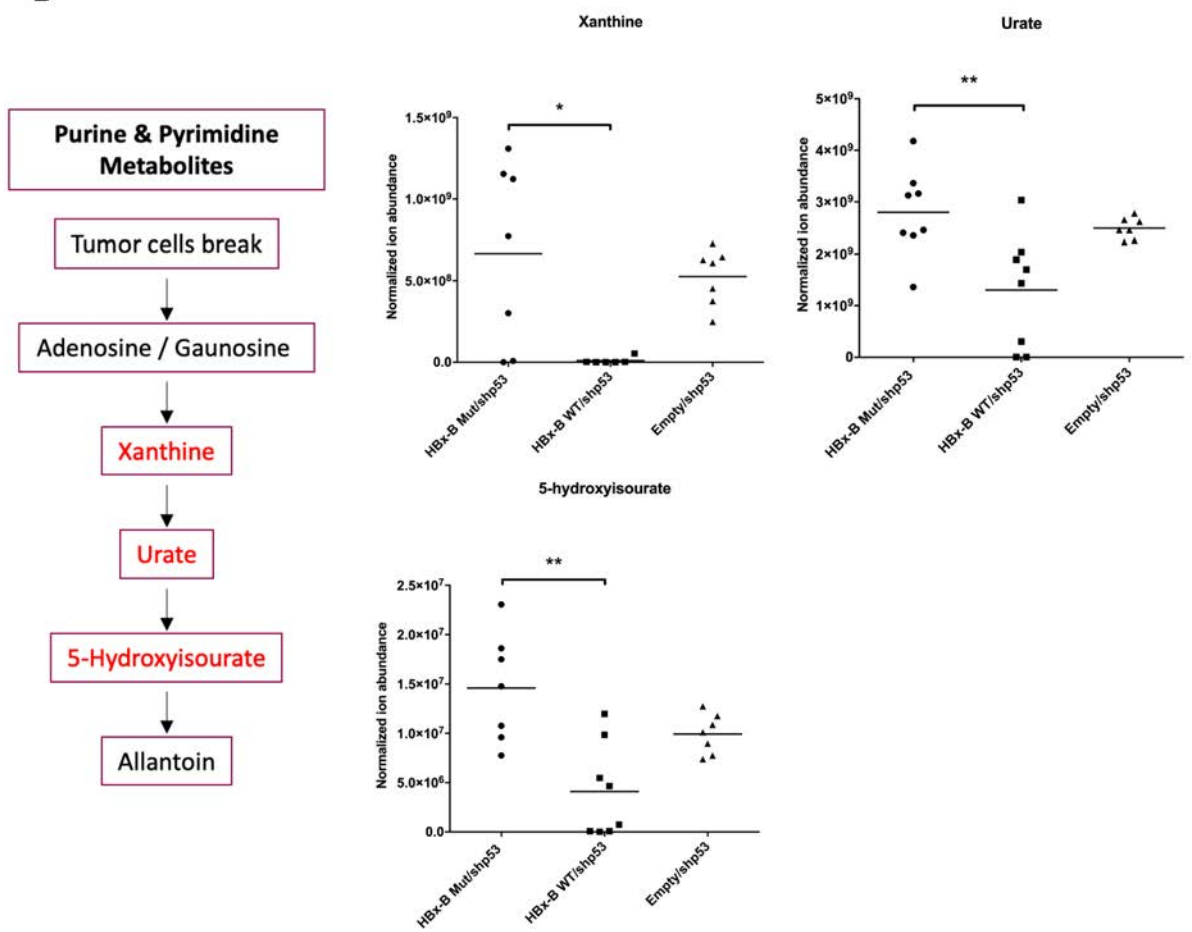
**D** KEGG pathways of DEGs found between normal and tumor tissues of HBx-B Mut



**Figure 22| RNA-seq result of normal and tumor tissues of HBx-B mutant injected animals.** (A) Heatmap of DEGs found between normal and tumor tissues of HBx-B Mut experimental animals. (B) KEGG functional classifications of DEGs found between normal and tumor tissues of HBx-B Mut experimental animals. (C) KEGG pathways enrichment of DEGs found between normal and tumor tissues of HBx-B Mut experimental animals. (D) KEGG pathways of DEGs found between normal and tumor tissues of HBx-B Mut experimental animals. N represents normal tissue; T represents tumor tissue. Red bars represent up-regulated genes. Blue bars represent down-regulated genes.



**B**



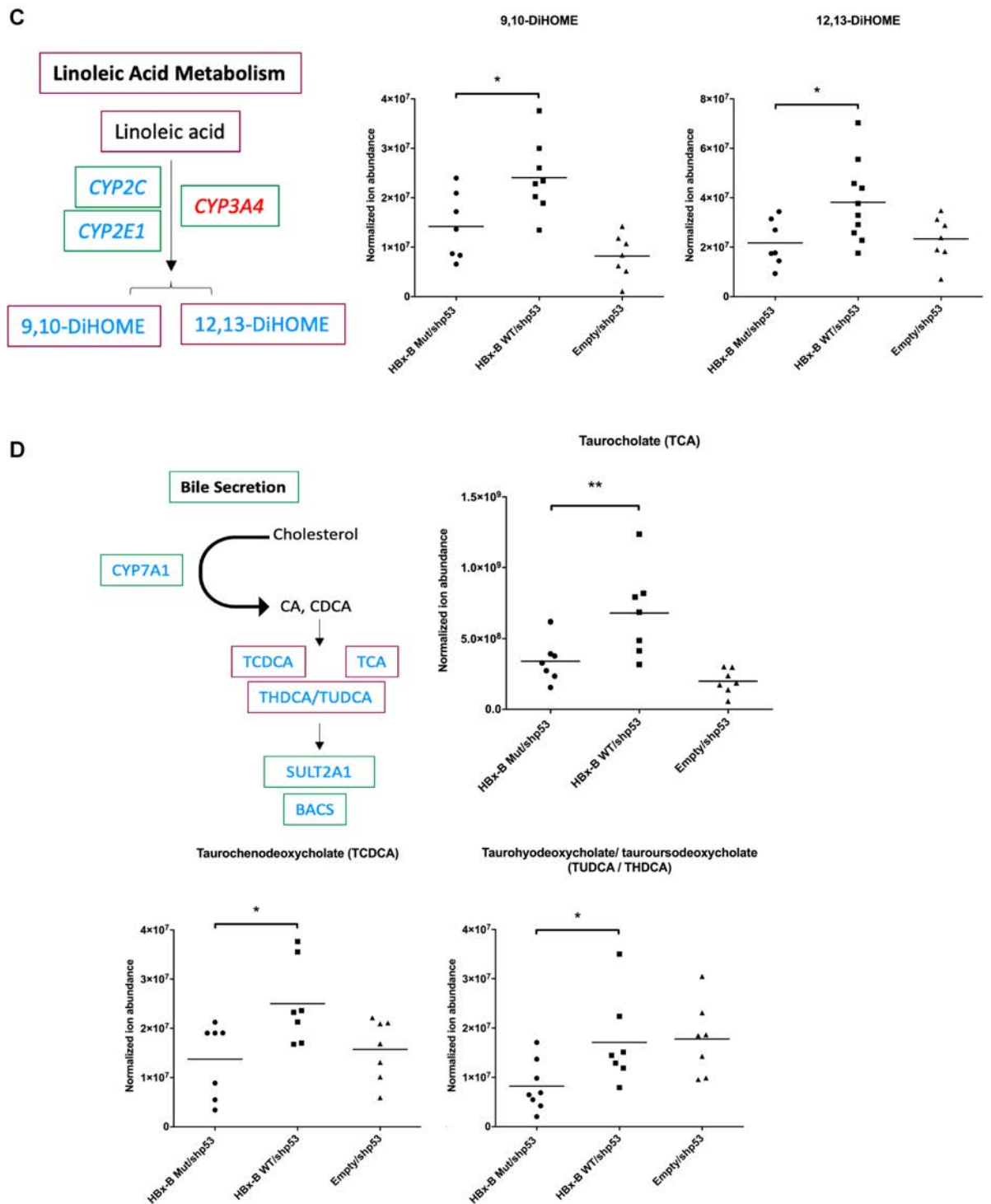


**Figure 23| Serum metabolites of HBx-B/shp53 injected animals.** (A) PLS-DA score plots of serum data using UPLC-Orbitrap-MS acquired at negative and positive ESI modes between HBx-B mutant and wild-type groups. The cumulative R2X, R2Y, and Q2 values of the score plots from data acquired at negative mode and positive mode were 0.550, 0.743 and 0.537, and 0.367, 0.843, 0.562 respectively, validating the classification of three groups in its score plots without overfitting. (B) Scatter plots of metabolites associated with purine and pyrimidine metabolism. (C) Scatter plots of metabolites associated with linoleic acid metabolism. (D) Scatter plots of metabolites associated with bile secretion. Mean  $\pm$  S.D.;  $p$ , unpaired student

*t*-test, \* $p \leq 0.05$ , \*\* $p \leq 0.01$ . Green box represents DEG identified by RNA-sequencing; violet box represents metabolite identified by UPLC-Orbitrap-MS. Blue word represents down-regulated DEG or lower abundance metabolite; red word represents up-regulated DEG or higher abundance metabolite.

### 3.5.3 KEGG pathways of HBx genotype C

Similarly, we first compared the RNA expression profiles in normal and tumor tissue of HBx-C Mut and HBx-C WT experimental groups with empty normal control group with the predisposal background of *shp53*. There were relatively higher genetic differences in RNA expression profile of normal tissues of HBx-C Mut, and HBx-C WT in referring to that of empty control groups. The results show 54 genes were up-regulated and 77 genes were down-regulated in normal tissues of HBx-C Mut compared with empty control; while 55 genes were up-regulated and 69 genes were down-regulated in normal tissues of HBx-C WT compared with normal empty control (**Figure 24A**). Large genetic differences in RNA expression profile of the tumors of HBx-C Mut and WT experimental groups compared to that of empty normal control, in which 68 genes were up-regulated and 259 genes were down-regulated in tumors of HBx-C Mut animals; while 150 genes were up-regulated and 286 genes were down-regulated in tumors of HBx-C WT animals (**Figure 24A**). There were 46 common DEGs identified in normal tissues of HBx-C WT and HBx-C Mut groups when compared to the empty normal control, in which 17 DEGs were up-regulated and 29 DEGs were down-regulated, including *Fah* and *Susd4*, which were also found in HBx genotype A and B injected animals (**Figure 24B**).

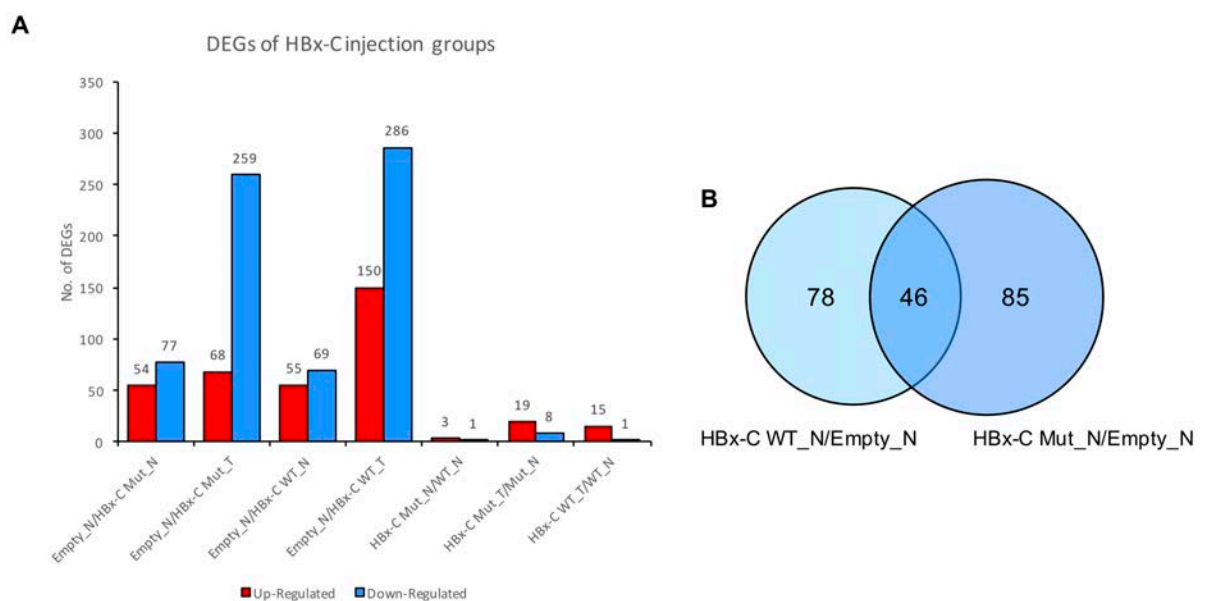


**Figure 24| Differentially expressed genes (DEGs) identified in HBx-C injected animal groups. (A)** Number of DEGs in HBx-C Mut (n = 2) normal liver tissue compared with empty control (n = 3) was 131; and that HBx-B WT (n = 3) normal liver tissue compared with empty

control was 327; while gene expression in tumor induced by HBx-C Mut (327 DEGs, n = 2) and HBx-C WT (436 DEGs, n = 3) had a diverse difference comparing to empty normal control. Only 4 genes were differentially expressed in normal tissue of HBx-C Mut group compared with HBx-C WT normal group. DEGs between tumor and normal tissue of HBx-C Mut groups was 27 and that in HBx-C WT groups was 16. Red bars represent up-regulated genes. Blue bars represent down-regulated genes. **(B)** Venn diagram showing overlapping DEGs identified in normal tissues of HBx-C WT and Mut injected animals in referencing to empty normal control. N represents normal tissue; T represents tumor tissue.

Comparing RNA expression profiles of the normal tissues in HBx-C Mut group to HBx-C WT group, four genes were found to be differentially expressed, including serine/threonine/tyrosine kinase 1 (*Styk1*), leucine-rich repeats and transmembrane domains 1 (*Lrtm1*) and N-acetyltransferase 8 (GCN5-related) family member 3 (*Nat8f3*) were up-regulated; while cysteine and glycine-rich protein 3 (*Csrp3*) was down-regulated (**Figure 24A and 25A**). Only *Lrtm1* and *Nat8f3* (up-regulated) were involved in the canonical KEGG pathways, in which *Lrtm1* was associated with axon guidance, while *Nat8f* was associated with metabolic pathways and alanine, aspartate and glutamate metabolism (**Figure 25B, 25C and 25D**).

When comparing RNA expression profiles of the tumor tissues and its adjacent normal tissues of HBx-C wild-type injected mice, 15 genes were up-regulated and only 1 gene was down-regulated (**Figure 24A and 26A**). These DEGs spanned across different branches of KEGG functional classifications, including cell growth and death, cell motility, cellular community – eukaryotes, signal transduction, folding, sorting and degradation, cancers: overview, cancers: specific types, infectious diseases: viral, amino acid metabolism, global and overview maps, development, digestive system, endocrine system and immune system (**Figure 26B**). The most significantly distorted KEGG pathways included microRNAs in cancer (DEGs = 3,  $q = 0.0102$ ) (**Figure 26C**). These three DEGs, solute carrier family 7 (cationic amino acid transporter), member 1 (*Slc7a1*), stathmin (*Stmn1*) and M-phase inducer phosphatase 1 (*Cdc25a*), were up-regulated in the tumor of HBx-C WT injected animals and found to be involved in the HCC progression induced by HBV.

Comparing the RNA expression profiles between tumor and normal tissues of HBx-C Mut injected animals, 27 DEGs were found, including 19 up-regulated genes and 8

down-regulated genes in the tumor tissues (**Figure 24A** and **27A**). These DEGs involved in cellular processes, environmental information processing, genetic information processing, human diseases, metabolism and organismal systems (**Figure 27B**). Although no KEGG pathway was significantly distorted by these DEGs, pathways such as thyroid hormone synthesis ( $q = 0.1322$ ), long-term potentiation ( $q = 0.1322$ ), gastric acid secretion ( $q = 0.1322$ ), aldosterone synthesis and secretion ( $q = 0.1322$ ), and Ras signalling pathway ( $q = 0.1322$ ) indicated the involvement of some DEGs (**Figure 27C** and **27D**).

Finally, we compared the RNA expression profiles from tumor tissues of HBx-C Mut and HBx-C WT injected animals. Twenty-eight DEGs were identified, in which 7 genes were up-regulated and 21 genes were down-regulated in the tumor of the HBx-C Mut injected animals (**Figure 24A** and **28A**). Cell death-inducing DNA fragmentation factor, alpha subunit-like effector A (*Cidea*) and tubulin, alpha 8 (*Tuba8*) were down-regulated in the apoptosis pathway, growth factor receptor bound protein 2-associated protein 1 (*Gab1*) and insulin-like growth factor 2 (*Igf2*) were up-regulated in the hepatocellular carcinoma, proteoglycans in cancer and Ras signalling pathways, while signal recognition particle 54B (*Srp54b*) was down-regulated in the protein export pathway (**Figure 28B**, **28C** and **28D**).

To summarize the RNA expression profiles of the wild-type and mutant HBx genotype C injected animals, as expected, only 4 DEGs found in normal tissues between HBx mutant and wild-type injected groups and no significant pathways were annotated. This indicated that the genetic background between the wild-type and mutant HBx genotype C injected animals were more or less the same. Next, only 15 DEGs were identified in tumor of HBx-C WT comparing with its corresponding normal tissues, and 3 of these DEGs with up-regulation were associated with the HCC progression induced by HBV. Thirdly, 27 DEGs were found in the tumor of HBx-C mutant injected animals compared to its normal counterparts. However, no KEGG pathway was significantly distorted by these DEGs. Lastly, we compared the RNA expression profiles in tumors of HBx-C WT and Mut injected groups, 28 DEGs were identified. Although these DEGs did not significantly distort the pathways, *Gab1* and *Igf2*, which were up-regulated in tumor found in HBx-C Mut group, were found to be associated with hepatocellular carcinoma, proteoglycans in cancer and Ras signalling pathways.

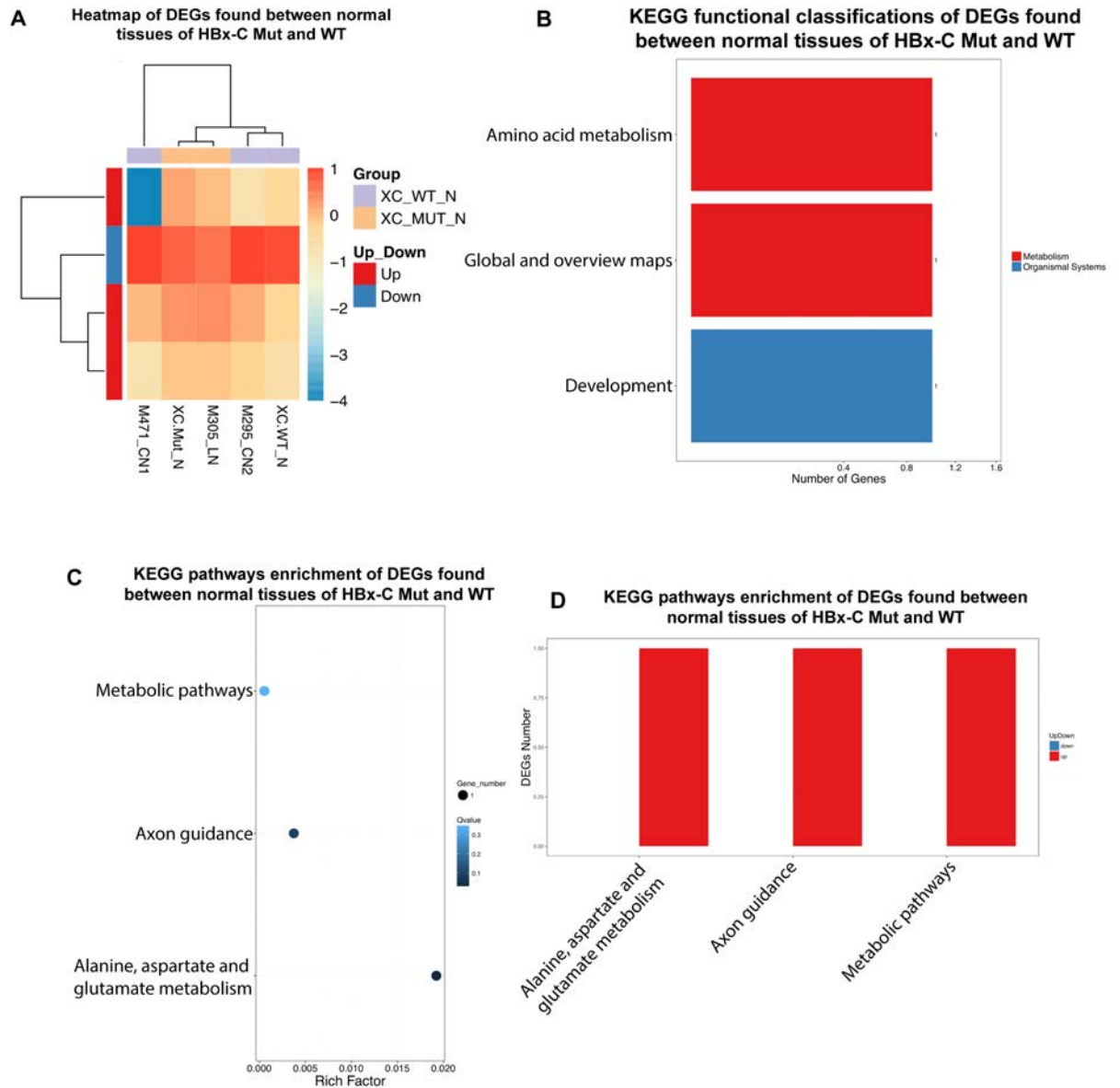
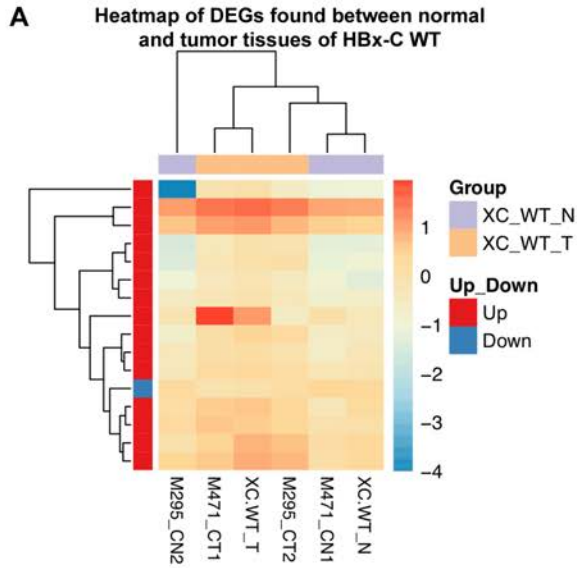
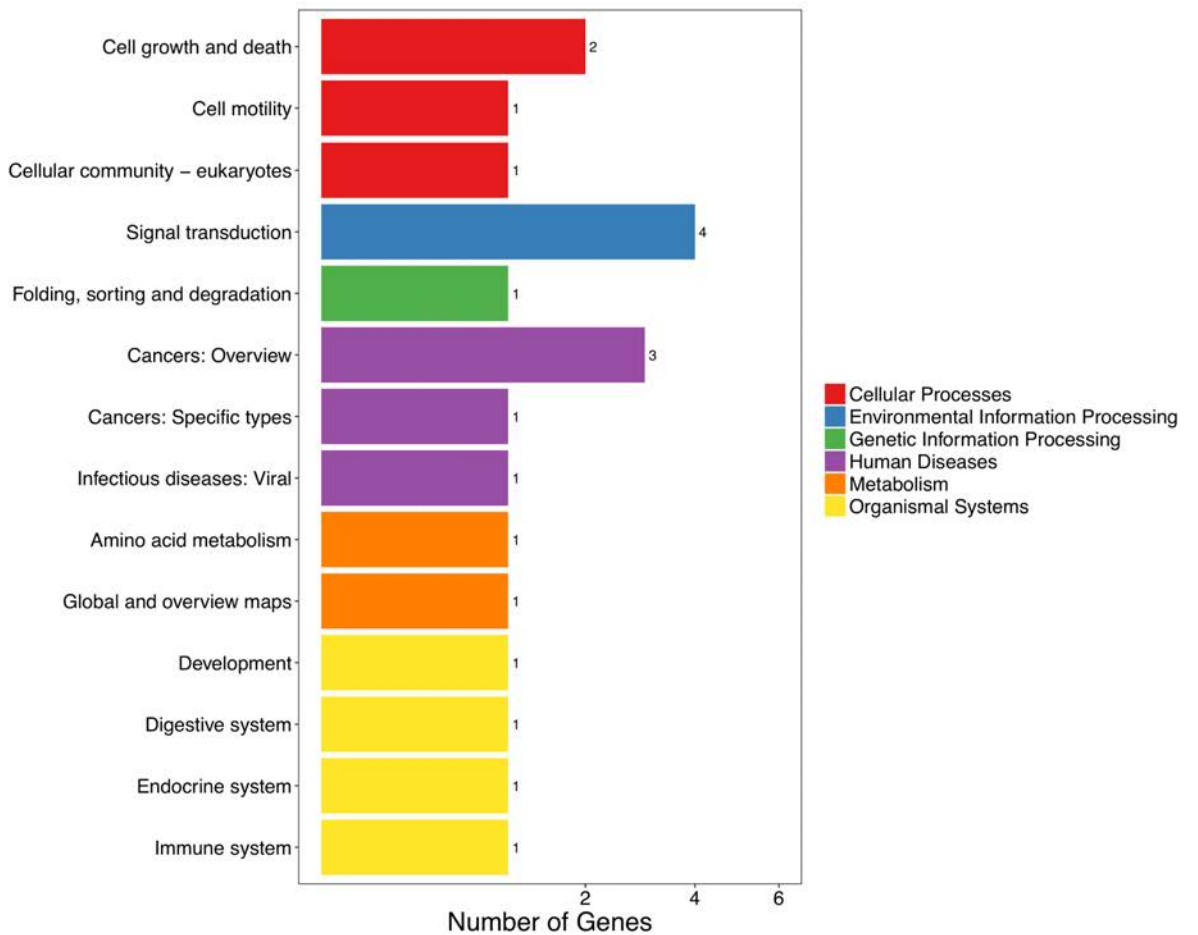


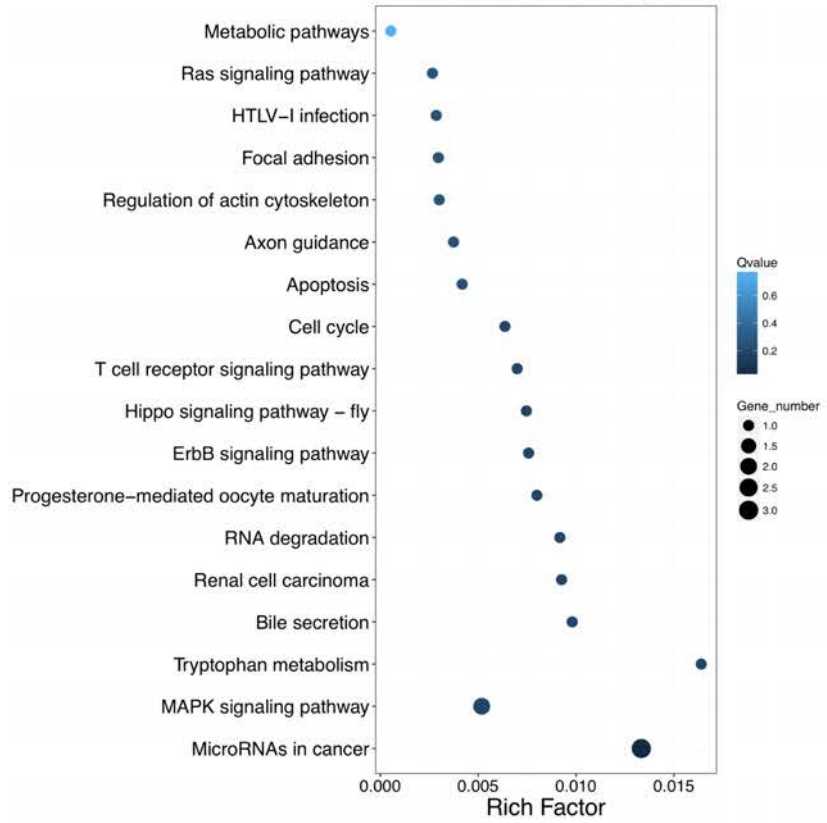
**Figure 25| RNA-seq result of normal tissues of HBx-C mutant and wild-type injected animals. (A)** Heatmap of DEGs found between normal tissues of HBx-C Mut and wild-type experimental animals. **(B)** KEGG functional classifications of DEGs found between normal tissues of HBx-C Mut and wild-type experimental animals. **(C)** KEGG pathways enrichment of DEGs found between normal tissues of HBx-C Mut and wild-type experimental animals. **(D)** KEGG pathways of DEGs found between normal tissues of HBx-C Mut and wild-type experimental animals. N represents normal tissue; T represents tumor tissue. Red bars represent up-regulated genes. Blue bars represent down-regulated genes.



**B** KEGG functional classifications of DEGs found between normal and tumor tissues of HBx-C WT



**C KEGG pathways enrichment of DEGs found between normal and tumor tissues of HBx-C WT**



**D KEGG pathways of DEGs found between normal and tumor tissues of HBx-C WT**

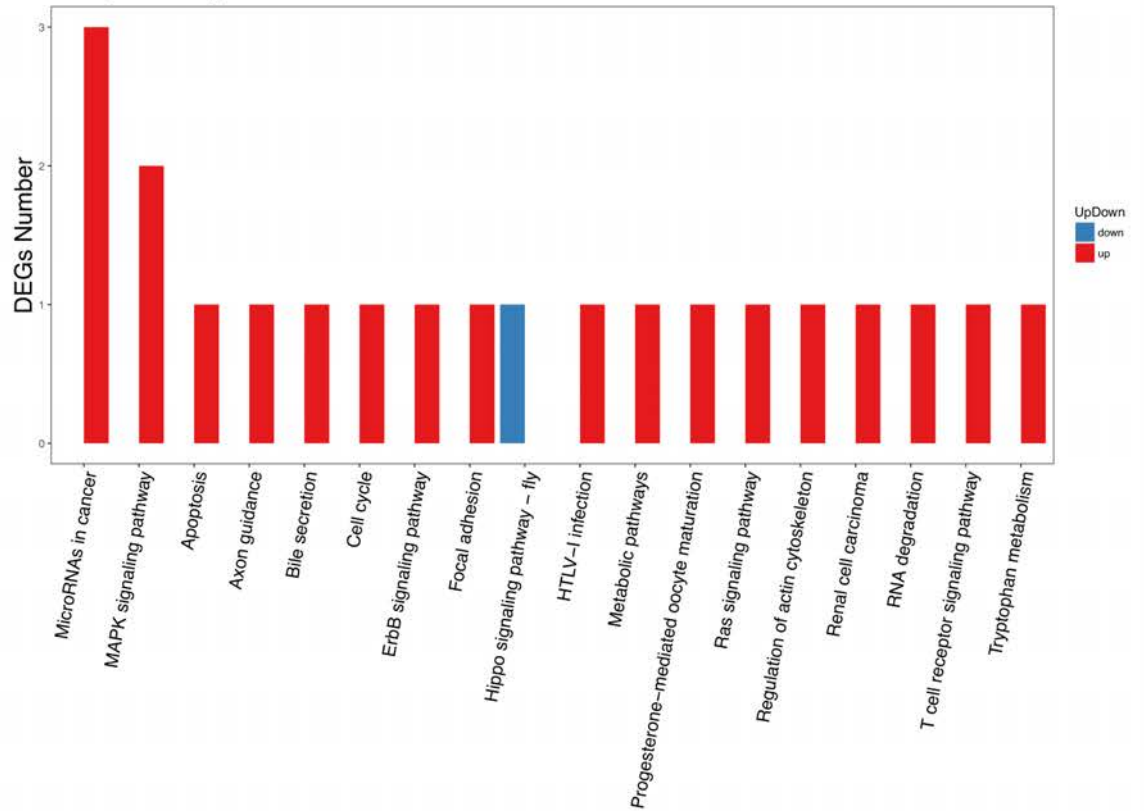
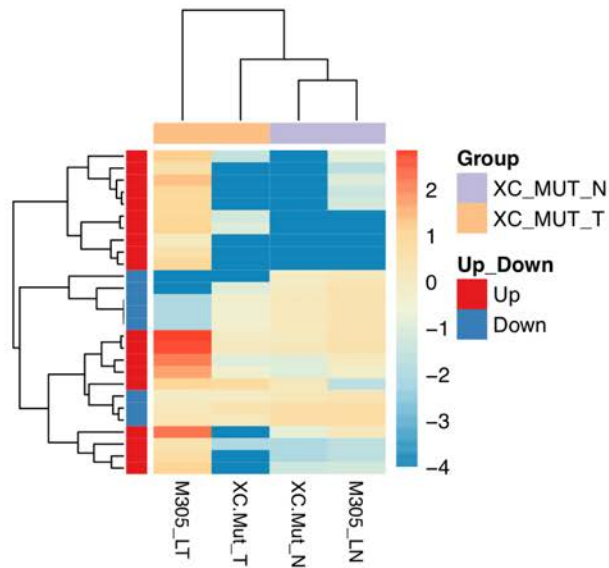
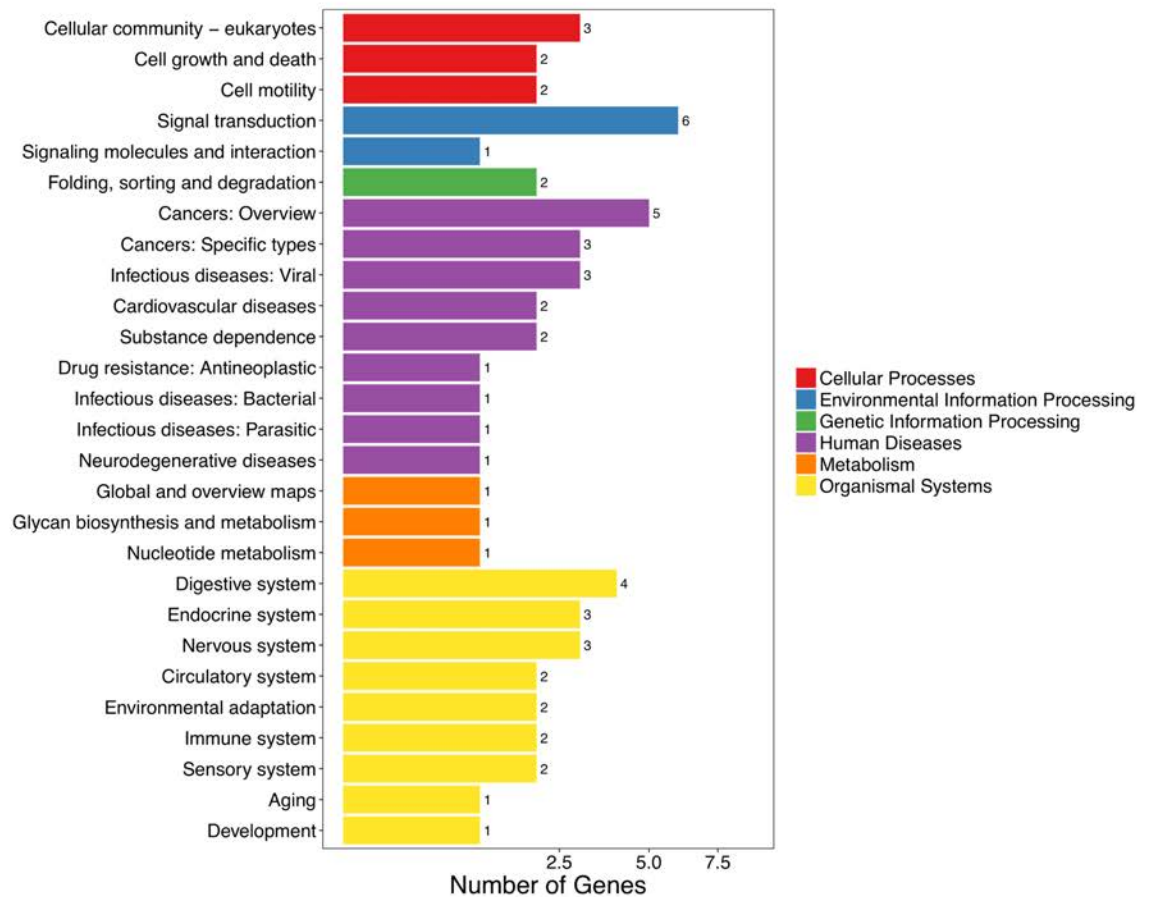


**Figure 26| RNA-seq result of normal and tumor tissues of HBx-C wild-type (WT) injected animals.** (A) Heatmap of DEGs found between normal and tumor tissues of HBx-C WT experimental animals. (B) KEGG functional classifications of DEGs found between normal and tumor tissues of HBx-C WT experimental animals. (C) KEGG pathways enrichment of DEGs found between normal and tumor tissues of HBx-C WT experimental animals. (D) KEGG pathways of DEGs found between normal and tumor tissues of HBx-C wild-type experimental animals. N represents normal tissue; T represents tumor tissue. Red bars represent up-regulated genes. Blue bars represent down-regulated genes.

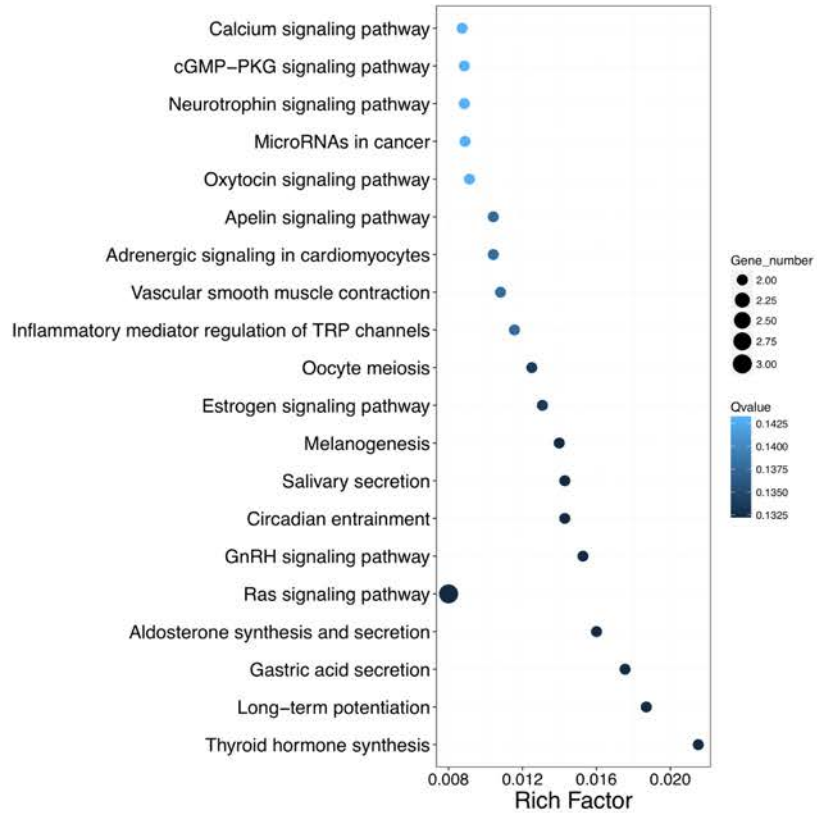
**A** Heatmap of DEGs found between normal and tumor tissues of HBx-C Mut



**B** KEGG functional classifications of DEGs found between normal and tumor tissues of HBx-C Mut



**C KEGG pathways enrichment of DEGs found between normal and tumor tissues of HBx-C Mut**



**D KEGG pathways of DEGs found between normal and tumor tissues of HBx-C Mut**

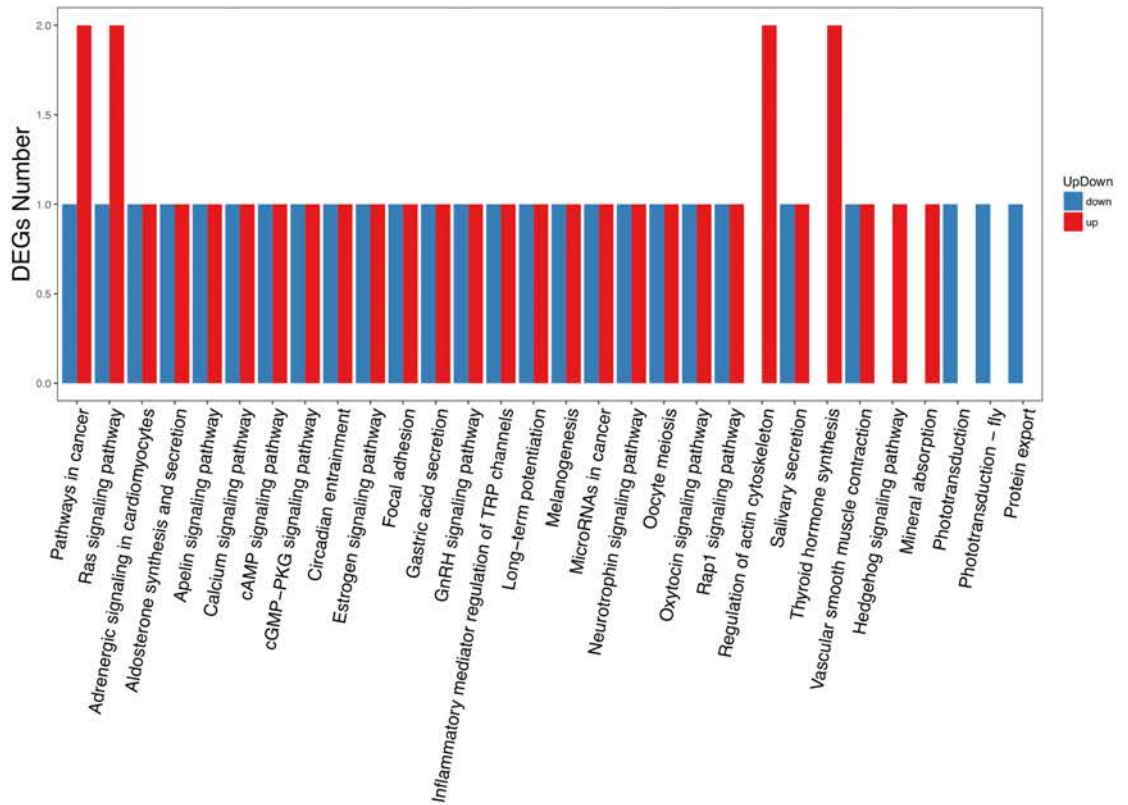
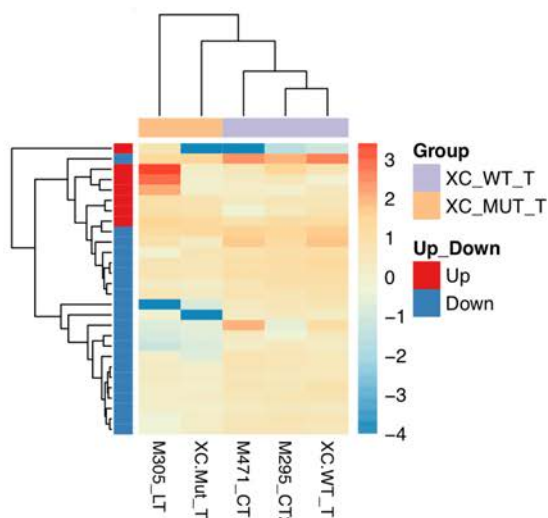
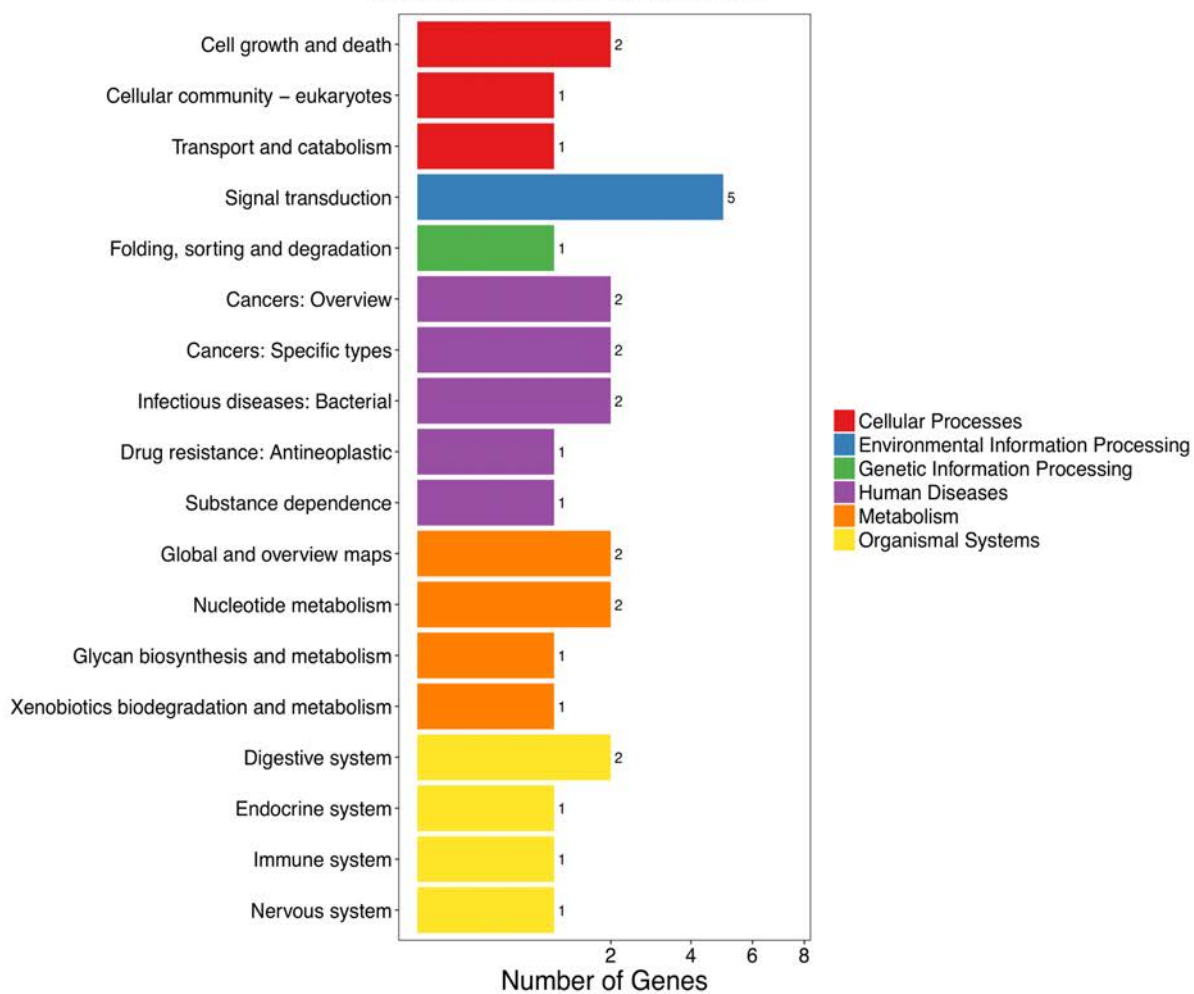


**Figure 27| RNA-seq result of normal and tumor tissues of HBx-C mutant (Mut) injected animals.** (A) Heatmap of DEGs found between normal and tumor tissues of HBx-C Mut experimental animals. (B) KEGG functional classifications of DEGs found between normal and tumor tissues of HBx-C Mut experimental animals. (C) KEGG pathways enrichment of DEGs found between normal and tumor tissues of HBx-C Mut experimental animals. (D) KEGG pathways of DEGs found between normal and tumor tissues of HBx-C Mut experimental animals. N represents normal tissue; T represents tumor tissue. Red bars represent up-regulated genes. Blue bars represent down-regulated genes.

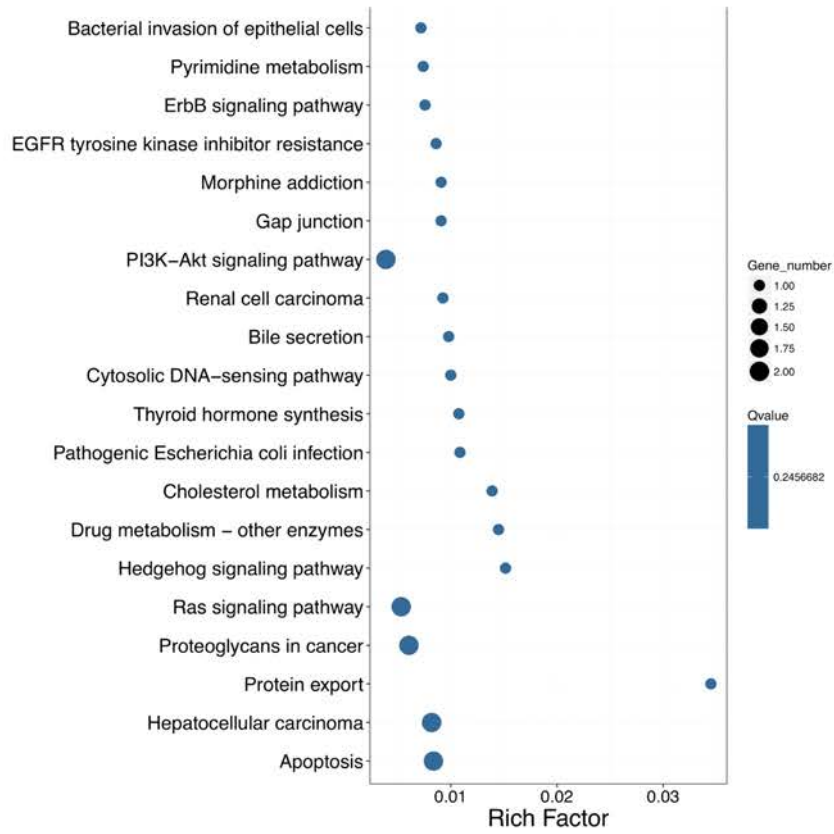
**A** Heatmap of DEGs found between tumor tissues of HBx-C Mut and WT



**B** KEGG functional classifications of DEGs found between tumor tissues of HBx-C Mut and WT



**C KEGG pathways enrichment of DEGs found between tumor tissues of HBx-C Mut and WT**



**D KEGG pathways of DEGs found between tumor tissues of HBx-C Mut and WT**

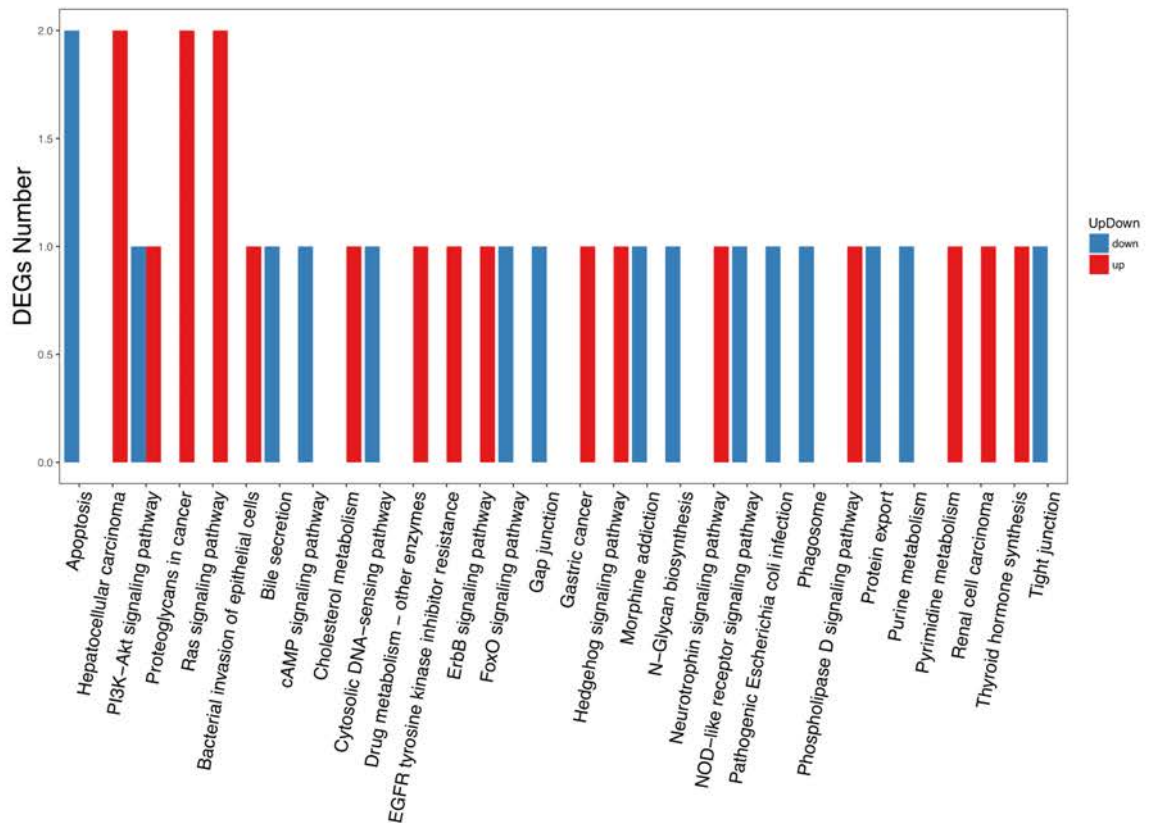


**Figure 28| RNA-seq result of tumor tissues of HBx-C mutant (Mut) and wild-type (WT) injected animals.** (A) Heatmap of DEGs found between tumor tissues of HBx-C Mut and WT experimental animals. (B) KEGG functional classifications of DEGs found between tumor tissues of HBx-C Mut and WT experimental animals. (C) KEGG pathways enrichment of DEGs found between tumor tissues of HBx-C Mut and WT experimental animals. (D) KEGG pathways of DEGs found between tumor tissues of HBx-C Mut and WT experimental animals. N represents normal tissue; T represents tumor tissue. Red bars represent up-regulated genes. Blue bars represent down-regulated genes.

### 3.5.4 KEGG pathways of HBx genotype D

We first compared the RNA expression profiles in normal and tumor tissue of HBx-D Mut and HBx-D WT experimental groups with empty normal control group with the co-injection of *shp53*. There were relatively high genetic differences in RNA expression profile of normal tissues of HBx-D Mut, HBx-D WT with the empty control group compared to that of genotypes A, B and C. This also reflected that HBx-D implied the severest tumor burden in our mouse model. According to the result, 87 genes were up-regulated and 161 genes were down-regulated in normal tissues of HBx-D Mut compared with empty control; while 119 genes were up-regulated and 168 genes down-regulated in normal tissues of HBx-D WT compared with empty control (**Figure 29A**). Large genetic differences in RNA expression profiles of the tumors of HBx-D Mut and WT experimental groups compared to that of empty normal control were observed, in which 164 genes were up-regulated and 307 genes were down-regulated in tumors of HBx-D Mut animals; while 464 genes were up-regulated, and 392 genes were down-regulated in tumors of HBx-D WT animals (**Figure 29A**). There were 139 common DEGs identified in normal tissues of HBx-D WT and HBx-D Mut groups in referencing to the empty normal control, in which 45 DEGs were up-regulated and 94 DEGs were down-regulated, including *Fah* and *Susd4*, which were commonly found in HBx genotype A, B and C injected animals (**Figure 29B**).

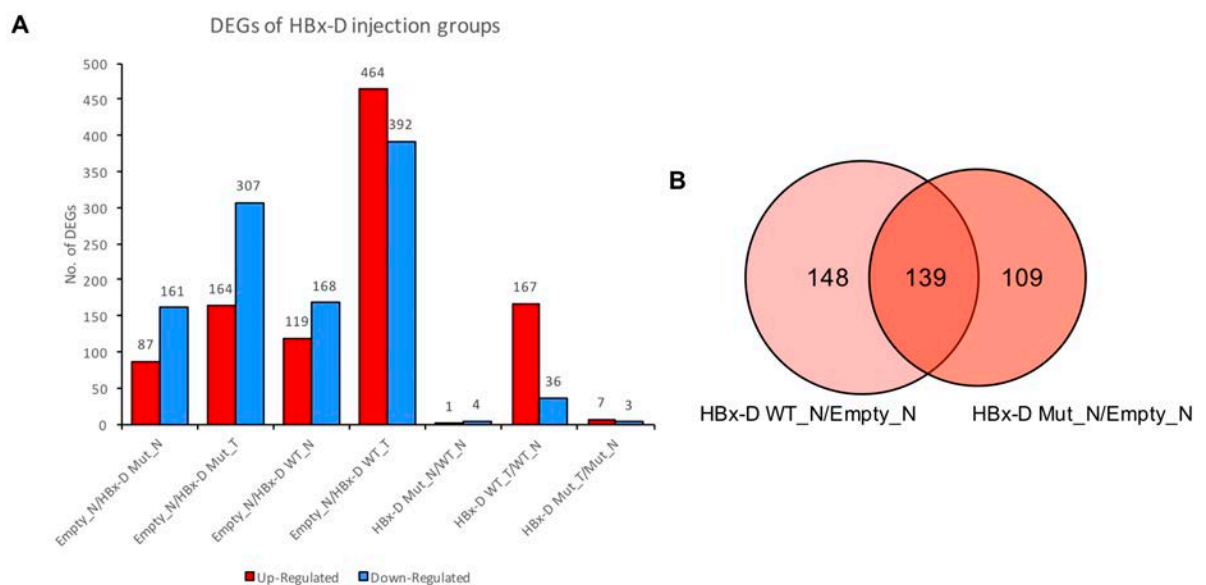


**Figure 29| Differentially expressed genes (DEGs) identified in HBx-D injected animal groups. (A)** Number of DEGs in HBx-D Mut (n = 3) normal liver tissue compared with empty control (n = 3) was 248; and that HBx-D WT (n = 3) normal liver tissue compared with empty

control was 287; while gene expression in tumor induced by HBx-D Mut (471 DEGs, n = 3) and HBx-D WT (856 DEGs, n = 3) had a diverse difference comparing to empty normal control. Only five genes were differentially expressed in normal tissue of HBx-D Mut group compared with HBx-D WT normal group. DEGs between tumor and normal tissue of HBx-D Mut groups was 10 and that in HBx-D WT groups was 203. Red bars represent up-regulated genes. Blue bars represent down-regulated genes. **(B)** Venn diagram showing overlapping DEGs identified in normal tissues of HBx-D WT and Mut injected animals in referencing to empty normal control. N represents normal tissue; T represents tumor tissue.

Comparing RNA expression profiles of normal tissues between HBx-D Mut and WT injected animals, only 5 genes were differentially expressed, in which only UDP glucuronosyltransferase 1 family, polypeptide A6A (*Ugt1a6a*) was up-regulated and eukaryotic translation initiation factor 5B (*Eif5b*), cyclin B1 interacting protein 1 (*Ccnblip1*), predicted gene 6710 (*Gm6710*) and zinc finger protein 820 (*Zfp820*) were down-regulated (**Figure 29A and 30A**). *Ugt1a6a* is involved in various metabolic pathways such as metabolism of xenobiotics by cytochrome P450, retinol metabolism and steroid metabolism, while *Eif5b* participates in RNA transport (**Figure 30B, 30C and 30D**).

Comparing RNA expression profiles of the tumor tissue to normal tissue of HBx-D WT injected animals, 203 DEGs were found, in which 167 genes were up-regulated and 36 gene were down-regulated in tumor (**Figure 29A and 31A**). These DEGs spanned across the common branches of KEGG functional classifications, included cellular processes, environmental information processing, genetic information processing, human diseases, metabolism and organismal systems. They highly associated with cellular community – eukaryotes under the cellular processes class (DEGs = 17), signal transduction under environmental information processing (DEGs = 41), translation under genetic information processing (DEGs = 2), cancers: overview under human diseases (DEGs = 31), global and overview maps under metabolism (DEGs = 26), and immune system under organismal system (DEGs = 20) (**Figure 31B**). The most significantly annotated KEGG pathways of these DEGs included arachidonic acid metabolism ( $q = 1.143 \times 10^{-6}$ ), linoleic acid metabolism ( $q = 3.437 \times 10^{-3}$ ), inflammatory mediator regulation of TRP channels ( $q = 3.437 \times 10^{-3}$ ), focal adhesion ( $q = 5.995 \times 10^{-3}$ ), steroid hormone biosynthesis ( $q = 6.441 \times 10^{-3}$ ), ECM-receptor interaction ( $q = 2.136 \times 10^{-2}$ ), retinol metabolism ( $q = 2.146 \times 10^{-2}$ ), chemical

carcinogenesis ( $q = 3.503 \times 10^{-2}$ ), and ErbB signalling pathway ( $q = 4.286 \times 10^{-2}$ ) (**Figure 31C and 31D**).

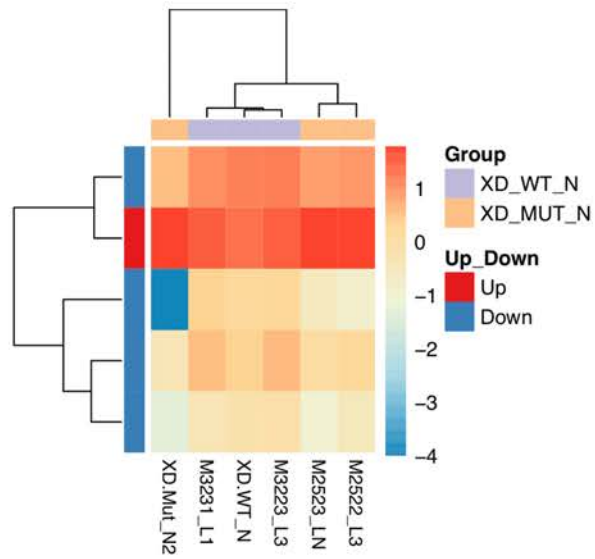
We then compared the RNA expression profiles between the normal and tumor tissues of HBX-D Mut injected animals, and 10 genes were differentially expressed in tumor with 7 up-regulated genes and 3 down-regulated genes (**Figure 29A and 32A**). These DEGs spanned across the KEGG functional classification as well, but no significant KEGG pathway was annotated by these DEGs (**Figure 32B, 32C and 32D**).

Finally, we compared the RNA expression profile between the tumor tissues of animals injected with wild-type and mutant HBx gene of genotype D. Thirteen genes were differentially expressed and all of these DEGs were down-regulated in tumor induced by mutant injected animals. These DEGs allocated in cellular processes, environmental information processing, human diseases, metabolism and organismal systems of KEGG functional classes and the most significantly annotated KEGG pathway was calcium signalling pathway (DEGs = 3,  $q = 0.0205$ ) (**Figure 29A and 33**).

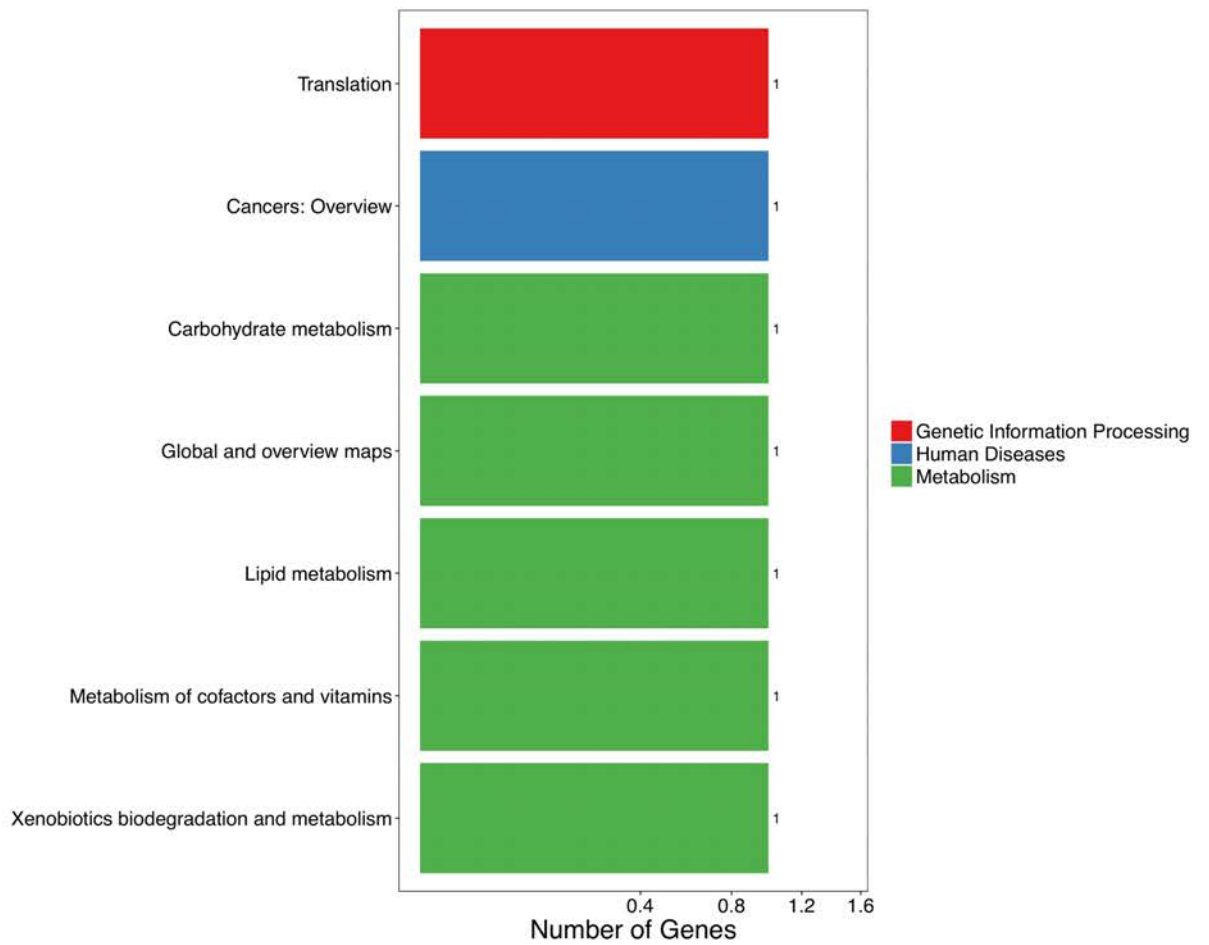
To summarize the expression profiles of the wild-type and mutant HBx genotype D injected animals, first, relatively high genetic differences were notified in HBx genotype D injected animals compared to empty control. This result consisted with tumor burden effect induced by HBx-D, which strongly promote formation of tumor nodules in our mouse model. However, only 5 DEGs were identified in normal tissues between HBx mutant and wild-type injected groups and no significant pathways were annotated. This suggested that the genetic background between the wild-type and mutant HBx genotype D injected animals were similar. Next, 203 DEGs were identified between the tumor and normal tissues of HBx-D WT injected animals, these DEGs involved in mostly metabolic pathways including arachidonic acid metabolism, linoleic acid metabolism, steroid hormone biosynthesis, and retinol metabolism; and canonical signalling pathways such as inflammatory mediator regulation of TRP channels, focal adhesion, ECM-receptor interaction, chemical carcinogenesis, and ErbB signalling pathway. Thirdly, only 10 DEGs were found in the tumor of HBx-D mutant injected animals compared to its wild-type counterparts and no KEGG pathway was significantly distorted by these DEGs. Lastly, we compared the RNA expression profiles in tumors of HBx-D WT and Mut injected groups, 13 DEGs were

identified with all found to be down-regulated in the tumor of HBx-D Mut injected animals.

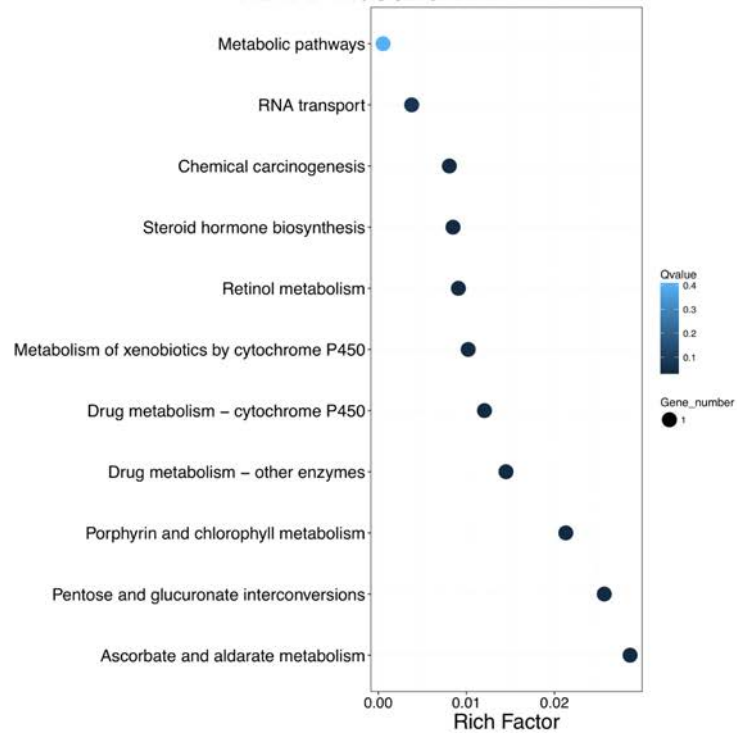
**A Heatmap of DEGs found between normal tissues of HBx-D Mut and WT**



**B KEGG functional classifications of DEGs found between normal tissues of HBx-D Mut and WT**



**C KEGG pathways enrichment of DEGs found between normal tissues of HBx-D Mut and WT**



**D KEGG pathways of DEGs found between normal tissues of HBx-D Mut and WT**

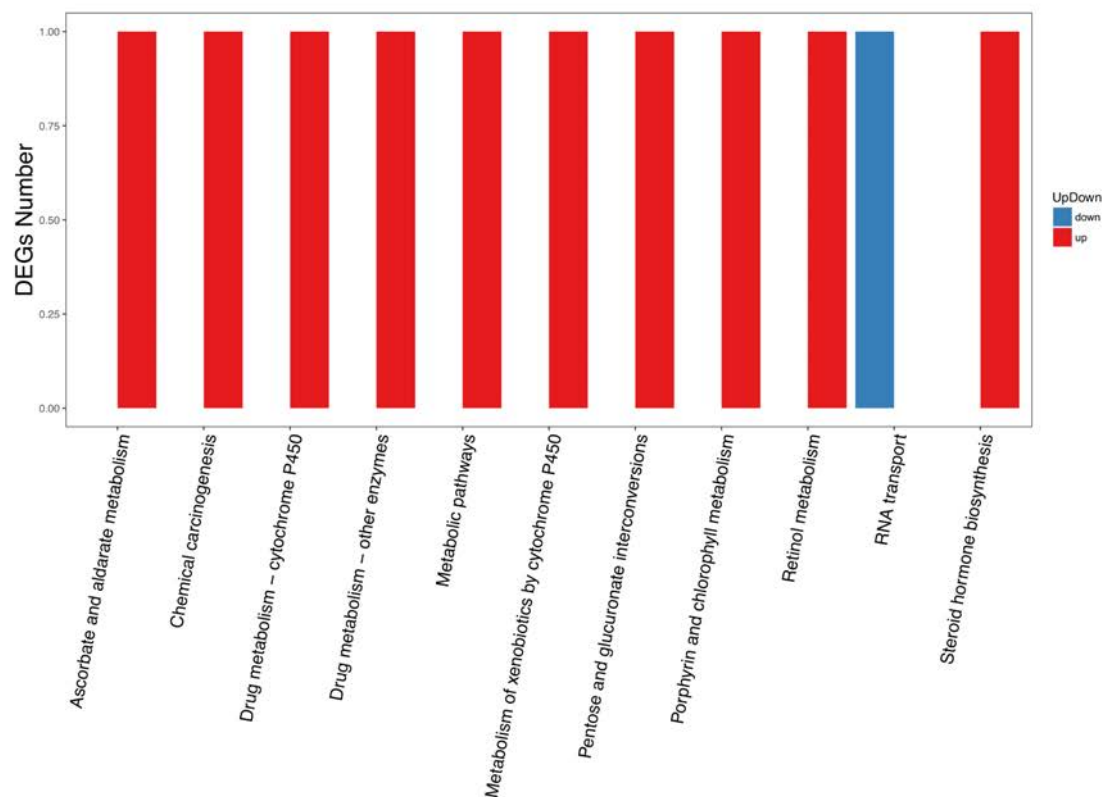
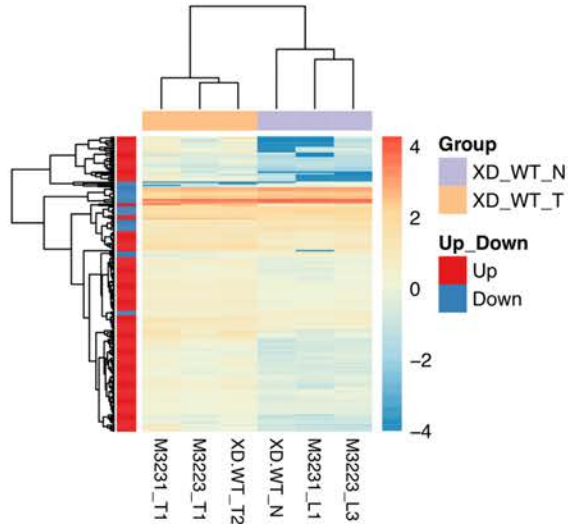


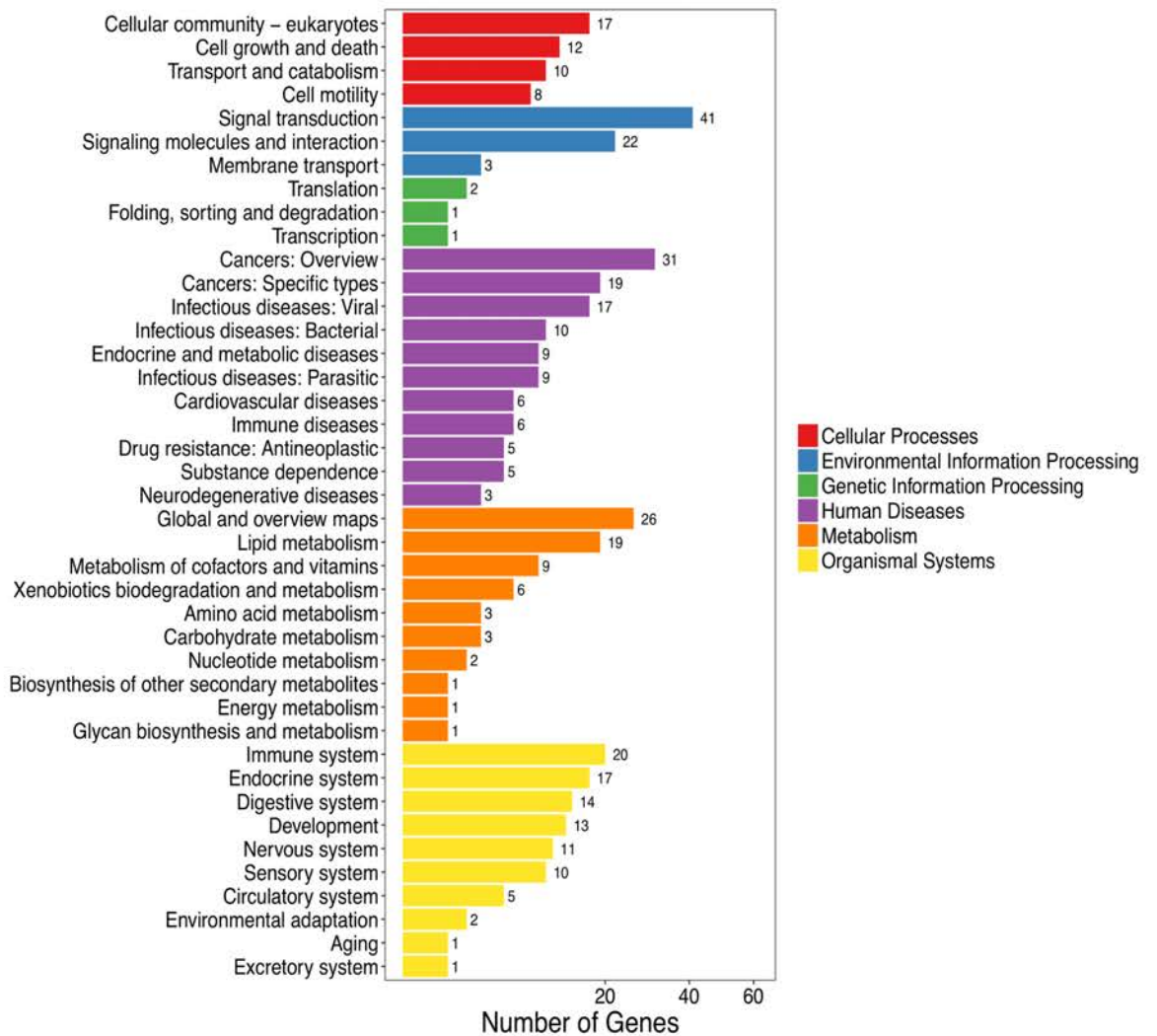
**Figure 30| RNA-seq result of normal tissues of HBx-D mutant (Mut) and wild-type (WT) injected animals. (A) Heatmap of DEGs found between normal tissues of HBx-D Mut and**

WT experimental animals. **(B)** KEGG functional classifications of DEGs found between normal tissues of HBx-D Mut and WT experimental animals. **(C)** KEGG pathways enrichment of DEGs found between normal tissues of HBx-D Mut and WT experimental animals. **(D)** KEGG pathways of DEGs found between normal tissues of HBx-D Mut and WT experimental animals. N represents normal tissue; T represents tumor tissue. Red bars represent up-regulated genes. Blue bars represent down-regulated genes.

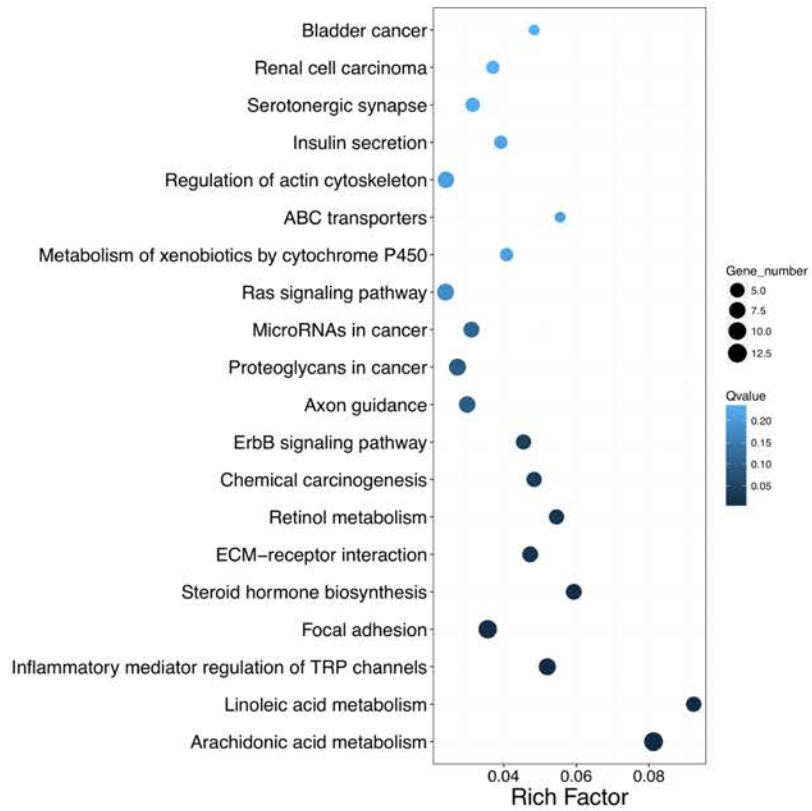
**A Heatmap of DEGs found between normal and tumor tissues of HBx-D WT**



**B KEGG functional classifications of DEGs found between normal and tumor tissues of HBx-D WT**



**C KEGG pathways enrichment of DEGs found between normal and tumor tissues of HBx-D WT**



**D KEGG pathways of DEGs found between normal and tumor tissues of HBx-D WT**

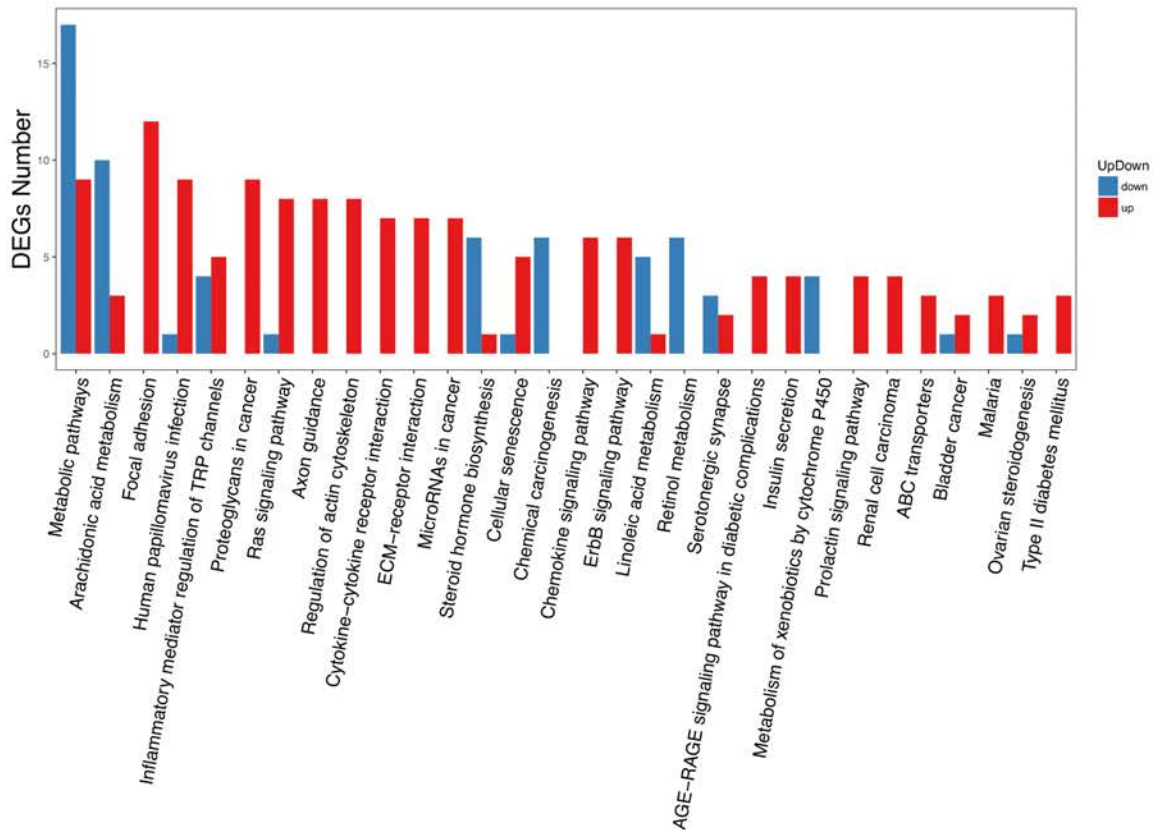
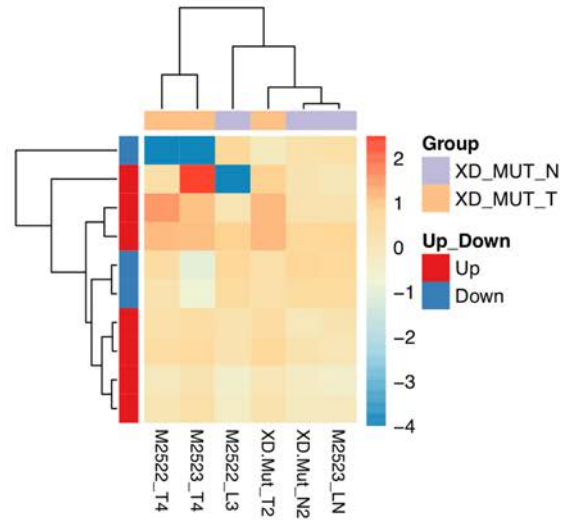
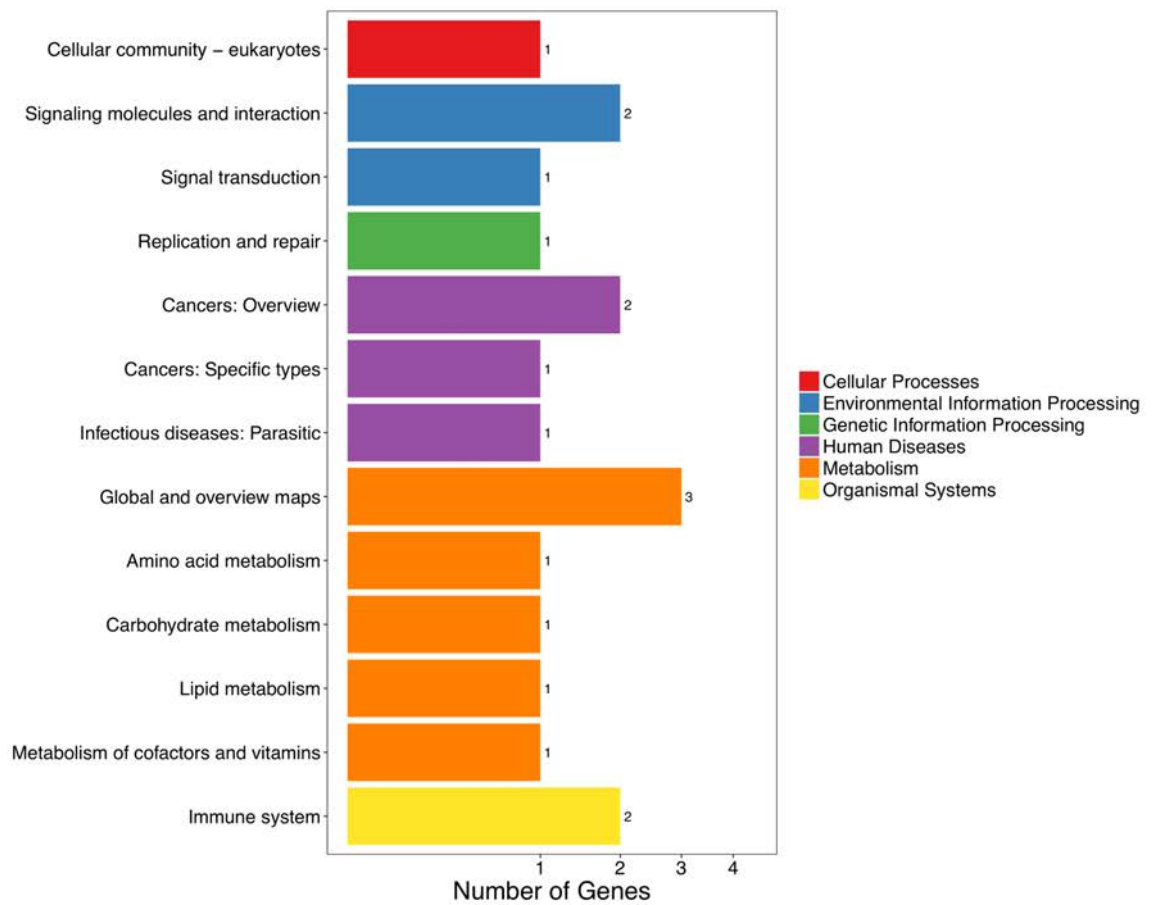


**Figure 31| RNA-seq result of normal and tumor tissues of HBx-D wild-type (WT) injected animals.** (A) Heatmap of DEGs found between normal and tumor tissues of HBx-D WT experimental animals. (B) KEGG functional classifications of DEGs found between normal and tumor tissues of HBx-D WT experimental animals. (C) KEGG pathways enrichment of DEGs found between normal and tumor tissues of HBx-D WT experimental animals. (D) KEGG pathways of DEGs found between normal and tumor tissues of HBx-D WT experimental animals. N represents normal tissue; T represents tumor tissue. Red bars represent up-regulated genes. Blue bars represent down-regulated genes.

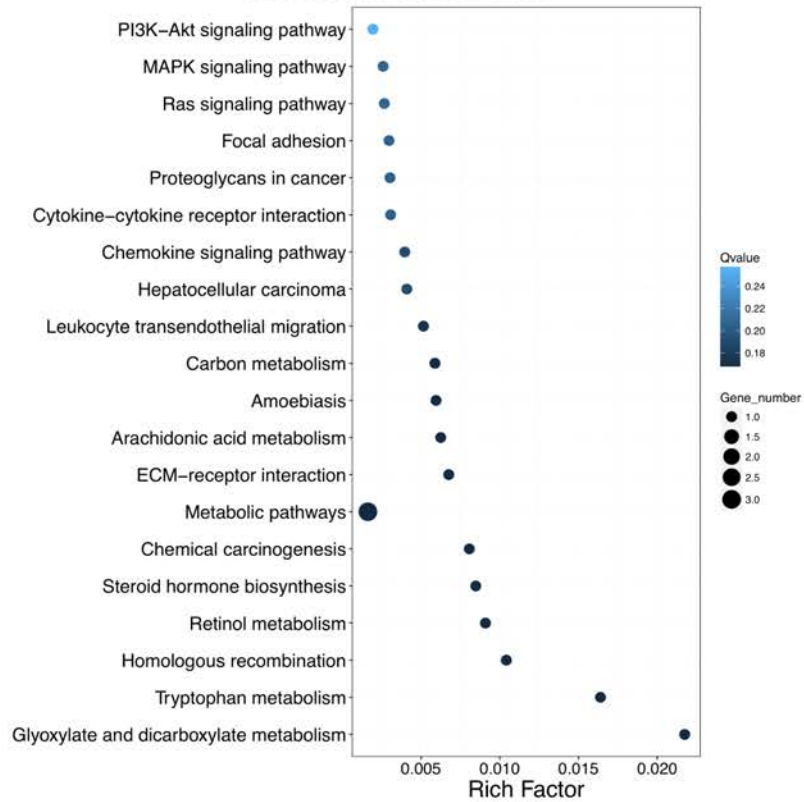
**A Heatmap of DEGs found between normal and tumor tissues of HBx-D Mut**



**B KEGG functional classifications of DEGs found between normal and tumor tissues of HBx-D Mut**



**C KEGG pathways enrichment of DEGs found between normal and tumor tissues of HBx-D Mut**



**D KEGG pathways of DEGs found between normal and tumor tissues of HBx-D Mut**

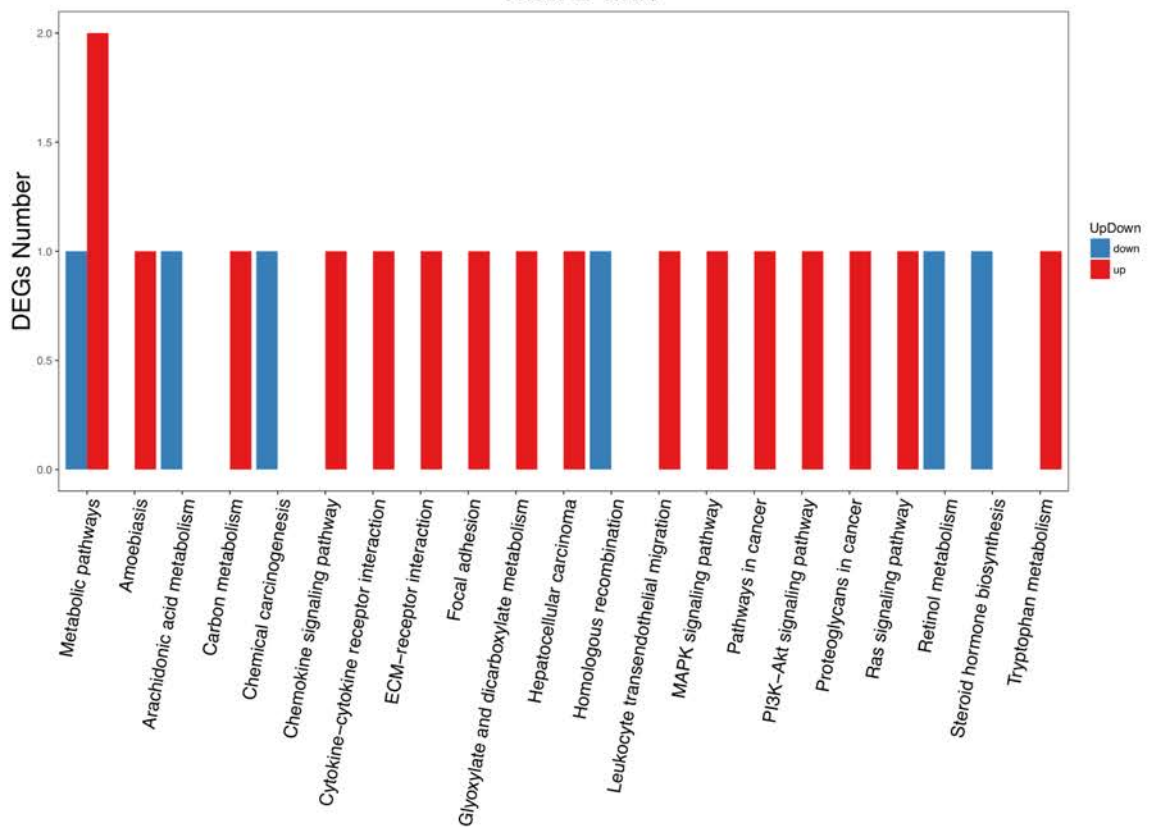
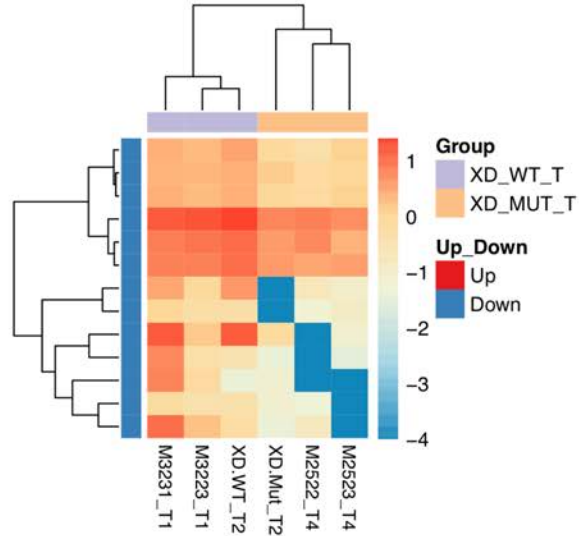
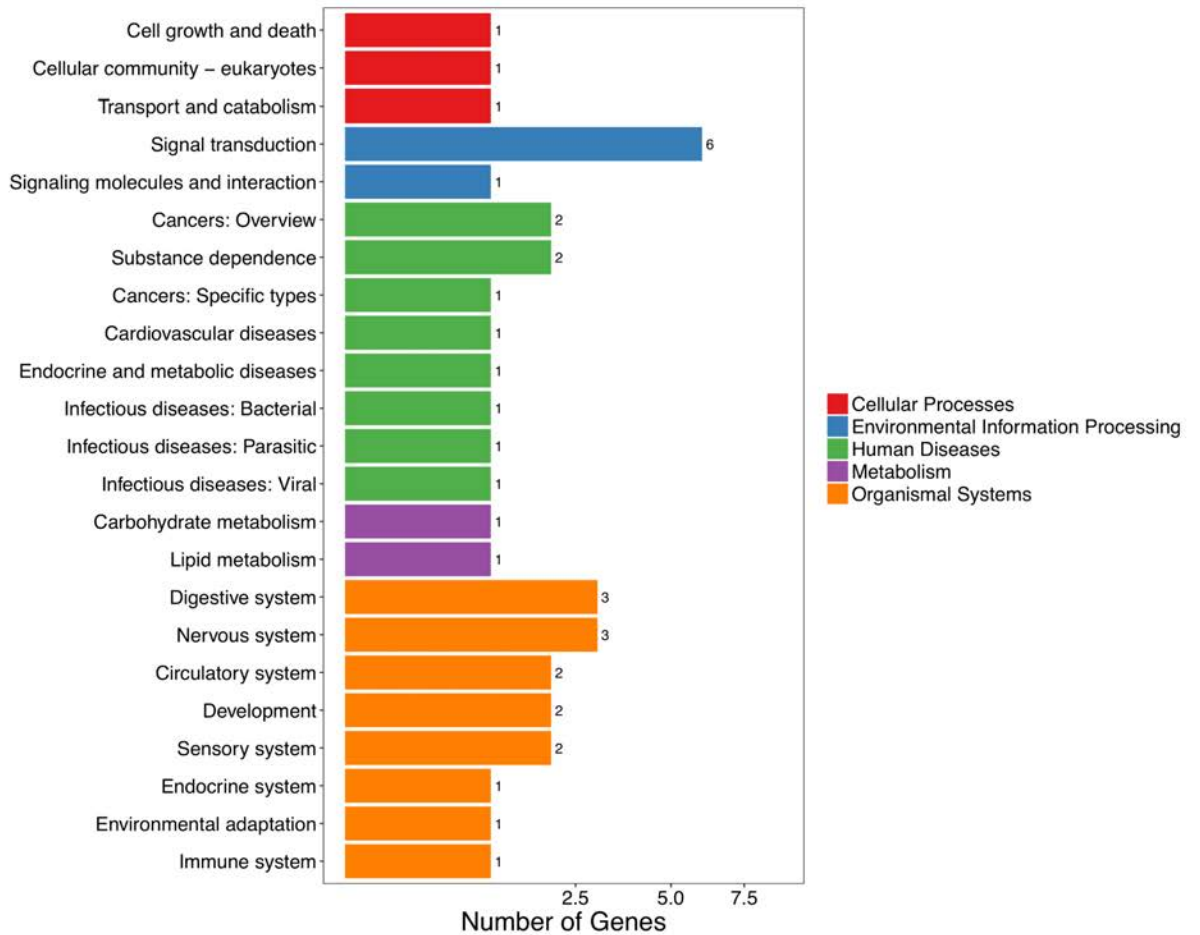


**Figure 32| RNA-seq result of normal and tumor tissues of HBx-D mutant (Mut) injected animals.** (A) Heatmap of DEGs found between normal and tumor tissues of HBx-D Mut experimental animals. (B) KEGG functional classifications of DEGs found between normal and tumor tissues of HBx-D Mut experimental animals. (C) KEGG pathways enrichment of DEGs found between normal and tumor tissues of HBx-D Mut experimental animals. (D) KEGG pathways of DEGs found between normal and tumor tissues of HBx-D Mut experimental animals. N represents normal tissue; T represents tumor tissue. Red bars represent up-regulated genes. Blue bars represent down-regulated genes.

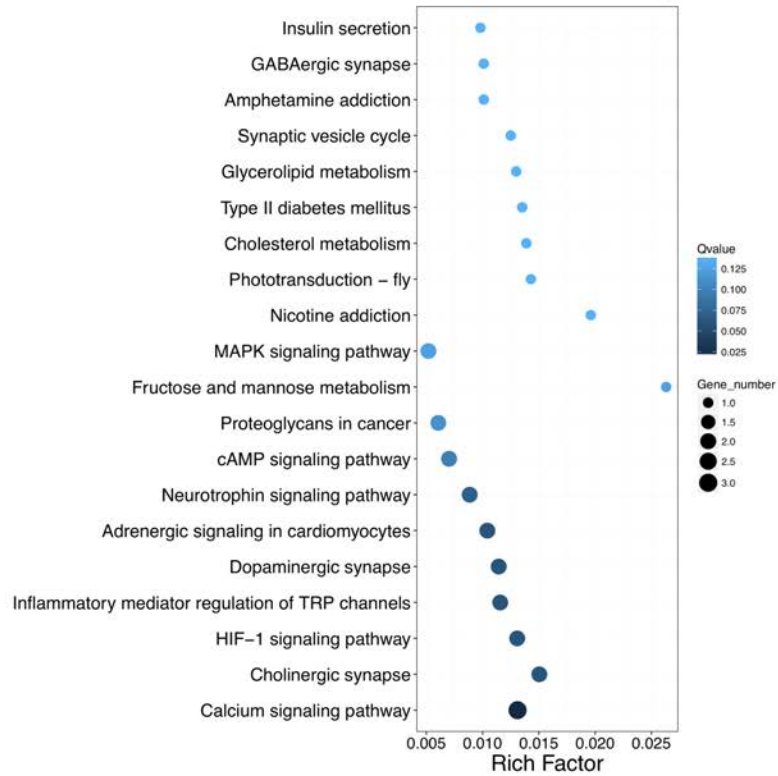
**A Heatmap of DEGs found between tumor tissues of HBx-D Mut and WT**



**B KEGG functional classifications of DEGs found between tumor tissues of HBx-D Mut and WT**



**C KEGG pathways enrichment of DEGs found between tumor tissues of HBx-D Mut and WT**



**D KEGG pathways of DEGs found between tumor tissues of HBx-D Mut and WT**

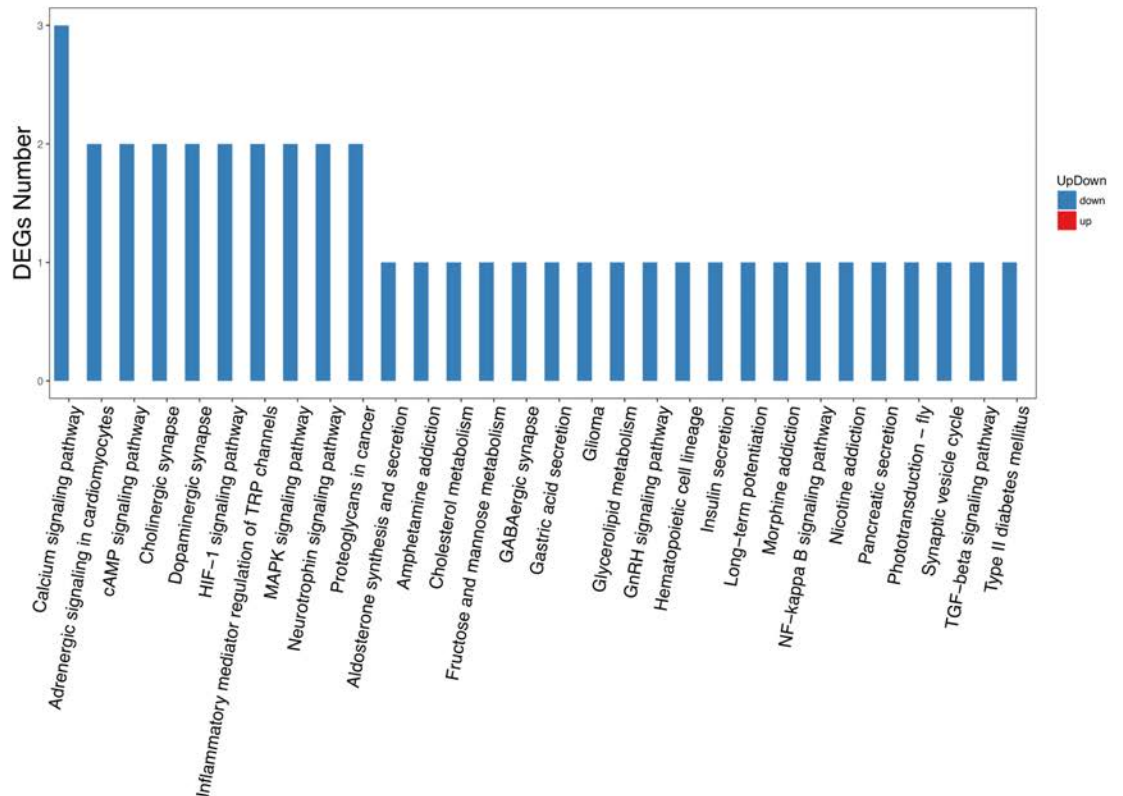


**Figure 33| RNA-seq result of tumor tissues of HBx-D mutant (Mut) and wild-type (WT) injected animals. (A) Heatmap of DEGs found between tumor tissues of HBx-D Mut and WT**

experimental animals. **(B)** KEGG functional classifications of DEGs found between tumor tissues of HBx-D Mut and WT experimental animals. **(C)** KEGG pathways enrichment of DEGs found between tumor tissues of HBx-D Mut and WT experimental animals. **(D)** KEGG pathways of DEGs found between tumor tissues of HBx-D Mut and WT experimental animals. N represents normal tissue; T represents tumor tissue. Red bars represent up-regulated genes. Blue bars represent down-regulated genes.

### 3.5.5 Low genetic difference between normal tissues of K130M/V131I mutant and wild-type variants of various HBx genotypes

In order to compare the genetic differences induced by genotypes A, B, C and D, DEGs were identified by comparing the RNA expression profiles in normal tissues of mutant to wild-type of the same genotype. From the comparison result, only a few genes were differentially expressed between the normal liver tissues of mice injected with various genotypes of the HBx gene (**Figure 34A**). Comparing the normal tissues of HBx-A Mut to HBx-A WT, only *Xlr3a* and *Fam47e* were found to be down-regulated (**Figure 34A** and **34C**). Comparing the normal tissues of HBx-B Mut to HBx-B WT, 3 genes were found to be differentially expressed: *Mup14* and *Eda* were up-regulated, *Gm5779* was down-regulated (**Figure 34**). Comparing the normal tissues of HBx-C Mut to HBx-C WT, 4 genes were found to be differentially expressed: *Styk1*, *Lrtm1* and *Nat8f3* were up-regulated, while *Csrp3* was down-regulated (**Figure 34**). In the comparison of normal tissues of HBx-D Mut to HBx-D WT, expression profiles of 5 genes were altered: *Ugt1a6a* was up-regulated, while *Eif5b*, *Ccnblip1*, *Gm6710* and *Zfp820* were down-regulated (**Figure 34**).

Few DEGs were identified in normal tissues between the mutant and wild-type groups of various genotypes, suggesting that the genetic background differences between mice injected with either mutant or wild-type HBx gene of the same genotype were low. Hence, any DEGs found exclusively in tumor groups were essential for tumor progression. Next, we compared the DEGs that were up-regulated and down-regulated in different genotypes to search for common DEGs induced by various genotypes. Surprisingly, no common DEGs could be found (**Figure 34B** and **34C**). This applied that these genotypes behaved exclusively upon integration into the host genome.

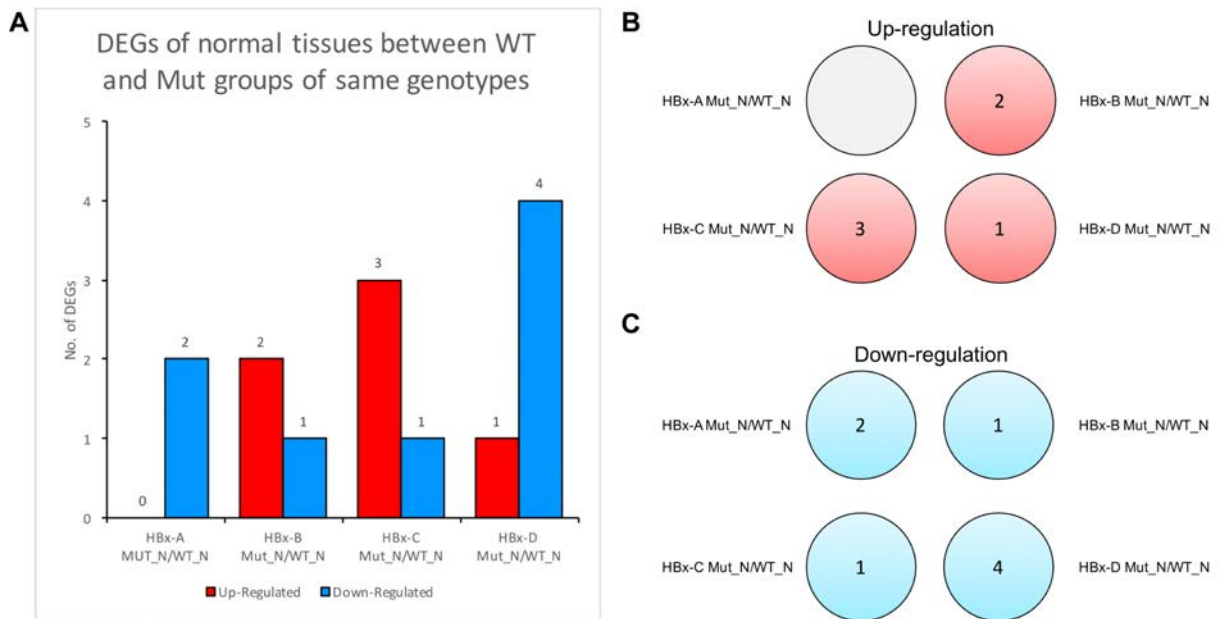


**Figure 34| Combinatorial analyses on DEGs identified from comparing the RNA expression profile of normal tissues between mutant (Mut) and wild-type (WT) of HBx genotype A, B, C and D. (A)** DEGs found between normal tissues of Mut and WT HBx genes of genotype A, B, C and D. **(B)** Venn diagram of up-regulated genes found in normal tissues of Mut and WT HBx genes of genotype A, B, C and D. There was no overlapping gene between compared genotypes. **(C)** Venn diagram of down-regulated genes found in normal tissues of Mut and WT HBx genes of genotype A, B, C and D. There was no overlapping gene between compared genotypes. N represents normal tissue; T represents tumor tissue. Red bars represent up-regulated genes. Blue bars represent down-regulated genes.

### 3.5.6 *Arhgap27* and *Pak6* were commonly up-regulated in the tumors of genotypes A, C and D of HBx wild-type gene

In order to discover the genes associated with tumor progression, we first aligned DEGs identified in tumors induced by wild-type HBx genotype A, C and D to discover the common DEGs expressed in all three genotypes. Since no solid tumor was isolated from HBx-B WT group, it was omitted in this comparison. There were 1498 DEGs identified in tumors induced by wild-type HBx genotype A in comparison to its normal tissues, in which 1100 DEGs were found to be up-regulated and 398 genes were found to be down-regulated (**Figure 35A**). This high gene variation might be due to the small sample size of tumor tissue. In tumors induced by wild-type HBx gene of genotype C, 16 DEGs were identified, in which 15 genes were up-regulated and only 1 gene was down-regulated (**Figure 35A**). In the comparison of tumor tissues to its adjacent normal tissues of HBx-D wild-type injected mice, a total of 203 DEGs were identified, in which 167 genes were up-regulated and 36 genes were down-regulated (**Figure 35A**). By aligning all these DEGs identified in tumors induced by wild-type HBx gene of each genotype, 7 genes were commonly up-regulated in tumor induced by wild-type HBx of genotype A and C (**Figure 35B**); while 93 genes were commonly altered in tumor induced by wild-type HBx of genotype A and D, in which 78 genes were up-regulated and 15 genes were down-regulated (**Figure 35B** and **35C**). Only 1 gene was commonly up-regulated in tumor induced by wild-type HBx gene of genotype C and D. Most importantly, p21 (RAC1) activated kinase 6 (*Pak6*) and Rho GTPase activating protein 27 (*Arhgap27*) were commonly up-regulated in all 3 different genotypes (**Figure 35D**). The mRNA expression level of *Pak6* and *Arhgap27* were further validated by qPCR in additional samples other than the RNA-sequenced samples (**Figure 36** and **37**). Significant up-regulation of *Pak6* was detected in both tumor and normal tissues of animals injected with HBx-WT genotype B, C and D, and in normal tissues of animals injected with HBx-WT genotype A (**Figure 36**). mRNA expression level of *Arhgap27* were significantly upregulated in both tumor and normal tissues of animals injected with genotype C and D, and in normal tissues of animals injected with genotype B (**Figure 37**). Additionally, in our study on RNA expression profiling of HBV-induced HCC patient samples with 18 HBV-positive tumor and 4 peripheral normal tissues, up-regulation of *PAK6* and *ARHGAP* genes were identified in the tumor tissues compared with its peripheral normal tissues (**unpublished data**).

**A** DEGs between tumor and normal tissue of WT variants of the same genotypes

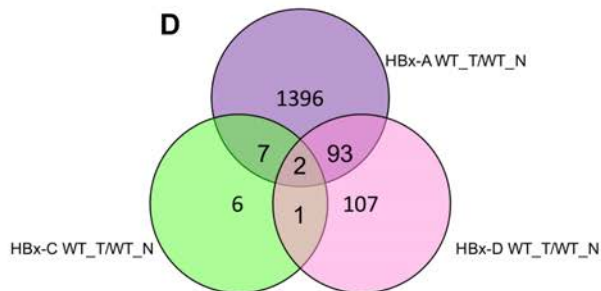
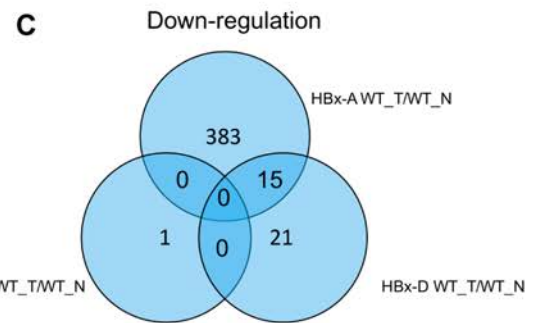
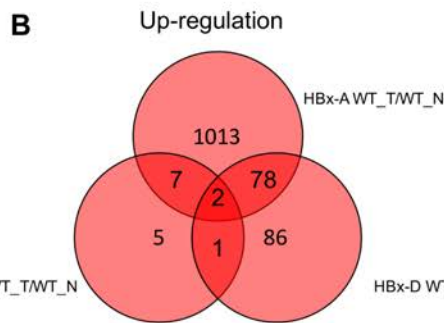
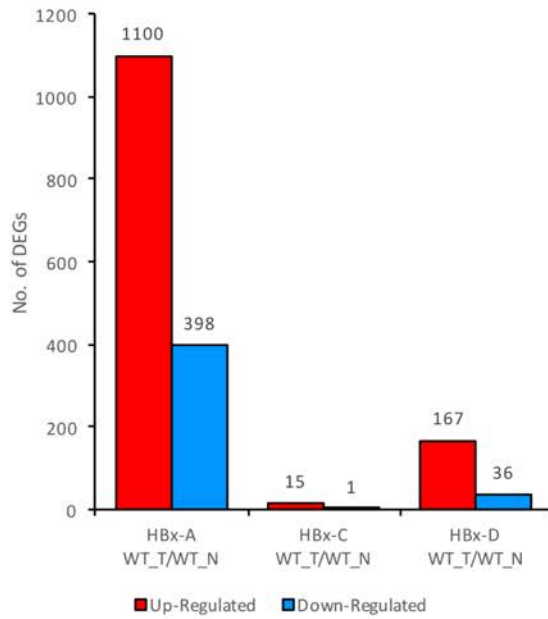


**Figure 35| Combinatorial analyses on DEGs identified from comparing the RNA expression profile of tumor induced by wild-type (WT) HBx gene to its corresponding normal tissues in the same genotype. (A)** DEGs identified from tumor induced by wild-type (WT) HBx gene compared to its corresponding normal tissues in genotype A, C and D. **(B)** Venn diagram of up-regulated genes found in tumor tissues of WT HBx genes of genotype A,

C and D. *Arhgap27* and *Pak6*, were commonly found in all three genotypes compared. (C) Venn diagram of down-regulated genes found in tumor tissues of WT HBx genes of genotype A, C and D. (D) Venn diagram combined both up-regulated and down-regulated genes found in tumor tissues of WT HBx genes of genotype A, C and D. N represents normal tissue; T represents tumor tissue. Red bars represent up-regulated genes. Blue bars represent down-regulated genes.

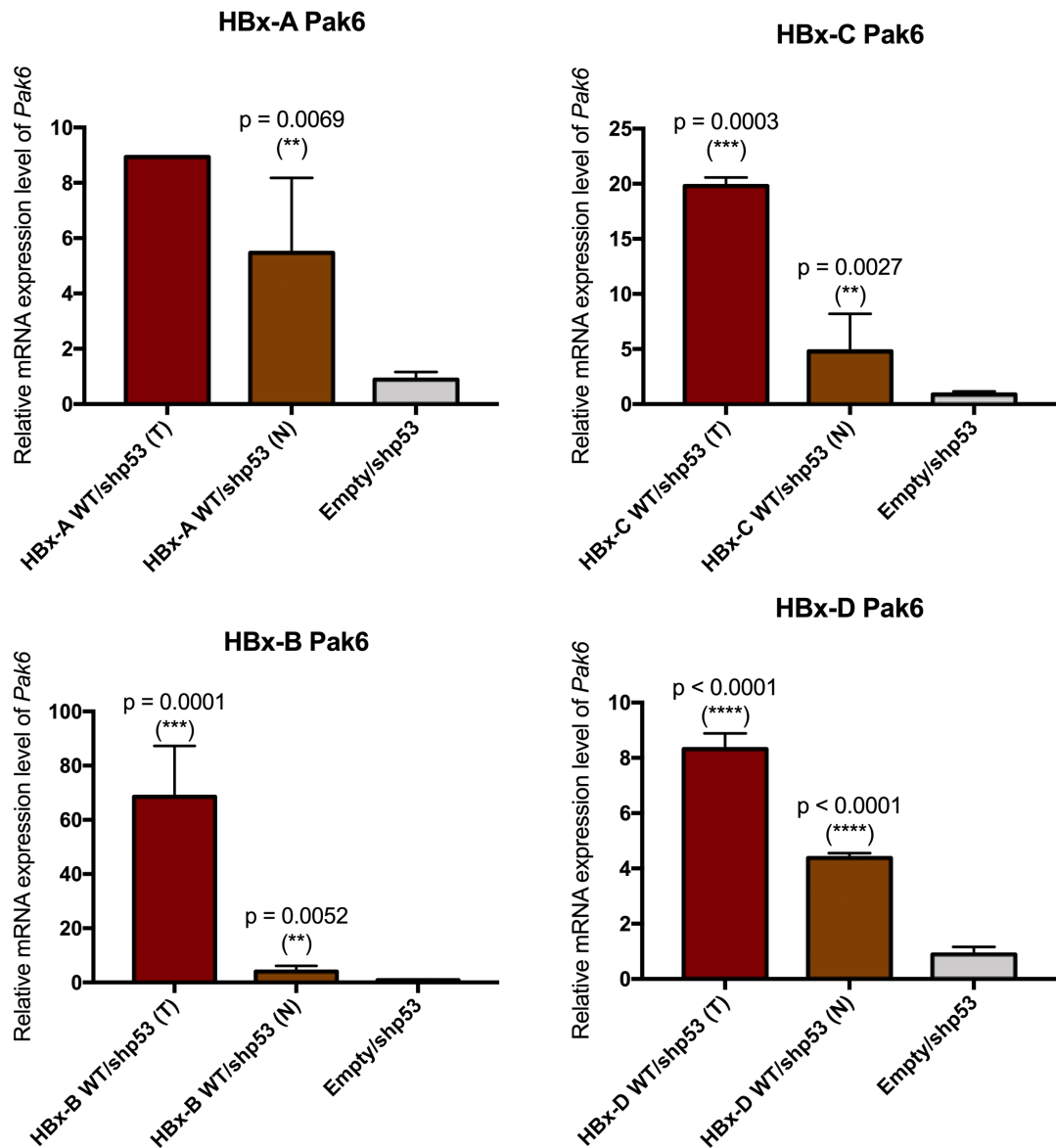


**Figure 36| The mRNA expression level of *Pak6* in animals injected with genotype A, B, C and D of HBx-WT variant by qPCR.** The relative mRNA expression level of *Pak6* in tumor and normal tissues was further validated by qPCR in additional samples other than those sent for RNA-sequencing. *Pak6* was significantly up-regulated in both tumor and normal tissues of animals injected with genotype B, C and D HBx-WT gene, and in normal tissues of animals

injected with genotype A HBx-WT gene compared with its expression level in normal tissues of empty control. T represents tumor tissue; N represent normal tissue. Mean  $\pm$  S.D.;  $p$ , unpaired student  $t$ -test,  $**p \leq 0.01$ ,  $***p \leq 0.001$ ,  $****p \leq 0.0001$ .

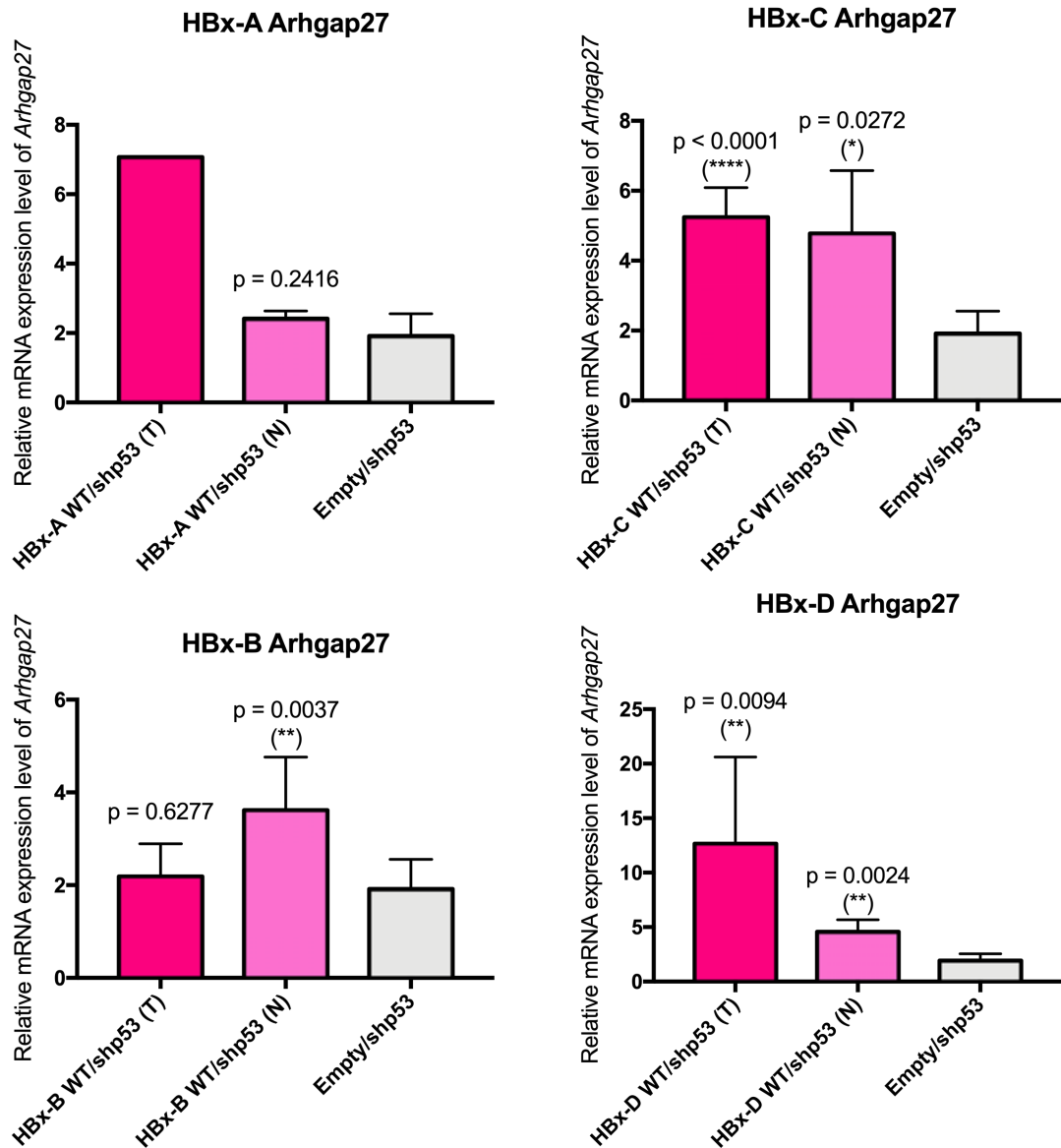


**Figure 37| The mRNA expression level of *Arhgap27* in animals injected with genotype A, B, C and D of HBx-WT variant by qPCR.** The relative mRNA expression level of *Arhgap27* in tumor and normal tissues was further validated by qPCR in additional samples other than those sent for RNA-sequencing. *Arhgap27* was significantly up-regulated in both tumor and normal tissues of animals injected with genotype C and D HBx-WT gene, and in normal tissues of animals injected with genotype B HBx-WT gene compared with its expression level in normal tissues of empty control. T represents tumor tissue; N represent normal tissue. Mean  $\pm$  S.D.;  $p$ , unpaired student  $t$ -test,  $*p \leq 0.05$ ,  $**p \leq 0.01$ ,  $****p \leq 0.0001$ .

### 3.5.7 *Igf2* was commonly up-regulated in the tumors of genotypes B, C and D of HBx mutant gene

Similarly, we aligned DEGs identified in tumors induced by K130M/V131I HBx genotype B, C and D in order to discover the common DEGs that expressed in all three genotypes. Since no solid tumor was isolated from HBx-A Mut group, it was omitted in this comparison. For genotype B, 235 genes were up-regulated and 142 genes were down-regulated in the tumor tissues compared to its adjacent normal tissues (**Figure 38A**). For genotype C, 19 genes were up-regulated and 8 genes were down-regulated in the tumor tissues compared to its adjacent normal tissues (**Figure 38A**). For genotype D, 7 genes were up-regulated, and 3 genes were down-regulated in the tumor tissues compared to its adjacent normal tissues (**Figure 38A**). Aligning the DEGs identified in tumor induced by K130M/V131I mutant HBx of all three genotypes, 4 genes including brain expressed X-linked 1 (*Bex1*), FYVE, RhoGEF and PH domain containing 3 (*Fgd3*), prostate stem cell antigen (*Psca*) and *modulator of apoptosis 1* (*Moap1*) were commonly altered in tumor of genotypes B and C (**Figure 38B, 38C and 38D**). Among these 4 genes, *Bex1*, *Fgd3* and *Psca* were up-regulated; while *Moap1* was up-regulated in tumor nodules isolated from HBx-B Mut group, but down-regulated in tumor nodules isolated from HBx-C Mut group. Another 4 genes including serine (or cysteine) peptidase inhibitor, clade B, member 6b (*Serpinb6b*), serine peptidase inhibitor, Kazal type 1 (*Spink1*), *Arhgap27* and *Susd4* were commonly altered in tumor of genotype B and D (**Figure 38B, 38C and 38D**), in which *Serpinb6b*, *Spink1* and *Arhgap27* were up-regulated; yet *Susd4* was down-regulated. Most important of all, only *Igf2* was commonly up-regulated in tumors induced by K130M/V131I mutant HBx of all three genotypes (**Figure 38B and 38D**). The mRNA expression level *Igf2* was further validated by qPCR in additional samples other than the samples that sent for RNA-sequencing (**Figure 39**). Significant up-regulation of *Igf2* was detected in both tumor and normal tissues of HBx-B Mut cohort and normal tissues of HBx-C Mut cohort (**Figure 39**). Additionally, compared the expression level of *IGF2* in HBV-positive clinical biopsy samples ( $n = 22$ ) to that of HBV-negative samples ( $n = 24$ ), we found that HBV-positive samples had higher expression of *IGF2* with average FPKM of 181.44; while HBV-negative samples had average FPKM of 158.50. Moreover, 55% of HBV-positive samples had expression level

above its average FPKM; while only 12.5% of HBV-negative samples had expression level above its average FPKM (**Figure 40**).

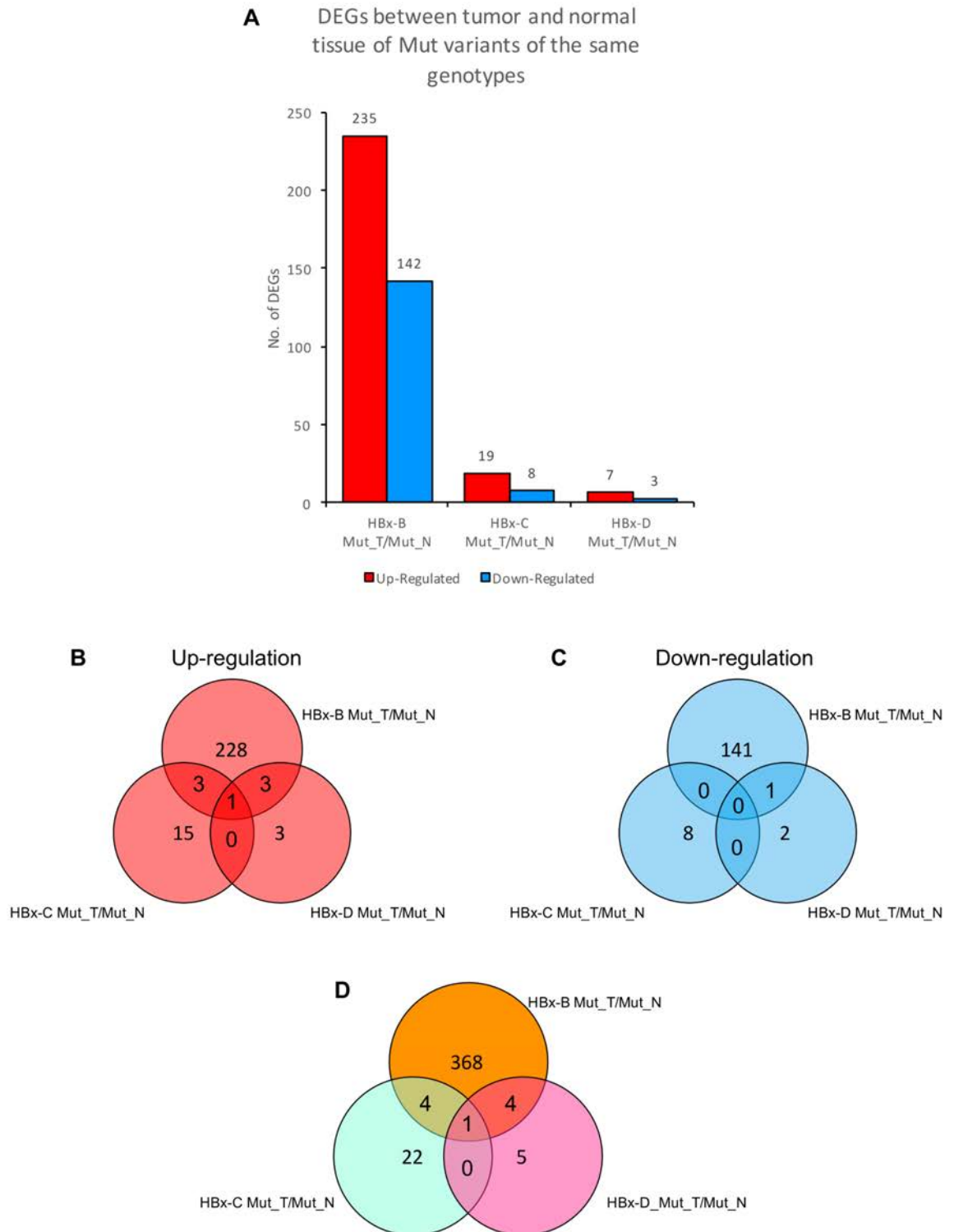


**Figure 38| Combinatorial analyses on DEGs identified from comparing the RNA expression profile of tumor induced by mutant (Mut) HBx gene to its corresponding normal tissues in the same genotype. (A) DEGs identified from tumor induced by HBx Mut**

gene compared to its corresponding normal tissues in genotype B, C and D. **(B)** Venn diagram of up-regulated genes found in tumor tissues of HBx Mut genes of genotype B, C and D. Only one gene, *Igf2*, was commonly found in all three genotypes compared. **(C)** Venn diagram of down-regulated genes found in tumor tissues of HBx Mut genes of genotype B, C and D. **(D)** Venn diagram combined both up-regulated and down-regulated genes found in tumor tissues of HBx Mut genes of genotype B, C and D. N represents normal tissue; T represents tumor tissue. Red bars represent up-regulated genes. Blue bars represent down-regulated genes.

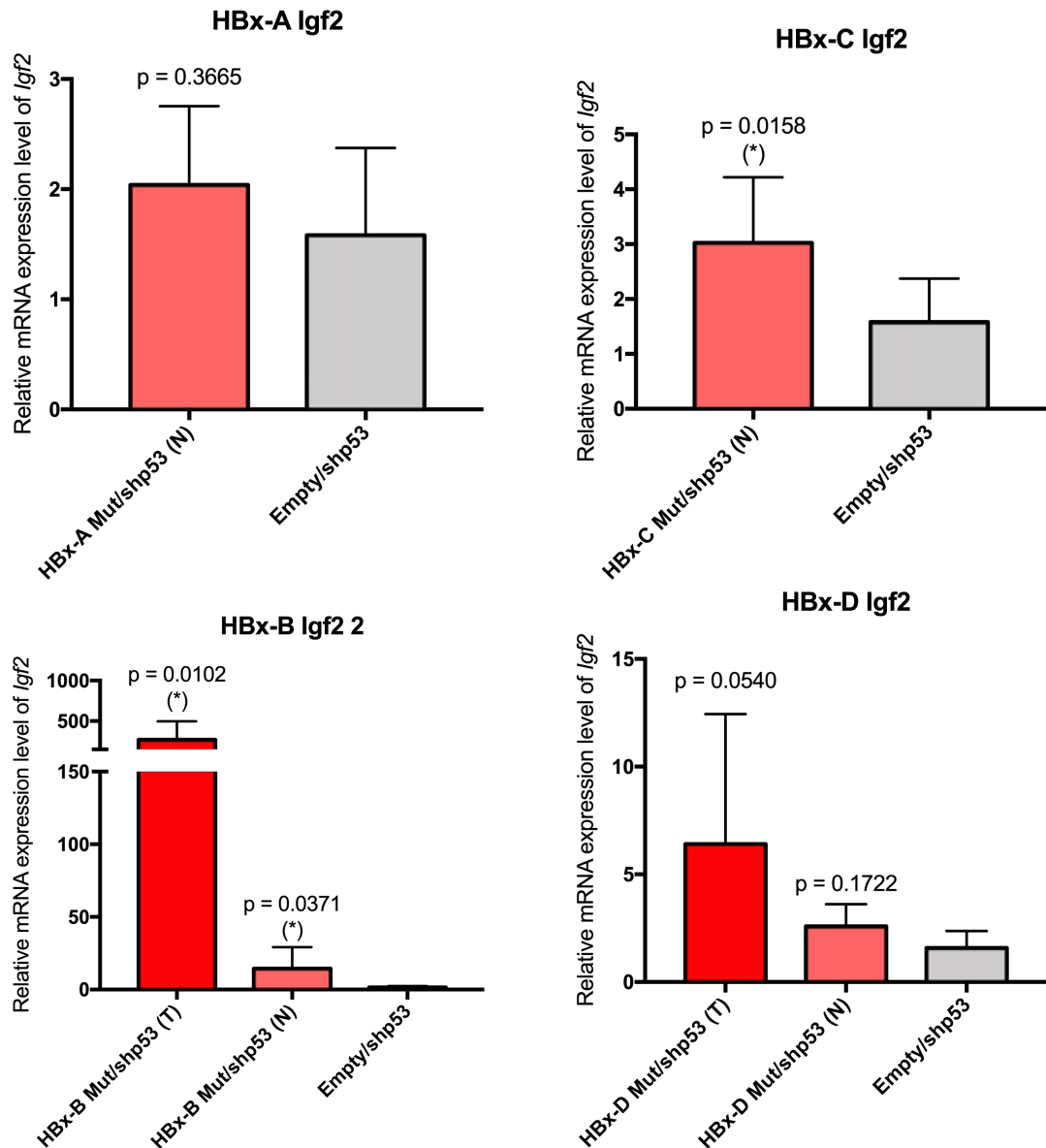


**Figure 39|** The mRNA expression level of *Igf2* in animals injected with genotype A, B, C and D of HBx-WT variant by qPCR. The relative mRNA expression level of *Igf2* in tumor and normal tissues was further validated by qPCR in additional samples other than those sent for RNA-sequencing. *Igf2* was significantly up-regulated in both tumor and normal tissues of animals injected with genotype B HBx-Mut gene, and in normal tissues of animals injected

with genotype C HBx-Mut gene compared with its expression level in normal tissues of empty control. T represents tumor tissue; N represent normal tissue. Mean  $\pm$  S.D.;  $p$ , unpaired student  $t$ -test,  $*p \leq 0.05$ .

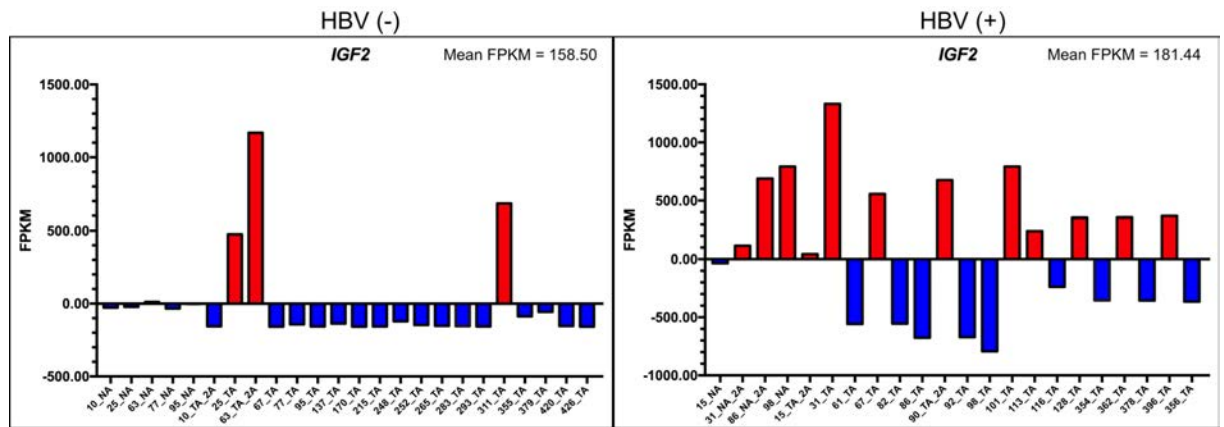


**Figure 40| Expression level of *IGF2* in HBV-positive and HBV-negative human biopsy samples.** Higher *IGF2* expression level was detected in both normal and tumor tissues of HBV-positive samples. NA, normal tissue; TA, tumor tissue; number, patient number; FPKM, fragments per kilobase million.

### 3.5.8 Biological roles of the common genes

With the common DEGs identified in the tumor tissues of both wild-type and mutant data set from various genotypes above, we performed the *Gene Ontology* (GO) classification of their roles on biological processes. Half of the genes (57/112 DEGs) were involved in the cellular process, and around 30% of the DEGs were involved in biological regulation, response to stimulus, and metabolic process. High proportion of these DEGs were associated with metabolic pathways (10/112 DEGs), focal adhesion (7/112 DEGs), regulation of actin cytoskeleton (6/112 DEGs), proteoglycans in cancer (6/112 DEGs) (**Figure 41**). From the top 20 KEGG pathways that we focused, *Pak1*, Rous sarcoma oncogene (*Src*), *Pak6*, SHC (Src homology 2 domain containing) transforming protein 2 (*Shc2*) involved in most of the pathways, in which *Pak1/Pak6* and *Src* are highly associated with pathways that regulating actin cytoskeleton, resulting in cell migration and invasion; while *Src* could also cooperate with *Shc2* in the Ras/Raf signalling pathway to regulate DNA repair.

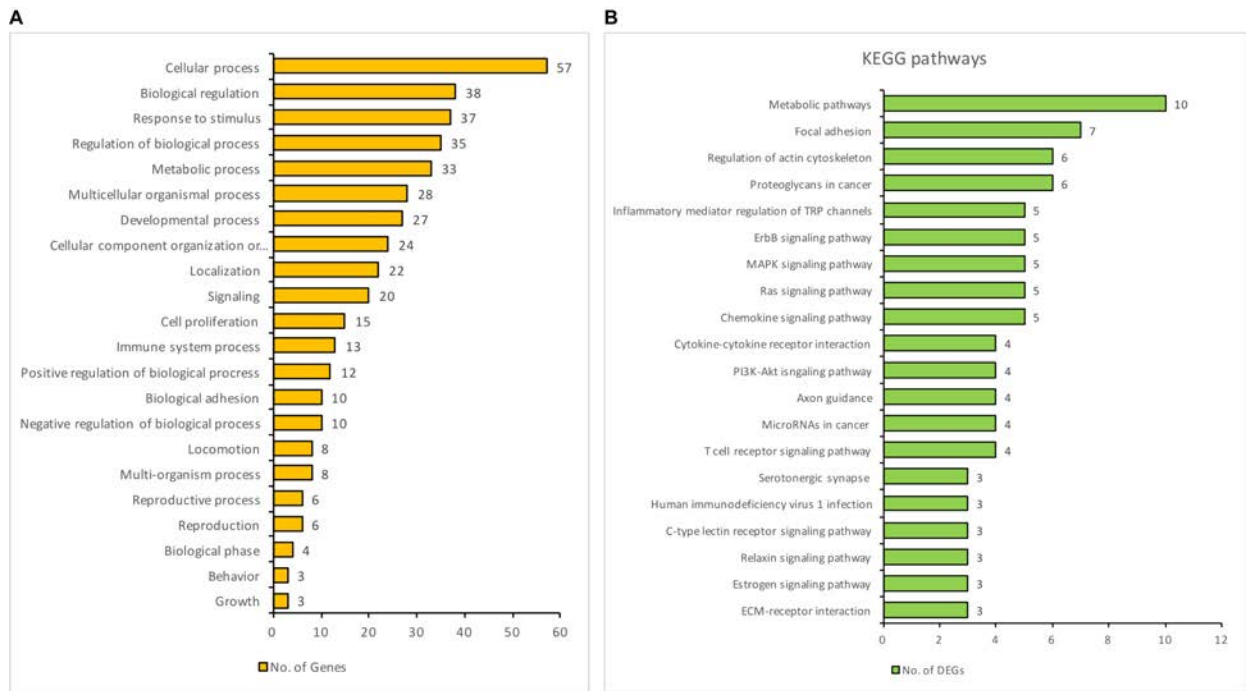


**Figure 41| Combinatorial analyses on common DEGs found in wild-type (WT) and mutant (Mut) tumor identified in Figure 35 and 36. (A) Biological processes of involved by these common DEGs. (B) KEGG pathways involved by these common DEGs.**

### 3.5.9 Arachidonic acid metabolism and HBx-induced HCC

While analysing the RNA-sequencing result, we found that genes involved in metabolic pathways were highly distorted. Most importantly, genes participated in the arachidonic acid (AA) metabolism were found to be altered in animals injected with various genotypes and variants of HBx gene, including prostaglandin-endoperoxide synthase 2 (*Ptgs2*) and leukotriene-B4 20-monooxygenase (*Cyp4f14* and *Cyp4f15*), which play role as pro-inflammatory factors, and arachidonate 12-lipoxygenase (*Alox12e*), which plays role as pro-carcinogenic factor. Therefore, we analysed the serum metabolite profiles of the experimental animals. From the RNA-sequencing result, genes involved in pro-inflammatory factors and pro-carcinogenic factor productions were significantly up-regulated, so metabolite profiles of prostaglandins, leukotriene B<sub>4</sub> and 12-hydroxyeicosatetraenoic acid (12-HETE), were mapped with commercially available reference standards or with online human metabolite database based on the mass fragmentation pattern and retention time. Taking serum metabolite profiles of HBx-B injected animals as example, pro-inflammatory factors, including leukotriene B<sub>4</sub>, prostaglandin B<sub>2</sub>, D<sub>2</sub> and E<sub>2</sub>, had significant higher abundance than the empty control (**Figure 42**). Additionally, the

pro-carcinogenic factor, 12-HETE, product of ALOX12 had significant higher abundance in the HBx-B injected animals compared with the empty control (**Figure 42**).

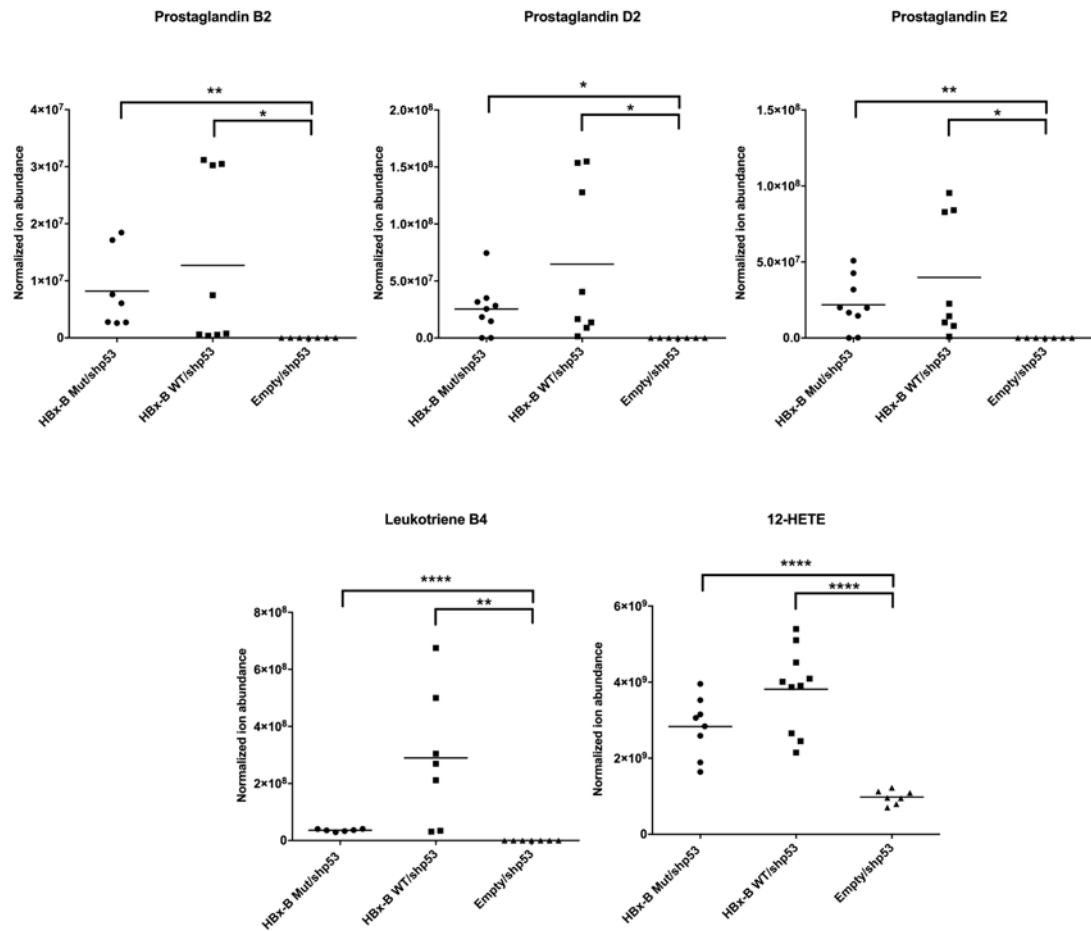


**Figure 42| Abundance of metabolites in arachidonic acid metabolism pathway.** Pro-inflammatory factors, including prostaglandin B2, D2 and E2, and leukotriene B<sub>4</sub> and pro-carcinogenic factor, 12-HETE, shown significant higher abundance than the empty control. Mean ± S.D.; *p*, unpaired student *t*-test, \**p* ≤ 0.05, \*\**p* ≤ 0.01, \*\*\*\**p* ≤ 0.0001.

## Chapter 4 - Discussion

### 4.1 HBx Genotype A

There was no significant difference in tumor burden rate and liver-to-whole-body weight ratio between experimental animals injected with either K130M/V131I mutant or wild-type variants of HBx genotype A in the context of *Trp53* knock-down. Both mutant and wild-type HBx of genotype A induced a low tumor burden with 0.4 and 0.5 tumor nodules per mouse, respectively. This indicated that both mutant and wild-type of HBx genotype A genes had low tumorigenic efficacy. However, there was a significant difference in the average liver-to-whole body weight ratio of mutant (7.235%) and wild-type HBx-A (7.002%) experimental animals compared with empty control animals (5.122%), indicating both mutant and wild-type variants of HBx-A gene could induce hepatomegaly. At the cellular level, both mutant and wild-type variants of HBx-A gene induced only mild inflammation, with no necrosis or fibrosis observed. This could suggest that both mutant and wild-type variants of HBx-A gene are less pathogenic. However, both mutant and wild-type of HBx-A gene could induce activation of AKT and WNT signalling pathways via phosphorylation of AKT and accumulation of non-phosphorylated CTNNB1 (**Figure 43**).

Comparing RNA expression profile between tissues from HBx-A Mut and WT with empty control, significant up-regulation of *Mup12* (169-fold increase) and *Mup14*, also known as prostaglandin D2 synthase (brain) (*Ptgds*) (>1000-fold increase) were detected. Both *Mup12* and *Mup14* encode for prostaglandin-H2 D-isomerase, which participated in the arachidonic acid (AA) metabolic pathway, a well-known inflammation related pathway. Prostaglandin-H2 D-isomerase converts prostaglandin H2 to prostaglandin D2 (PGD<sub>2</sub>), which is a pro-inflammatory factor that could increase vascular permeability. However, genes that encode for CYP2 proteins family were significantly down-regulated (>2-fold). The CYP2 proteins are associated with the production of anti-inflammatory factors. Thus, combining these finding, we suggested that HBx-A induced higher inflammation than empty control via activation of arachidonic acid metabolism by increasing pro-inflammatory factor, PGD<sub>2</sub>, and reducing anti-inflammatory factors by down-regulating CYP2 proteins production. Comparing RNA expression profiles between the normal tissues of HBx-A Mut and WT, only 2 genes were differentially expressed. This implied that the genetic backgrounds of both groups were similar. Although more than thousands of DEGs

were identified in the tumor of the HBx-A WT animal compared to its normal tissues, only one tumor sample was sequenced in the group. Thus, convincing conclusion cannot be drawn. On the other hand, *Fah* and *Susd4* were commonly down-regulated in HBx genotype A, B, C and D mutant and wild-type variants injected experimental animals. The down-regulation of *Fah* was due to the *Fah*-deficient genetic background of our experimental animals, even though *Fah* cDNA was included in the expression vector, its expression level could not be comparable with wild-type control, this was proven by the RT-PCR and IHC result that lower expression level of *Fah* was detected compared with wild-type control. The role of *SUSD4* in cancer progression is not well-studied. However, a recent *in vitro* study shown that growth and migration of breast cancer cells were inhibited by over-expression of *SUSD4* (112). While comparing the tumors induced by wild-type HBx gene of genotype A, C and D, *Arhgap27* and *Pak6* were the common DEGs identified in all groups (**Figure 43**). The roles of *Arhgap27* and *Pak6* in disease progression will be discussed in the later section.

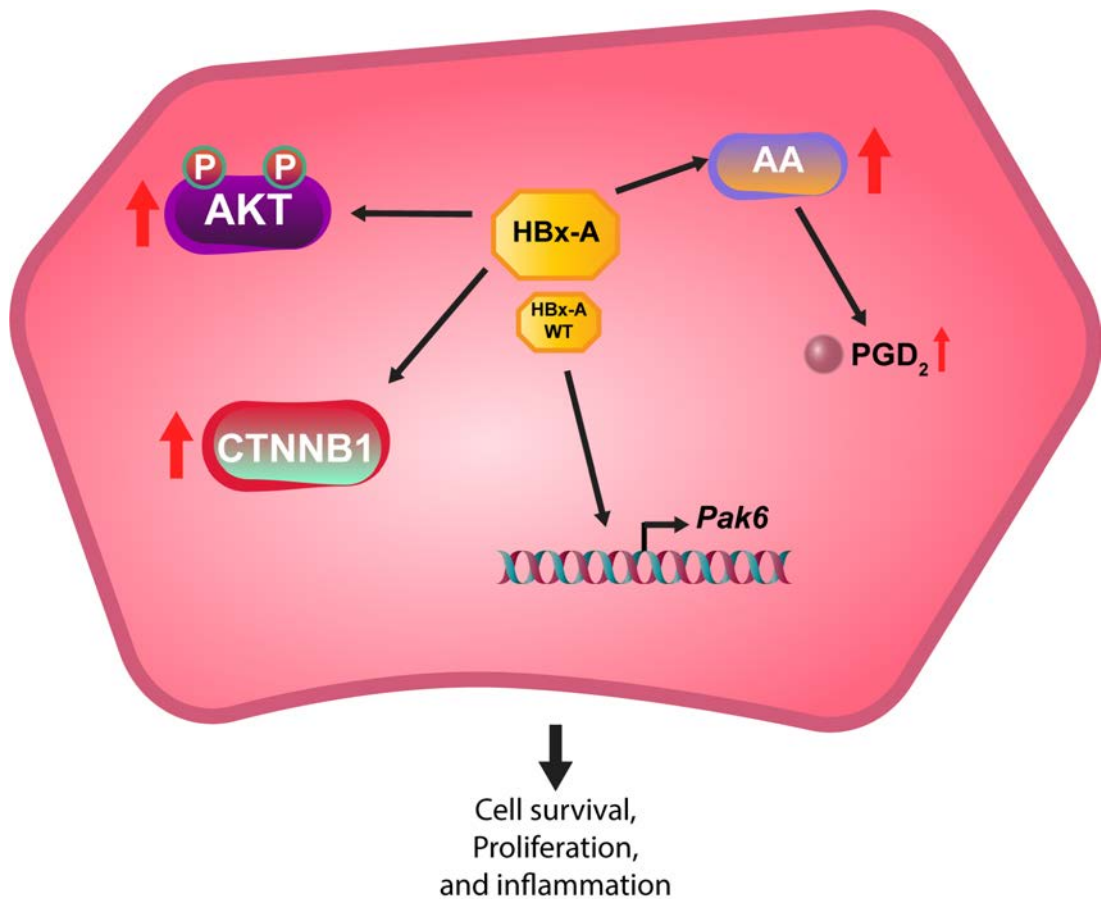


**Figure 43| Proposed schematic pathways involved in disease progression by HBx-A gene.** Increased level of phosphorylation of AKT (pAKT) and CTNNB1 was observed in hepatocytes of HBx-A injected animals. In addition, hepatitis as a result of HBx-A gene injection could be induced via activation of arachidonic acid metabolism by increasing pro-inflammatory factor, PGD<sub>2</sub>, and reducing anti-inflammatory factors by down-regulating CYP2 proteins production.

#### **4.2 HBx Genotype B**

K130M/V131I mutant variant of HBx-B gene induced higher tumor burden than its wild-type counterpart and significantly increased the liver weight of experimental animals. Although there was no significant difference in tumor burden efficacy between HBx-B Mut and HBx-B WT experimental groups, HBx-B Mut injected mice displayed a trend toward higher tumor burden than HBx-B WT counterpart ( $p = 0.1272$ ), in which HBx-B Mut induced 1.2 tumor nodules per mouse; while HBx-B WT induced 0.2 tumor nodules per mouse.

At the cellular level, hepatocytes of HBx-B Mut and WT injected mice were larger than those of empty control and *Fah*/SB11 non-injected mice, indicating hepatomegaly. In addition, severe inflammation, mild necrosis and fibrosis were observed in livers injected with HBx-B Mut indicating the development of chronic hepatitis. We found that higher degree of inflammation was observed in Asian-related genotypes B and C. Experimental animals injected with both mutant and wild-type HBx genes of genotype C induced severe inflammation, and HBx-B experimental groups induced moderate degree of inflammation; while both HBx-A and HBx-D experimental groups only induced mild inflammation. Therefore, it was believed that genotype B and C of HBx genes had a stronger effect on inducing inflammation, hence might promote necrosis and fibrosis development. Comparing RNA expression profiles between normal and tumor tissues from HBx-B Mut and WT with empty control, significant up-regulation of pro-inflammatory production genes, such as *Mup14* (274-fold increase) and prostaglandin-endoperoxide synthase 1 (*Ptgs1*) (26-fold increase) were detected. Upregulation of *Mup14* and *Ptgs1* increased the production of pro-inflammatory factors in the AA metabolic pathway. In addition, genes encoding LTB<sub>4</sub> 20-monooxygenase were down-regulated. LTB<sub>4</sub> 20-monooxygenase is an enzyme that converts LTB<sub>4</sub> to 20-OH-LTB<sub>4</sub>, the down-regulation of genes encoding LTB<sub>4</sub> 20-monooxygenase caused the accumulation of LTB<sub>4</sub> in cells. LTB<sub>4</sub> is also known to be a pro-inflammatory factor that attracts leukocytes to the injured tissue (113). Moreover, LTB<sub>4</sub> could also activate MEK/ERK and PI3K/AKT pathways through the interaction with the G protein-coupled receptors BLT2 in human pancreatic cancer cells (114, 115). However, genes encoding CYP2 proteins family were significantly down-regulated (~2-fold). In addition, the abundance of pro-inflammatory factors, such as prostaglandins B<sub>2</sub>, D<sub>2</sub>, E<sub>2</sub>, and LTB<sub>4</sub>, were significantly higher in serum of HBx injected animals compared with empty control (**Figure 42**). Thus, combining these finding, HBx-B induced inflammation via activation of AA metabolism by increasing pro-inflammatory factors, such as PGD<sub>2</sub> and LTB<sub>4</sub>, and reducing anti-inflammatory factors by down-regulating CYP2 proteins production (**Figure 44**). Furthermore, *Alox12e* was up-regulated in tumor induced by HBx-B Mut. ALOX12 has been described as a potential pro-carcinogenic enzyme (116), ALOX12 was shown to be associated with proliferation and anti-apoptosis of hepatocytes and its product 12-HETE had significant higher abundance in the serum of HBx injected animals compared with the empty control (**Figure 42**).

Furthermore, ALOX12 was reported in various cancers, such as esophageal squamous cell carcinoma, rectal cancer and breast cancer (117). Therefore, it is believed that higher abundance of 12-HETE due to up-regulation of *Alox12e* might be contributing to promoting tumor progression of HBV infected patients. Interestingly, we found that all DEGs involved in arginine biosynthesis pathway, including genes coding for aspartate transaminase, glutaminase, ornithine carbamoyltransferase, ASL and ASS were down-regulated in our RNA-seq result. Other researchers have reported that HCC was arginine auxotrophy due to the loss of ASS (118-120), suggesting that HBx-B Mut-induced HCC could also be auxotrophic to arginine.

Both IHC and Western blot analyses confirmed the over-expression of either HBx-B Mut or WT could activate phosphorylation of AKT and overexpress CTNNB1 in our injected mice. Moreover, the protein level of FOXO1 was significantly reduced in HBx-B Mut group. FOXO1 is a transcriptional factor that mediates the expression of downstream target genes involved in cell proliferation, apoptosis, cell cycle arrest and metabolism (121, 122). FOXO1 is also a downstream target of AKT, which can be phosphorylated by pAKT and be translocated to cytoplasm, then subsequently be degraded by ubiquitination (121) (**Figure 44**). Therefore, we proposed that HBx-B mutant variant increased cell proliferation and promoted cell cycle progression by activating AKT phosphorylation, which in turn, phosphorylated and translocated FOXO1 to cytoplasm for ubiquitination, resulting in reduced FOXO1 abundance in cells. In transcriptional analysis, both HBx-B Mut and WT induced over-expression of *Afp*, *Myc* and *Ccnd1*.

RNA-seq was performed to quantify the RNA expression level differences between tumor and its peripheral normal tissue of HBx-B injected mice. Few DEGs were identified in normal tissues of HBx-B Mut and WT animals compared with the empty normal control. There were low genetic background differences in RNA expression profiles between normal tissues of HBx-B Mut and WT, with only 3 DEGs identified and no significant pathways annotated. This suggests that the genetic background between the wild-type and mutant HBx genotype B injected animals were similar and DEGs found in tumor tissues were highly associated with disease progression. RNA expression profiles of genetic difference between the tumor and normal tissues in HBx-B Mut injected animals identified 377 DEGs. These DEGs were highly associated with metabolic pathways, such as arachidonic acid metabolism, bile

secretion, biosynthesis of amino acid and steroid hormone biosynthesis, and canonical signalling pathways including chemical carcinogenesis, focal adhesion, Ras signalling pathway, inflammatory mediator regulation of TRP channels, and ECM-receptor intermediation. Moreover, the participation of metabolic disorder was also confirmed by metabolomics analysis using the serum extracted from the HBx-B injected animals. Most importantly, *Igf2* was the only common DEG that identified in tumor induced by K130M/V131I mutant HBx of genotype B, C and D (**Figure 44**). The role of *Igf2* will be described in the later section.

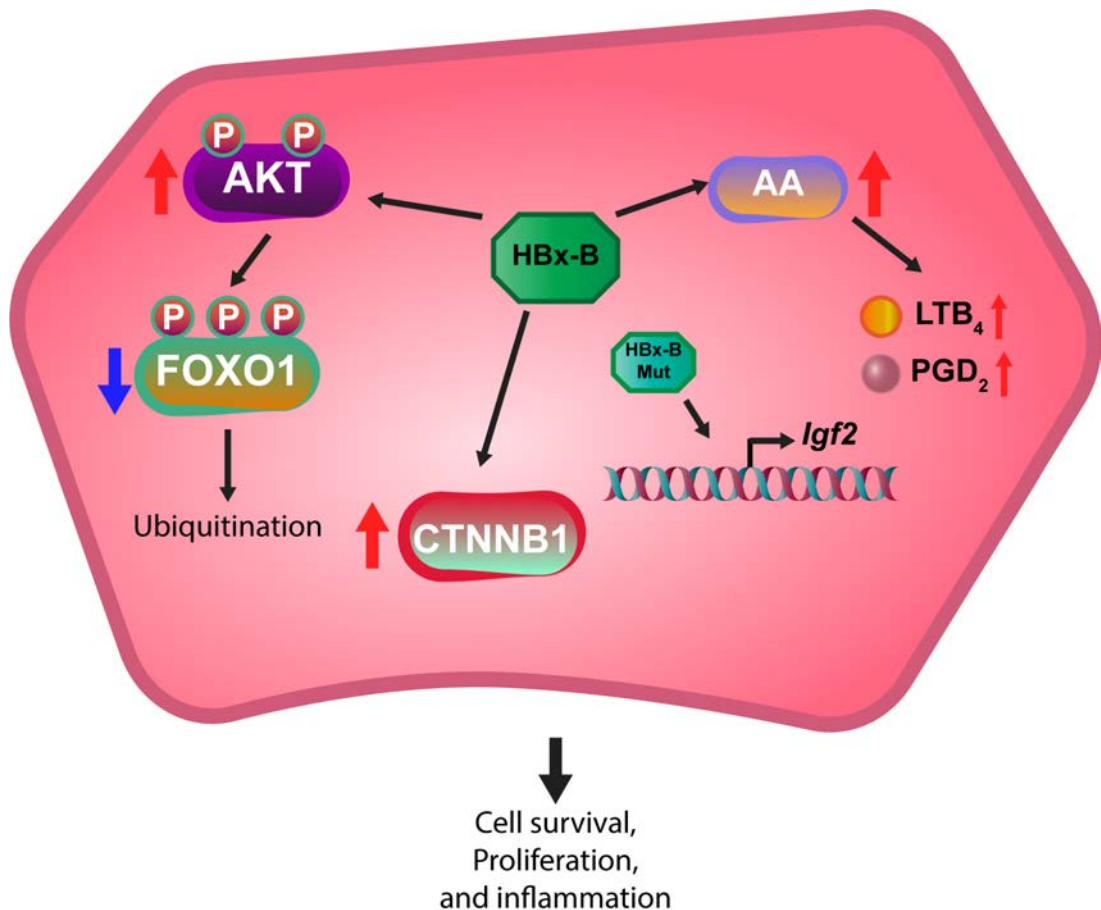


**Figure 44| Proposed schematic pathways involved in disease progression by HBx-B gene.** HBx-B mutant and wild-type of HBx-B gene induces phosphorylation of AKT (pAKT), which enters the nucleus to phosphorylate FOXO1. Phosphorylated FOXO1 gets transported to the cytoplasm, where it undergoes ubiquitination and hence the reduction in FOXO1 protein levels. On the other hand, increased level of CTNNB1 was observed in hepatocytes of HBx-B injected animals. In addition, hepatitis could be induced via activation of arachidonic acid metabolism by accumulation of pro-inflammatory factors, such as PGD<sub>2</sub> and LTB<sub>4</sub>. Furthermore, *Igf2* expression level was significantly increased in tumors of HBx-B Mut injected animals.

### 4.3 HBx Genotype C

There was no significant difference in tumor burden rate and liver-to-whole-body weight ratio between experimental animals injected with either mutant or wild-type variants of HBx genotype C in the context of *Trp53* knock-down. However, HBx gene of genotype C could induce more aggressive tumor progression than genotype A and B, with mutant induced development of 2.3 tumor nodules per mouse and wild-type induced 1.4 tumor nodules per mouse. This suggests that both mutant and wild-type of HBx genotype C genes have strong tumorigenic efficacy. Moreover, there was a significant difference in the average liver-to-whole body weight ratio of mutant (7.418%) and wild-type HBx-C (7.626%) experimental animals compared with empty control animals, this revealed both mutant and wild-type variants of HBx-C gene could induce hepatomegaly. At the cellular level, severe inflammation was observed in specimens from both mutant and wild-type variants of HBx-C gene, and pathological signs of binuclei, pyknotic nuclei, mitotic figure, karyocytomegaly, necrosis and fibrosis were also observed. This indicates that both mutant and wild-type variants of HBx-C gene have strong pathogenic ability. Both mutant and wild-type of HBx-C gene could induce activation of AKT and WNT signalling pathways via phosphorylation of AKT and accumulation of non-phosphorylated CTNNB1 (**Figure 45**). Additionally, while investigating the molecular pathways induced by over-expression of HBx in injected animals, suppression of PPARG was observed in HBx-C WT over-expressing animals (**Figure 17D**). Studies had shown that PPARG could regulate the cytoplasmic CTNNB1 level (123, 124), therefore, we proposed that over-expression of HBx suppressed PPARG, hence, preventing its ability of driving CTNNB1 for ubiquitination, resulting in accumulation of CTNNB1 in cytoplasmic of hepatocytes, excessed CTNNB1 would translocated into the nucleus and activate the transcription of its targeting genes (**Figure 45**).

Comparison on the RNA expression profiles of the normal tissues between HBx-C Mut and WT, only 4 DEGs were identified and these genes were scattered in different KEGG pathways. Small number of DEGs found between normal and wild-type groups also suggests that the genetic backgrounds of both groups were similar to each another. Comparing RNA expression profile between tissues from HBx-C Mut and WT with empty control, significant up-regulation of pro-inflammatory factors production genes, such as *Mup12* (55-fold increase) and *Mup14* (>2700-fold increase)

were detected. Additionally, *Cyp4f15*, which encodes for LTB<sub>4</sub> 20-monooxygenase was significantly down-regulated (~3-fold decrease) in tumors induced by HBx-C Mut and WT genes, this causes accumulation of LTB<sub>4</sub> in cells (**Figure 45**). Moreover, genes encoding for secretory phospholipase A2 (PLA2G), which converts lecithin into AA, were significantly up-regulated in tumors induced by HBx-C Mut and WT genes. On the other hand, genes the encode for CYP2 proteins family were significantly down-regulated (~2-fold). The CYP2 proteins are associated with the production of anti-inflammatory factors. Taken together, HBx-C induces inflammation via activation of arachidonic acid metabolism by increasing pro-inflammatory factor, PGD<sub>2</sub>, and reducing anti-inflammatory factors by down-regulating CYP2 proteins production.

Among the 16 DEGs identified in the tumor of the HBx-C WT animal compared to its normal tissues, *Slc7a1* and *Stmn1* were suggested to be related to HBV-induced HCC. The expression of *Slc7a1* and *Stmn1* were regulated by the microRNAs, *miR-122* and *miR-223*, respectively. *miR-122*, repressor of *Slc7a1*, was known to be regulated by up-stream HBV mRNAs and it was well identified as down-regulated miRNAs in HCC (125, 126). *miR-122* is a liver specific microRNAs and well characterized with its inverse linear correlation with HBV gene expression and replication (126). In our study, up-regulation of *Slc7a1* might be due to suppression of *miR-122* by over-expression of HBx gene (127). Besides, *miR-223* was another well-known down-regulated miRNA in HCC and reported with negative correlation to *Stmn1* expression (128). Most importantly, a recent study on the effect of HBx to miRNAs in HepG2 cells revealed that the expression level of *miR-223* could be repressed by expression of HBx gene (127), which supports our result and suggests that expression of HBx represses *miR-223*, which in turns up-regulates *Stmn1*, resulting in promoting HCC progression. Taken together, HCC progression by up-regulation of *Slc7a1* and *Stmn1* in our experiment model were due to repression of *miR-122* and *miR-223* under HBx over-expression (**Figure 45**).

Among the DEGs found in tumor of HBx-C Mut groups compared to the adjacent normal tissue or tumor of HBx-C WT groups, *Igf2* was found to be highly up-regulated (>6 fold-increase) (**Figure 45**). The effect of *Igf2* on HCC had been reported since 2004 that over-expression of *Igf2* could promote progression of HCC (129). Moreover, IGF-II was also an up-stream substrate of insulin-like growth factor 1 receptor

(IGF1R), upon binding of IGF-II to IGF1R, down-stream cascades of PI3K/AKT and RAS signalling pathways would be activated. Therefore, over-expression of HBx promotes HCC development via up-regulation of *Igf2*, resulting in activation of PI3K/AKT signalling pathway.

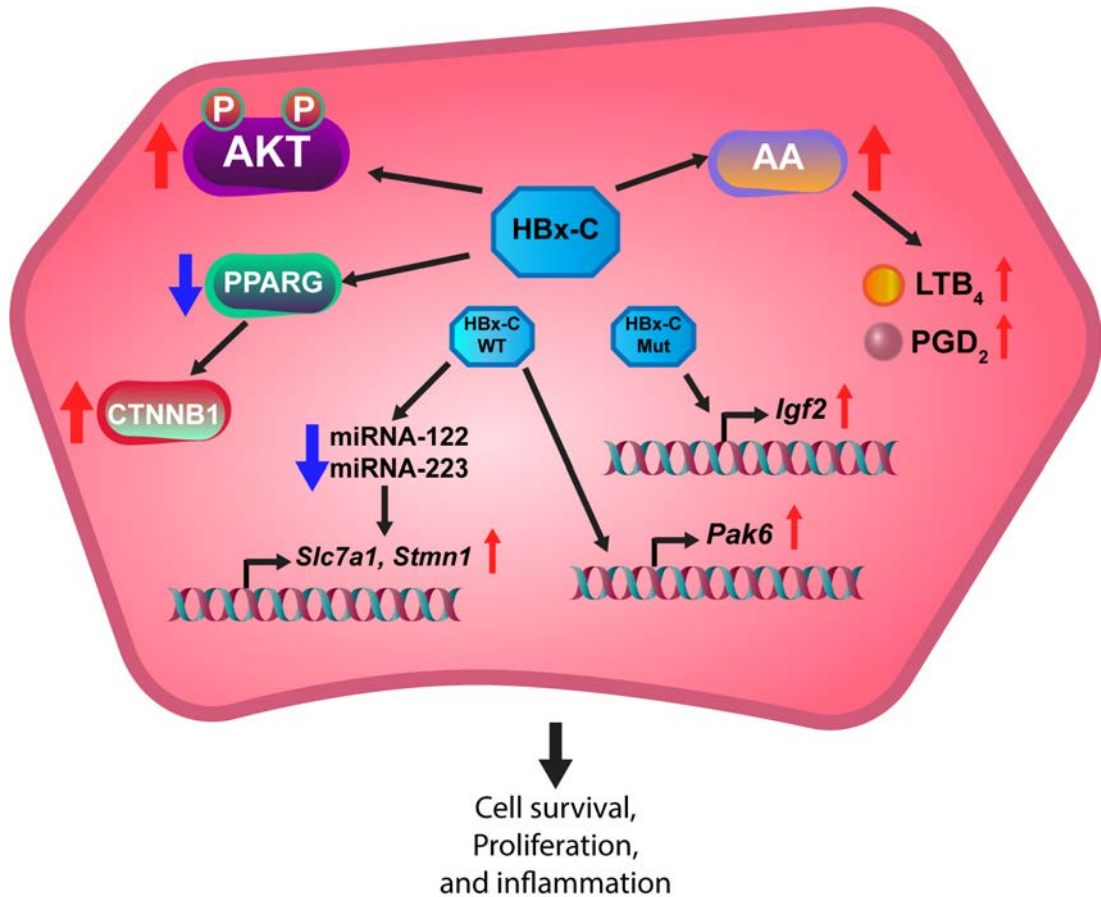


**Figure 45| Proposed schematic pathways involved in disease progression by HBx-C gene.** Increased protein levels of pAKT and CTNNB1 were observed in hepatocytes of HBx-C injected animals. In addition, hepatitis could be induced via activation of arachidonic acid metabolism by accumulation of pro-inflammatory factors, such as PGD<sub>2</sub> and LTB<sub>4</sub>. Furthermore, *Igf2* expression level was significantly increased in tumor of HBx-C Mut injected animals. While *Pak6*, *Slc7a1* and *Stmn1* expression levels were significantly up-regulated by HBx-C WT gene.

#### 4.4 HBx genotype D

Amongst the four genotypes analyzed, HBx genotype D was the most tumorigenic. Mutant variant (average tumor nodules per mouse = 7.6) of HBx-D could significantly promote tumor nodule formation compared to its wild-type counterparts (average

tumor nodules per mouse = 3.1) and, as discussed in the previous section, average liver-to-whole body weight ratio of HBx genotype D injected mice was significantly higher than empty control groups. Combining the result of liver-to-whole body weight ratio of all genotypes, we can conclude that hepatomegaly was induced by HBx gene in a genotype independent manner.

Our previous study had shown that HBx genotype D induced accumulation of CTNNB1 in hepatocytes (54). Therefore, to further study this genotype, RNA-seq was performed to determine the genetic differences between tumors induced by mutant and wild-type variants of HBx-D gene. Similar to genotypes A, B and C, significant up-regulation of pro-inflammatory factors production genes, such as *Mup12* (~32-fold increase) and *Mup14* (~640-fold increase), and down-regulation of *Cyp4f14* were detected in HBx-D Mut and WT experimental groups compared to empty control. In addition, genes that encode for CYP2 proteins family were significantly down-regulated (~2-fold). Taken together, HBx-D also induces inflammation via activation of arachidonic acid metabolism by increasing pro-inflammatory factors and reducing anti-inflammatory factors by down-regulating CYP2 proteins production (**Figure 46**).

From RNA-seq result, only 5 DEGs were found in normal tissues of mutant injected animals against normal tissue of wild-type injected animals. This result was consistent with genotypes A, B and C that were analyzed in this project, which showed that mutant and wild-type HBx genes did not cause large expression difference in normal tissue. However, K130M/V131I mutant variants of the HBx gene possess a stronger tumor induction effect, since HBx mutant variants of genotypes B, C and D were more susceptible to tumor nodule formation. In order to identify the genes that contributed to tumor formation, a total of 203 DEGs were identified in tumor induced by HBx-D wild-type compared to its normal tissues. These DEGs mainly associated with inflammation-related pathways, such as arachidonic acid metabolism and inflammatory mediator regulation of TRP channels. Besides, a significant number of DEGs (12 DEGs) were associated with focal adhesion pathway that regulates cell survival and motility.

On the other hand, only 10 DEGs were identified in tumors of HBx-D mutant in referring to its normal tissues. Within these 10 DEGs, *Igf2*, a gene that codes for the

up-stream activator epidermal growth factor (EGF) of various cancer pathways, such as Ras, MAPK and PI3K/AKT signalling pathways, was up-regulated (3.6-fold increase) in the tumor samples (**Figure 46**). This provides further support that HBx induced HCC progression via activation of PI3K/AKT signalling pathway. Finally, 13 DEGs were identified in tumors induced by HBx-D mutant gene in referring to tumors induced by HBx-D wild-type gene. Interestingly, all these DEGs were down-regulated.

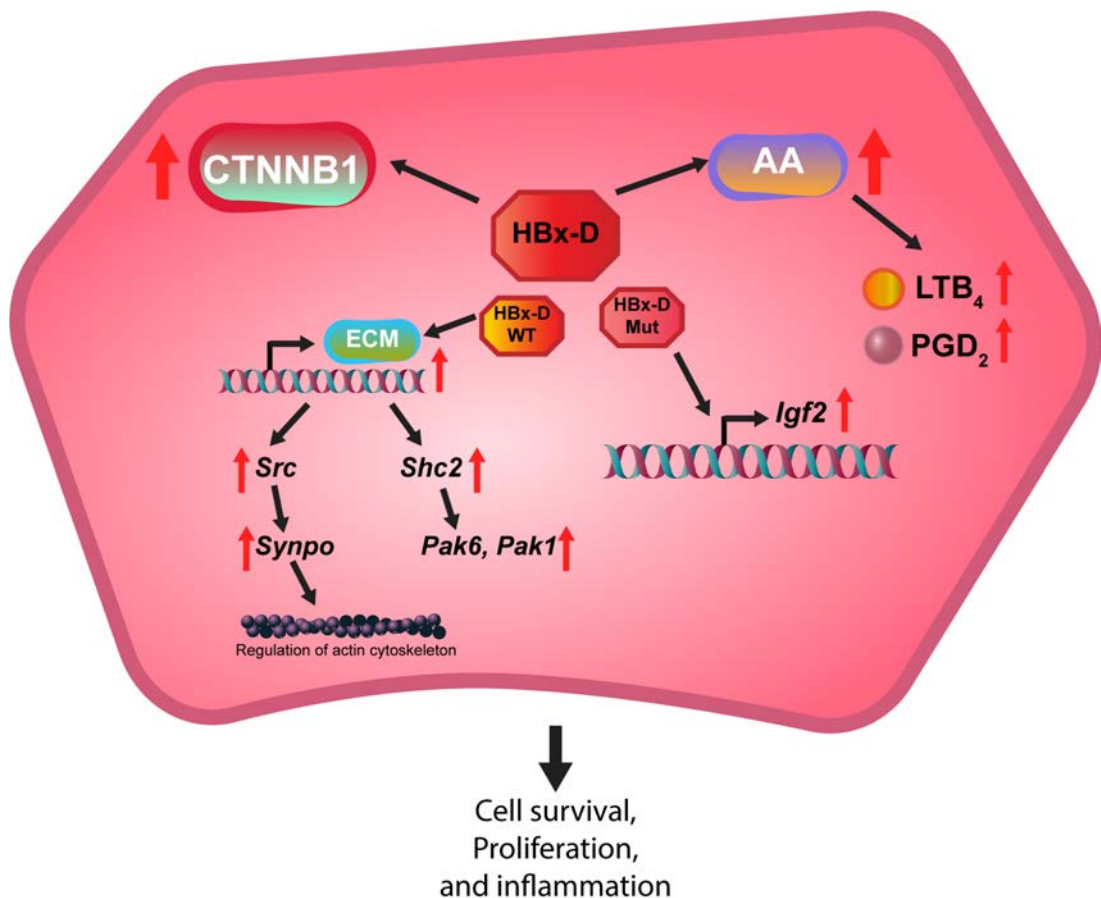


**Figure 46| Proposed schematic pathways involved in disease progression by HBx-D gene.** Increased protein level of CTNNB1 were observed in hepatocytes of HBx-D injected animals. In addition, hepatitis could be induced via activation of arachidonic acid metabolism by accumulation of pro-inflammatory factors, such as PGD<sub>2</sub> and LTB<sub>4</sub>. Furthermore, *Igf2* expression level was significantly increased in tumor of HBx-D Mut injected animals. While expression levels of genes encoding for extra-cellular matrix (ECM), *Src*, *Shc2*, *Synpo*, *Pak1*, and *Pak6* were significantly up-regulated by HBx-D WT gene.

#### ***4.5 Arhgap27 and Pak6 were commonly up-regulated in the tumors of genotypes A, C and D of HBx wild-type gene***

*Arhgap27* and *Pak6* were commonly up-regulated in tumors induced by wild-type HBx of genotypes A, C and D, and a significant co-occurrence of *ARHGAP27* and *PAK6* was reported in TCGA liver cancer database (cBioPortal). *Arhgap27* had an average of 2.7-fold up-regulation and *Pak6* had an average of 8.28-fold upregulation (**Table 7**). Both *Arhgap27* and *Pak6* encode proteins involved in Ras homologous (Rho) family proteins. The three well-studied Rho family proteins are RAC1, CDC42 and RHOA, which enhance morphologic transformation induced by activated RAS (130, 131). Rho-family proteins are small GTP-binding proteins that interconverts between GDP-bound form (inactive) and GTP-bound form (active) (132). The active Rho-GTP interacts with a wide spectrum of effectors that regulated a variety of cellular pathways including cytoskeletal dynamics, motility, cytokinesis and transcriptional activity (132). *Arhgap27* encodes for Rho GTPase-activating protein (RhoGAP) that inactivate Rho by promoting GTP hydrolysis (133). The up-regulation of *Arhgap27* might imply inactivation of Rho proteins. However, there is contradicting evidence that RhoGAP inactivates Rho, but yet activation of Rho is associated with morphologic transformation (132). Therefore, up-regulation of *Arhgap27* might be the result of a feed-back mechanism from over-activation of RAC/PAK signalling pathway, since diaphanous 1 (*Diaph1*), which encodes for a down-stream molecule mDia1, of RHO signalling pathways was significantly up-regulated (4.6-fold increase) in tumors induced by HBx-A WT and HBx-D WT genes (**Figure 47** and **Table 7**).

*Pak6*, which encodes for the down-stream molecule PAK, was significantly up-regulated in tumors of all genotypes. PAK is an effector of RAC proteins, where activation of RAC cascade triggers actin polymerization and induces membrane protrusion and cell spreading, resulting in mesenchymal cell morphology (134) (**Figure 47**). It possesses oncogenic roles that regulate cell proliferation, cell survival, adhesion and migration (135) and over-expression of PAKs had been reported in various human malignancies such as prostate, colorectal, bladder, melanoma, breast, and ovarian carcinoma (135). Finally, transmembrane protein 117 (*Tmem117*) was one of the common genes that up-regulated in tumor of genotype C and D HBx wild-

type groups, since these 2 groups induced similar tumor burden effect. This suggests that *Tmem117* might be an important gene for tumor progression. Recently, TMEM117 was reported as a novel transmembrane protein that involved in endoplasmic reticulum (ER) stress-mediated cell death signalling by regulating mitochondrial membrane potential, reactive oxygen species (ROS) level and Caspase-3 activity (136). It has been reported that *TMEM117* knock-down by short hairpin RNA led to membrane potential loss, ROS levels increase, ER stress sensor C/EBP homologous protein up-regulation, and Caspase-3 activation, resulting in cell death (136).

#### ***4.6 Igf2 was commonly up-regulated in the tumors of genotypes B, C and D of HBx mutant gene***

A common DEG, *Igf2*, which was identified in tumors induced by K130M/V131I mutant HBx gene of genotype B, C and D, was highly up-regulated (70-fold increase) (**Table 7**). Additionally, in our study on RNA expression profiling of human clinical samples, we found that HBV-positive samples had higher expression of *IGF2* with average FPKM compared to that of HBV-negative samples and 55% of HBV-positive samples had expression level above its average FPKM (**Figure 40**). *Igf2* encodes for a mitogenic peptide, namely insulin-like growth factor 2 (IGF2). Over-expression of *IGF2* has been reported in various cancers, such as colorectal, breast, prostate and lung cancer, and is associated with poor prognosis (137, 138). IGF2 activates insulin/IGF signalling cascades via the binding with IGF1 receptor (IGF1R), insulin receptor isoform A (IR-A) and IGF1R-IR-A hybrid receptor. The insulin/IGF signalling pathway regulates cell growth, proliferation and survival (138) (**Figure 47**). To initiate the signalling cascade, other IGF components such as IGF1, IGF2 mRNA binding protein (IGF2BPs and IMPs), and IGF binding proteins (IGFBPs) that regulate post-transcriptional and post-translational events of IGFs, as well as IGF receptors including IGF1R and IGF2R are required (138). In human adults, IGF2 is continuously secreted, and up-regulation of *IGF2* was reported in both childhood and adult malignancies and significantly increase risk of hepatoblastoma development (138). Researches had shown that binding of IGF2 onto IGF1R could activate PI3K/AKT pathway in esophageal squamous cell carcinoma (138). Importantly, IGF/AKT/mTOR signalling pathway could be activated by loss of p53, since *IGFBPs*

are also target genes of p53 (138). In our study, IGFBP-related genes such as *Igf2bp3*, *Igfbp1*, and *Igfbp2* were up-regulated in our RNA sequencing result. In heterozygous *Trp53* mice, over-expression of *Igf2* could accelerate tumor formation (139). Besides, according to the IPA result, *Igf2*, *prostate stem cell antigen (PscA)* and *Fgd3* commonly found in mutant HBx gene of genotype B and C, together with *Spink1* and *Arhgap27*, commonly found in mutant HBx gene of genotype B and D were associated with liver tumor development. According to a previous study on gene expression profiling of HCC patients acquired from various risk factors, *IGF2* was one of the differentially expressed gene that only found in HBV-induced HCC cases (140), this further confirmed the importance of *Igf2* in HCC progression induced by over-expression of HBx gene with *Trp53* knock-down background in our study. Additionally, this study also revealed that about 88% of the tumors from HBV-induced HCC patients ( $n = 8$ ) were SPINK1-positive by IHC staining (140), consistent with our RNA-seq results.

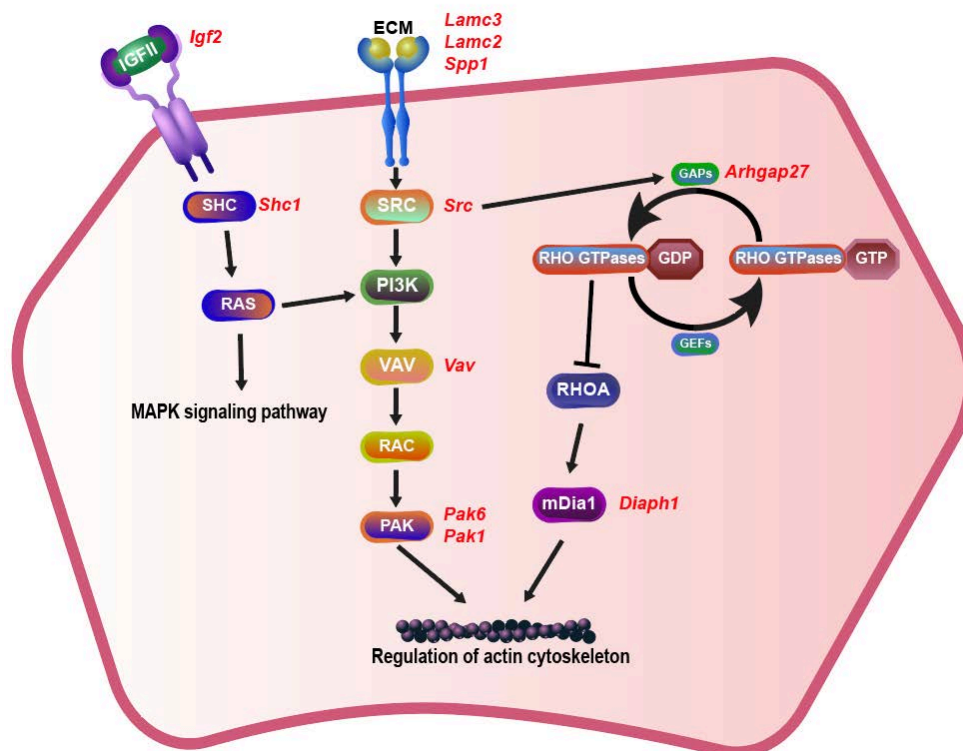


**Figure 47| Proposed schematic genetic pathways involved in disease progression by HBx gene.** HBx induced up-regulation of *Igf2* and *Shc1* in the MAPK signalling pathway. Moreover, up-regulation of genes producing extracellular matrix (ECM), such as *Lamc3*, *Lamc2* and *Spp1*, were detected in HBx injected animals. Along this signalling cascade pathway, *Src*, *Vav*, *Pak6* and *Pak1* were up-regulated. A strong association exists between this signalling pathway with actin content in cells in the context of HBx over-expression.

Gene	Gene Name	HBx-A WT_T	HBx-C WT_T	HBx-D WT_T	HBx-B Mut_T	HBx-C Mut_T	HBx-D Mut_T
<i>Igf2</i>	Insulin-like growth factor 2				5.3	7.3	3.6
<i>Pak6 / Pak1* / Pak3**</i>	P21 (RAC1) activated kinase 6 / 1 / 3	3.3 / 3.8*	2.6	3.1 / 1.3*	3.6	5.9**	
<i>Arhgap27</i>	Rho GTPase activating protein 27	1.5	1.1	1.6			1.3
<i>Shc1</i>	Src homology 2 domain-containing transforming protein C1	4.8		3.3			
<i>Lamc3 / Lamc2*</i>	Laminin gamma 3 / 2			5.1	4.5 / 3.6*		
<i>Spp1</i>	Secreted phosphoprotein 1	3.8		2.1	3.8		
<i>Src</i>	Rous sarcoma oncogene	1.8		1.7	1.6		
<i>Vav1</i>	Vav 1 oncogene	1.8					
<i>Diaph1</i>	Diaphanous related formin 1	1.9		2.0	2.0		

**Table 7| Expression level of genes in proposed schematic genetic pathways induced by HBx expression.** Table shown the log 2 mRNA expression level of genes involved in the genetic pathways induced by HBx gene. The log 2 expression level was in comparison with its normal tissue of corresponding group.

#### **4.7 Contributions of the study and future directions**

We found that different genotypes of HBx would induce HCC progression via different signalling pathways, in which HBx\_K130M/V131I mutant variant of genotype B tends to activate the AKT/FOXO1 pathway; while genotype C tends to activate the PPARG/CTNNB1 pathway, therefore, for better treatment strategy, patients should perform a pre-treatment diagnosis of the infected HBV genotypes for a better treatment regime. In this study, we found that AKT inhibitor (AZD5363) could significantly repress the growth of HBV infected cell line (SNU-449) and HBx-B Mut and WT transfected HHL7 cell lines (**Figure 48**). Therefore, AZD5363 could be a potential treatment to HBV genotype B infected patients. On the other hand, in our previous study, we found that DAW22, a natural compound extracted from the

*Ferula ferulaeoides*, could target AKT, ERK and CTNNB1 in malignant peripheral nerve sheath tumor. Accounting for the multiple targeting role of DAW22, and different genotypes of HBx would activate different signalling pathways, AKT/FOXO1 signalling pathway was dominantly activated in genotype B HBx injected animals; while PPARG/CTNNB1 was predominantly activated in genotype C HBx injected animals, therefore, it would be interesting to find out if DAW22 could suppress the tumor progression in animals injected with various genotypes of HBx gene in the future (141).

Additionally, different degrees of pathological signs were observed in HBx experimental animals, severe inflammation was observed in HBx genotype B and C injected animals, fibrosis and necrosis were observed in HBx genotype B injected animals. During further validating the contribution of inflammation to HCC progression, we found that genes in the AA metabolic pathway, the well-known metabolic pathway that associated with inflammation, were highly distorted, and the inflammatory factors, including various prostaglandins and leukotriene, had significant higher abundance in the serum of the HBx-B injected animals than that of the empty control. Therefore, we believed that inflammation might play a critical role in promoting HCC progression and minimizing the inflammation event might be able to slow down the disease progression. In our lab, we found that sodium tanshinone IIA sulfonate (STS), a water-soluble compound extracted from the roots of *Salvia miltiorrhiza*, could suppress inflammation in oleic acid and palmitic acid treated hepatic cell lines. Therefore, inhibiting inflammation by STS could be a new treatment regime for HBV infected patients. However, further experiments should be performed to confirm its effect *in vitro* and *in vivo* before clinical trial (142).

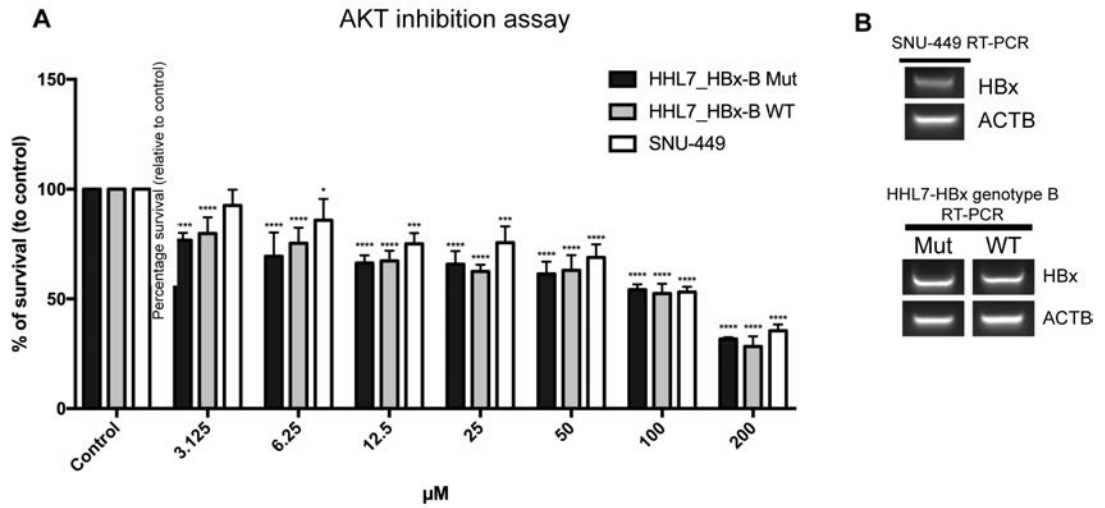


**Figure 48| Survival rate of HBx expressing cell lines under different concentrations of AKT protein kinase inhibitor (AZD5363).** Mean  $\pm$  S.D.;  $p$ , ordinary one-way ANOVA, \*,  $p \leq 0.05$ , \*\*\*,  $p \leq 0.001$ , \*\*\*\*,  $p \leq 0.0001$ . Representative RT-PCR analyses for the HBx genes in SNU-449 and transfected HHL7 cells.

## Chapter 5 – Conclusion

For a better understanding on the contributions of HBV on HCC development, and discovering the molecular mechanisms induced by various genotypes of HBV, we used the transgenic mouse model to compare the tumorigenic efficiency of K130M/V131 mutant and wild-type variants of HBx in genotypes A, B, C and D in this study. The disease progression pathways in both transcriptional and translational aspects were analyzed, with the consideration of the metabolomics influenced by the HBx gene. In summary, the most tumorigenic HBx gene was genotype D for both wild-type and mutant variants; while genotype A was the least tumorigenic HBx genotype. Mutant variant of genotype B had a stronger tumor burden than its wild-type counterpart; while both wild-type and mutant of genotype C induced similar tumorigenic evidence as mutant of genotype B.

In general, both wild-type and mutant variants of all HBx genotypes played an important role in hepatitis via activation of the arachidonic acid metabolic pathway. Significant up-regulation of *Mup14* and down-regulation of *Cyp4f14* or *Cyp4f15* caused accumulation of pro-inflammatory factors, such as various prostaglandins and  $LTB_4$ , in the liver; while suppression of anti-inflammatory factors such as EETs production by down-regulating CYP2 encoding genes was also observed in mutant and wild-type variants of all HBx genotypes (**Figure 49**). In addition, HBx could also alter metabolism of various metabolites including linoleic acid, retinol, and steroid hormone, which could contribute to disease progression.

At the transcriptional level, *Igf2* was identified as a commonly up-regulated gene in tumors induced by genotypes B, C and D HBx mutant variants; while *Arhgap27* and *Pak6* were commonly up-regulated in tumors induced by genotypes A, C and D HBx wild-type variants. Up-regulation of *Igf2* has been reported to be associated with PI3K/AKT and MAPK signalling pathways; while *Pak6* has been shown to participate in actin cytoskeleton regulation via RAC/PAK signalling pathway. Moreover, significant co-occurrence of *PAK6* and *ARHGAP27* was reported in TCGA liver cancer database, and *IGF2* had tendency to co-occur with *PAK6* as well, these provided us the hints that these candidate genes might play vital roles in promoting tumor development in HBV infected patients. Additionally, at the translational level by focusing on the protein abundance in HBx injected animals, the role of CTNNB1

in tumor development was further confirmed and, interestingly, we found that different genotypes of HBx gene accelerated tumor progression by activating different signalling pathways predominantly. HBx-B mutant variant promoted tumor progression via phosphorylation of AKT in PI3K/AKT signalling pathway and reduced FOXO1 production, and the growth of HBx-B infected cells could be suppressed by AKT inhibitor; while HBx-C wild-type variant promoted tumor progression by suppressing the activity of PPARG, hence caused accumulation of CTNNB1 in cells, excess CTNNB1 would translocated into nucleus of hepatocytes and trigger the transcription of its downstream targeting genes (**Figure 47**) (109). Based on our findings, we suggested that HBV-infected patients should perform a genotype screening before targeted treatment with inhibitors. Generally, preventing inflammation might be a potential regime to slow down HBV-induced tumor development.

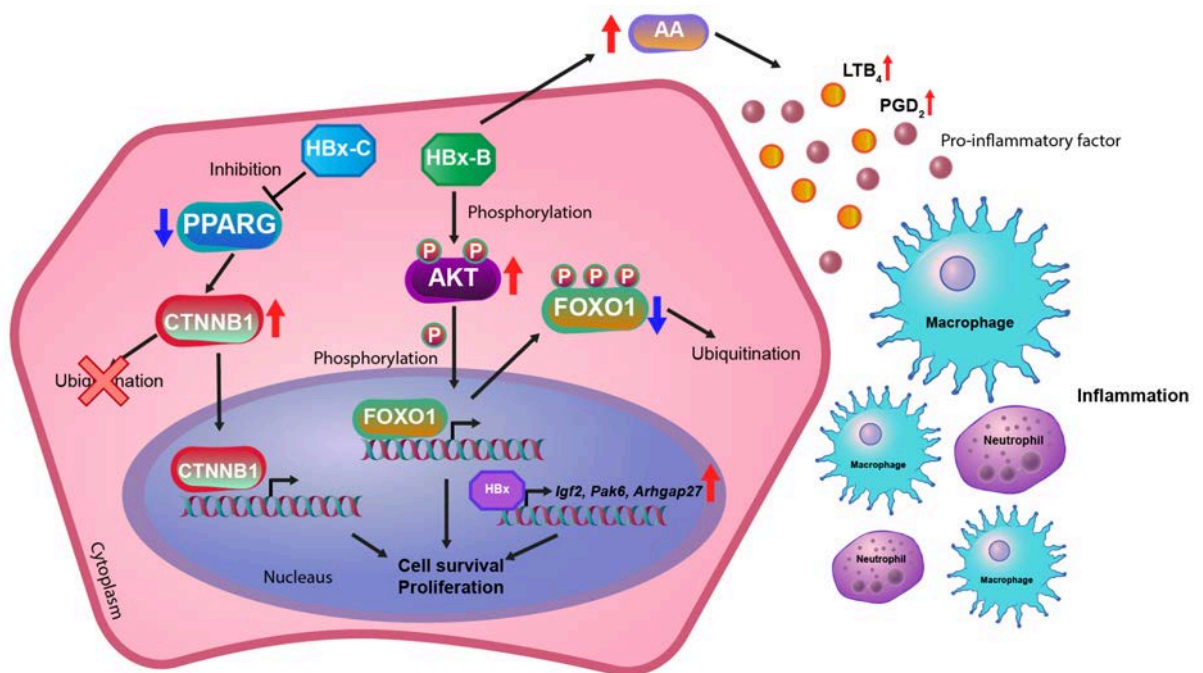


**Figure 49| Summarized proposed schematic pathways involved in disease progression by HBx gene.** Different genotypes of HBx gene could induce tumor progression via activating different signalling pathways predominantly. HBx-B gene induced phosphorylation of AKT (pAKT), which entered the nucleus to phosphorylate FOXO1. Phosphorylated FOXO1 was transported to the cytoplasm, where it underwent ubiquitination, resulting FOXO1 protein reduction. On the other hand, HBx-C gene suppressed PPARG, resulting in accumulation of CTNNB1 in hepatocytes, and excessed CTNNB1 could translocate into nucleus of hepatocyte and trigger expression of downstream target genes. In addition, hepatitis could be induced

via activation of arachidonic acid metabolism by accumulation of pro-inflammatory factors, such as PGD<sub>2</sub> and LTB<sub>4</sub>. Furthermore, *Igf2* expression level was significantly increased in tumor of HBx Mut injected animals. While expression levels of *Pak6* and *Arhgap27* were significantly up-regulated by HBx WT gene.

## References

1. Akinyemiju T, Abera S, Ahmed M, Alam N, Alemayohu MA, Allen C, Al-Raddadi R, et al. The Burden of Primary Liver Cancer and Underlying Etiologies From 1990 to 2015 at the Global, Regional, and National Level Results From the Global Burden of Disease Study 2015. *Jama Oncology* 2017;3:1683-1691.
2. Laursen L. A preventable cancer. *Nature* 2014;516:S2-3.
3. Ganeshan D, Szklaruk J, Kundra V, Kaseb A, Rashid A, Elsayes K. Imaging Features of Fibrolamellar Hepatocellular Carcinoma. *American Journal of Roentgenology* 2014;202:544-552.
4. Ganeshan D, Szklaruk J, Kaseb A, Kattan A, Elsayes KM. Fibrolamellar hepatocellular carcinoma: multiphasic CT features of the primary tumor on pre-therapy CT and pattern of distant metastases. *Abdom Radiol (NY)* 2018.
5. Parkin DM, Ohshima H, Srivatanakul P, Vatanasapt V. Cholangiocarcinoma - Epidemiology, Mechanisms of Carcinogenesis and Prevention. *Cancer Epidemiology Biomarkers & Prevention* 1993;2:537-544.
6. Blechacz B. Cholangiocarcinoma: Current Knowledge and New Developments. *Gut Liver* 2017;11:13-26.
7. Gaballah AH, Jensen CT, Palmquist S, Pickhardt PJ, Duran A, Broering G, Elsayes KM. Angiosarcoma: clinical and imaging features from head to toe. *Br J Radiol* 2017;90:20170039.
8. Ananthkrishnan A, Gogineni V, Saeian K. Epidemiology of Primary and Secondary Liver Cancers. *Semin Intervent Radiol* 2006;23:47-63.
9. Siegel RL, Miller KD, Jemal A. Cancer Statistics, 2018. *Ca-a Cancer Journal for Clinicians* 2018;68:7-30.
10. WHO. GUIDELINES FOR THE PREVENTION, CARE AND TREATMENT OF PERSONS WITH CHRONIC HEPATITIS B INFECTION, MARCH 2015; 2015.
11. Brunetto MR, Oliveri F, Colombatto P, Moriconi F, Ciccoross P, Coco B, Romagnoli V, et al. Hepatitis B Surface Antigen Serum Levels Help to Distinguish Active From Inactive Hepatitis B Virus Genotype D Carriers. *Gastroenterology* 2010;139:483-490.
12. Lok ASF, McMahon BJ. Chronic Hepatitis B: Update 2009. *Hepatology* 2009;50:661-662.

13. McMahon BJ. The Natural History of Chronic Hepatitis B Virus Infection. *Hepatology* 2009;49:S45-S55.
14. Castera L. Noninvasive Methods to Assess Liver Disease in Patients With Hepatitis B or C. *Gastroenterology* 2012;142:1293-+.
15. Park SH, Kim CH, Kim DJ, Suk KT, Cheong JY, Cho SW, Hwang SG, et al. Usefulness of Multiple Biomarkers for the Prediction of Significant Fibrosis in Chronic Hepatitis B. *Journal of Clinical Gastroenterology* 2011;45:361-365.
16. Zhang YG, Wang BE, Wang TL, Ou XJ. Assessment of hepatic fibrosis by transient elastography in patients with chronic hepatitis B. *Pathology International* 2010;60:284-290.
17. Papatheodoridis G, Buti M, Cornberg M, Janssen H, Mutimer D, Pol S, Raimondo G, et al. EASL Clinical Practice Guidelines: Management of chronic hepatitis B virus infection. *Journal of Hepatology* 2012;57:167-185.
18. Bam RA, Birkus G, Babusis D, Cihlar T, Yant SR. Metabolism and antiretroviral activity of tenofovir alafenamide in CD4(+) T-cells and macrophages from demographically diverse donors. *Antiviral Therapy* 2014;19:669-677.
19. Bam RA, Yant SR, Cihlar T. Tenofovir alafenamide is not a substrate for renal organic anion transporters (OATs) and does not exhibit OAT-dependent cytotoxicity. *Antiviral Therapy* 2014;19:687-692.
20. Ringehan M, McKeating JA, Protzer U. Viral hepatitis and liver cancer. *Philosophical Transactions of the Royal Society B-Biological Sciences* 2017;372.
21. Yan H, Zhong GC, Xu GW, He WH, Jing ZY, Gao ZC, Huang Y, et al. Sodium taurocholate cotransporting polypeptide is a functional receptor for human hepatitis B and D virus. *Elife* 2012;1.
22. Yan H, Peng B, He WH, Zhong GC, Qi YH, Ren BJ, Gao ZC, et al. Molecular Determinants of Hepatitis B and D Virus Entry Restriction in Mouse Sodium Taurocholate Cotransporting Polypeptide. *Journal of Virology* 2013;87:7977-7991.
23. Barrera A, Guerra B, Notvall L, Lanford RE. Mapping of the hepatitis B virus pre-S1 domain involved in receptor recognition. *Journal of Virology* 2005;79:9786-9798.
24. Glebe D, Urban S, Knoop EV, Cag N, Krass P, Grun S, Bulavaite A, et al. Mapping of the hepatitis B virus attachment site by use of infection-inhibiting preS1 lipopeptides and tupaia hepatocytes. *Gastroenterology* 2005;129:234-245.

25. Schulze A, Schieck A, Ni Y, Mier W, Urban S. Fine Mapping of Pre-S Sequence Requirements for Hepatitis B Virus Large Envelope Protein-Mediated Receptor Interaction. *Journal of Virology* 2010;84:1989-2000.
26. Neuveut C, Wei Y, Buendia MA. Mechanisms of HBV-related hepatocarcinogenesis. *J Hepatol* 2010;52:594-604.
27. Grimm D, Thimme R, Blum HE. HBV life cycle and novel drug targets. *Hepatol Int* 2011;5:644-653.
28. Kramvis A, Kew M, Francois G. Hepatitis B virus genotypes. *Vaccine* 2005;23:2409-2423.
29. Shi WF, Zhang Z, Ling C, Zheng WM, Zhu CD, Carr MJ, Higgins DG. Hepatitis B virus subgenotyping: History, effects of recombination, misclassifications, and corrections. *Infection Genetics and Evolution* 2013;16:355-361.
30. Sunbul M. Hepatitis B virus genotypes: global distribution and clinical importance. *World J Gastroenterol* 2014;20:5427-5434.
31. Ayub A, Ashfaq UA, Haque A. HBV Induced HCC: Major Risk Factors from Genetic to Molecular Level. *Biomed Research International* 2013.
32. Zhang Q, Cao G. Genotypes, mutations, and viral load of hepatitis B virus and the risk of hepatocellular carcinoma: HBV properties and hepatocarcinogenesis. *Hepat Mon* 2011;11:86-91.
33. Gong DY, Chen EQ, Huang FJ, Leng XH, Cheng X, Tang H. Role and Functional Domain of Hepatitis B Virus X Protein in Regulating HBV Transcription and Replication in Vitro and in Vivo. *Viruses-Basel* 2013;5:1261-1271.
34. Ghany M, Liang TJ. Drug targets and molecular mechanisms of drug resistance in chronic hepatitis B. *Gastroenterology* 2007;132:1574-1585.
35. Cao GW. Clinical relevance and public health significance of hepatitis B virus genomic variations. *World Journal of Gastroenterology* 2009;15:5761-5769.
36. Churin Y, Roderfeld M, Roeb E. Hepatitis B virus large surface protein: function and fame. *Hepatobiliary Surgery and Nutrition* 2015;4:1-10.
37. Tarocchi M, Polvani S, Marroncini G, Galli A. Molecular mechanism of hepatitis B virus-induced hepatocarcinogenesis. *World Journal of Gastroenterology* 2014;20:11630-11640.

38. Lin CM, Wang GM, Jow GM, Chen BF. Functional analysis of hepatitis B virus pre-s deletion variants associated with hepatocellular carcinoma. *Journal of Biomedical Science* 2012;19.
39. Chiu AP, Tschida BR, Lo LH, Moriarity BS, Rowlands DK, Largaespada DA, Keng VW. Transposon mouse models to elucidate the genetic mechanisms of hepatitis B viral induced hepatocellular carcinoma. *World J Gastroenterol* 2015;21:12157-12170.
40. Kay A, Zoulim F. Hepatitis B virus genetic variability and evolution. *Virus Research* 2007;127:164-176.
41. Yeung P, Wong DKH, Lai CL, Fung J, Seto WK, Yuen MF. Association of Hepatitis B Virus Pre-S Deletions with the Development of Hepatocellular Carcinoma in Chronic Hepatitis B. *Journal of Infectious Diseases* 2011;203:646-654.
42. Na B, Huang ZM, Wang Q, Qi ZX, Tian YJ, Lu CC, Yu JW, et al. Transgenic Expression of Entire Hepatitis B Virus in Mice Induces Hepatocarcinogenesis Independent of Chronic Liver Injury. *Plos One* 2011;6.
43. Shen T, Yan XM, Zhang JP, Wang JL, Zuo RX, Li L, Wang LP. Evolution of Hepatitis B Virus in a Chronic HBV-Infected Patient over 2 Years. *Hepat Res Treat* 2011;2011:939148.
44. Qu LS, Kuai XL, Liu TT, Chen TY, Ni ZP, Shen XZ. Pre-S Deletion and Complex Mutations of Hepatitis B Virus Related to Young Age Hepatocellular Carcinoma in Qidong, China. *Plos One* 2013;8.
45. Zhang DK, Dong PL, Zhang K, Deng LB, Bach C, Chen W, Li FF, et al. Whole genome HBV deletion profiles and the accumulation of preS deletion mutant during antiviral treatment. *Bmc Microbiology* 2012;12.
46. Brechot C, Kremsdorf D, Soussan P, Pineau P, Dejean A, Paterlini-Brechot P, Tiollais P. Hepatitis B virus (HBV)-related hepatocellular carcinoma (HCC): Molecular mechanisms and novel paradigms. *Pathologie Biologie* 2010;58:278-287.
47. Lu JW, Hsia Y, Tu HC, Hsiao YC, Yang WY, Wang HD, Yuh CH. Liver Development and Cancer Formation in Zebrafish. *Birth Defects Research Part C- Embryo Today-Reviews* 2011;93:157-172.
48. Tian Y, Yang WB, Song JX, Wu YZ, Ni B. Hepatitis B Virus X Protein-Induced Aberrant Epigenetic Modifications Contributing to Human Hepatocellular Carcinoma Pathogenesis. *Molecular and Cellular Biology* 2013;33:2810-2816.

49. Hsieh YH, Hsu JL, Su IJ, Huang WY. Genomic instability caused by hepatitis B virus: into the hepatoma inferno. *Frontiers in Bioscience-Landmark* 2011;16:2586-2597.
50. Matsuda Y, Ichida T. Impact of hepatitis B virus X protein on the DNA damage response during hepatocarcinogenesis. *Medical Molecular Morphology* 2009;42:138-142.
51. Qadri I, Fatima K, AbdeL-Hafiz H. Hepatitis B virus X protein impedes the DNA repair via its association with transcription factor, TFIIH. *Bmc Microbiology* 2011;11.
52. van de Klundert MAA, van Hemert FJ, Zaaier HL, Kootstra NA. The Hepatitis B Virus X Protein Inhibits Thymine DNA Glycosylase Initiated Base Excision Repair. *Plos One* 2012;7.
53. Cha MY, Kim CM, Park YM, Ryu WS. Hepatitis B virus X protein is essential for the activation of Wnt/beta-catenin signalling in hepatoma cells. *Hepatology* 2004;39:1683-1693.
54. Keng VW, Tschida BR, Bell JB, Largaespada DA. Modeling hepatitis B virus X-induced hepatocellular carcinoma in mice with the Sleeping Beauty transposon system. *Hepatology* 2011;53:781-790.
55. Lin X, Xu X, Huang QL, Liu YQ, Zheng DL, Chen WN, Lin JY. Biological impacts of "hot-spot" mutations of hepatitis B virus X proteins are genotype B and C differentiated. *World Journal of Gastroenterology* 2005;11:4703-4708.
56. Lindh M, Gustavson C, Mardberg K, Norkrans G, Dhillon AP, Horal P. Mutation of nucleotide 1,762 in the core promoter region during hepatitis B e seroconversion and its relation to liver damage in hepatitis B e antigen carriers. *Journal of Medical Virology* 1998;55:185-190.
57. Lindh M, Gustavson C, Mardberg K, Norkrans G, Dhillon AP, Horal P. Mutation of nucleotide 1,762 in the core promoter region during hepatitis B e seroconversion and its relation to liver damage in hepatitis B e antigen carriers. *J Med Virol* 1998;55:185-190.
58. Lin X, Xu X, Huang QL, Liu YQ, Zheng DL, Chen WN, Lin JY. Biological impacts of "hot-spot" mutations of hepatitis B virus X proteins are genotype B and C differentiated. *World J Gastroenterol* 2005;11:4703-4708.
59. Ng SA, Lee C. Hepatitis B virus X gene and hepatocarcinogenesis. *J Gastroenterol* 2011;46:974-990.

60. Lin CL, Liao LY, Wang CS, Chen PJ, Lai MY, Chen DS, Kao JH. Basal core-promoter mutant of hepatitis B virus and progression of liver disease in hepatitis B e antigen-negative chronic hepatitis B. *Liver International* 2005;25:564-570.
61. Kuang SY, Jackson PE, Wang JB, Lu PX, Munoz A, Qian GS, Kensler TW, et al. Specific mutations of hepatitis B virus in plasma predict liver cancer development. *Proc Natl Acad Sci U S A* 2004;101:3575-3580.
62. Datta S, Chatterjee S, Veer V, Chakravarty R. Molecular biology of the hepatitis B virus for clinicians. *J Clin Exp Hepatol* 2012;2:353-365.
63. Lizzano RA, Yang B, Clippinger AJ, Bouchard MJ. The C-terminal region of the hepatitis B virus X protein is essential for its stability and function. *Virus Research* 2011;155:231-239.
64. Luo N, Cai Y, Zhang J, Tang WX, Slagle BL, Wu XL, He S. The C-terminal region of the hepatitis B virus X protein is required for its stimulation of HBV replication in primary mouse hepatocytes. *Virus Research* 2012;165:170-178.
65. Ma NF, Lau SH, Hu L, Xie D, Wu J, Yang J, Wang Y, et al. COOH-terminal truncated HBV X protein plays key role in hepatocarcinogenesis. *Clinical Cancer Research* 2008;14:5061-5068.
66. Toh ST, Jin Y, Liu LZ, Wang JB, Babrzadeh F, Gharizadeh B, Ronaghi M, et al. Deep sequencing of the hepatitis B virus in hepatocellular carcinoma patients reveals enriched integration events, structural alterations and sequence variations. *Carcinogenesis* 2013;34:787-798.
67. Sze KMF, Chu GKY, Lee JMF, Ng IOL. C-terminal truncated hepatitis B virus x protein is associated with metastasis and enhances invasiveness by c-jun/matrix metalloproteinase protein 10 activation in hepatocellular carcinoma. *Hepatology* 2013;57:131-139.
68. Kew MC. Hepatitis B virus x protein in the pathogenesis of hepatitis B virus-induced hepatocellular carcinoma. *Journal of Gastroenterology and Hepatology* 2011;26:144-152.
69. Yip WK, Cheng ASL, Zhu RX, Lung RWM, Tsang DPF, Lau SSK, Chen YC, et al. Carboxyl-Terminal Truncated HBx Regulates a Distinct MicroRNA Transcription Program in Hepatocellular Carcinoma Development. *Plos One* 2011;6.
70. Totoki Y, Tatsuno K, Covington KR, Ueda H, Creighton CJ, Kato M, Tsuji S, et al. Trans-ancestry mutational landscape of hepatocellular carcinoma genomes. *Nature Genetics* 2014;46:1267-1273.

71. Schulze K, Imbeaud S, Letouze E, Alexandrov LB, Calderaro J, Rebouissou S, Couchy G, et al. Exome sequencing of hepatocellular carcinomas identifies new mutational signatures and potential therapeutic targets. *Nature Genetics* 2015;47:505-U106.
72. Amaddeo G, Cao Q, Ladeiro Y, Imbeaud S, Nault JC, Jaoui D, Mathe YG, et al. Integration of tumour and viral genomic characterisations in HBV-related hepatocellular carcinomas. *Gut* 2015;64:820-829.
73. Chittmittrapap S, Chieochansin T, Chaiteerakij R, Treeprasertsuk S, Klaikaew N, Tangkijvanich P, Komolmit P, et al. Prevalence of Aflatoxin Induced p53 Mutation at Codon 249 (R249s) in Hepatocellular Carcinoma Patients with and without Hepatitis B Surface Antigen (HBsAg). *Asian Pacific Journal of Cancer Prevention* 2013;14:7675-7679.
74. Jiang WD, Wang XW, Unger T, Forgues M, Kim JW, Hussain SP, Bowman E, et al. Cooperation of tumor-derived HBx mutants and p53-249(ser) mutant in regulating cell proliferation, anchorage-independent growth and aneuploidy in a telomerase-immortalized normal human hepatocyte-derived cell line. *International Journal of Cancer* 2010;127:1011-1020.
75. Bard-Chapeau EA, Nguyen AT, Rust AG, Sayadi A, Lee P, Chua BQ, New LS, et al. Transposon mutagenesis identifies genes driving hepatocellular carcinoma in a chronic hepatitis B mouse model. *Nat Genet* 2014;46:24-32.
76. Collier LS, Carlson CM, Ravimohan S, Dupuy AJ, Largaespada DA. Cancer gene discovery in solid tumours using transposon-based somatic mutagenesis in the mouse. *Nature* 2005;436:272-276.
77. Dupuy AJ, Rogers LM, Kim J, Nannapaneni K, Starr TK, Liu P, Largaespada DA, et al. A modified sleeping beauty transposon system that can be used to model a wide variety of human cancers in mice. *Cancer Res* 2009;69:8150-8156.
78. Keng VW, Sia D, Sarver AL, Tschida BR, Fan D, Alsinet C, Sole M, et al. Sex bias occurrence of hepatocellular carcinoma in Poly7 molecular subclass is associated with EGFR. *Hepatology* 2013;57:120-130.
79. Keng VW, Villanueva A, Chiang DY, Dupuy AJ, Ryan BJ, Matisse I, Silverstein KA, et al. A conditional transposon-based insertional mutagenesis screen for genes associated with mouse hepatocellular carcinoma. *Nat Biotechnol* 2009;27:264-274.

80. O'Donnell KA, Keng VW, York B, Reineke EL, Seo D, Fan D, Silverstein KA, et al. A Sleeping Beauty mutagenesis screen reveals a tumor suppressor role for Ncoa2/Src-2 in liver cancer. *Proc Natl Acad Sci U S A* 2012;109:E1377-1386.
81. Rahrmann EP, Collier LS, Knutson TP, Doyal ME, Kuslak SL, Green LE, Malinowski RL, et al. Identification of PDE4D as a proliferation promoting factor in prostate cancer using a Sleeping Beauty transposon-based somatic mutagenesis screen. *Cancer Res* 2009;69:4388-4397.
82. Rahrmann EP, Watson AL, Keng VW, Choi K, Moriarity BS, Beckmann DA, Wolf NK, et al. Forward genetic screen for malignant peripheral nerve sheath tumor formation identifies new genes and pathways driving tumorigenesis. *Nat Genet* 2013;45:756-766.
83. Riordan JD, Keng VW, Tschida BR, Scheetz TE, Bell JB, Podetz-Pedersen KM, Moser CD, et al. Identification of rtl1, a retrotransposon-derived imprinted gene, as a novel driver of hepatocarcinogenesis. *PLoS Genet* 2013;9:e1003441.
84. Starr TK, Allaei R, Silverstein KA, Staggs RA, Sarver AL, Bergemann TL, Gupta M, et al. A transposon-based genetic screen in mice identifies genes altered in colorectal cancer. *Science* 2009;323:1747-1750.
85. Chen L, Jenjaroenpun P, Pillai AM, Ivshina AV, Ow GS, Efthimios M, Zhiqun T, et al. Transposon insertional mutagenesis in mice identifies human breast cancer susceptibility genes and signatures for stratification. *Proc Natl Acad Sci U S A* 2017;114:E2215-E2224.
86. Kodama T, Newberg JY, Kodama M, Rangel R, Yoshihara K, Tien JC, Parsons PH, et al. Transposon mutagenesis identifies genes and cellular processes driving epithelial-mesenchymal transition in hepatocellular carcinoma. *Proc Natl Acad Sci U S A* 2016;113:E3384-3393.
87. Rangel R, Lee SC, Hon-Kim Ban K, Guzman-Rojas L, Mann MB, Newberg JY, Kodama T, et al. Transposon mutagenesis identifies genes that cooperate with mutant Pten in breast cancer progression. *Proc Natl Acad Sci U S A* 2016;113:E7749-E7758.
88. Morris SM, Davison J, Carter KT, O'Leary RM, Trobridge P, Knoblauch SE, Myeroff LL, et al. Transposon mutagenesis identifies candidate genes that cooperate with loss of transforming growth factor-beta signalling in mouse intestinal neoplasms. *Int J Cancer* 2017;140:853-863.

89. Moriarity BS, Otto GM, Rahrman EP, Rathe SK, Wolf NK, Weg MT, Manlove LA, et al. A Sleeping Beauty forward genetic screen identifies new genes and pathways driving osteosarcoma development and metastasis. *Nat Genet* 2015;47:615-624.
90. Been RA, Linden MA, Hager CJ, DeCoursin KJ, Abrahante JE, Landman SR, Steinbach M, et al. Genetic signature of histiocytic sarcoma revealed by a sleeping beauty transposon genetic screen in mice. *PLoS One* 2014;9:e97280.
91. Heltemes-Harris LM, Larson JD, Starr TK, Hubbard GK, Sarver AL, Largaespada DA, Farrar MA. Sleeping Beauty transposon screen identifies signalling modules that cooperate with STAT5 activation to induce B-cell acute lymphoblastic leukemia. *Oncogene* 2016;35:3454-3464.
92. Starr TK, Scott PM, Marsh BM, Zhao L, Than BL, O'Sullivan MG, Sarver AL, et al. A Sleeping Beauty transposon-mediated screen identifies murine susceptibility genes for adenomatous polyposis coli (*Apc*)-dependent intestinal tumorigenesis. *Proc Natl Acad Sci U S A* 2011;108:5765-5770.
93. Zanesi N, Balatti V, Riordan J, Burch A, Rizzotto L, Palamarchuk A, Cascione L, et al. A Sleeping Beauty screen reveals NF- $\kappa$ B activation in CLL mouse model. *Blood* 2013;121:4355-4358.
94. Bell JB, Podetz-Pedersen KM, Aronovich EL, Belur LR, McIvor RS, Hackett PB. Preferential delivery of the Sleeping Beauty transposon system to livers of mice by hydrodynamic injection. *Nat Protoc* 2007;2:3153-3165.
95. Wiesner SM, Decker SA, Larson JD, Ericson K, Forster C, Gallardo JL, Long C, et al. De novo induction of genetically engineered brain tumors in mice using plasmid DNA. *Cancer Res* 2009;69:431-439.
96. Ivics Z, Hackett PB, Plasterk RH, Izsvak Z. Molecular reconstruction of Sleeping Beauty, a Tc1-like transposon from fish, and its transposition in human cells. *Cell* 1997;91:501-510.
97. Mikkelsen JG, Yant SR, Meuse L, Huang Z, Xu H, Kay MA. Helper-Independent Sleeping Beauty transposon-transposase vectors for efficient nonviral gene delivery and persistent gene expression in vivo. *Mol Ther* 2003;8:654-665.
98. Dupuy AJ, Fritz S, Largaespada DA. Transposition and gene disruption in the male germline of the mouse. *Genesis* 2001;30:82-88.

99. Keng VW, Yae K, Hayakawa T, Mizuno S, Uno Y, Yusa K, Kokubu C, et al. Region-specific saturation germline mutagenesis in mice using the Sleeping Beauty transposon system. *Nat Methods* 2005;2:763-769.
100. Luo G, Ivics Z, Izsvak Z, Bradley A. Chromosomal transposition of a Tc1/mariner-like element in mouse embryonic stem cells. *Proc Natl Acad Sci U S A* 1998;95:10769-10773.
101. Suda T, Liu D. Hydrodynamic gene delivery: its principles and applications. *Mol Ther* 2007;15:2063-2069.
102. Grompe M, al-Dhalimy M, Finegold M, Ou CN, Burlingame T, Kennaway NG, Soriano P. Loss of fumarylacetoacetate hydrolase is responsible for the neonatal hepatic dysfunction phenotype of lethal albino mice. *Genes Dev* 1993;7:2298-2307.
103. Wangensteen KJ, Wilber A, Keng VW, He Z, Matisse I, Wangensteen L, Carson CM, et al. A facile method for somatic, lifelong manipulation of multiple genes in the mouse liver. *Hepatology* 2008;47:1714-1724.
104. Geurts AM, Yang Y, Clark KJ, Liu G, Cui Z, Dupuy AJ, Bell JB, et al. Gene transfer into genomes of human cells by the sleeping beauty transposon system. *Mol Ther* 2003;8:108-117.
105. Carlson CM, Frandsen JL, Kirchhof N, McIvor RS, Largaespada DA. Somatic integration of an oncogene-harboring Sleeping Beauty transposon models liver tumor development in the mouse. *Proc Natl Acad Sci U S A* 2005;102:17059-17064.
106. Tschida BR, Largaespada DA, Keng VW. Mouse models of cancer: Sleeping Beauty transposons for insertional mutagenesis screens and reverse genetic studies. *Semin Cell Dev Biol* 2014;27:86-95.
107. Hackett PB, Jr., Aronovich EL, Hunter D, Urness M, Bell JB, Kass SJ, Cooper LJ, et al. Efficacy and safety of Sleeping Beauty transposon-mediated gene transfer in preclinical animal studies. *Curr Gene Ther* 2011;11:341-349.
108. Yoshino H, Hashizume K, Kobayashi E. Naked plasmid DNA transfer to the porcine liver using rapid injection with large volume. *Gene Ther* 2006;13:1696-1702.
109. Sidiropoulos K, Viteri G, Sevilla C, Jupe S, Webber M, Orlic-Milacic M, Jassal B, et al. Reactome enhanced pathway visualization. *Bioinformatics* 2017;33:3461-3467.

110. Zucman-Rossi J. Molecular classification of hepatocellular carcinoma. *Dig Liver Dis* 2010;42 Suppl 3:S235-241.
111. Tiu RV, Mountantonakis SE, Dunbar AJ, Schreiber MJ, Jr. Tumor lysis syndrome. *Semin Thromb Hemost* 2007;33:397-407.
112. Englund E, Reitsma B, King BC, Escudero-Esparza A, Owen S, Orimo A, Okroj M, et al. The human complement inhibitor Sushi Domain-Containing Protein 4 (SUSD4) expression in tumor cells and infiltrating T cells is associated with better prognosis of breast cancer patients. *Bmc Cancer* 2015;15.
113. Saeki K, Yokomizo T. Identification, signalling, and functions of LTB4 receptors. *Semin Immunol* 2017;33:30-36.
114. Azrad M, Turgeon C, Demark-Wahnefried W. Current evidence linking polyunsaturated Fatty acids with cancer risk and progression. *Front Oncol* 2013;3:224.
115. Tong WG, Ding XZ, Talamonti MS, Bell RH, Adrian TE. LTB4 stimulates growth of human pancreatic cancer cells via MAPK and PI-3 kinase pathways. *Biochem Biophys Res Commun* 2005;335:949-956.
116. Wang D, Dubois RN. Eicosanoids and cancer. *Nat Rev Cancer* 2010;10:181-193.
117. Mashima R, Okuyama T. The role of lipoxygenases in pathophysiology; new insights and future perspectives. *Redox Biol* 2015;6:297-310.
118. Delage B, Fennell DA, Nicholson L, McNeish I, Lemoine NR, Crook T, Szlosarek PW. Arginine deprivation and argininosuccinate synthetase expression in the treatment of cancer. *Int J Cancer* 2010;126:2762-2772.
119. Ensor CM, Holtsberg FW, Bomalaski JS, Clark MA. Pegylated arginine deiminase (ADI-SS PEG20,000 mw) inhibits human melanomas and hepatocellular carcinomas in vitro and in vivo. *Cancer Res* 2002;62:5443-5450.
120. Wu LN, Li L, Meng SC, Qi RZ, Mao ZB, Lin M. Expression of argininosuccinate synthetase in patients with hepatocellular carcinoma. *Journal of Gastroenterology and Hepatology* 2013;28:365-368.
121. Xing YQ, Li A, Yang Y, Li XX, Zhang LN, Guo HC. The regulation of FOXO1 and its role in disease progression. *Life Sci* 2018;193:124-131.
122. Wang Y, Zhou YM, Graves DT. FOXO Transcription Factors: Their Clinical Significance and Regulation. *Biomed Research International* 2014.

123. Jansson EA, Are A, Greicius G, Kuo IC, Kelly D, Arulampalam V, Pettersson S. The Wnt/beta-catenin signalling pathway targets PPARgamma activity in colon cancer cells. *Proc Natl Acad Sci U S A* 2005;102:1460-1465.
124. Liu J, Farmer SR. Regulating the balance between peroxisome proliferator-activated receptor gamma and beta-catenin signalling during adipogenesis. A glycogen synthase kinase 3beta phosphorylation-defective mutant of beta-catenin inhibits expression of a subset of adipogenic genes. *J Biol Chem* 2004;279:45020-45027.
125. Xie KL, Zhang YG, Liu J, Zeng Y, Wu H. MicroRNAs Associated With HBV Infection And HBV-related HCC. *Theranostics* 2014;4:1176-1192.
126. Chen YN, Shen A, Rider PJ, Yu Y, Wu KL, Mu YX, Hao Q, et al. A liver-specific microRNA binds to a highly conserved RNA sequence of hepatitis B virus and negatively regulates viral gene expression and replication. *Faseb Journal* 2011;25:4511-4521.
127. Yu GF, Chen XZ, Chen SD, Ye WP, Hou KL, Liang M. MiR-19a, miR-122 and miR-223 are differentially regulated by hepatitis B virus X protein and involve in cell proliferation in hepatoma cells. *Journal of Translational Medicine* 2016;14.
128. Imura S, Yamada S, Saito Y, Iwahashi S, Arakawa Y, Ikemoto T, Morine Y, et al. miR-223 and Stathmin-1 Expression in Non-tumor Liver Tissue of Patients with Hepatocellular Carcinoma. *Anticancer Research* 2017;37:5877-5883.
129. Iizuka N, Oka M, Tamesa T, Hamamoto Y, Yamada-Okabe H. Imbalance in expression levels of insulin-like growth factor 2 and H19 transcripts linked to progression of hepatocellular carcinoma. *Anticancer Research* 2004;24:4085-4089.
130. Khosravifar R, Solski PA, Clark GJ, Kinch MS, Der CJ. Activation of Rac1, Rhoa, and Mitogen-Activated Protein-Kinases Is Required for Ras Transformation. *Molecular and Cellular Biology* 1995;15:6443-6453.
131. Qiu RG, Abo A, McCormick F, Symons M. Cdc42 regulates anchorage-independent growth and is necessary for Ras transformation. *Molecular and Cellular Biology* 1997;17:3449-3458.
132. Prudnikova TY, Rawat SJ, Chernoff J. Molecular pathways: targeting the kinase effectors of RHO-family GTPases. *Clin Cancer Res* 2015;21:24-29.
133. Peck J, Douglas G, Wu CH, Burbelo PD. Human RhoGAP domain-containing proteins: structure, function and evolutionary relationships. *Febs Letters* 2002;528:27-34.

134. Nakamura F. FilGAP and its close relatives: a mediator of Rho-Rac antagonism that regulates cell morphology and migration. *Biochemical Journal* 2013;453:17-25.
135. Radu M, Semenova G, Kosoff R, Chernoff J. PAK signalling during the development and progression of cancer. *Nature Reviews Cancer* 2014;14:13-25.
136. Tamaki T, Kamatsuka K, Sato T, Morooka S, Otsuka K, Hattori M, Sugiyama T. A novel transmembrane protein defines the endoplasmic reticulum stress-induced cell death pathway. *Biochem Biophys Res Commun* 2017;486:149-155.
137. Livingstone C. IGF2 and cancer. *Endocr Relat Cancer* 2013;20:R321-339.
138. Brouwer-Visser J, Huang GS. IGF2 signalling and regulation in cancer. *Cytokine Growth Factor Rev* 2015;26:371-377.
139. Haley VL, Barnes DJ, Sandovici I, Constancia M, Graham CF, Pezzella F, Buhemann C, et al. Igf2 pathway dependency of the Trp53 developmental and tumour phenotypes. *EMBO Mol Med* 2012;4:705-718.
140. Marshall A, Lukk M, Kutter C, Davies S, Alexander G, Odom DT. Global gene expression profiling reveals SPINK1 as a potential hepatocellular carcinoma marker. *PLoS One* 2013;8:e59459.
141. Li XX, Zhang SJ, Chiu AP, Lo LH, Huang J, Rowlands DK, Wang J, et al. Targeting of AKT/ERK/CTNNB1 by DAW22 as a potential therapeutic compound for malignant peripheral nerve sheath tumor. *Cancer Med* 2018;7:4791-4800.
142. Li XX, Lu XY, Zhang SJ, Chiu AP, Lo LH, Largaespada DA, Chen QB, et al. Sodium tanshinone IIA sulfonate ameliorates hepatic steatosis by inhibiting lipogenesis and inflammation. *Biomed Pharmacother* 2019;111:68-75.